

# Fractional Insulators and their Parent Hamiltonians

---

Dissertation zur Erlangung des  
naturwissenschaftlichen Doktorgrades  
der Julius-Maximilians-Universität Würzburg

vorgelegt von

**Vera Schnells**

aus Leverkusen

Würzburg 2019



Eingereicht am 08.04.2019

bei der Fakultät für Physik und Astronomie

1. Gutachter: PD Dr. Martin Greiter
  2. Gutachter: Prof. Dr. Haye Hinrichsen
- der Dissertation

Vorsitzender: Prof. Dr. Edwin Batke

1. Prüfer: PD Dr. Martin Greiter
  2. Prüfer: Prof. Dr. Haye Hinrichsen
  3. Prüfer: Prof. Dr. Friedrich Reinert
- im Promotionskolloquium

Tag des Promotionskolloquiums: 19.07.2019

# Acknowledgments

I am deeply grateful to my advisor Martin Greiter. He graciously guided and influenced my professional growth since the beginning of my doctoral studies. Most importantly, he served to me as a mentor and model of how to be a methodically thorough and passionate physicist. This entire work would not have been possible without his ideas, physical insight and our endless discussions.

I also wish to deeply thank Ronny Thomale for his professional guidance and endless support during my PhD. Time and again, he inspired me with his motivation and bold research ideas.

My gratefulness also belongs to all members of the Institute for Theoretical Physics I at University of Würzburg, who have created a welcoming atmosphere during all the years.

Finally, I want to express my endless gratitude to my parents and my sister, who are and have always been my support and motivation.



# Abstract

In the past few years, two-dimensional quantum liquids with fractional excitations have been a topic of high interest due to their possible application in the emerging field of quantum computation and cryptography. This thesis is devoted to a deeper understanding of known and new fractional quantum Hall states and their stabilization in local models. We pursue two different paths, namely chiral spin liquids and fractionally quantized, topological phases.

The chiral spin liquid is one of the few examples of spin liquids with fractional statistics. Despite its numerous promising properties, the microscopic models for this state proposed so far are all based on non-local interactions, making the experimental realization challenging. In the first part of this thesis, we present the first local parent Hamiltonians, for which the Abelian and non-Abelian chiral spin liquids are the exact and, modulo a topological degeneracy, unique ground states. We have developed a systematic approach to find an annihilation operator of the chiral spin liquid and construct from it a many-body interaction which establishes locality. For various system sizes and lattice geometries, we numerically find largely gapped eigenspectra and confirm to an accuracy of machine precision the uniqueness of the chiral spin liquid as ground state of the respective system. Our results provide an exact spin model in which fractional quantization can be studied.

Topological insulators are one of the most actively studied topics in current condensed matter physics research. With the discovery of the topological insulator, one question emerged: Is there an interaction-driven set of fractionalized phases with time reversal symmetry? One intuitive approach to the theoretical construction of such a fractional topological insulator is to take the direct product of a fractional quantum Hall state and its time reversal conjugate. However, such states are well studied conceptually and do not lead to new physics, as the idea of taking a state and its mirror image together without any entanglement between the states has been well understood in the context of topological insulators. Therefore, the community has been looking for ways to implement some topological interlocking between different spin species. Yet, for all practical purposes so far, time reversal symmetry has appeared to limit the set of possible fractional states to those with no interlocking between the two spin species.

In the second part of this thesis, we propose a new universality class of fractionally quantized, topologically ordered insulators, which we name “fractional insulator”. Inspired by the fractional quantum Hall effect, spin liquids, and fractional Chern insulators, we develop a wave function approach to a new class of topological order in a two-dimensional crystal of spin-orbit coupled electrons. The idea is simply to allow the topological order to violate time reversal symmetry, while all locally observable quantities remain time reversal invariant. We refer to this situation as “topological time reversal symmetry breaking”. Our state is based on the Halperin double layer states and can be viewed as a two-layer system of an  $\uparrow$ -spin and a  $\downarrow$ -spin sphere. The construction starts off with Laughlin states for the  $\uparrow$ -spin and  $\downarrow$ -spin electrons and an interflavor term, which creates correlations between the two layers. With a careful parameter choice, we obtain a state preserving time reversal symmetry locally, and label it the “311-state”. For systems of up to six  $\uparrow$ -spin and six  $\downarrow$ -spin electrons, we manage to construct an approximate parent Hamiltonian with a physically realistic, local interaction.



# Zusammenfassung

In den letzten Jahren waren zweidimensionale Quantenflüssigkeiten mit fraktionalem Anregungen aufgrund ihrer möglichen Anwendung auf dem aufstrebenden Forschungsgebiet der Quantencomputer und Quantenkryptographie von großem Interesse. Diese Dissertation hat sich zum Ziel gesetzt, einem tieferen Verständnis bekannter und neuer fraktionaler Quanten-Hall-Zustände und ihrer Stabilisierung in lokalen Modellen beizutragen. In diesem Zusammenhang werden zwei Themen betrachtet: Chirale Spinflüssigkeiten und fraktional quantisierte, topologische Phasen.

Die chirale Spinflüssigkeit ist eines der wenigen Beispiele für Spinflüssigkeiten mit fraktionaler Statistik. Trotz ihrer zahlreichen vielversprechenden Eigenschaften beruhen die bisher vorgeschlagenen mikroskopischen Modelle für diesen Zustand alle auf nichtlokalen Wechselwirkungen. Dies erschwert eine experimentelle Realisierung. Im ersten Teil dieser Dissertation stellen wir die ersten Eltern-Hamiltonoperatoren vor, für die die Abelschen und nicht-Abelschen chiralen Spinflüssigkeiten die exakten und, abgesehen von einer topologischen Entartung, einzigen Grundzustände sind. Wir haben eine Methode entwickelt, um ausgehend von einem Vernichtungsoperator für die chirale Spinflüssigkeit eine lokale Mehrkörper-Wechselwirkung zu konstruieren. Numerisch finden wir für verschiedene Systemgrößen und Gittergeometrien Eigenspektren mit großer Anregungslücke und können mit Maschinengenauigkeit die Eindeutigkeit der chiralen Spinflüssigkeit als Grundzustand des jeweiligen Systems bestätigen. Damit liefern unsere Ergebnisse ein exaktes Spinmodell, in dem fraktionale Quantisierung untersucht werden kann.

Topologische Isolatoren sind derzeit eines der am häufigsten untersuchten Themen in der Physik der kondensierten Materie. Mit ihrer Entdeckung kam die Frage auf: Gibt es eine verschränkte Gruppe fraktionaler Phasen mit Zeitumkehrsymmetrie? Ein intuitiver Ansatz für die theoretische Konstruktion eines solchen fraktionalem topologischen Isolators besteht darin, das direkte Produkt eines fraktionalem Quanten-Hall-Zustands und seines Zeitumkehrkonjugats zu bilden. Solche Zustände bringen jedoch konzeptionell keinen Mehrwert, da Systeme bestehend aus einem Zustand und seinem Spiegelbild ohne zusätzliche Verschränkung im Kontext der topologischen Isolatoren im Detail erforscht sind. Daher wird aktuell nach Möglichkeiten gesucht, eine topologische Verschränkung zwischen verschiedenen Spinarten umzusetzen. Für alle Anwendungen in der Praxis scheint die Zeitumkehrsymmetrie jedoch die Menge möglicher fraktionaler Zustände auf solche ohne Verschränkung zwischen den beiden Spinspezies zu begrenzen.

Im zweiten Teil dieser Dissertation schlagen wir eine neue Universalitätsklasse von fraktional quantisierten, topologisch geordneten Isolatoren vor, die wir “fraktionalem Isolator” nennen. Inspiriert vom fraktionalem Quanten-Hall-Effekt, Spin-Flüssigkeiten und fraktionalem Chern-Isolatoren entwickeln wir eine Wellenfunktion, die eine neue Klasse topologischer Ordnung in einem zweidimensionalen Kristall aus Spin-Orbit-gekoppelten Elektronen beschreibt. Unser Ansatz basiert darauf, die topologische Ordnung gegen die Zeitumkehrsymmetrie verstoßen zu lassen, während alle lokal beobachtbaren Größen zeitumkehrinvariant sind. Wir bezeichnen diese Situation als “topologische Zeitumkehrsymmetriebrechung”. Unser Zustand basiert auf den Halperin-Doppelschichtzuständen und kann als ein Zweischichtensystem aus einer  $\uparrow$ -Spin- und einer  $\downarrow$ -Spin-Sphäre betrachtet werden. Die Konstruktion beginnt mit zwei Laughlin-Zuständen für die  $\uparrow$ -Spin- und  $\downarrow$ -Spin-Elektronen und einem Wechselwirkungsterm, der eine Verschränkung zwischen den beiden Schichten erzeugt. Wir erhalten einen neuen Zustand, den “311-Zustand”, der lokal zeitumkehrinvari-

ant ist. Für Systeme mit bis zu sechs  $\uparrow$ -Spin- und sechs  $\downarrow$ -Spin-Elektronen finden wir einen approximativen Eltern-Hamiltonoperator mit einer physikalisch realistischen, lokalen Wechselwirkung.



# List of Publications

1. P. S. Häfliger, S. Gerber, R. Pramod, V. Schnells, B. dalla Piazza, R. Chati, V. Pomjakushin, K. Conder, E. Pomjakushina, L. Le Dreau, N. B. Christensen, O. F. Syljurasen, B. Normand, and H. M. Rønnow, *Quantum and thermal ionic motion, oxygen isotope effect, and superexchange distribution in  $\text{La}_2\text{CuO}_4$* , Physical Review B **89**, 085113 (2014)
2. M. Moretti Sala, V. Schnells, S. Boseggia, L. Simonelli, A. Al-Zein, J. G. Vale, L. Paolasini, E. C. Hunter, R. S. Perry, D. Prabhakaran, A. T. Boothroyd, M. Krisch, G. Monaco, H. M. Rønnow, D. F. McMorrow, and F. Mila, *Evidence of quantum dimer excitations in  $\text{Sr}_3\text{Ir}_2\text{O}_7$* , Physical Review B **92**, 024405 (2015)
3. M. Greiter, V. Schnells, and R. Thomale, *The 1D Ising model and the topological Kitaev chain*, Annals of Physics **351**, 1026 (2014)
4. —, *Laughlin states and their quasiparticle excitations on the torus*, Physical Review B **93**, 245156 (2016)
5. —, *Method to identify parent Hamiltonians for trial states*, Physical Review B **98**, 081113 (2018)
6. V. Schnells, R. Thomale, and M. Greiter, *Fractional insulators* , to be published (2019)
7. —, *Local parent Hamiltonian for the chiral spin liquid* , to be published (2019)



# Contents

<b>1</b>	<b>Introduction</b>	1
<b>2</b>	<b>Review of the Laughlin state and its formalism</b>	5
2.1	Landau level quantization in the plane	5
2.2	The Laughlin state in the plane	6
2.3	Quasihole and quasiparticle excitations	7
2.4	Landau level quantization on the sphere	8
2.5	The Laughlin state on the sphere	10
2.6	Extension to multi-component systems	11
<b>3</b>	<b>Chiral spin liquids</b>	13
3.1	The Haldane-Shastry model	13
3.2	The Abelian chiral spin liquid	18
3.3	The non-Abelian chiral spin liquid	22
<b>4</b>	<b>Local parent Hamiltonian for the chiral spin liquid</b>	27
4.1	Introduction	27
4.2	A local parent Hamiltonian for the chiral spin liquid	28
4.2.1	Annihilation operator in 1d	28
4.2.2	Annihilation operator in 2d	28
4.2.3	Direct verification of the annihilation property	29
4.2.4	Construction of a parent Hamiltonian	31
4.2.5	Establishing locality	32
4.3	Tensor representation of operators	35
4.3.1	Representation of rotations	35
4.3.2	Spherical tensor operators	35
4.3.3	Product of tensor operators	37
4.3.4	Decomposition of tensor products	38
4.3.5	Structure of the parent Hamiltonian	40
4.4	Implementation details	42
4.4.1	Numerical decomposition of tensor operators	42
4.4.2	From a small Hamiltonian to a parent Hamiltonian	47
4.4.3	Calculation of the eigenspectra	49
4.5	Results for a local parent Hamiltonian of the chiral spin liquid	50
4.5.1	Spin 1/2, two-site interaction	50
4.5.2	Spin 1/2, three-site interaction	50
4.5.3	Spin 1/2, four-site interaction	51
4.5.4	Spin 1, two-site interaction	52

4.5.5	Spin 1, three-site interaction	52
4.5.6	Spin 3/2, two-site interaction	54
4.6	Numerical validation of spin 1/2 systems	55
4.6.1	Two-site interaction	55
4.6.2	Three-site interaction	60
4.6.3	Four-site interaction	61
4.7	Numerical validation of spin 1 systems	63
4.7.1	Two-site interaction	63
4.7.2	Three-site interaction	66
<b>5</b>	<b>Topological insulators</b>	<b>73</b>
5.1	Overview	73
5.2	Basic properties of topological insulators	76
5.3	Time reversal and Kramers pairs	77
5.4	Absence of backscattering in 2D topological insulators	78
5.5	TKNN and Chern invariants	79
5.6	Graphene band structure and the Haldane model	80
5.7	Edge states of Chern insulators	81
5.8	2D Topological insulators in HgTe/CdTe quantum wells	83
5.9	$\mathbb{Z}_2$ -invariant	85
5.10	3D topological insulators	86
<b>6</b>	<b>Fractional insulators</b>	<b>89</b>
6.1	Introduction	89
6.2	Properties of the 311-state	93
6.2.1	Construction of the 311-state	93
6.2.2	Angular momentum calculation and rotational invariance	94
6.2.3	Effective field theory of the 311-state	98
6.2.4	Pair correlation function	98
6.3	Construction of a parent Hamiltonian	102
6.3.1	Pseudopotentials	102
6.3.2	The Hamiltonian Finder - General method	111
6.3.3	The Hamiltonian Finder - Approximate parent Hamiltonians	113
6.3.4	Finding an approximate parent Hamiltonian for the 311-state	115
6.3.5	Relative angular momentum resolved analysis	117
6.3.6	Real space potentials	118
6.4	Numerical results for the 311-state	125
6.4.1	Numerical construction of the wave function	125
6.4.2	Pair correlation function	128
6.4.3	Relative angular momentum resolved correlators	130
6.4.4	Construction and analysis of a parent Hamiltonian	133
6.4.5	Real space potentials for the 311-state	138
<b>7</b>	<b>Conclusion</b>	<b>141</b>
<b>A</b>	<b>Angular momentum algebra and spin operators</b>	<b>143</b>
<b>B</b>	<b>Tensor decompositions of spin operators</b>	<b>145</b>
B.1	One spin operator	145
B.2	Two spin operators	145
B.3	Three spin operators	146
B.4	Four spin operators	149

Contents	xiii
<b>C The Jacobi theta function</b> .....	151
<b>D Mathematica notebooks for tensor decompositions</b> .....	153
<b>References</b> .....	163



# Chapter 1

## Introduction

One of the most fascinating aspects of condensed matter physics is the discovery and classification of new phases of matter. For decades, different phases could be characterized by the Landau-Ginzburg theory of symmetry breaking [83; 84]. Only with the experimental discovery of the integer and fractional quantum Hall effect [80; 140], and its theoretical explanation by Laughlin [86], this paradigm was broken. A new class of states was found which does not break any symmetries, but instead is characterized by the notion of *topological order* [139; 144]. Such states are characterized by properties such as the quantized Hall conductance or the number of edge modes, which depend on the topology of the system. While the integer quantum Hall effect can be explained by a single-particle picture, strong electronic correlations require a many-body theory to describe the fractional quantum Hall states.

Among these topological states of matter, especially two-dimensional quantum liquids with fractional excitations have been a topic of high interest in the past few years [132; 150]. This is due to their possible application in the emerging field of quantum computation and cryptography [79; 105]. In such systems, the elementary excitations carry only a fraction of the quantum numbers of the particles. The fractional quantum Hall state is the most prominent state in which fractional quantization was analyzed on a unified footing [86; 63; 5]. It is noteworthy that fractional statistics can only occur in one- and two-dimensional systems, where a winding number can be defined [45; 149].

This thesis is devoted to a deeper understanding of known and new fractional quantum Hall states and their stabilization in local models. To set the theoretical background for our research projects, we review the Laughlin formalism to describe fractionally quantized Hall states in Chapter 2. Haldane was the first to extend the Laughlin formalism to a spherical geometry [53], which offers the advantage that it does not have a boundary, making this geometry particularly suited for the investigation of bulk properties. We therefore analyze the Laughlin state, its elementary excitations and its extension to multi-component systems both in planar and spherical geometries.

In Section 3.1 of Chapter 3, we introduce the Haldane-Shastry model, which describes a spin-1/2 chain with a Heisenberg interaction falling off as  $1/r^2$  with increasing distance  $r$ . This integrable model reveals a direct relationship of the spin chain to the fractional quantum Hall effect [74]. The Abelian chiral spin liquid (CSL), which we introduce in Section 3.2 as one of the few examples of a spin liquid with fractional statistics, may be considered as the two-dimensional analog of the Haldane-Shastry model. For spin systems with  $s > 1/2$ , the spinon excitations of the CSL have non-Abelian statistics. This class of non-Abelian CSLs, introduced in 2009 [45], is detailed in Section 3.3.

Although the CSL has many promising properties, it took almost two decades for a microscopic model to emerge. The first exact parent Hamiltonian for the Abelian CSL was constructed by Schroeter et al. [125], and, for a system with periodic boundary conditions, an approximate parent Hamiltonian for the non-Abelian CSL has been proposed [42], which becomes exact in the thermodynamic limit. However, the major problem of both parent Hamiltonians is their lack of locality, making such models challenging to achieve experimentally.

In Chapter 4, we present the first local parent Hamiltonians, for which the Abelian and non-Abelian CSLs are exact ground states [124]. The construction of such a parent Hamiltonian is highly complex since

it has to meet several criteria: it has to be Hermitian, invariant under spatial translations and  $SU(2)$ -spin rotations, the CSL has to be the exact and unique ground state, and the model should be local. We have developed a method to systematically solve this problem, which is presented in Section 4.2. First, an annihilation operator  $\Omega$  of the CSL has to be constructed, as detailed in Sections 4.2.1-4.2.3. Second, in Section 4.2.4, the Hermitian product  $\Omega^\dagger\Omega$  is taken. Section 4.2.5 explains that we need a many-body interaction with at least four particles to obtain a local interaction. And to establish  $SU(2)$ -invariance under spin rotations, the expression  $\Omega^\dagger\Omega$  is projected onto its scalar component in Section 4.3, in which we also explain how to decompose arbitrary tensor products into irreducible representations under  $SU(2)$ -spin rotations.

The parent Hamiltonian expressions in Section 4.3.5 are difficult to apprehend. To develop a better intuition about the underlying model, we decompose the Hamiltonian into simple scalar spin terms. Performing this task by hand is intricate and becomes unfeasible for more complex tensor expressions. We have developed an exact numerical technique, which is presented in Section 4.4.1. Implemented as a *Mathematica*-program, the technique allows to decompose generic tensor expressions into simple products of spin operators. We construct the Hamiltonians for spin-1/2, spin-1 and spin-3/2 systems, and present our results in Section 4.5. Overall, these models represent an exact spin model in which fractional quantization can be studied.

To determine whether the CSL is the *unique* ground state of our parent Hamiltonians, we perform exact diagonalization studies [16; 109; 107]. This becomes numerically challenging due to the exponential growth of the Hilbert space with system size. In Sections 4.4.2 and 4.4.3, we explain details of our implementation, including which lattice geometries and sizes were investigated. Our numerical results in Section 4.6 show an eigenspectrum with large gaps and confirm to an accuracy of machine precision that the Abelian CSL is the unique ground state for our Hamiltonian with spin  $s = 1/2$ . In Section 4.7, the uniqueness of the non-Abelian CSL for our Hamiltonian with spin  $s = 1$  is confirmed for all geometries. We hereby provide an exact spin model in which fractional quantization with Abelian and non-Abelian statistics can be studied.

In Chapter 5, we review the path that led to the discovery of topological insulators and the current state of research. Both the integer and fractional quantum Hall effect require strong magnetic fields for their realization. Therefore, soon after their discovery, the quest for systems exhibiting dissipationless edge modes without any magnetic field began. Haldane was the first to propose a lattice analog to the integer quantum Hall state without an orbital magnetic field [55], which is called the ‘‘Haldane model’’. Systems with this property are called ‘‘Chern insulators’’. For decades, an experimental realization remained unachieved. In 2005, Kane and Mele theoretically proposed a time reversal-invariant system exhibiting a so-called quantum spin Hall state [75]. Based on the spin-orbit coupling of graphene, they combined two copies of a Haldane model such that the  $\uparrow$ -spin electrons manifest a chiral quantum Hall effect, while the  $\downarrow$ -spin electrons manifest an anti-chiral quantum Hall effect.

To create an experimentally more attainable system, Bernevig et al. [12] followed up on an idea by Molenkamp et al. [111; 108] and theoretically investigated semiconductors with an inverted band structure, predicting a quantum phase transition in type-III HgTe/CdTe quantum wells between a trivial insulator phase and quantum spin-Hall phase beyond a critical thickness of the well. Only one year later, in 2007, this prediction could be confirmed experimentally [81]. A system exhibiting the quantum spin-Hall effect, also labeled ‘‘topological insulator’’, is a new topological state of matter, characterized by a bulk insulating gap and a pair of gapless edge states, protected by time reversal symmetry. Currently, topological insulators [64; 116; 9] are one of the most actively studied topics in condensed matter physics.

With the discovery of the topological insulator, one question became apparent: Is there an interaction-driven set of fractionalized phases with time reversal symmetry? The idea is to take, similar to the construction of a topological insulator, two copies of a system exhibiting a fractional quantum Hall effect for each spin species, creating a fractional topological insulator. The first step toward such a state was achieved with the realization of a lattice analog of the fractional quantum Hall effect, the ‘‘fractional Chern insulator’’ [106; 128; 141; 121; 114; 155]. One intuitive approach to the theoretical construction of a fractional topological insulator is to take the direct product of a fractional quantum Hall state and its time reversal conjugate. Several wave functions and model interactions for such fractional topological insulators have been constructed [114; 95; 130].



However, such states are well studied conceptually and do not lead to new physics, as the idea of taking a state and its mirror image together without any entanglement between the states has been well understood in the context of topological insulators. So effectively replacing the IQH state (for the topological insulator) by a fractional quantum Hall state for the fractional topological insulator does not give rise to profoundly new physics, since the fractionalization and the symmetry protection do not entangle. Therefore, the community has been looking for ways to implement some topological interlocking between different spin species [137]. Yet, for all practical purposes so far, time reversal symmetry has appeared to limit the set of possible fractional states to those with no interlocking between both “layers” of  $\uparrow$ - and  $\downarrow$ -spins [133].

In Chapter 6, we propose a new universality class of fractionally quantized, topologically ordered insulators, which we name “fractional insulator” [123]. Inspired by the fractional quantum Hall effect, spin liquids, and fractional Chern insulators, we develop a wave function approach to a new class of topological order in a two-dimensional crystal of spin-orbit coupled electrons.

The idea is simply to allow the topological order to violate time reversal symmetry, while all locally observable quantities are time reversal invariant. We refer to this situation as “topological time reversal symmetry breaking”. The class of fractional insulators includes the previously established fractional topological insulators as a trivial case. To observe the violation of time reversal symmetry, one has to perform a non-local probe, for instance measuring the fractionally valued, statistical parameter for the quasiparticles.

In Section 6.2, we construct a fractionally quantized Hall wave function, describing  $\uparrow$ -spin and  $\downarrow$ -spin electrons in a two dimensional continuum subject to perpendicular magnetic fields of equal magnitude but opposite direction, in the spherical geometry. Our state is inspired by the Halperin double layer states [62] and can be viewed as a two-layer system of an  $\uparrow$ -spin and a  $\downarrow$ -spin sphere. The construction starts off with Laughlin states for the  $\uparrow$ -spin and  $\downarrow$ -spin electrons and an interflavor term, which entangles the two spin species. With a specific parameter choice, which is detailed in this section, we obtain a state preserving time reversal symmetry locally, and label it the “311-state”. As we are dealing with a two-layer system in which the magnetic fields point in opposite directions, the calculation of angular momenta is subtle. We explain it in Section 6.2.2.

The important question is whether our 311-state can be stabilized for a reasonable interaction profile among the electrons. To answer this question, we have developed a numerical technique to identify exact or approximate parent Hamiltonians. We label this technique the “Hamiltonian Finder method” [41] and provide a detailed explanation in Sections 6.3.1-6.3.4. To analyze the accuracy of our approximate parent Hamiltonian, we introduce relative angular momentum resolved correlators in Section 6.3.5, which allow to compare the inter- and intralayer correlations of the 311-state to the exact ground state of the parent Hamiltonian. Section 6.3.6 explains how to represent the parent Hamiltonian as a real space interaction potential, which allows to develop an intuition of our model.

The task of finding a parent Hamiltonian is numerically challenging, since we are effectively dealing with a direct product of two quantum Hall Hilbert spaces, and hence exponentially large Hilbert spaces. For systems of up to six  $\uparrow$ -spin and six  $\downarrow$ -spin electrons, we manage to construct an approximate parent Hamiltonian with a physically realistic, local interaction. The numerical results are presented in Section 6.4.

We conclude with a brief summary of our results in Chapter 7. In the Appendices A and B, we provide additional material for the interested reader on the angular momentum algebra and tensor decompositions. Appendix C lists the essential properties of the Jacobi theta functions, and in Appendix D, we print our *Mathematica*-notebooks for the implementation of a generic tensor decomposition.



## Chapter 2

# Review of the Laughlin state and its formalism

At the core of this thesis is the description and analysis of novel quantum Hall systems. It is therefore worthwhile to review Laughlin's theory [86; 53; 62; 87; 17; 112] for a series of fractionally quantized Hall states, as it provides the basic formalism to treat more complicated systems. Here, we summarize the main results crucial for this thesis. We follow the notation of [37], which provides a thorough discussion of the theory.

### 2.1 Landau level quantization in the plane

The motion of a free charged particle moving in a plane perpendicular to a magnetic field with strength  $B$  is

$$H = \frac{1}{2M} \left( \mathbf{p} + \frac{e}{c} \mathbf{A} \right)^2, \quad (2.1.1)$$

where  $M$  is the particle mass and  $-e < 0$  is its charge. The gauge field  $\mathbf{A}$  is minimally coupled to the canonical momentum  $\mathbf{p}$ . It is convenient to choose the symmetric gauge  $\mathbf{A} = \frac{1}{2} B \mathbf{r} \times \mathbf{e}_z$  for this problem, since rotational symmetry around the origin is preserved and angular momentum is a good quantum number.

By introducing cyclotron ladder operators  $a$  and  $a^\dagger$ , the Hamiltonian (2.1.1) can be put into harmonic oscillator form

$$H = \hbar\omega_c \left( a^\dagger a + \frac{1}{2} \right), \quad (2.1.2)$$

with the cyclotron frequency  $\omega_c = eB/Mc$ . For a detailed derivation, the reader is referred to [37]. The magnetic field quenches the kinetic energy into discrete energy levels, the so-called Landau levels,

$$E_n = \hbar\omega_c \left( n + \frac{1}{2} \right), \quad n \in \mathbb{N}_0. \quad (2.1.3)$$

In the unperturbed system without magnetic field, the density of states is proportional to the area of the system,  $g_0(E) = M/(2\pi\hbar^2)$ . Adding a magnetic field results into a density of states of  $g(E) = 1/(\hbar\omega_c)$ . Since the average density of states, taken over a sufficiently large energy range, is not altered by the addition of a magnetic field, the resulting energy levels must be highly degenerate. The degeneracy per unit area amounts to

$$N_\Phi = \frac{g_0(E)}{g(E)} = \frac{eB}{\hbar c} = \frac{1}{2\pi l^2}, \quad (2.1.4)$$

where we have introduced the magnetic length  $l = \sqrt{\hbar c/(eB)}$ , which is independent of any material parameters. Thus, in every level  $n$ , one Dirac flux quantum  $\Phi_0 = \hbar c/e$  is required per state, and  $N_\Phi$  corresponds to the number of flux quanta per unit area.

Analytically, to describe the motion of a charged particle in a two-dimensional plane perpendicular to a magnetic field, it is convenient to introduce complex coordinates  $z = x + iy$  and their complex conjugates  $\bar{z} = x - iy$ . In the following, we will focus on the energy level  $n = 0$ , the so-called lowest Landau level (LLL). The real space basis state of the LLL is

$$\phi_0(z) := \phi_0(z, \bar{z}) = \frac{1}{\sqrt{2\pi l^2}} \exp\left(-\frac{1}{4l^2}|z|^2\right). \quad (2.1.5)$$

To shorten notation, we will set  $l = 1$  from now on and will not keep track of the normalization of the wave functions.

Extending to a  $N$ -particle system, the wave function of the LLL can be obtained by antisymmetrizing the single-particle basis states (2.1.5),

$$\begin{aligned} \psi(z_1, \dots, z_N) &= \mathcal{A}\{z_1^0 z_2^1 \dots z_N^{N-1}\} \cdot \prod_{i=1}^N e^{-\frac{1}{4}|z_i|^2} \\ &= \prod_{i<j}^N (z_i - z_j) \prod_{i=1}^N e^{-\frac{1}{4}|z_i|^2}. \end{aligned} \quad (2.1.6)$$

The most generic  $N$ -particle wave function for the LLL is

$$\psi(z_1, \dots, z_N) = P(z_1, \dots, z_N) \prod_{i<j}^N (z_i - z_j) \prod_{i=1}^N e^{-\frac{1}{4}|z_i|^2}, \quad (2.1.7)$$

with a symmetric polynomial  $P$  in the coordinates  $z_i$ .

A key quantity for the analysis of quantum Hall systems is the filling fraction, which is defined by the number of particles divided by the number of states, and thus the number of flux quanta, in each Landau level in the thermodynamic limit,

$$\frac{1}{\nu} := \left. \frac{\partial N_\Phi}{\partial N} \right|_{N \rightarrow \infty}. \quad (2.1.8)$$

## 2.2 The Laughlin state in the plane

If the filling fraction is  $0 < \nu < 1$ , the LLL is only partly filled and the corresponding state of  $N$  particles is highly degenerate, since the number of possible configurations is  $\propto \frac{N_\Phi!}{N!(N_\Phi - N)!}$ . Laughlin made an inspired guess for the wave function of a system driven by Coulomb interaction and with  $\nu = 1/m$ ,

$$\psi_m(z_1, \dots, z_N) = \prod_{i<j}^N (z_i - z_j)^m \prod_{i=1}^N e^{-\frac{1}{4}|z_i|^2}. \quad (2.2.1)$$

This wave function minimizes the Coulomb energy by attaching additional zeros onto the particle positions. The prefactor thus vanishes with a zero of order  $m$  when two particles approach each other, keeping the particles away from each other effectively. This minimizes the repulsive Coulomb interaction. The smallest component of relative angular momentum between the particles is  $m$ , which is the uniquely defining property of the Laughlin state. The exponential factor quickly decreases when the particles move away from the origin, and the wave function peaks at configurations which balance these two effects. The Laughlin state is incompressible and describes a circular droplet of uniform density [145]. To preserve antisymmetry,  $m$  must be odd.

Numerically, this approximate ground state is well confirmed for systems with small particle number  $N$  [25], the overlap with the exact ground state being  $> 99.9\%$ . Although impressive, one has to take into account, that due to the complexity of the calculation, only small systems are accessible numerically. Even with modern super-computers, calculations for particle numbers beyond the order  $\mathcal{O}(10^1)$  are not feasible. Thus, even though the overlap equals almost 1, for macroscopic systems, which are of order  $\mathcal{O}(10^{23})$ , the overlap will vanish.

An exact parent Hamiltonian for the Laughlin state was first constructed by Haldane [53]. Its construction and analysis will be detailed in Section 6.3.1.

## 2.3 Quasihole and quasiparticle excitations

In a fractionally quantized Hall system, there are two types of elementary charged excitations above the incompressible ground state: the quasihole and the quasiparticle excitation. The wave function of a quasihole at position  $\xi$  is

$$\psi_{\xi}^{\text{QH}}(z_1, \dots, z_N) = \prod_{i=1}^N (z_i - \xi) \prod_{i<j}^N (z_i - z_j)^m \prod_{i=1}^N e^{-\frac{1}{4}|z_i|^2}. \quad (2.3.1)$$

The electron density vanishes at point  $\xi$ , a ‘‘hole’’ has been created in the electron liquid. Physically, this can be achieved by adiabatically inserting one Dirac flux quantum at position  $\xi$ , inducing an electrical field

$$\oint \mathbf{E} \cdot d\mathbf{s} = E_{\varphi} \cdot 2\pi r = \frac{1}{c} \frac{\partial \phi}{\partial t}, \quad (2.3.2)$$

which increases the canonical angular momentum by  $\hbar$ ,

$$\Delta L_z = \frac{e}{2\pi c} \int \frac{\partial \phi}{\partial t} dt = \frac{e}{2\pi c} \cdot \phi_0 = \hbar. \quad (2.3.3)$$

The charge of the quasihole can be determined by inserting  $m$  Dirac flux quanta into the system at position  $\xi$  and thus creating  $m$  quasiholes. The corresponding wave function then is

$$\psi_{\xi}^{m \text{QHs}}(z_1, \dots, z_N) = \prod_{i=1}^N (z_i - \xi)^m \prod_{i<j}^N (z_i - z_j)^m \prod_{i=1}^N e^{-\frac{1}{4}|z_i|^2}. \quad (2.3.4)$$

Overall, a full hole of charge  $e$  has been created. It follows that the quasihole charge must be  $e/m$ . Analytically, a quasihole can be identified as a zero in the wave function which does not coincide with any of the electrons.

A quasiparticle excitation is created by inserting a Dirac flux quantum in the opposite direction as compared to the construction of the quasihole. As a result, the canonical angular momentum is decreased by  $\hbar$ . Mathematically, this process is achieved by removing one zero from the Laughlin state. The wave function of a quasiparticle at position  $\xi$  therefore contains a derivative operator,

$$\psi_{\xi}^{\text{QE}}(z_1, \dots, z_N) = \prod_{i=1}^N e^{-\frac{1}{4}|z_i|^2} \prod_{i=1}^N \left( 2 \frac{\partial}{\partial z_i} - \bar{\xi} \right) \prod_{i<j}^N (z_i - z_j)^m. \quad (2.3.5)$$

Note that, in contrast to the quasihole excitation, the quasiparticle wave function is not an exact eigenstate of Haldane’s parent Hamiltonian.

The most intriguing prediction of Laughlin’s theory is that both quasiparticles obey fractional statistics with an exchange phase  $\alpha = \pi\nu$  [63; 5]. This can be calculated by adiabatically exchanging the position of two quasiholes (or quasiparticles) [5].

The fractionalization is a direct consequence of the two-dimensionality of the physical system. To explain this briefly, we consider two particles located at coordinates  $\mathbf{r}_1$  and  $\mathbf{r}_2$ . Since the particles are indistinguishable, the probability of particle 1 being at position  $\mathbf{r}_1$  and particle 2 being at position  $\mathbf{r}_2$  must be equal to the probability of the particles being at each others position,

$$|\Psi(\mathbf{r}_1, \mathbf{r}_2)|^2 = |\Psi(\mathbf{r}_2, \mathbf{r}_1)|^2.$$

The two wave functions therefore fulfill

$$\Psi(\mathbf{r}_1, \mathbf{r}_2) = e^{i\alpha} \Psi(\mathbf{r}_2, \mathbf{r}_1),$$

and the exchange phase  $\alpha$  can be any real number. Now, if we exchange the particles twice without changing the sense (either clockwise or counterclockwise), the system comes back into its initial state. If  $\Psi_f$  denotes the final state, it must be

$$\Psi_f(\mathbf{r}_1, \mathbf{r}_2) \stackrel{!}{=} e^{2i\alpha} \Psi(\mathbf{r}_1, \mathbf{r}_2). \quad (2.3.6)$$

In three or more spatial dimensions, the exchange path of one particle encircling the other can always be deformed into the identity operator without passing through the point  $\mathbf{r}_1 = \mathbf{r}_2$ . Therefore,

$$\Psi_f(\mathbf{r}_1, \mathbf{r}_2) = \Psi(\mathbf{r}_1, \mathbf{r}_2)$$

and thus  $\alpha = 0$  or  $\pi$ , leading to either Bose or Fermi statistics.

Leinaas and Myrheim were the first to demonstrate that the above consideration does not hold for strictly two-dimensional systems [92], since the exchange path cannot be continuously contracted without passing through the other point. Expression (2.3.6) still holds. However,  $\alpha$  can be any real number. Such particles are labeled ‘‘anyons’’.

## 2.4 Landau level quantization on the sphere

Moving from a plane to a sphere for the description of a two-dimensional electron gas can be beneficial, since the sphere does not have a boundary. Haldane formulated the Laughlin formalism in this geometry for the LLL [53]. Only in 2011, it was extended to higher Landau levels by Greiter [36]. Working on the sphere therefore is well suited to study the bulk properties of a quantized Hall system.

The formalism has also been extended to the torus [59; 40], another often studied geometry, which is equivalent to a plane with periodic boundary conditions. It is the only manifold with a nonzero genus ( $g = 1$ ), giving rise to topological degeneracies.

We study a sphere with radius  $R$ , placed in a radial magnetic field  $B = \hbar c s_0 / e R^2$  with  $e > 0$ , and  $\nabla \times \mathbf{A} = B \mathbf{e}_r$ . According to Dirac’s monopole quantization condition [22], the number of magnetic flux quanta  $2s_0$  piercing through the surface of the sphere must be integer. The single-particle Hamiltonian is

$$H = \frac{\mathbf{\Lambda}^2}{2MR^2} = \frac{\omega_c}{2s_0} \mathbf{\Lambda}^2, \quad (2.4.1)$$

with the cyclotron frequency  $\omega_c = eB/M$  and the effective mass  $M$  of the particle. The dynamical angular momentum is

$$\mathbf{\Lambda} = \mathbf{r} \times (-i\nabla + e\mathbf{A}(\mathbf{r})), \quad (2.4.2)$$

while the canonical angular momentum is the sum

$$\mathbf{L} = \mathbf{\Lambda} + s_0 \mathbf{e}_r, \quad (2.4.3)$$

satisfying the Lie algebra. Given an eigenstate  $|\Psi\rangle$ , specified below, we set the eigenvalue of the angular momentum as

$$\mathbf{L}|\Psi\rangle = s(s+1)|\Psi\rangle. \quad (2.4.4)$$

It follows that  $s = s_0 + n$  with  $n \in \mathbb{N}_0$ , while  $s$  and  $s_0$  can be integer or half-integer. For the LLL ( $n = 0$ ),  $s = s_0$ . The eigenstates of (2.4.1) can be derived via

$$\Lambda^2 = L^2 - s_0^2, \quad (2.4.5)$$

giving the Landau levels with index  $n$ ,

$$E_n = \omega_c \left[ \left( n + \frac{1}{2} \right) + \frac{n(n+1)}{2s_0} \right]. \quad (2.4.6)$$

To formulate eigenstates in a spherical geometry, Haldane [53] introduced spinor coordinates, defined by

$$\begin{aligned} u &= \cos\left(\frac{\theta}{2}\right) \exp\left(\frac{i\varphi}{2}\right), \\ v &= \sin\left(\frac{\theta}{2}\right) \exp\left(-\frac{i\varphi}{2}\right), \end{aligned} \quad (2.4.7)$$

such that a position on the sphere is described by

$$\mathbf{e}_r = \mathbf{\Omega}(u, v) := (u, v) \boldsymbol{\sigma} \begin{pmatrix} \bar{u} \\ \bar{v} \end{pmatrix}. \quad (2.4.8)$$

The vector  $\boldsymbol{\sigma} = (\sigma_x, \sigma_y, \sigma_z)$  consists of the three Pauli matrices

$$\sigma_x = \begin{pmatrix} 0 & 1 \\ 1 & 0 \end{pmatrix}, \quad \sigma_y = \begin{pmatrix} 0 & -i \\ i & 0 \end{pmatrix}, \quad \sigma_z = \begin{pmatrix} 1 & 0 \\ 0 & -1 \end{pmatrix}. \quad (2.4.9)$$

In the LLL, the angular momentum operator can be rewritten in terms of the spinor coordinates as

$$\mathbf{L} = \frac{1}{2}(u, v) \boldsymbol{\sigma} \begin{pmatrix} \partial_u \\ \partial_v \end{pmatrix}. \quad (2.4.10)$$

A complete orthogonal basis spanning the LLL is expressed by the states

$$\psi_{m,0}^s(u, v) = \mathcal{N} u^{s+m} v^{s-m} \quad (2.4.11)$$

with

$$m = -s, -s+1, \dots, s.$$

The normalization  $\mathcal{N}$  can be derived from the integral

$$\frac{1}{4\pi} \int d\Omega \bar{u}^{S+m'} \bar{v}^{S-m'} u^{s+m} v^{s-m} = \frac{(s+m)!(s-m)!}{(2s+1)!} \delta_{mm'}, \quad (2.4.12)$$

where the solid angle is  $d\Omega = \sin\theta d\theta d\phi$ . The eigenvalues of the basis states are

$$\begin{aligned} L^z \psi_{m,0}^s &= m \psi_{m,0}^s, \\ H \psi_{m,0}^s &= \frac{1}{2} \omega_c \psi_{m,0}^s. \end{aligned} \quad (2.4.13)$$

To describe a particle in the LLL at a position  $\mathbf{\Omega}(\alpha, \beta)$ , with spinor coordinates  $(\alpha, \beta)$ ,  $|\alpha|^2 + |\beta|^2 = 1$ ,

$$\mathbf{\Omega}(\alpha, \beta) = (\alpha, \beta) \boldsymbol{\sigma} \begin{pmatrix} \bar{\alpha} \\ \bar{\beta} \end{pmatrix}, \quad (2.4.14)$$

Haldane introduced ‘‘coherent states’’ [53] specified by the equation

$$\{\mathbf{\Omega}(\alpha, \beta) \cdot \mathbf{L}\} \psi_{(\alpha, \beta), 0}^s(u, v) = s \psi_{(\alpha, \beta), 0}^s(u, v). \quad (2.4.15)$$

Its solution is

$$\psi_{(\alpha, \beta), 0}^s(u, v) = (\bar{\alpha}u + \bar{\beta}v)^{2s}. \quad (2.4.16)$$

It is also possible to create two particle-coherent LLL states, which will be further detailed in Section 6.3.1.

It is worth mentioning that the formalism can be extended to higher Landau levels [36]. The basic idea is to describe the Hilbert space of a charged particle on a sphere with a magnetic monopole in the center by two mutually commuting SU(2) angular momentum algebras. The first algebra for the cyclotron momentum  $\mathbf{S}$ , consists of operators that raise or lower eigenstates from one Landau to the next. The operators for the second algebra correspond to the guiding center momentum  $\mathbf{L}$ , and rotate the eigenstates on the sphere while preserving the Landau level index.

## 2.5 The Laughlin state on the sphere

Given  $N$  particles on a sphere, the Laughlin state with  $\nu = 1/m$  [53] is

$$\psi_m[u, v] = \prod_{i < j}^N (u_i v_j - u_j v_i)^m. \quad (2.5.1)$$

Here,  $[u, v]$  is a short-hand notation for  $(u_1, \dots, u_N, v_1, \dots, v_N)$ . Its flux can be calculated by counting the zeros each particle sees, giving  $2s_0 = m(N - 1)$ .

The state is invariant under spatial rotations on the sphere,

$$\mathbf{L}_{\text{tot}} \psi_m = 0, \quad (2.5.2)$$

since each individual factor  $(u_i v_j - u_j v_i)$  commutes with the total angular momentum

$$\mathbf{L}_{\text{tot}} = \sum_{i=1}^N \mathbf{L}_i. \quad (2.5.3)$$

In this geometry, the interaction part of the parent Hamiltonian can be constructed using pseudopotentials. This procedure was first proposed by Haldane [53] and will be explained in further detail in Section 6.3.1. With addition of the kinetic part of the Hamiltonian (2.4.1), this model is the parent Hamiltonian of the Laughlin state (2.5.1).

The wave function for the quasihole excitation on the sphere at position  $\mathbf{\Omega}(\alpha, \beta)$  is

$$\psi_{(\alpha, \beta)}^{\text{QH}}[u, v] = \prod_{i=1}^N (\beta u_i - \alpha v_i) \prod_{i < j}^N (u_i v_j - u_j v_i)^m. \quad (2.5.4)$$

For the quasiparticle excitation, we get

$$\psi_{(\alpha, \beta)}^{\text{QE}}[u, v] = \prod_{i=1}^N \left( \bar{\beta} \frac{\partial}{\partial u_i} - \bar{\alpha} \frac{\partial}{\partial v_i} \right) \prod_{i < j}^N (u_i v_j - u_j v_i)^m \quad (2.5.5)$$



in this geometry. As can be easily verified, the number of flux quanta through the sphere is increased (decreased) by one,  $s = 2s_0 \pm 1$ , while the projected total angular momentum,  $\mathbf{\Omega}(\alpha, \beta) \cdot \mathbf{L}_{\text{tot}}$ , is decreased (increased) by  $N/2$  for the quasihole (quasiparticle) state compared to the LLL.

## 2.6 Extension to multi-component systems

A multi-component extension of the Laughlin state was proposed by Halperin [62], who considered electrons with degrees of freedom in addition to the two-dimensional coordinates. This can be spin degrees of freedom, but also a system with electrons confined to different layers is possible. This formalism will be of specific interest to us in Chapter 6, so that we provide a brief introduction here.

Consider a two-level system with  $N_\uparrow$  ( $N_\downarrow$ ) particles in the first (second) layer being denoted by coordinates  $z_i$  ( $w_k$ ). The straight-forward generalization of the Laughlin state to a two-component system is described by the wave function [38]

$$\begin{aligned} \Psi_{m_\uparrow, m_\downarrow, n}[z, w] = & \prod_{i < j} (z_i - z_j)^{m_\uparrow} \prod_{k < l} (w_k - w_l)^{m_\downarrow} \prod_i \prod_k (z_i - w_k)^n \\ & \cdot \exp\left(-\sum_i (|z_i|^2 + |w_i|^2)/4l_b^2\right). \end{aligned} \quad (2.6.1)$$

The function argument  $[z, w]$  stands for  $(z_1, \dots, z_{N_\uparrow}, w_1, \dots, w_{N_\downarrow})$ . This wave function can, for instance, describe particles with spin 1/2. For a fermionic system, both  $m_\uparrow$  and  $m_\downarrow$  have to be odd. The mixed term

$$\prod_i \prod_k (z_i - w_k)^n \quad (2.6.2)$$

introduces a correlation between the two types of particles. Usually, states of the form of (2.6.1) are referred to as  $(m_\uparrow, m_\downarrow, n)$ -states or Halperin states. They have very similar properties compared to the Laughlin state. For instance, the relative angular momentum between two particles of type  $\uparrow$  ( $\downarrow$ ) is never less than  $m_\uparrow$  ( $m_\downarrow$ ), and it is never less than  $n$  for particles of opposite spin.

Formulating the wave function (2.6.1) in spherical geometry yields

$$\begin{aligned} \Psi_{m_\uparrow, m_\downarrow, n}[u_i, v_i, a_k, b_k] = & \\ & \prod_{i < j} (u_i v_j - u_j v_i)^{m_\uparrow} \prod_{k < l} (a_k b_l - a_l b_k)^{m_\downarrow} \prod_i \prod_k (u_i a_k - v_i b_k)^n. \end{aligned} \quad (2.6.3)$$

As in the single-layer case, for a system of  $N_\uparrow$  electrons in the first layer and  $N_\downarrow$  electrons in the second layer, the flux through each layer can be calculated to be

$$2s_\uparrow = N_{\Phi, \uparrow} = m_\uparrow(N_\uparrow - 1) + nN_\downarrow, \quad (2.6.4)$$

and

$$2s_\downarrow = N_{\Phi, \downarrow} = m_\downarrow(N_\downarrow - 1) + nN_\uparrow. \quad (2.6.5)$$

Combining the two equations, in matrix form we get

$$\begin{pmatrix} N_{\Phi, \uparrow} \\ N_{\Phi, \downarrow} \end{pmatrix} = \begin{pmatrix} m_\uparrow & n \\ n & m_\downarrow \end{pmatrix} \begin{pmatrix} N_\uparrow \\ N_\downarrow \end{pmatrix} - \begin{pmatrix} m_\uparrow \\ m_\downarrow \end{pmatrix}. \quad (2.6.6)$$

If the electrons in both layers are subject to the same magnetic field, the number of flux quanta seen in each layer is identical,  $N_{\Phi, \uparrow} = N_{\Phi, \downarrow} = N_\Phi$ . The filling fraction for each layer is obtained via (2.1.8). For

an explicit expression, we take the thermodynamic limit ( $N_i \gg 1$  for  $i = \uparrow, \downarrow$ ). Using (2.6.6) to express the particle numbers in terms of the flux quanta,

$$\begin{pmatrix} N_\uparrow \\ N_\downarrow \end{pmatrix} = \begin{pmatrix} m_\uparrow & n \\ n & m_\downarrow \end{pmatrix}^{-1} \left[ \begin{pmatrix} 1 \\ 1 \end{pmatrix} N_\Phi + \begin{pmatrix} m_\uparrow \\ m_\downarrow \end{pmatrix} \right], \quad (2.6.7)$$

we get

$$\begin{pmatrix} \nu_\uparrow \\ \nu_\downarrow \end{pmatrix} = \frac{\partial}{\partial N_\Phi} \begin{pmatrix} N_\uparrow \\ N_\downarrow \end{pmatrix} = \frac{1}{m_\uparrow m_\downarrow - n^2} \begin{pmatrix} m_\downarrow - n \\ m_\uparrow - n \end{pmatrix}. \quad (2.6.8)$$

The total filling fraction of the two layers is

$$\nu_{\text{tot}} = \nu_\uparrow + \nu_\downarrow = \frac{m_\uparrow + m_\downarrow - 2n}{m_\uparrow m_\downarrow - n^2}. \quad (2.6.9)$$

There are several interesting examples of the Halperin state. The  $(3, 3, 1)$ -state has filling fraction  $\nu = 1/2$  and is a genuine quantum Hall state. It has been observed in bilayer samples [134]. Another example is the  $(3, 3, 2)$ -state with  $\nu = 2/5$ , which competes with the spin-polarized hierarchy state that occurs at the same filling [72].

## Chapter 3

# Chiral spin liquids

The chiral spin liquid (CSL) [73; 74; 89; 160; 125] is an example of a two-dimensional system obeying fractional statistics. It is a spin liquid which violates time reversal (T) and parity (P) symmetry. Being conceptually closely related, the system may be viewed as an extension of the Haldane-Shastry model to two dimensions.

In case of the Abelian or spin  $s = 1/2$  CSL, it is essentially a Laughlin state with filling fraction  $\nu = 1/2$  for spin flips on a two-dimensional lattice. The liquid supports spinon excitations, which are deconfined and obey fractional statistics. The spinons of the CSL are quasiparticles with spin  $1/2$  and no charge. They exhibit quantum-number fractionalization and carry only half of the spin as compared to the excitations of conventional magnetically ordered systems with spin 1.

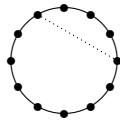
In 2009, Greiter and Thomale proposed a novel CSL state for a  $s = 1$  antiferromagnet, the non-Abelian chiral spin liquid (NACSL) [45; 136]. As for the Abelian CSL, the spinon excitations are deconfined, but in this state, they obey non-Abelian statistics, making the system interesting for the field of quantum computation and cryptography. As suggested by [45], the concept can be extended to systems with  $s > 1$ .

In the following, we first briefly review the Haldane-Shastry model and summarize the main properties of the Abelian and non-Abelian CSL.

### 3.1 The Haldane-Shastry model

The Haldane-Shastry model [54; 127; 70; 57; 126; 58; 77; 78; 21; 88; 11; 10; 44] plays a unique role among the integrable models of spin  $1/2$  Heisenberg chains. Apart from being solvable by the asymptotic Bethe ansatz, its ground state and several excited states (those with fully polarized spins of the spinon excitations) can be written down in closed form. Furthermore, the model reveals a direct relationship of the spin chain to the fractional quantum Hall effect (FQHE) [74].

Let a spin- $1/2$  chain of  $N$  sites,  $N \in 2\mathbb{N}$ , with periodic boundary conditions be wrapped onto a unit circle. Each site may be expressed as a complex number,



$$\eta_\alpha = e^{i\frac{2\pi}{N}\alpha} \quad \text{with } \alpha = 1, \dots, N.$$

The Haldane-Shastry Hamiltonian then is

$$H^{\text{HS}} = \left(\frac{2\pi}{N}\right)^2 \sum_{\alpha < \beta}^N \frac{\mathbf{S}_\alpha \mathbf{S}_\beta}{|\eta_\alpha - \eta_\beta|^2}, \quad (3.1.1)$$

with the chord distance  $|\eta_\alpha - \eta_\beta|$  between sites  $\alpha$  and  $\beta$ . The interaction decreases with  $1/r^2$ . The Hamiltonian is invariant under translations, time reversal, parity and global  $SU(2)$ -spin rotations,

$$\mathbf{S}_{\text{tot}} = \sum_{\alpha=1}^N \mathbf{S}_\alpha, \quad [H^{\text{HS}}, \mathbf{S}_{\text{tot}}] = 0. \quad (3.1.2)$$

In addition, the model possesses a special internal symmetry, generated by the rapidity operator,

$$\mathbf{\Lambda} = \frac{i}{2} \sum_{\substack{\alpha, \beta=1 \\ \alpha \neq \beta}}^N \frac{\eta_\alpha + \eta_\beta}{\eta_\alpha - \eta_\beta} \mathbf{S}_\alpha \times \mathbf{S}_\beta, \quad [H^{\text{HS}}, \mathbf{\Lambda}] = 0. \quad (3.1.3)$$

Since the rapidity operator transforms as a vector under spin rotations,

$$[S_{\text{tot}}^i, \Lambda^j] = i \varepsilon^{ijk} \Lambda^k, \quad (3.1.4)$$

it does not commute with the total spin. Thus, the operators  $\mathbf{S}_{\text{tot}}$  and  $\mathbf{\Lambda}$  generate an infinite dimensional associative algebra of the Haldane-Shastry model, the Yangian  $Y(sl_2)$  [24; 19].

The exact ground state of the Haldane-Shastry model is

$$|\psi_0^{\text{HS}}\rangle = \sum_{\{z_1, \dots, z_M\}} \psi_0^{\text{HS}}(z_1, \dots, z_M) S_{z_1}^+ \cdots S_{z_M}^+ |\underbrace{\downarrow \downarrow \dots \downarrow}_{\text{all } N \text{ spins } \downarrow}\rangle, \quad (3.1.5)$$

where the sum includes all possible configurations of distributing  $M = N/2$   $\uparrow$ -spins on the  $N$ -site chain, and

$$\psi_0^{\text{HS}}(z_1, z_2, \dots, z_M) = \prod_{i < j}^M (z_i - z_j)^2 \prod_{i=1}^M z_i. \quad (3.1.6)$$

The ground state is a spin singlet, which implies that the wave function does not alter with the quantization axis taken to be an arbitrary direction in spin space.

*Proof.* Since  $S_{\text{tot}}^z |\psi_0^{\text{HS}}\rangle = 0$ , it is sufficient to demonstrate that  $|\psi_0^{\text{HS}}\rangle$  is annihilated by  $S_{\text{tot}}^-$ :

$$\begin{aligned} S_{\text{tot}}^- |\psi_0^{\text{HS}}\rangle &= \sum_{\alpha=1}^N S_\alpha^- \sum_{\{z_1, \dots, z_M\}} \psi_0^{\text{HS}}(z_1, z_2, \dots, z_M) S_{z_1}^+ \cdots S_{z_M}^+ |\downarrow \downarrow \dots \downarrow\rangle \\ &= \sum_{\{z_2, \dots, z_M\}} \underbrace{\sum_{\alpha=1}^N \psi_0^{\text{HS}}(\eta_\alpha, z_2, \dots, z_M)}_{=0} S_{z_2}^+ \cdots S_{z_M}^+ |\downarrow \downarrow \dots \downarrow\rangle, \end{aligned} \quad (3.1.7)$$

since  $\psi_0^{\text{HS}}(\eta_\alpha, z_2, \dots, z_M)$  contains only powers  $\eta_\alpha^1, \eta_\alpha^2, \dots, \eta_\alpha^{N-1}$  and

$$\sum_{\alpha=1}^N \eta_\alpha^m = N \delta_{m,0} \pmod{N}. \quad (3.1.8)$$

□

The proof of the singlet property is even simpler, if the Haldane-Shastry state is constructed via a Gutzwiller projection. This will be detailed below.

Furthermore, the state is real and thus parity and time-reversal invariant.

*Proof.* Since  $\bar{z}_i z_i = 1$ , we have

$$(z_i - z_j)^2 = -z_i z_j |z_i - z_j|^2. \quad (3.1.9)$$

Hence, (3.1.6) can be rewritten as

$$\begin{aligned} \psi_0^{\text{HS}}(z_1, z_2, \dots, z_M) &= - \prod_{i < j}^M |z_i - z_j|^2 \prod_{i < j}^M z_i z_j \prod_{i=1}^M z_i \\ &= - \prod_{i < j}^M |z_i - z_j|^2 \prod_{i=1}^M G(z_i), \end{aligned} \quad (3.1.10)$$

where

$$G(\eta_\alpha) = (\eta_\alpha)^{\frac{N}{2}} = \begin{cases} +1 & \alpha \text{ even} \\ -1 & \alpha \text{ odd.} \end{cases} \quad (3.1.11)$$

Parity invariance is now straight-forward: Under parity, the coordinates transform as  $\eta_\alpha \rightarrow \eta_{-\alpha} = \bar{\eta}_\alpha$  and thus  $z_i \rightarrow \bar{z}_i$ . Since  $\psi_0^{\text{HS}}$  is real, it is unaltered under a parity transformation. Under time reversal [32],

$$i \rightarrow -i, \quad \mathbf{S}_\alpha \rightarrow -\mathbf{S}_\alpha, \quad |s, m\rangle \rightarrow i^{2m} |s, -m\rangle,$$

thus  $z_i \rightarrow \bar{z}_i$ ,  $S_\alpha^+ \rightarrow -S_\alpha^-$ , and  $|\downarrow\downarrow \dots \downarrow\rangle \rightarrow (-i)^N |\uparrow\uparrow \dots \uparrow\rangle$ . The Haldane-Shastry state (3.1.5) thus transforms as

$$\begin{aligned} &\sum_{\{z_1, \dots, z_M\}} \psi_0^{\text{HS}}(z_1, \dots, z_M) S_{z_1}^+ \dots S_{z_M}^+ |\downarrow\downarrow \dots \downarrow\rangle \\ \rightarrow &\sum_{\{z_1, \dots, z_M\}} \psi_0^{\text{HS}}(z_1, \dots, z_M) S_{z_1}^- \dots S_{z_M}^- |\uparrow\uparrow \dots \uparrow\rangle. \end{aligned} \quad (3.1.12)$$

Since the state is a singlet, it follows that it is time-reversal symmetric. □

If we set the momentum of the vacuum state  $|\downarrow\downarrow \dots \downarrow\rangle$  to  $p = 0$ , the Haldane-Shastry state has momentum

$$p_0 = -\frac{\pi}{2}N, \quad (3.1.13)$$

and energy

$$E_0 = -\frac{\pi^2}{24} \left( N + \frac{5}{N} \right). \quad (3.1.14)$$

A detailed derivation of (3.1.13) and (3.1.14) can be found in [37].

A straight-forward construction of the Haldane-Shastry wave function is to Gutzwiller project from a completely filled one-dimensional band, in which there are as many spin-1/2 particles as there are sites [51; 29; 96; 76; 50; 98; 30]:

$$|\psi_0^{\text{HS}}\rangle = P_{\text{GW}} |\psi_{\text{SD}}^N\rangle, \quad |\psi_{\text{SD}}^N\rangle := \prod_{q \in \mathcal{I}} c_{q\uparrow}^\dagger c_{q\downarrow}^\dagger |0\rangle. \quad (3.1.15)$$

The Gutzwiller projector

$$P_{\text{GW}} := \prod_{i=1}^N (1 - c_{i\uparrow}^\dagger c_{i\uparrow} c_{i\downarrow}^\dagger c_{i\downarrow}) \quad (3.1.16)$$

eliminates doubly occupied sites. The interval  $\mathcal{I}$  contains  $M = N/2$  adjacent momenta. The resulting state (3.1.15) is identical to the Haldane-Shastry state (3.1.5).

*Proof.* If the lattice constant is  $a = 2\pi/N$ , the creation operators in momentum space are obtained via a Fourier transformation

$$c_q^\dagger = \sum_{\alpha=1}^N e^{i\frac{2\pi}{N}\alpha q} c_\alpha^\dagger = \sum_{\alpha=1}^N \eta_\alpha^q c_\alpha^\dagger, \quad (3.1.17)$$

where the momentum can take the values  $q = 0, 1, \dots, N-1$ . Then, the unnormalized single particle momentum eigenstates are

$$\phi_q(z) = \langle z|q\rangle = \langle 0|c_z c_q^\dagger|0\rangle = z^q. \quad (3.1.18)$$

From now on, expressions with creation and annihilation operators without spin index hold for both spin orientations  $\uparrow$  and  $\downarrow$ , so that  $c_{z_i} := c_{z_i, \alpha}$ ,  $\alpha = \uparrow, \downarrow$ . Given  $M$  fermions with adjacent momenta  $q \in \mathcal{I} = [q_1, q_1 + M - 1]$ , the corresponding wave function is

$$\phi_{\mathcal{I}}(z_1, z_2, \dots, z_M) = \prod_{i=1}^M z_i^{q_1} \cdot \mathcal{A} \{z_1^0 z_2^1 \dots z_M^{M-1}\} = \prod_{i=1}^M z_i^{q_1} \prod_{i<j}^M (z_i - z_j). \quad (3.1.19)$$

The Gutzwiller state (3.1.15) can be rewritten as

$$|\psi_0^{\text{HS}}\rangle = \sum_{\{z_1, \dots, z_M; w_1, \dots, w_M\}} \phi_{\mathcal{I}}(z_1, \dots, z_M) \phi_{\mathcal{I}}(w_1, \dots, w_M) \cdot c_{z_1 \uparrow}^\dagger \dots c_{z_M \uparrow}^\dagger c_{w_1 \downarrow}^\dagger \dots c_{w_M \downarrow}^\dagger |0\rangle, \quad (3.1.20)$$

since it is the sum of all possible configurations in which  $M$   $\uparrow$ -spin (coordinates  $z_i$ ) and  $M$   $\downarrow$ -spin (coordinates  $w_i$ ) particles distributed on  $N$  distinct lattice sites.

We define  $\tilde{\mathcal{I}}$  as the set containing all those momenta not contained in  $\mathcal{I}$ , and the coordinates  $w_1, \dots, w_M$  are all sites not occupied by  $\uparrow$ -spin electrons. We wish to express  $\phi_{\mathcal{I}}(w_1, \dots, w_M)$  in (3.1.20) in terms of  $\phi_{\mathcal{I}}(z_1, \dots, z_M)$ :

$$\begin{aligned} \phi_{\mathcal{I}}(w_1, \dots, w_M) &= \langle 0|c_{w_M} \dots c_{w_1} \prod_{q \in \mathcal{I}} c_q^\dagger |0\rangle \\ &= \text{sign}[z; w] \cdot \langle 0| \prod_{q \in \mathcal{I}} c_q \prod_{q \in \tilde{\mathcal{I}}} c_q c_{z_1}^\dagger \dots c_{z_M}^\dagger \prod_{q \in \mathcal{I}} c_q^\dagger |0\rangle \\ &= \text{sign}[z; w] \cdot \langle 0| \prod_{q \in \tilde{\mathcal{I}}} c_q c_{z_1}^\dagger \dots c_{z_M}^\dagger |0\rangle \\ &= \text{sign}[z; w] \cdot \phi_{\tilde{\mathcal{I}}}^*(z_1, \dots, z_M) \\ &= \text{sign}[z; w] \cdot \prod_{i=1}^M \bar{z}_i^M \cdot \phi_{\mathcal{I}}^*(z_1, \dots, z_M) \\ &= \text{sign}[z; w] \cdot \prod_{i=1}^M G(z_i) \cdot \phi_{\mathcal{I}}^*(z_1, \dots, z_M), \end{aligned} \quad (3.1.21)$$

where

$$\text{sign}[z; w] \equiv \langle 0|c_{w_M} \dots c_{w_1} c_{z_M} \dots c_{z_1} \prod_{q \in \tilde{\mathcal{I}}} c_q^\dagger \prod_{q \in \mathcal{I}} c_q^\dagger |0\rangle \quad (3.1.22)$$

is the sign obtained by ordering the  $z$ - and  $w$ -coordinates according to the lattice site indices  $\alpha$ . Then, we have

$$\text{sign}[z; w] \cdot c_{z_1 \uparrow}^\dagger \dots c_{z_M \uparrow}^\dagger c_{w_1 \downarrow}^\dagger \dots c_{w_M \downarrow}^\dagger |0\rangle = S_{z_1}^+ \dots S_{z_M}^+ \underbrace{|\downarrow \downarrow \dots \downarrow\rangle}_{\text{all } N \text{ spins } \downarrow}. \quad (3.1.23)$$

Therefore, the Gutzwiller state (3.1.20) can be expressed as

$$|\psi_0^{\text{HS}}\rangle = \sum_{\{z_1, \dots, z_M\}} |\phi_{\mathcal{I}}(z_1, \dots, z_M)|^2 \prod_{i=1}^M G(z_i) S_{z_1}^+ \dots S_{z_M}^+ |\downarrow \downarrow \dots \downarrow\rangle, \quad (3.1.24)$$

which is identical to (3.1.10).

□

The singlet property of the Haldane-Shastry state can now be easily proven: The construction via Gutzwiller projection starts off with a singlet state,

$$\mathbf{S}_{\text{tot}} |\psi_{\text{SD}}^N\rangle = 0, \quad (3.1.25)$$

since this state is designed to fill each single particle state with  $\uparrow$ - and  $\downarrow$ -spin particles. The commutator of the Gutzwiller projector with all local spin operators vanishes, and thus the projector commutes with the total spin,

$$[\mathbf{P}_{\text{GW}}, \mathbf{S}_\alpha] = [\mathbf{P}_{\text{GW}}, \mathbf{S}_{\text{tot}}] = 0. \quad (3.1.26)$$

Consequently,

$$\mathbf{S}_{\text{tot}} |\psi_0^{\text{HS}}\rangle = 0, \quad (3.1.27)$$

implying that the Haldane-Shastry state is a singlet.

Free spinons are the elementary excitation of this model. The wave function for a spinon excitation, carrying spin 1/2 but no charge, at site  $\eta_\alpha$  is constructed analogously to the wave function for quasi-hole excitations in a FQH liquid, as detailed in Section 2.3. For an odd number of sites  $N$  and  $M = (N - 1)/2$   $\uparrow$ -spins, the one-spinon wave function is

$$\psi_{\alpha\downarrow}(z_1, z_2, \dots, z_M) = \prod_{i=1}^M (\eta_\alpha - z_i) \psi_0^{\text{HS}}(z_1, z_2, \dots, z_M), \quad (3.1.28)$$

with  $\psi_0^{\text{HS}}$  defined in (3.1.6). Since  $S_{\text{tot}}^z \psi_{\alpha\downarrow} = -\frac{1}{2} \psi_{\alpha\downarrow}$  and  $S_{\text{tot}}^- \psi_{\alpha\downarrow} = 0$ , the spinon has the same transformation properties as a spinor under rotations. This is a fractionally quantized excitation since the spin of the spinon is 1/2, while the Hilbert space is built up from spin flips, carrying spin 1.

However, the localized spinon (3.1.28) is not an eigenstate of  $H^{\text{HS}}$ . Through Fourier transformation of this state, exact momentum eigenstates are constructed,

$$\psi_{m\downarrow}(z_1, z_2, \dots, z_M) = \sum_{\alpha=1}^N (\bar{\eta}_\alpha)^m \psi_{\alpha\downarrow}(z_1, z_2, \dots, z_M). \quad (3.1.29)$$

The integer  $m$  is the momentum quantum number, which has to fulfill  $m \in \{0, 1, \dots, M\}$ , since  $\psi_{\alpha\downarrow}(z_1, z_2, \dots, z_M)$  contains only powers  $\eta_\alpha^0, \eta_\alpha^1, \dots, \eta_\alpha^M$  and

$$\sum_{\alpha=1}^N \bar{\eta}_\alpha^m \eta_\alpha^n = \delta_{m,n \bmod N}. \quad (3.1.30)$$

The physical spinon momentum  $p_m$  can be obtained by translating (3.1.29) by one lattice spacing around the unit circle,

$$T_{\text{lat}} |\psi_{m\downarrow}\rangle = e^{i(p_0 + p_m)} |\psi_{m\downarrow}\rangle. \quad (3.1.31)$$

Setting  $p_0 = -\frac{\pi}{2}N$ , the momentum is

$$p_m = \pi - \frac{2\pi}{N} \left( m + \frac{1}{4} \right). \quad (3.1.32)$$

The wave function for two spinons at sites  $\eta_\alpha$  and  $\eta_\beta$  is

$$\psi_{\alpha\beta}(z_1, z_2, \dots, z_M) = \prod_{i=1}^M (\eta_\alpha - z_i)(\eta_\beta - z_i) \psi_0^{\text{HS}}(z_1, z_2, \dots, z_M), \quad (3.1.33)$$

for a chain with  $N$  even and  $M = (N-2)/2$ . The momentum eigenstate of the Haldane-Shastry Hamiltonian then is

$$\psi_{mn}(z_1, z_2, \dots, z_M) = \sum_{\alpha, \beta=1}^N (\bar{\eta}_\alpha)^m (\bar{\eta}_\beta)^n \psi_{\alpha\beta}(z_1, z_2, \dots, z_M), \quad (3.1.34)$$

with  $M \geq m \geq n \geq 0$ .

Between two spinon excitations, there is no spin exchange [57], following from the commutativity of  $H^{\text{HS}}$  with  $\mathbf{\Lambda}$ . The spinons constitute an ideal gas of particles obeying fractional statistics [150; 56; 43].

### 3.2 The Abelian chiral spin liquid

The model can be extended to two dimensions. We consider a system of spins on a square lattice with lattice constant one. Its ground state wave function for a circular droplet with open boundary conditions containing  $N$  electrons is

$$|\psi_0^{\text{CSL}}\rangle = \sum_{z_1, \dots, z_M} \psi_0^{\text{CSL}}(z_1, \dots, z_M) S_{z_1}^+ \dots S_{z_M}^+ |\downarrow \downarrow \dots \downarrow\rangle, \quad (3.2.1)$$

where  $M = N/2$  and the ground state wave function,

$$\psi_0^{\text{CSL}}[z] = \langle z_1, \dots, z_M | \psi \rangle = \prod_{j < k}^M (z_j - z_k)^2 \prod_{j=1}^M G(z_j) e^{-\pi/2 |z_j|^2}, \quad (3.2.2)$$

is, apart from the gauge factors  $G(z_j)$ , formally equivalent to the Laughlin wave function at filling fraction  $\nu = 1/2$ . The complex coordinates  $z_i = x_i + iy_i$  indicate the positions of the electrons with  $\uparrow$ -spin on the lattice,  $x, y \in \mathbb{Z}$ . Lattice sites without an associated coordinate  $z_i$  are occupied by  $\downarrow$ -spin electrons. The factor  $G(z) = (-1)^{(x+1)(y+1)}$  is a gauge sign, ensuring that the wave function describes a spin singlet. The sign of each lattice site is indicated in Figure 3.1. The exponential factor in (3.2.2) corresponds to a fictitious magnetic field of strength  $2\pi/\text{plaquet}$ . The state violates the discrete symmetries of time-reversal and parity.

For a CSL with periodic boundary conditions on a lattice with  $N$  sites and equal periods,  $L_1 = L_2 = L$ , Schroeter et al. [125] wrote down the wave function, following Haldane and Rezayi [60],

$$\begin{aligned} \langle z_1, \dots, z_M | \psi \rangle = \psi_0^{\text{CSL}}[z] &= \prod_{\nu=1}^2 \vartheta_{\frac{1}{2}, \frac{1}{2}} \left( \frac{\pi}{L} [\mathcal{Z} - Z_\nu] \right) \prod_{i < j}^M \vartheta_{\frac{1}{2}, \frac{1}{2}} \left( \frac{\pi}{L} [z_i - z_j] \right)^2 \\ &\cdot \prod_{j=1}^M G(z_j) e^{\pi/2 (z_j^2 - |z_j|^2)}, \end{aligned} \quad (3.2.3)$$

with  $\mathcal{Z} = \sum_i z_i$  being the center-of-mass coordinate, and  $Z_1, Z_2$  its zeros. They can be chosen anywhere inside of the principal region  $0 \leq \Re(Z_1) < L$  and  $0 \leq \Im(Z_1) < L$ , but have to fulfill the condition  $Z_1 + Z_2 = L + iL$ . Thus, one zero is free to choose and reflects the topological degeneracy of the CSL on the torus, yielding two linearly independent ground states. The odd Jacobi theta function  $\vartheta_{\frac{1}{2}, \frac{1}{2}}(w)$  in (3.2.3) is further explained in Appendix C. The two ground states are strictly periodic on the torus, translationally invariant under lattice transformations and spin singlets.



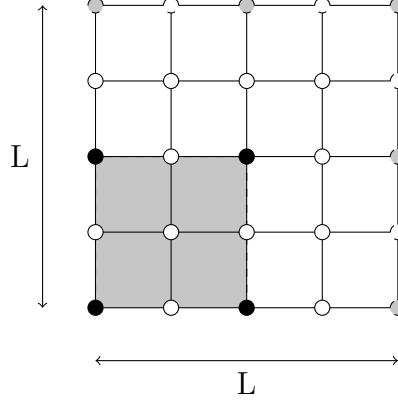


**Fig. 3.1** The CSL is defined on a square lattice with equal length  $L$  per side and  $N = L^2$  sites. It is  $N = 16$ . The open (shaded) circles correspond to lattice sites with  $G(z) = +1$  ( $G(z) = -1$ ). The shaded sites create a sublattice with twice the original lattice spacing. The shaded region in the figure is the doubled unit cell.

*Proof.* Similar to the Haldane-Shastry state, to prove the singlet property of the CSL state, it is sufficient to prove that  $S_{\text{tot}}^- |\psi_0^{\text{CSL}}\rangle = 0$ , since  $S_{\text{tot}}^z |\psi_0^{\text{CSL}}\rangle = 0$  holds by construction. Now, we have

$$\begin{aligned} S_{\text{tot}}^- |\psi_0^{\text{CSL}}\rangle &= \sum_{\alpha=1}^N S_{\alpha}^- \sum_{\{z_1, \dots, z_M\}} \psi_0^{\text{HS}}(z_1, z_2, \dots, z_M) S_{z_1}^+ \dots S_{z_M}^+ |\downarrow \downarrow \dots \downarrow\rangle \\ &= \sum_{\{z_2, \dots, z_M\}} \underbrace{\sum_{\alpha=1}^N \psi_0^{\text{CSL}}(\eta_{\alpha}, z_2, \dots, z_M)}_{=0} S_{z_2}^+ \dots S_{z_M}^+ |\downarrow \downarrow \dots \downarrow\rangle. \end{aligned} \quad (3.2.4)$$

The identity

$$\sum_{\alpha=1}^N \psi_0^{\text{CSL}}(\eta_{\alpha}, z_2, \dots, z_M) = 0 \quad (3.2.5)$$

is a special case of the Perelomov identity [110; 46], which holds for all lattice sums of  $e^{-\frac{\pi}{2}|\eta_{\alpha}|^2} G(\eta_{\alpha})$  times an arbitrary analytic function of  $\eta_{\alpha}$ . The identity was originally derived from the properties of the Jacobi  $\vartheta$ -functions, and many analytical results available for the CSL, such as the singlet property for Abelian and non-Abelian CSL states, rely on this identity. A proof of (3.2.5) is contained in [46].

□

Analogously to the construction of the Haldane-Shastry state via Gutzwiller projection, the CSL state can be obtained by projecting from a completely filled LLL with  $M = N/2$   $\uparrow$ -spin and  $M$   $\downarrow$ -spin electrons [89; 35],

$$|\psi_0^{\text{CSL}}\rangle = P_{\text{GW}} |\psi_{\text{SD},2d}^N\rangle, \quad (3.2.6)$$

with  $|\psi_{\text{SD},2d}^N\rangle$  being the Slater determinant wave function for the LLL filled once with  $M$   $\uparrow$ -spins and once with  $M$   $\downarrow$ -spins. The Gutzwiller projector  $P_{\text{GW}}$  is defined in (3.1.16).

The state (3.2.6) is equivalent to (3.2.1).

*Proof.* Similar to the derivation for the Haldane-Shastry model, the Gutzwiller state (3.2.6) can be rewritten as

$$|\psi_0^{\text{CSL}}\rangle = \sum_{\{z_1, \dots, z_M; w_1, \dots, w_M\}} \phi(z_1, \dots, z_M) \phi(w_1, \dots, w_M) \cdot c_{z_1 \uparrow}^\dagger \dots c_{z_M \uparrow}^\dagger c_{w_1 \downarrow}^\dagger \dots c_{w_M \downarrow}^\dagger |0\rangle, \quad (3.2.7)$$

where  $\phi(z_1, \dots, z_M)$  is the wave function of a filled LLL in a fictitious magnetic field with flux  $\pi$  per plaquet,

$$\phi[z] = \prod_{i < j}^M (z_i - z_j) \prod_{i=1}^M e^{-\frac{\pi}{4}|z_i|^2}. \quad (3.2.8)$$

The coordinates  $z_i$  ( $w_i$ ) label sites with  $\uparrow$ -spin ( $\downarrow$ -spin) particles.

At the same time, we can rewrite (3.2.2),

$$\psi_0^{\text{CSL}}[z] = \prod_{j=1}^M \left( G(z_j) e^{-\frac{M\pi}{N}|z_j|^2} \prod_{\substack{k=1 \\ (k \neq j)}}^M (z_j - z_k) \right). \quad (3.2.9)$$

Kalmeyer and Laughlin [74] have proven that

$$\prod_{\substack{\alpha=1 \\ (\alpha \neq k)}}^N (\zeta_\alpha - z_k) = -C_0 G(z_k) e^{\frac{\pi}{4}|z_k|^2}, \quad (3.2.10)$$

where  $\zeta_\alpha$  are lattice sites and  $C_0$  is constant in the thermodynamic limit.

Inserting this into (3.2.9) yields

$$\psi_0^{\text{CSL}}[z] = \prod_{\substack{j,k=1 \\ (k \neq j)}}^M (z_j - z_k) \left[ \prod_{k=1}^M \prod_{\substack{\alpha=1 \\ (\zeta_\alpha \neq z_k)}}^N (\zeta_\alpha - z_k) \right]^{-1} (-C_0)^N. \quad (3.2.11)$$

The coordinates  $\zeta_\alpha$  run over all lattice sites, the coordinates  $z_j$  are the locations of the  $\uparrow$ -spins.

Taking  $\{w_1, w_2, \dots, w_M\}$  as the locations of the sites occupied with  $\downarrow$ -spin particles, we have

$$\prod_{k=1}^M \prod_{\substack{\alpha=1 \\ (\zeta_\alpha \neq z_k)}}^N (\zeta_\alpha - z_k) = \prod_{\substack{j,k=1 \\ (k \neq j)}}^M (z_j - z_k) \prod_{\alpha,l=1}^M (w_\alpha - z_l). \quad (3.2.12)$$

Then, (3.2.11) takes the simple form

$$\psi_0^{\text{CSL}}[z] = \left[ \prod_{\alpha,l=1}^M (w_\alpha - z_l) \right]^{-1} (-C_0)^N. \quad (3.2.13)$$

This form of the CSL manifests the inversion symmetry of the ground state, since interchanging  $\uparrow$ - and  $\downarrow$ -spins (interchanging  $z_l$  and  $w_\alpha$ ) only results in a global sign change. Therefore, the amplitude for a specific spin configuration is equal to the amplitude of its spin-flipped image.

The sign obtained by ordering the  $z$ - and  $w$ -coordinates according to the lattice positions is

$$\text{sign}[z; w] \equiv \langle 0 | c_{w_{N-M\downarrow}} \dots c_{w_1\downarrow} c_{z_M\uparrow} \dots c_{z_1\uparrow} |\downarrow \dots \downarrow\rangle. \quad (3.2.14)$$

Since

$$\prod_{j < k}^M (z_j - z_k) \prod_{j, l=1}^M (z_j - w_l) \prod_{l < m}^M (w_l - w_m) = \text{const.} \cdot \text{sign}[z; w], \quad (3.2.15)$$

(3.2.13) can be rewritten as

$$\psi_0^{\text{CSL}}[z] = \text{sign}[z; w] \phi[z] \phi[w] \cdot \text{const}, \quad (3.2.16)$$

which is equivalent to (3.2.7).

□

In the framework of this construction, the singlet property of the CSL becomes evident: The Slater determinant  $|\psi_{\text{SD},2d}^N\rangle$  is clearly a singlet, and the Gutzwiller operator commutes with the spin operator of every local site, see (3.1.26). Thus,  $|\psi_0^{\text{CSL}}\rangle$  is a singlet itself. Moreover, this construction illustrates that the CSL is invariant under lattice transformations. Therefore, it can be defined on any lattice of interest (square, triangular, ...).

In analogy to the spinon excitation in the Haldane-Shastry model, the wave function for a spinon excitation at position  $\eta_\alpha$  of the CSL with open boundary conditions reads

$$\psi_\alpha^{\text{CSL}}(z_1, \dots, z_M) = \prod_{j=1}^M (\eta_\alpha - z_j) \prod_{j=1}^M G(z_j) \prod_{j < k}^M (z_j - z_k)^2 \prod_{j=1}^M e^{-\frac{\pi}{2}|z_j|^2}. \quad (3.2.17)$$

The momentum wave function is given through Fourier transformation,

$$\psi_m^{\text{CSL}}(z_1, \dots, z_M) = \sum_{\alpha=1}^N (\eta_\alpha)^m \psi_\alpha^{\text{CSL}}(z_1, \dots, z_M). \quad (3.2.18)$$

Constructing the CSL state via Gutzwiller projection lets us also express spinon excitations elegantly. For a system with  $L$   $\downarrow$ -spin spinons at positions  $\eta_1, \dots, \eta_L$ , the state is

$$|\psi_{\eta_1, \dots, \eta_L}^{\text{CSL}}\rangle = P_{\text{GW}} c_{\eta_1 \uparrow} \cdots c_{\eta_L \uparrow} |\psi_{\text{SD},2d}^{N+L}\rangle, \quad (3.2.19)$$

where  $N + L = 2M$  has to be an even integer. The fractional spin  $1/2$  of the spinons is nicely illustrated in this form: The electron annihilation operators  $c_\eta$  create inhomogeneities in spin and charge before the projection, which enforces one particle per site and thus restores the homogeneity in the charge distribution. Since the projector commutes with the spin, the final wave function is a neutral object of spin  $1/2$ .

Since the spinon coordinates  $\eta$  do not have to coincide with lattice points, we can define a winding number and with that a statistical parameter via a Berry phase upon adiabatic interchange of the excitations.

The spinons obey half-fermi statistics, both in the sense of Haldane's exclusion principle and in the sense of the Berry phase. The phase, obtained by adiabatically exchanging two spinons by moving them counterclockwise around each other, is  $\pi/2$ ,

$$|\psi\rangle \rightarrow e^{i\frac{\pi}{2}} |\psi\rangle. \quad (3.2.20)$$

A holon excitation carries a positive unit charge and no spin. It can be constructed from spinon excitations by annihilating one electron at the spinon position, which now must coincide with a lattice point. As an example, the CSL with  $L$  holons at sites  $\eta_1, \dots, \eta_L$  is

$$|\psi_{\eta_1 \circ \dots \eta_L}^{\text{CSL}}\rangle = c_{\eta_1 \downarrow} \cdots c_{\eta_L \downarrow} P_{\text{GW}} c_{\eta_1 \uparrow} \cdots c_{\eta_L \uparrow} |\psi_{\text{SD},2d}^{N+L}\rangle \quad (3.2.21)$$

with  $N + L = 2M$  an even integer again.

### 3.3 The non-Abelian chiral spin liquid

In the previous models, the spinon excitations possessed Abelian fractional statistics. However, extending the concept to systems with higher spin ( $s > 1/2$ ), CSL states with non-Abelian statistics can be constructed [45]. Systems with such a property are candidates for applications in quantum computation and cryptography [79]. After one braiding of two non-Abelian anyons, the corresponding wave function undergoes a matrix rotation instead of simply achieving an additional phase factor [143], making such systems an ideal candidate for encoding quantum information. For  $s = 1$ , the CSL state is the analogue of the bosonic Pfaffian state, for  $s > 1$ , the CSLs correspond to the Read-Rezayi series at filling  $\nu \geq 3/2$ .

The Pfaffian state is an example of a quantized Hall state supporting quasiparticle excitations with non-Abelian statistics. It was independently discovered by Moore and Read [100], and by Wen, Wilczek and Greiter [47; 48]. The latter authors proposed the Pfaffian state as a candidate for the experimentally measured Hall plateau at filling fraction  $\nu = 5/2$ , which is equivalent to a filling fraction  $\nu = 1/2$  in the second Landau level. Their proposal was strongly supported experimentally by the direct measurement of the quasihole charge recently [23; 118].

The Pfaffian wave function initially proposed by Moore and Read [100] is

$$\psi_0(z_1, z_2, \dots, z_N) = \text{Pf} \left( \frac{1}{z_i - z_j} \right) \prod_{i < j}^N (z_i - z_j)^m \prod_{i=1}^N e^{-\frac{1}{4}|z_i|^2}, \quad (3.3.1)$$

where the particle number  $N$  is even, and the exponent  $m$  is even (odd) for fermions (bosons). The Pfaffian is

$$\text{Pf} \left( \frac{1}{z_i - z_j} \right) := \mathcal{A} \left\{ \frac{1}{z_1 - z_2} \cdot \dots \cdot \frac{1}{z_{N-1} - z_N} \right\}. \quad (3.3.2)$$

It is the fully antisymmetrized sum over all possible pairings of the  $N$  particle coordinates. Given an analytic function  $\varphi(\mathbf{x})$ , and a matrix

$$M_{ij} = \begin{cases} 0 & \text{for } i = j, \\ \varphi(\mathbf{x}_i - \mathbf{x}_j) & \text{for } i \neq j, \end{cases} \quad (3.3.3)$$

the square of the Pfaffian is equal to the determinant of the matrix,

$$\text{Pf}(\varphi(\mathbf{x}_i - \mathbf{x}_j))^2 = \det(M_{ij}). \quad (3.3.4)$$

The inverse Landau level filling fraction is

$$\frac{1}{\nu} = \frac{\partial N_{\Phi}}{\partial N} = \frac{\partial(m(N-1) - 1)}{\partial N} = m. \quad (3.3.5)$$

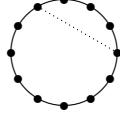
Obviously, the state is a combination of a Laughlin state at filling  $\nu = 1/m$  and a Pfaffian which implements p-wave pairing correlations but leaves the filling fraction unaltered. Since the Pfaffian is antisymmetric, it changes the statistics from bosonic to fermionic or vice versa. The state vanishes as the  $(3m-1)$ -th power as three particles approach each other. Thus, there can be at most two particles at the same position among each triplet of particles.

In spherical geometry, the Pfaffian wave function is [48]

$$\psi_0[u, v] = \text{Pf} \left( \frac{1}{u_i v_j - u_j v_i} \right) \prod_{i < j}^N (u_i v_j - u_j v_i)^m, \quad (3.3.6)$$

for a system of  $N$  particles at Landau level filling  $\nu = 1/m$  on a sphere pierced by  $2s_0 = m(N-1) - 1$  magnetic flux quanta. Again,  $m$  is even (odd) for fermions (bosons).

The one-dimensional analog of a non-Abelian chiral spin liquid can be achieved by extending the Haldane-Shastry model to spin  $s = 1$  systems. We consider a one-dimensional lattice with periodic boundary conditions and an even number of sites  $N$  on a unit circle embedded in the complex plane.



$N$  sites with spin 1 on unit circle:

$$\eta_\alpha = e^{i\frac{2\pi}{N}\alpha} \quad \text{with } \alpha = 1, \dots, N$$

If the spin of each site is  $s = 1$ , the ground state wave function is expressed by a Pfaffian state supplemented by a phase factor [37],

$$\psi_0^{s=1}(z_1, z_2, \dots, z_N) = \text{Pf} \left( \frac{1}{z_i - z_j} \right) \prod_{i < j}^N (z_i - z_j) \prod_{i=1}^N z_i. \quad (3.3.7)$$

At sites  $z_i$ , re-normalized spin flips  $\tilde{S}_\alpha^+$  are located, which act on a vacuum with all spins in the  $S^z = -1$  state,

$$|\psi_0^{s=1}\rangle = \sum_{\{z_1, \dots, z_N\}} \psi_0^{s=1}(z_1, \dots, z_N) \tilde{S}_{z_1}^+ \cdots \tilde{S}_{z_N}^+ |-1\rangle_N. \quad (3.3.8)$$

The sum extends over all possibilities of distributing the  $N$  “particles” over the  $N$  lattice sites, including double occupation. The re-normalized spin flips are defined by

$$\tilde{S}_\alpha^+ := \frac{S_\alpha^z + 1}{2} S_\alpha^+, \quad (3.3.9)$$

and the vacuum state is

$$|-1\rangle_N \equiv \otimes_{\alpha=1}^N |1, -1\rangle_\alpha. \quad (3.3.10)$$

A detailed analysis of this state and the derivation of its parent Hamiltonian can be found in [37].

A generalization to arbitrary spin  $s$  is achieved by combining  $2s$  copies of the Haldane-Shastry ground state with spin 1/2, and projecting the spin on each site onto spin  $s$  [37]. Considering a  $N$  particle system, the resulting wave function is

$$\psi_0^s(z_1, \dots, z_{sN}) = \prod_{m=1}^{2s} \left( \prod_{\substack{i,j=(m-1)M+1 \\ i < j}}^{mM} (z_i - z_j)^2 \right) \prod_{i=1}^{sN} z_i, \quad (3.3.11)$$

with  $M = N/2$ , having notable similarity to the Read-Rezayi states in the quantum Hall effect [120]. By rewriting the state into

$$|\psi_0^s\rangle = \left[ \sum_{\{z_1, \dots, z_M\}} \psi_0^{\text{HS}}(z_1, \dots, z_M) \tilde{S}_{z_1}^+ \cdots \tilde{S}_{z_M}^+ \right]^{2s} |-s\rangle_N, \quad (3.3.12)$$

its construction based on the Haldane-Shastry state becomes evident. In the vacuum state, all spins are maximally polarized in the negative  $z$ -direction,

$$|-s\rangle_N := \otimes_{\alpha=1}^N |s, -s\rangle_\alpha. \quad (3.3.13)$$

In a basis where  $S^z$  is diagonal, the re-normalized spin flip operators can be written as

$$\tilde{S}^+ = \frac{1}{s - S^z + 1} S^+. \quad (3.3.14)$$

(3.3.14) implies that

$$S^-(\tilde{S}^+)^n |s, -s\rangle = n(\tilde{S}^+)^{n-1} |s, -s\rangle. \quad (3.3.15)$$

The previous considerations for one-dimensional systems help to derive the wave function for the non-Abelian chiral spin liquid (NACSL) living in two dimensions. Greiter and Thomale [45] introduced a wave function for a circular droplet with open boundary conditions occupying  $N$  sites of a triangular or square lattice  $s = 1$  antiferromagnet. It is expressed by a Pfaffian state supplemented by a gauge factor  $G(z)$ ,

$$\psi_0^1(z_1, z_2, \dots, z_N) = \text{Pf} \left( \frac{1}{z_i - z_j} \right) \prod_{i < j}^N (z_i - z_j) \prod_{i=1}^N G(z_i) e^{-(\pi/2)|z_i|^2}. \quad (3.3.16)$$

The ‘‘particles’’ at complex coordinates  $z_i$  are re-normalized spin flips  $\tilde{S}_\alpha^+$  acting on a vacuum with all spins in the  $S^z = -1$  state,

$$|-1\rangle_N := \otimes_{\alpha=1}^N |1, -1\rangle_\alpha. \quad (3.3.17)$$

The NACSL state then is

$$|\psi_0^1\rangle = \sum_{\{z_1, \dots, z_N\}} \psi_0^1(z_1, \dots, z_N) \tilde{S}_{z_1}^+ \cdots \tilde{S}_{z_N}^+ |-1\rangle_N, \quad (3.3.18)$$

where we sum over all possible distributions of  $N$  particles on  $N$  lattice sites, allowing also double occupation, and the re-normalized spin flips are defined by

$$\tilde{S}_\alpha^+ := \frac{S_\alpha^z + 1}{2} S_\alpha^+. \quad (3.3.19)$$

As proven in [45], the state is a spin singlet. It trivially violates parity and time-reversal symmetry, which takes  $z \rightarrow \bar{z}$ .

Generalized to a spin  $s$  system [42], the NACSL state can be written as

$$|\psi_0^s\rangle = \sum_{\{z_1, \dots, z_{sN}\}} \psi_0^s(z_1, \dots, z_{sN}) \tilde{S}_{z_1}^+ \cdots \tilde{S}_{z_{sN}}^+ |-s\rangle_N. \quad (3.3.20)$$

In the ‘‘vacuum’’ state, all spins are maximally polarized in the negative  $\hat{z}$ -direction,

$$|-s\rangle_N := \otimes_{\alpha=1}^N |s, -s\rangle_\alpha. \quad (3.3.21)$$

In a basis in which  $S^z$  is diagonal, the renormalized spin flip operators are

$$\tilde{S}_\alpha^+ = \frac{1}{s - S_\alpha^z + 1} S_\alpha^+. \quad (3.3.22)$$

The wave function is a bosonic Read-Rezayi state,

$$\psi_0^s[z] = \prod_{m=1}^{2s} \left( \prod_{\substack{i,j=(m-1)M+1 \\ i < j}}^{mM} (z_i - z_j)^2 \right) \prod_{i=1}^{sN} G(z_i) e^{-\frac{1}{4}|z_i|^2}, \quad (3.3.23)$$

with  $M = N/2$ , and the function is understood to be completely symmetrized over the coordinates  $z_i$ .

The spinon excitations of (3.3.16) and the half vortex quasiparticles of the Moore-Read quantum Hall state [100] can be analogously derived. As an example, four  $\downarrow$ -spin spinon excitations at coordinates  $\eta_1, \eta_2, \eta_3$  and  $\eta_4$  are generated by simply replacing the Pfaffian in (3.3.16) by

$$\text{Pf} \left( \frac{(z_i - \eta_1)(z_j - \eta_2)(z_i - \eta_3)(z_j - \eta_4) + (i \leftrightarrow j)}{z_i - z_j} \right). \quad (3.3.24)$$

Each spinon carries spin 1/2.





## Chapter 4

# Local parent Hamiltonian for the chiral spin liquid

### 4.1 Introduction

Despite the promising properties of the CSL, it took almost two decades for a microscopic model to emerge. A first attempt was made by Wen et al., who proposed a parent Hamiltonian for a two-dimensional system with a chiral spin state, but not a liquid, as a ground state [146]. One subtlety of the system is the fact that for long-range chiral order to be stabilized, nearest-neighbor Heisenberg interactions are insufficient [6]. Schroeter et al. were the first to construct a parent Hamiltonian for which the Abelian CSL on a square lattice is an exact and, apart from the twofold topological degeneracy, the unique zero-energy ground state [125]. In 2014, they extended their method to construct a parent Hamiltonian for the family of non-Abelian CSL [42], which they introduced in 2009 [45].

The problem of these parent Hamiltonians, however, is twofold: The Hamiltonian for the non-Abelian CSL [42] is only exact in the thermodynamic limit and, more importantly, both of them lack locality. Such models are challenging to achieve experimentally. The question remains whether the CSL can be realized in more realistic spin models. In this chapter, we present local spin Hamiltonians for which the Abelian or the non-Abelian CSL is the exact ground state. These Hamiltonians are, in many respects, a generalization of the Haldane-Shastry model to two dimensions. Moreover, they represent an exact spin model in which fractional quantization can be studied. Similar to [125; 138], our method to find a parent Hamiltonian relies on the singlet property of the CSL, allowing for a spherical tensor decomposition of the introduced annihilation operator.

To find out whether the CSL is the *unique* ground state modulo topological degeneracy of the proposed parent Hamiltonian, we perform exact diagonalization studies for different system sizes. An adapted kernel-sweeping method, introduced in [138], is applied to allow for an efficient implementation of the complex Hamiltonians, reducing the number of computations significantly.

We manage to construct local parent Hamiltonians for spin-1/2 and spin-1 systems with largely gapped eigenspectrums. Through numerical study of the obtained Hamiltonians on various lattice geometries, we confirm that the CSL (for the spin-1/2 system) and the NACSL (for the spin-1 system) are the unique ground states. Our models work on all investigated lattices, making an experimental realization more attainable.

The results presented in this chapter are product of a joint collaboration of Martin Greiter, Ronny Thomale and the author of this thesis [124].

## 4.2 A local parent Hamiltonian for the chiral spin liquid

We wish to construct a local parent Hamiltonian for the Abelian and non-Abelian chiral spin liquid (CSL). The final Hamiltonian has to meet several criteria: Apart from being Hermitian, it should be invariant under space translations and  $SU(2)$ -spin rotations. Moreover, the CSL state has to be the unique ground state and the Hamiltonian should be local in order to be experimentally viable. Without any technique, the task to find such a Hamiltonian seems dauntingly complex. To solve this problem, we have developed a method to systematically construct such a Hamiltonian for systems with spin  $s = 1/2$  and  $s = 1$ . Additionally, for  $s = 3/2$  systems, we have found a longer range parent Hamiltonian.

In the first step of this method, an annihilation operator for the ground state is set up. Since the CSL state, living in a two-dimensional system, shares many similarities with the Haldane-Shastry state, living in a one-dimensional system, we take the Haldane-Shastry model (3.1.1) as a template for the CSL parent Hamiltonian. Therefore, in the following Section 4.2.1, we first set up an annihilation operator for the 1d-system, and then, in Section 4.2.2, extend it to a 2d-system. In contrast to the one-dimensional system, the CSL state in 2D breaks explicitly time-reversal and parity symmetry. Hence, the two-dimensional parent Hamiltonian does not have these symmetries.

In the next step, detailed in Section 4.2.4, a parent Hamiltonian obeying the trivial symmetries of the CSL is constructed out of the annihilation operator. In Section 4.2.5, locality of the Hamiltonian is successfully established by extending the original annihilation operator from a two-spin term to a three- and even four-spin term.

### 4.2.1 Annihilation operator in 1d

The defining condition for the annihilation operator is

$$\Omega_\alpha^{s,1d} |\psi_0^{\text{HS}}\rangle = 0. \quad (4.2.1)$$

We choose

$$\Omega_\alpha^{s,1d} = \sum_{\substack{\mu=1 \\ (\mu \neq \alpha)}}^N \frac{\eta_\alpha + \eta_\mu}{\eta_\alpha - \eta_\mu} (S_\alpha^-)^{2s} S_\mu^-. \quad (4.2.2)$$

This annihilation operator is associated with one lattice site  $\alpha$  and contains a sum over all other lattice sites. Compared to [37], we added a factor  $\eta_\alpha + \eta_\mu$ . This does not alter the annihilation property of the operator, but its prefactor becomes time-reversal invariant, since it is purely imaginary,

$$\frac{\bar{\eta}_\alpha + \bar{\eta}_\mu}{\bar{\eta}_\alpha - \bar{\eta}_\mu} = -\frac{\eta_\alpha + \eta_\mu}{\eta_\alpha - \eta_\mu}. \quad (4.2.3)$$

In the following, we will abbreviate

$$M_{\alpha\mu} := \frac{\eta_\alpha + \eta_\mu}{\eta_\alpha - \eta_\mu}. \quad (4.2.4)$$

### 4.2.2 Annihilation operator in 2d

The extension to two-dimensional CSL states is straightforward by setting up the annihilation operator analogously to the one-dimensional case (4.2.2). The defining condition for the annihilation operator is

$$\Omega_\alpha^{s,2d} |\psi_0^{\text{CSL}}\rangle = 0 \quad (4.2.5)$$

with

$$\Omega_\alpha^{s,2d} = \sum_{\substack{\mu=1 \\ (\mu \neq \alpha)}}^N \frac{\vartheta_{a,b}(\eta_\alpha - \eta_\mu|\tau)}{\vartheta_{\frac{1}{2},\frac{1}{2}}(\eta_\alpha - \eta_\mu|\tau)} (S_\alpha^-)^{2s} S_\mu^-. \quad (4.2.6)$$

We define

$$M_{\alpha\mu}^{ab} := \vartheta_{a,b}(\eta_\alpha - \eta_\mu|\tau) / \vartheta_{\frac{1}{2},\frac{1}{2}}(\eta_\alpha - \eta_\mu|\tau), \quad (4.2.7)$$

and  $\vartheta_{a,b}(z|\tau)$  is the Jacobi theta function, further explained in Appendix C. The index tuple  $(a, b)$  can take values  $(0, 0)$ ,  $(\frac{1}{2}, 0)$  or  $(0, \frac{1}{2})$ . We will omit the superscript “2d” from now on.

### 4.2.3 Direct verification of the annihilation property

We wish to prove that the above-mentioned tensor operators annihilate the ground state of the respective system.

*One-dimensional system with spin  $s = 1/2$ :* The operator (4.2.2) annihilates the Haldane-Shastry ground state (3.1.5), since

$$\begin{aligned} \Omega_\alpha^{s,1d} |\psi_0^{\text{HS}}\rangle &= \sum_{\substack{\beta=1 \\ \beta \neq \alpha}}^N \frac{\eta_\alpha + \eta_\beta}{\eta_\alpha - \eta_\beta} S_\alpha^- S_\beta^- \sum_{\{z_1, \dots, z_M\}} \psi_0^{\text{HS}}(z_1, z_2, \dots, z_M) S_{z_1}^+ \dots S_{z_M}^+ |\downarrow \dots \downarrow\rangle \\ &= \sum_{\{z_3, \dots, z_M\}} \underbrace{\sum_{\substack{\beta=1 \\ \beta \neq \alpha}}^N (\eta_\alpha + \eta_\beta) \frac{\psi_0^{\text{HS}}(\eta_\alpha, \eta_\beta, z_3, \dots, z_M)}{\eta_\alpha - \eta_\beta}}_{=0} S_{z_3}^+ \dots S_{z_M}^+ |\downarrow \dots \downarrow\rangle. \end{aligned} \quad (4.2.8)$$

The term

$$\begin{aligned} &(\eta_\alpha + \eta_\beta) \frac{\psi_0^{\text{HS}}(\eta_\alpha, \eta_\beta, z_3, \dots, z_M)}{\eta_\alpha - \eta_\beta} \\ &= (\eta_\alpha^2 - \eta_\beta^2) \eta_\alpha \eta_\beta \prod_{i=3}^M (\eta_\alpha - z_i)^2 (\eta_\beta - z_i)^2 z_i \prod_{3 \leq i < j}^M (z_i - z_j)^2 \end{aligned}$$

contains only powers of  $\eta_\beta^1, \eta_\beta^2, \dots, \eta_\beta^{N-1}$  and

$$\sum_{\alpha=1}^N \eta_\alpha^m = N \delta_{m,0} \text{ mod } N. \quad (4.2.9)$$

□

The complex conjugate of the annihilation operator,  $\bar{\Omega}_\alpha^{s,1d}$ , also annihilates the CSL state. The proof is almost identical to the above calculation, since

$$(\bar{\eta}_\alpha + \bar{\eta}_\beta) \frac{\psi_0^{\text{HS}}(\eta_\alpha, \eta_\beta, z_3, \dots, z_M)}{\bar{\eta}_\alpha - \bar{\eta}_\beta} = -(\eta_\alpha + \eta_\beta) \frac{\psi_0^{\text{HS}}(\eta_\alpha, \eta_\beta, z_3, \dots, z_M)}{\eta_\alpha - \eta_\beta}$$

again contains only powers of  $\eta_\beta^1, \eta_\beta^2, \dots, \eta_\beta^{N-1}$ .

*One-dimensional system with arbitrary spin  $s$ :* The proof is slightly more involved. We first examine the action of the spin operator  $(S_\alpha^-)^{2s} S_\mu^-$  on the ground state (3.3.12). Since the Haldane-Shastry wave

function  $\psi_0^{\text{HS}}(z_1, \dots, z_M)$  vanishes whenever two arguments  $z_i$  coincide, one of the arguments in the  $2s$  copies in (3.3.12) must be equal to  $\eta_\alpha$ . Due to the invariance of the Haldane-Shastry wave function under interchange of the  $z_i$ , and the fact that each configuration in the sum over  $\{z_1, \dots, z_M\}$  is counted only once, we may choose without loss of generality  $z_1 = \eta_\alpha$ . At site  $\mu$ , there can be  $0, 1, 2, \dots, 2s$  re-normalized spin flips  $\tilde{S}_\mu^+$  in state (3.3.12). Again, due to the invariance of the Haldane-Shastry state under interchange of the  $z_i$ , we may assume that the first  $n$  spin flips are present in the first  $n$  copies. A combinatorial factor  $\binom{2s}{n}$  then takes into account all permutations.

$$\begin{aligned}
& (S_\alpha^-)^{2s} S_\mu^- |\psi_0^{\text{HS}}\rangle \\
&= (S_\alpha^-)^{2s} S_\mu^- \sum_{n=0}^{2s} \binom{2s}{n} \left[ \sum_{\{z_3, \dots, z_M\}} \psi_0^{\text{HS}}(\eta_\alpha, \eta_\mu, z_3, \dots) \tilde{S}_\alpha^+ \tilde{S}_\mu^+ \tilde{S}_{z_3}^+ \cdots \tilde{S}_{z_M}^+ \right]^n \\
&\quad \cdot \left[ \sum_{\{z_2, \dots, z_M\} \neq \eta_\mu} \psi_0^{\text{HS}}(\eta_\alpha, z_2, \dots) \tilde{S}_\alpha^+ \tilde{S}_{z_2}^+ \cdots \tilde{S}_{z_M}^+ \right]^{2s-n} | -s \rangle_N \\
&= (2s)! 2s \left[ \sum_{\{z_2, \dots, z_M\}} \psi_0^{\text{HS}}(\eta_\alpha, \eta_\mu, z_3, \dots, z_M) \tilde{S}_{z_3}^+ \cdots \tilde{S}_{z_M}^+ \right] \\
&\quad \cdot \sum_{n=1}^{2s} \binom{2s-1}{n-1} \left[ \sum_{\{z_3, \dots, z_M\}} \psi_0^{\text{HS}}(\eta_\alpha, \eta_\mu, z_3, \dots, z_M) \tilde{S}_\mu^+ \tilde{S}_{z_3}^+ \cdots \tilde{S}_{z_M}^+ \right]^{n-1} \\
&\quad \cdot \left[ \sum_{\{z_2, \dots, z_M\} \neq \eta_\mu} \psi_0^{\text{HS}}(\eta_\alpha, z_2, \dots, z_M) \tilde{S}_{z_2}^+ \cdots \tilde{S}_{z_M}^+ \right]^{2s-n} | -s \rangle_N \\
&= (2s)! 2s \left[ \sum_{\{z_3, \dots, z_M\}} \psi_0^{\text{HS}}(\eta_\alpha, \eta_\mu, z_3, \dots, z_M) \tilde{S}_{z_3}^+ \cdots \tilde{S}_{z_M}^+ \right] \\
&\quad \cdot \left[ \sum_{\{z_2, \dots, z_M\}} \psi_0^{\text{HS}}(\eta_\alpha, z_2, \dots, z_M) \tilde{S}_{z_2}^+ \cdots \tilde{S}_{z_M}^+ \right]^{2s-1} | -s \rangle_N, \tag{4.2.10}
\end{aligned}$$

where we have used (3.3.15). Applying the entire operator (4.2.2) onto the ground state then results in

$$\begin{aligned}
\Omega_\alpha^{s,1d} |\psi_0^{\text{HS}}\rangle &= (2s)! 2s \\
&\quad \cdot \left[ \sum_{\{z_3, \dots, z_M\}} \underbrace{\sum_{\mu=1}^N (\eta_\alpha + \eta_\mu) \frac{\psi_0^{\text{HS}}(\eta_\alpha, \eta_\mu, z_3, \dots, z_M)}{\eta_\alpha - \eta_\mu}}_{=0} \tilde{S}_{z_3}^+ \cdots \tilde{S}_{z_M}^+ \right] \\
&\quad \cdot \left[ \sum_{\{z_2, \dots, z_M\}} \psi_0^{\text{HS}}(\eta_\alpha, z_2, \dots, z_M) \tilde{S}_{z_2}^+ \cdots \tilde{S}_{z_M}^+ \right]^{2s-1} | -s \rangle_N, \tag{4.2.11}
\end{aligned}$$

where we have used that

$$\begin{aligned}
& (\eta_\alpha + \eta_\mu) \frac{\psi_0^{\text{HS}}(\eta_\alpha, \eta_\mu, z_3, \dots, z_M)}{\eta_\alpha - \eta_\mu} \\
&= (\eta_\alpha + \eta_\mu)(\eta_\alpha - \eta_\mu) \eta_\alpha \eta_\mu \prod_{i=3}^M (\eta_\alpha - z_i)^2 (\eta_\mu - z_i)^2 z_i \prod_{3 \leq i < j}^M (z_i - z_j)^2
\end{aligned}$$

vanishes for  $\mu = \alpha$  and contains only powers  $\eta_\mu^1, \eta_\mu^2, \dots, \eta_\mu^{N-2}$ . Note that the calculation for  $\bar{\Omega}_\alpha^{s,1\text{d}}$  is almost identical, since

$$(\bar{\eta}_\alpha + \bar{\eta}_\mu) \frac{\psi_0^{\text{HS}}(\eta_\alpha, \eta_\mu, z_3, \dots, z_M)}{\bar{\eta}_\alpha - \bar{\eta}_\mu} = -(\eta_\alpha + \eta_\mu) \frac{\psi_0^{\text{HS}}(\eta_\alpha, \eta_\mu, z_3, \dots, z_M)}{\eta_\alpha - \eta_\mu}$$

vanishes also for  $\mu = \alpha$  and contains only powers  $\eta_\mu^2, \eta_\mu^3, \dots, \eta_\mu^{N-1}$ .

□

*Two-dimensional system with arbitrary spin  $s$ :* The considerations for the Haldane-Shastry wave function  $\psi_0^{\text{HS}}$  up to (4.2.10) also hold for the CSL state  $\psi_0^{\text{CSL}}$ , leading to

$$\begin{aligned}
\Omega_\alpha^{s,2\text{d}} |\psi_0^{\text{CSL}}\rangle &= (2s)! 2s \\
&\cdot \left[ \sum_{\{z_3, \dots, z_M\}} \underbrace{\sum_{\substack{\mu=1 \\ (\mu \neq \alpha)}}^N \vartheta_{a,b}(\eta_\alpha - \eta_\mu | \tau) \frac{\psi_0^{\text{CSL}}(\eta_\alpha, \eta_\mu, z_3, \dots, z_M)}{\vartheta_{\frac{1}{2}, \frac{1}{2}}(\eta_\alpha - \eta_\mu | \tau)}}_{=0} \tilde{S}_{z_3}^+ \cdots \tilde{S}_{z_M}^+ \right] \\
&\cdot \left[ \sum_{\{z_2, \dots, z_M\}} \psi_0^{\text{CSL}}(\eta_\alpha, z_2, \dots, z_M) \tilde{S}_{z_2}^+ \cdots \tilde{S}_{z_M}^+ \right]^{2s-1} | -s \rangle_N. \tag{4.2.12}
\end{aligned}$$

As in the proof of the singlet property of the CSL state (3.2.5), we have used a special case of the Perelomov identity to proof that the first term vanishes.

□

#### 4.2.4 Construction of a parent Hamiltonian

From the annihilation operator (4.2.6), we now wish to construct a parent Hamiltonian for the Abelian chiral spin liquid state for spin  $s = 1/2$  systems (3.2.3) and for the non-Abelian chiral spin liquid state for arbitrary spin  $s > 1/2$  (3.3.23). The Hamiltonian has to fulfill several criteria: It should be Hermitian and invariant under spatial translations and  $SU(2)$ -spin rotations.

The product of our annihilation operator with its Hermitian conjugate,  $\Omega^s \dagger \Omega^s$ , is itself Hermitian and positive semi-definite. Consequently, the CSL state is a zero-energy ground state of the product operator. It becomes translationally invariant by summing over all possible lattices sites, giving the first template for our parent Hamiltonian

$$H^s = \sum_{\alpha=1}^N \Omega_\alpha^s \dagger \Omega_\alpha^s. \tag{4.2.13}$$

The Hamiltonian contains a scalar, vector, and higher-order tensor components which all have to annihilate the state  $|\psi_0\rangle$  individually. For the one-dimensional case, the preliminary Hamiltonian is

$$H^s = \sum_{\substack{\alpha, \mu, \nu \\ (\alpha \neq \mu, \nu)}}^N \bar{M}_{\alpha\mu} M_{\alpha\nu} (S_\alpha^+)^{2s} (S_\alpha^-)^{2s} S_\mu^+ S_\nu^-. \quad (4.2.14)$$

In two dimensions, the coefficients  $M_{\alpha\beta}$  simply have to be generalized to  $M_{\alpha\beta}^{ab}$ .

Since the CSL state is a spin singlet state, the final Hamiltonian has to fulfill  $SU(2)$ -symmetry. Therefore, we project the Hamiltonian  $H^s$  onto its scalar component,  $H_0^s = \{H^s\}_0$ . Still, the CSL is the ground state of the scalar Hamiltonian, since the following theorem holds:

If an operator  $M$  annihilates a singlet state  $\psi_S$ , also each of its irreducible components are annihilation operators.

*Proof.* According to the Wigner-Eckart theorem, in the basis of angular momentum eigenstates, matrix elements of spherical tensor operators can be expressed as the product of a Clebsch-Gordan coefficient [7] and a factor independent of the orientation of the angular momentum. Given a spherical tensor operator  $T^{(k)}$ , the matrix element of its  $q$ -th component in an angular momentum resolved basis can be decomposed into

$$\langle n, j, m | T_q^{(k)} | n', j', m' \rangle = \langle j', m', k, q | j, m \rangle \langle n, j | T^{(k)} | n', j' \rangle. \quad (4.2.15)$$

Here,  $|n, j, m\rangle$  are the eigenstates with  $j$  the total angular momentum number,  $L^2 |n, j, m\rangle = \hbar^2 j(j+1) |n, j, m\rangle$ , and  $m$  the  $z$ -component,  $L_z |n, j, m\rangle = \hbar m |n, j, m\rangle$ . All remaining quantum numbers are expressed by  $n$ . The first factor on the right of (4.2.15) is a Clebsch-Gordan coefficient for coupling  $j'$  with  $k$  to give  $j$ . The second factor, traditionally written as a bracket with double lines, is the reduced matrix element depending only on the total (or relative) angular momentum. Applying a tensor on a state can then be written as

$$T_q^{(k)} |n', j', m'\rangle = \sum_{j, m} \langle j', m', k, q | j, m \rangle \langle n, j | T^{(k)} | n', j' \rangle |n, j, m\rangle. \quad (4.2.16)$$

Since  $\psi_S$  is a singlet state,  $\psi_S = \beta |n, 0, 0\rangle$  holds for some constant  $\beta$ , thus  $j' = m' = 0$  in (4.2.16). The Clebsch-Gordan coefficients then vanish unless  $k = j$  and  $q = m$ . Given an operator  $M$  which annihilates the CSL state, it can be decomposed into its irreducible tensor components,  $M_q = \sum_k \alpha_k T_q^{(k)}$ ,  $|q| \leq k$ . Inserted into (4.2.16), we get for all  $k$

$$0 = M_q \psi_S = \sum_k \alpha_k \langle n', k | T^{(k)} | n, 0 \rangle |n', k, q\rangle =: \sum_k \gamma_k |n', k, q\rangle. \quad (4.2.17)$$

Since the basis states  $|n', k, q\rangle$  with different  $k$  are orthogonal, it follows that each of the coefficients  $\gamma_k$  has to be zero. Thus, all operators  $T_q^{(k)}$  are annihilation operators of  $\psi_S$ .

□

We have developed an exact numerical technique to project a tensor operator onto its singlet component and decompose it into scalar spin operator products. It will be presented in detail in Section 4.4.1. In Section 4.5, we apply the above procedure to construct the final parent Hamiltonians for different system setups.

#### 4.2.5 Establishing locality

There are two problems with the model constructed so far: First, the Hamiltonian  $H_0^s$  is long-ranged, since it decreases as  $1/r$  with the distance, such that the spatial integral in one as well as two dimensions is diverging. Second, the Hamiltonian is not periodic in two dimensions. The factor  $M_{\alpha\beta}^{ab}$  acquires the following phases under translations:

$$\begin{aligned}
z \rightarrow z + 1 &: e^{2\pi i(a - \frac{1}{2})}, \\
z \rightarrow z + \tau &: e^{2\pi i(b - \frac{1}{2})}
\end{aligned} \tag{4.2.18}$$

due to the quasi-periodicity of the  $\vartheta$ -function, as explained in Appendix C. For specific values of the parameters  $a, b$ , the phase shift is

a,b	$z \rightarrow z + 1$	$z \rightarrow z + \tau$
$0, \frac{1}{2}$	-	+
$\frac{1}{2}, 0$	+	-
$0, 0$	-	-

The cure to both problems [124] is to replace the annihilation operator  $\Omega_\alpha^s$  in (4.2.6), by

$$\Omega_{\alpha\beta}^s = \sum_{\substack{\mu \\ (\mu \neq \alpha, \beta)}} M_{\alpha\mu}^{ab} M_{\beta\mu}^{ab} (S_\alpha^-)^{2s} (S_\beta^-)^{2s} S_\mu^-. \tag{4.2.19}$$

The new annihilation operator for one-dimensional systems is derived by replacing the prefactors  $M_{\alpha\mu}^{ab}$  by  $M_{\alpha\mu}$  in (4.2.19).

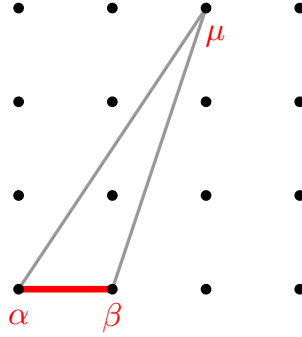


**Fig. 4.1** Schematic of the interaction of the two-site annihilation operator  $\Omega_{\alpha\beta}^s$  with an arbitrary external site  $\mu$  on a square lattice. The interaction decreases as  $1/r^2$ .

The resulting Hamiltonian is then

$$H^{s,2} = \sum_{\langle \alpha, \beta \rangle} \Omega_{\alpha\beta}^{s\dagger} \Omega_{\alpha\beta}^s, \tag{4.2.20}$$

establishing an interaction of two neighboring sites  $\alpha, \beta$  with an external site  $\mu$ . We call this a “two-site” Hamiltonian. The sum goes only over neighboring sites in all lattice directions. Again, for the final Hamiltonian, we project (4.2.20) onto its scalar component,  $H_0^{s,2} := \{H^{s,2}\}_0$ .

For the two-dimensional system, the choice of the parameters  $(a, b)$  in (4.2.19) can be  $(0, 0)$ ,  $(\frac{1}{2}, 0)$  or  $(0, \frac{1}{2})$ , thereby choosing one of the three even  $\vartheta$ -functions in the nominator of the prefactor  $M_{\alpha\mu}^{ab}$  of the annihilation operator  $\Omega_{\alpha\beta}^s$ . To treat the boundaries in  $x$ - and  $y$ -direction symmetrically,  $(0, 0)$  is the best choice. The three choices lead to three different Hamiltonians which are locally equivalent.

In the two-site Hamiltonian (4.2.20), the interaction decreases as  $1/r^2$ , thus being still long-ranged for two-dimensional systems, as depicted in Figure 4.1. However, extending the logic from above, we can easily increase the locality in our Hamiltonian. Instead of a two-site interaction with an external site, as in (4.2.20), it is possible to introduce an interaction over three neighboring sites

$$H^{s,3} = \sum_{\langle \alpha, \beta, \gamma \rangle} \Omega_{\alpha\beta\gamma}^{s\dagger} \Omega_{\alpha\beta\gamma}^s, \tag{4.2.21}$$

with

$$\Omega_{\alpha\beta\gamma}^s = \sum_{\substack{\mu \\ (\mu \neq \alpha, \beta, \gamma)}} M_{\alpha\mu}^{ab} M_{\beta\mu}^{a'b'} M_{\gamma\mu}^{a''b''} (S_{\alpha}^{-})^{2s} (S_{\beta}^{-})^{2s} (S_{\gamma}^{-})^{2s} S_{\mu}^{-}, \quad (4.2.22)$$

or even a four-site interaction

$$H^{s,4} = \sum_{\langle \alpha, \beta, \gamma, \delta \rangle} \Omega_{\alpha\beta\gamma\delta}^{s\dagger} \Omega_{\alpha\beta\gamma\delta}^s, \quad (4.2.23)$$

with

$$\Omega_{\alpha\beta\gamma\delta}^s = \sum_{\substack{\mu \\ (\mu \neq \alpha, \beta, \gamma, \delta)}} M_{\alpha\mu}^{ab} M_{\beta\mu}^{a'b'} M_{\gamma\mu}^{a''b''} M_{\delta\mu}^{a'''b'''} (S_{\alpha}^{-})^{2s} (S_{\beta}^{-})^{2s} (S_{\gamma}^{-})^{2s} (S_{\delta}^{-})^{2s} S_{\mu}^{-}. \quad (4.2.24)$$

The three-site Hamiltonian falls off as  $1/r^3$  with distance. Consequently, the integral in two spatial dimensions is finite when taking the limit of large distances, corresponding to the low energy regime,

$$\int_{r_0}^{R_0} 2\pi r dr \frac{1}{r^3} = 2\pi \left[ -\frac{1}{r} \right]_{r_0}^{R_0} = \frac{2\pi}{r_0} - \frac{2\pi}{R_0} \longrightarrow \frac{2\pi}{r_0} \quad \text{as } R_0 \longrightarrow \infty. \quad (4.2.25)$$

The four-site Hamiltonian falls off as  $1/r^4$ . Its integral in two spatial dimensions is local in the infrared cutoff,

$$\int_{r_0}^{R_0} 2\pi r dr \frac{1}{r^4} = 2\pi \left[ -\frac{1}{2r^2} \right]_{r_0}^{R_0} = \frac{\pi}{r_0^2} - \frac{\pi}{R_0^2} \longrightarrow \frac{\pi}{r_0^2} \quad \text{as } R_0 \longrightarrow \infty. \quad (4.2.26)$$

This implies that both parent Hamiltonians are local, the four-site system even more than the three-site system.

For the three-site operator (4.2.22), there is a subtlety in the choice of the parameters  $(a, b)$ ,  $(a', b')$  and  $(a'', b'')$ , since we have to impose periodicity when translating  $\eta_{\mu}$  by 1 or by  $\tau$  in the complex plane. This is fulfilled for the choice

$$(a, b) = (0, 0), \quad (a', b') = \left( \frac{1}{2}, 0 \right) \quad \text{and} \quad (a'', b'') = \left( 0, \frac{1}{2} \right). \quad (4.2.27)$$

The operator is not symmetric under permutations of the site indices  $\alpha, \beta, \gamma$ . However, the symmetry is established in the final Hamiltonian since we sum over all permutations of nearest-neighboring sites.

In case of the four-site interaction (4.2.23), there are multiple choices for the parameters  $(a, b)$ ,  $(a', b')$ ,  $(a'', b'')$  and  $(a''', b''')$  in the  $\vartheta$ -functions of operator (4.2.24) which have to fulfill the required periodic boundary conditions. The easiest way is to set all parameters equal,  $(a, b) = (a', b') = (a'', b'') = (a''', b''')$ . Still, there remain three choices since we can choose one of the three  $\vartheta$ -functions for the parameters  $(a, b)$ . We have opted for the rotationally invariant choice,  $(a, b) = (0, 0)$ , as will be further detailed in Section 4.5.

In Sections 4.4-4.7, we construct rotationally invariant and non-invariant versions of our parent Hamiltonians with a two-, three- and four-site interaction and analyze them numerically on the square and the triangular lattice.



### 4.3 Tensor representation of operators

We want our final parent Hamiltonian to be invariant under translations as well as  $SU(2)$ -spin rotations. The last condition entails that the Hamiltonian transforms as a scalar under spin rotations. Our construction of the parent Hamiltonian starts from the annihilation operator (4.2.6), which transforms as a higher order tensor. For instance, the operator  $\Omega_{\alpha,\beta}$  consists of spin products proportional to  $\mathbf{S}_\alpha^- \mathbf{S}_\beta^- \mathbf{S}_\mu^-$ ,  $\mu \neq \alpha, \beta$ , and is therefore a third order tensor. Therefore, to obtain the final Hamiltonian, the scalar component has to be projected out of the operator product.

In theory, this can be achieved by hand. This, however, becomes unfeasible for slightly more involved tensor expressions. We therefore have developed an exact numerical technique to easily project out the scalar component and decompose it into scalar spin operator products, which will be presented in Section 4.4. Before presenting our technique, we review the rotation properties of tensor operators and how to project and decompose them.

#### 4.3.1 Representation of rotations

A spherical tensor operator is defined by its transformation properties under rotations. The generator of  $SU(2)$ -rotations is the angular momentum operator  $\mathbf{J}$ . The operator

$$R_\omega = e^{-i\mathbf{J}\cdot\omega} \quad (4.3.1)$$

rotates a state vector around the axis  $\omega$  by an angle  $|\omega|$ .

The eigenstates  $|j, m\rangle$  of the total angular momentum  $\mathbf{J}$  and its  $z$ -component, with eigenvalues  $j(j+1)$  and  $m$ , form a complete orthonormal basis. They transform under rotations as

$$R_\omega |j, m\rangle = \sum_{m'=-j}^j |j, m'\rangle d_{m'm}^{(j)}(\omega). \quad (4.3.2)$$

Obviously, a rotation only changes  $m$ , the total angular momentum is conserved. In (4.3.2), the matrix elements are

$$d_{m'm}^{(j)}(\omega) = \langle j, m' | e^{-i\mathbf{J}\cdot\omega} | j, m \rangle. \quad (4.3.3)$$

This so-called Wigner d-matrix describes an irreducible,  $2j+1$ -dimensional representation of the group  $SU(2)$  [148].

#### 4.3.2 Spherical tensor operators

It is straightforward to determine the transformation properties of operators: Rotations are required to leave the expectation value of an operator  $\mathbf{A}$  unaltered,

$$\langle \psi' | \mathbf{A}' | \psi \rangle = \langle \psi' | \mathbf{A} | \psi \rangle. \quad (4.3.4)$$

Here, a prime stands for a rotated object. Therefore, the transformation has to be unitary,  $R_\omega^{-1} = R_\omega^\dagger$ . Since state vectors transform under rotations as

$$|\psi\rangle \rightarrow |\psi'\rangle = R_\omega |\psi\rangle, \quad (4.3.5)$$

the operator must transform as

$$\mathbf{A}' = R_\omega \mathbf{A} R_\omega^{-1}. \quad (4.3.6)$$

Scalar operators are invariant under rotations

$$\mathbf{A}_{sc} = R_\omega \mathbf{A}_{sc} R_\omega^{-1}, \quad (4.3.7)$$

and thus, they commute with the generators of rotation,

$$[\mathbf{A}_{sc}, \mathbf{J}] = 0. \quad (4.3.8)$$

Scalars are irreducible tensors of order zero.

Vectors, which are irreducible tensors of order one, are a set of three operators, such as the position vector  $\mathbf{r}$  and the angular momentum operator  $\mathbf{J}$ . In general, an irreducible tensor operator of order  $j$ ,  $T^{(j)}$ , has  $2j + 1$  components  $T^{(j)m}$ ,  $m = -j, \dots, j$ . Under rotations, they transform according to

$$R_\omega T^{(j)m} R_\omega^{-1} = \sum_{m'=-j}^j T^{(j)m'} d_{m'm}^{(j)}(\omega). \quad (4.3.9)$$

The coefficients  $d_{m'm}^{(j)}(\omega)$  are defined in (4.3.3).

Rewriting (4.3.9) for infinitesimal rotations

$$R_\epsilon = e^{-i\mathbf{J}\epsilon} \approx 1 - i\mathbf{J}\epsilon, \quad (4.3.10)$$

ignoring higher terms beyond first order, we obtain the commutation relation with the angular momentum operator,

$$[\mathbf{J}, T^{(j)m}] = \sum_{m'=-j}^j T^{(j)m'} \langle j, m' | \mathbf{J} | j, m \rangle. \quad (4.3.11)$$

Remembering that

$$\begin{aligned} J^z |j, m\rangle &= m |j, m\rangle, \\ J^\pm |j, m\rangle &= \sqrt{j(j+1) - m(m \pm 1)} |j, m \pm 1\rangle, \end{aligned} \quad (4.3.12)$$

leads to the commutation relations with the angular momentum components

$$[J^z, T^{(j)m}] = m T^{(j)m}, \quad (4.3.13)$$

$$[J^\pm, T^{(j)m}] = \sqrt{j(j+1) - m(m \pm 1)} T^{(j)m \pm 1}, \quad (4.3.14)$$

where  $J^\pm := J^x \pm iJ^y$ .

When acting on an angular momentum eigenstate  $|j, m\rangle$ , the tensor  $T_m^{(j)}$  increases its eigenvalue by  $m$ , as can be demonstrated by the application of the  $J^z$ -operator,

$$\begin{aligned} J^z T^{(j)m} |j', m'\rangle &= [J^z, T^{(j)m}] |j', m'\rangle + T^{(j)m} J^z |j', m'\rangle \\ &= (m + m') T^{(j)m} |j', m'\rangle. \end{aligned} \quad (4.3.15)$$

In the spherical basis, the components of a vector  $\mathbf{V} = (V_x, V_y, V_z)$ , up to an overall normalization factor, are

$$V^{m=1} = -\frac{V^x + iV^y}{\sqrt{2}}, \quad V^{m=0} = V^z, \quad V^{m=-1} = \frac{V^x - iV^y}{\sqrt{2}}. \quad (4.3.16)$$

This follows from the commutation relation

$$[J^i, V^j] = i\epsilon^{ijk}V^k.$$

### 4.3.3 Product of tensor operators

The tensor product of two irreducible representations  $T^{(l)}$  and  $T^{(m)}$ ,  $l, m \in \mathbb{N}_0$ , of a group or Lie algebra is not irreducible in general. Its decomposition into irreducible pieces is called the Clebsch-Gordan problem. In the  $SU(2)$ -case, assuming  $l \geq m$ , the direct product decomposes as follows

$$T^{(l)} \otimes T^{(m)} \cong T^{(l-m)} \oplus T^{(l-m+1)} \oplus \dots \oplus T^{(l+m)}. \quad (4.3.17)$$

The  $J^z$ -quantum number  $m$  of a product of two tensors

$$T^{(j_1)^{m_1}} T^{(j_2)^{m_2}} \quad (4.3.18)$$

is the sum of the  $J^z$ -quantum numbers of the individual tensors,  $m = m_1 + m_2$ . This can be directly seen by using (4.3.13).

Using Clebsch-Gordan coefficients, two tensor operators can be combined to produce a tensor of order  $j$ ,

$$T^{(j)^m} = \sum_{m_1=-j_1}^{j_1} \sum_{m_2=-j_2}^{j_2} T^{(j_1)^{m_1}} T^{(j_2)^{m_2}} \langle j_1, m_1; j_2, m_2 | j, m \rangle, \quad (4.3.19)$$

with the Clebsch-Gordan coefficients  $\langle j_1, m_1; j_2, m_2 | j, m \rangle$ . This expression can be simplified if we take into account that all Clebsch-Gordan coefficients with  $m \neq m_1 + m_2$  vanish. The expression reduces to one summation,

$$T^{(j)^m} = \sum_{m_1=\max\{-j_1, -j_2+m\}}^{\min\{j_1, j_2+m\}} T^{(j_1)^{m_1}} T^{(j_2)^{m-m_1}} \langle j_1, m_1; j_2, m-m_1 | j, m \rangle. \quad (4.3.20)$$

To prove that the left hand side of (4.3.19) is an irreducible tensor of order  $j$ , its transformation properties under rotations may be considered:

$$\begin{aligned} R_{\omega} T^{(j)^m} R_{\omega}^{-1} &= \sum_{m_1, m_2} R_{\omega} T^{(j_1)^{m_1}} R_{\omega}^{-1} R_{\omega} T^{(j_2)^{m_2}} R_{\omega}^{-1} \langle j_1, m_1; j_2, m_2 | j, m \rangle \\ &= \sum_{m'_1, m'_2} T^{(j_1)^{m'_1}} T^{(j_2)^{m'_2}} \\ &\quad \cdot \sum_{m_1, m_2} \langle j_1, m'_1; j_2, m'_2 | e^{-i\mathbf{J}\cdot\boldsymbol{\omega}} | j_1, m_1; j_2, m_2 \rangle \langle j_1, m_1; j_2, m_2 | j, m \rangle \\ &= \sum_{m'_1, m'_2} T^{(j_1)^{m'_1}} T^{(j_2)^{m'_2}} \sum_{j', m'} \langle j_1, m'_1; j_2, m'_2 | j', m' \rangle \langle j', m' | e^{-i\mathbf{J}\cdot\boldsymbol{\omega}} | j, m \rangle \\ &= \sum_{m'} T^{(j)^{m'}} d_{m'm}^{(j)}(\boldsymbol{\omega}). \end{aligned} \quad (4.3.21)$$

For the derivation, the completeness relations

$$\sum_{m_1=-j_1}^{j_1} \sum_{m_2=-j_2}^{j_2} |j_1, m_1; j_2, m_2\rangle \langle j_1, m_1; j_2, m_2| = 1, \quad (4.3.22)$$

$$\sum_{j=|j_1-j_2|}^{j_1+j_2} \sum_{m=-j}^j |j, m\rangle \langle j, m| = 1, \quad (4.3.23)$$

of the Clebsch–Gordan algebra have been inserted.

With the knowledge of (4.3.19), we can now decompose the product of two tensors into its irreducible components,

$$T^{(j_1)^{m_1}} T^{(j_2)^{m_2}} = \sum_{j=|j_1-j_2|}^{j_1+j_2} \sum_{m=-j}^j T^{(j)^m} \langle j, m | j_1, m_1; j_2, m_2 \rangle. \quad (4.3.24)$$

The projection of the above tensor product onto its  $j'$ -th order component then simply is

$$\{T^{(j_1)^{m_1}} T^{(j_2)^{m_2}}\}_{j'} = T^{(j')^{m_1+m_2}} \langle j', m_1 + m_2 | j_1, m_1; j_2, m_2 \rangle, \quad (4.3.25)$$

where  $T^{(j)^{m_1+m_2}}$  is defined in (4.3.20).

In the following, we will frequently use the projection of a tensor product onto its scalar component,

$$\begin{aligned} \{T^{(j_1)^m} T^{(j_2)^{-m}}\}_0 = \\ \langle 0, 0 | j_1, m; j_2, -m \rangle \sum_{m'=-\min\{j_1, j_2\}}^{\min\{j_1, j_2\}} T^{(j_1)^{m'}} T^{(j_2)^{-m'}} \langle j_1, m'; j_2, -m' | 0, 0 \rangle. \end{aligned} \quad (4.3.26)$$

In Appendix B, the tensor decomposition of spin products with up to three spin operators will be listed.

#### 4.3.4 Decomposition of tensor products

For tensors consisting only of a few spin operators, the decomposition of the scalar component can be done analytically. However, with an increasing number of operators in a tensor, the decomposition becomes soon too intricate to be executable by hand. At this point, it is useful to employ numerical methods which can decompose the expression in a fraction of time. For this purpose, we have developed an exact numerical technique which projects a tensor expression onto its scalar component and decomposes it into simple scalar spin terms. In this section, we explain how the decomposition can be executed analytically. The following Section 4.4.1 then introduces our numerical technique.

As a shorthand notation, we label tensors of  $N$ -th order which are a product of  $N$  spin operators by  $T_{i_1, i_2, \dots, i_N}$ . Their  $m = N$ -component is

$$T_{i_1, i_2, \dots, i_N}^N := S_{i_1}^+ S_{i_2}^+ \dots S_{i_N}^+. \quad (4.3.27)$$

The spin indices are not necessarily different.

To illustrate how to proceed with an analytical decomposition, we present in the following the steps to obtain the scalar component of a very simple expression, the tensor product of  $T_{\alpha\beta}^0$  and  $T_{\mu\nu}^0$  with  $\alpha \neq \beta \neq \mu, \nu$  but allowing  $\mu = \nu$ . Both tensors are of order 2, so that  $j_1 = j_2 = 2$ . Using (4.3.26), we can write the tensor product as

$$\{T_{\alpha\beta}^0 T_{\mu\nu}^0\}_0 = \langle 0, 0 | 2, 0; 2, 0 \rangle \sum_{m=-2}^2 T_{\alpha\beta}^m T_{\mu\nu}^{-m} \langle 2, m; 2, -m | 0, 0 \rangle. \quad (4.3.28)$$

With (B.2.4) and the Clebsch–Gordan coefficients

$$\langle 2, m; 2, -m | 0, 0 \rangle = \frac{(-1)^m}{\sqrt{5}}, \quad (4.3.29)$$

we obtain

$$\begin{aligned} 5 \{T_{\alpha\beta}^0 T_{\mu\nu}^0\}_0 &= \sum_{m=-2}^2 (-1)^m T_{\alpha\beta}^m T_{\mu\nu}^{-m} \\ &= S_{\alpha}^{-} S_{\beta}^{-} S_{\mu}^{+} S_{\nu}^{+} \\ &\quad + (S_{\alpha}^z S_{\beta}^{-} + S_{\alpha}^{-} S_{\beta}^z) (S_{\mu}^z S_{\nu}^{+} + S_{\mu}^{+} S_{\nu}^z) \\ &\quad + \frac{1}{6} (4S_{\alpha}^z S_{\beta}^z - S_{\alpha}^{+} S_{\beta}^{-} - S_{\alpha}^{-} S_{\beta}^{+}) (4S_{\mu}^z S_{\nu}^z - S_{\mu}^{+} S_{\nu}^{-} - S_{\mu}^{-} S_{\nu}^{+}) \\ &\quad + (S_{\alpha}^z S_{\beta}^{+} + S_{\alpha}^{+} S_{\beta}^z) (S_{\mu}^z S_{\nu}^{-} + S_{\mu}^{-} S_{\nu}^z) \\ &\quad + S_{\alpha}^{+} S_{\beta}^{+} S_{\mu}^{-} S_{\nu}^{-}. \end{aligned} \quad (4.3.30)$$

This expression can be rewritten such that the scalar transformation property under spin rotations becomes apparent. Since

$$\mathbf{1} \otimes \mathbf{1} \otimes \mathbf{1} \otimes \mathbf{1} = 3 \cdot \mathbf{0} \oplus 6 \cdot \mathbf{1} \oplus 6 \cdot \mathbf{2} \oplus 3 \cdot \mathbf{3} \oplus \mathbf{4},$$

only three scalars can be formed from four spin operators. For  $\alpha \neq \beta \neq \mu, \nu$ , three such scalars are

$$(\mathbf{S}_{\alpha} \mathbf{S}_{\beta})(\mathbf{S}_{\mu} \mathbf{S}_{\nu}), \quad (\mathbf{S}_{\alpha} \mathbf{S}_{\mu})(\mathbf{S}_{\beta} \mathbf{S}_{\nu}), \quad \text{and} \quad (\mathbf{S}_{\beta} \mathbf{S}_{\mu})(\mathbf{S}_{\alpha} \mathbf{S}_{\nu}).$$

Note that since  $\alpha \neq \beta$ , only the order  $\mathbf{S}_{\mu}$  vs.  $\mathbf{S}_{\nu}$  in the products is relevant. If we were to allow for  $\alpha = \beta$  in addition to  $\mu = \nu$ , we would need to write the last scalar as  $\mathbf{S}_{\alpha}(\mathbf{S}_{\beta} \mathbf{S}_{\mu})\mathbf{S}_{\nu}$ . As an ansatz, we may try

$$5 \{T_{\alpha\beta}^0 T_{\mu\nu}^0\}_0 = a (\mathbf{S}_{\alpha} \mathbf{S}_{\beta})(\mathbf{S}_{\mu} \mathbf{S}_{\nu}) + b [(\mathbf{S}_{\alpha} \mathbf{S}_{\mu})(\mathbf{S}_{\beta} \mathbf{S}_{\nu}) + (\mathbf{S}_{\beta} \mathbf{S}_{\mu})(\mathbf{S}_{\alpha} \mathbf{S}_{\nu})] \quad (4.3.31)$$

where we have used the invariance of the tensor product under interchange of  $\alpha$  and  $\beta$ . The task is now to find the values of the parameters  $a$  and  $b$ . For a generic system beyond this example, the task can be formulated as follows: A tensor  $T$  is given whose scalar component  $\{T\}_0$  shall be decomposed. There is a set  $\{A_i\}$  of possible scalar terms, which can occur in the decomposition. Thus, we have to solve the system of linear equations

$$\{T\}_0 = \sum_i a_i A_i \quad (4.3.32)$$

for the parameters  $a_i \in \mathbb{R}$ . For more complicated tensors, in which a large number of possible scalar spin products can occur, this step becomes intricate.

Back to our example: Since the  $S_{\alpha}^{-} S_{\beta}^{-}$  term in (4.3.30) originates from the second term in (4.3.31), it follows immediately that  $b = 2$ . To obtain  $a$ , we write out the second term in (4.3.31) for  $\alpha \neq \beta \neq \mu, \nu$ ,

$$\begin{aligned} &2 [(\mathbf{S}_{\alpha} \mathbf{S}_{\mu})(\mathbf{S}_{\beta} \mathbf{S}_{\nu}) + (\mathbf{S}_{\beta} \mathbf{S}_{\mu})(\mathbf{S}_{\alpha} \mathbf{S}_{\nu})] \\ &= \frac{1}{2} (2S_{\alpha}^z S_{\mu}^z + S_{\alpha}^{+} S_{\mu}^{-} + S_{\alpha}^{-} S_{\mu}^{+}) (2S_{\beta}^z S_{\nu}^z + S_{\beta}^{+} S_{\nu}^{-} + S_{\beta}^{-} S_{\nu}^{+}) \\ &\quad + \text{same with } \alpha \leftrightarrow \beta \\ &= S_{\alpha}^{+} S_{\beta}^{+} S_{\mu}^{-} S_{\nu}^{-} + S_{\alpha}^{-} S_{\beta}^{-} S_{\mu}^{+} S_{\nu}^{+} \\ &\quad + S_{\alpha}^z S_{\mu}^z (S_{\beta}^{+} S_{\nu}^{-} + S_{\beta}^{-} S_{\nu}^{+}) + S_{\beta}^z S_{\mu}^z (S_{\alpha}^{+} S_{\nu}^{-} + S_{\alpha}^{-} S_{\nu}^{+}) \\ &\quad + (S_{\alpha}^{+} S_{\mu}^{-} + S_{\alpha}^{-} S_{\mu}^{+}) S_{\beta}^z S_{\nu}^z + (S_{\beta}^{+} S_{\mu}^{-} + S_{\beta}^{-} S_{\mu}^{+}) S_{\alpha}^z S_{\nu}^z \\ &\quad + \frac{1}{2} (S_{\alpha}^{+} S_{\beta}^{-} + S_{\alpha}^{-} S_{\beta}^{+}) (S_{\mu}^{+} S_{\nu}^{-} + S_{\mu}^{-} S_{\nu}^{+}) + 4S_{\alpha}^z S_{\beta}^z S_{\mu}^z S_{\nu}^z. \end{aligned} \quad (4.3.33)$$

Subtracting this from (4.3.30), we obtain

$$\begin{aligned}
& 5 \{T_{\alpha\beta}^0 T_{\mu\nu}^0\}_0 - 2 [(\mathbf{S}_\alpha \mathbf{S}_\mu)(\mathbf{S}_\beta \mathbf{S}_\nu) + (\mathbf{S}_\beta \mathbf{S}_\mu)(\mathbf{S}_\alpha \mathbf{S}_\nu)] \\
&= \frac{1}{6} (4S_\alpha^z S_\beta^z - S_\alpha^+ S_\beta^- - S_\alpha^- S_\beta^+) (4S_\mu^z S_\nu^z - S_\mu^+ S_\nu^- - S_\mu^- S_\nu^+) \\
&\quad - \frac{1}{2} (S_\alpha^+ S_\beta^- + S_\alpha^- S_\beta^+) (S_\mu^+ S_\nu^- + S_\mu^- S_\nu^+) - 4 S_\alpha^z S_\beta^z S_\mu^z S_\nu^z \\
&= -\frac{4}{3} S_\alpha^z S_\beta^z S_\mu^z S_\nu^z \\
&\quad - \frac{2}{3} (S_\alpha^+ S_\beta^- + S_\alpha^- S_\beta^+) S_\mu^z S_\nu^z - \frac{2}{3} S_\alpha^z S_\beta^z (S_\mu^+ S_\nu^- + S_\mu^- S_\nu^+) \\
&\quad - \frac{1}{3} (S_\alpha^+ S_\beta^- + S_\alpha^- S_\beta^+) (S_\mu^+ S_\nu^- + S_\mu^- S_\nu^+) \\
&= -\frac{4}{3} (\mathbf{S}_\alpha \mathbf{S}_\beta)(\mathbf{S}_\mu \mathbf{S}_\nu), \tag{4.3.34}
\end{aligned}$$

or

$$5 \{T_{\alpha\beta}^0 T_{\mu\nu}^0\}_0 = -\frac{4}{3} (\mathbf{S}_\alpha \mathbf{S}_\beta)(\mathbf{S}_\mu \mathbf{S}_\nu) + 2 [(\mathbf{S}_\alpha \mathbf{S}_\mu)(\mathbf{S}_\beta \mathbf{S}_\nu) + (\mathbf{S}_\beta \mathbf{S}_\mu)(\mathbf{S}_\alpha \mathbf{S}_\nu)] \tag{4.3.35}$$

As an aside, the Clebsch–Gordan coefficient

$$\langle 2, 0; 2, 0 | 1, 0 \rangle = 0 \tag{4.3.36}$$

in (4.3.28) implies that the tensor product of  $T_{\alpha\beta}^0$  and  $T_{\mu\nu}^0$  has no vector component, i.e.,

$$\{T_{\alpha\beta}^0 T_{\mu\nu}^0\}_1 = 0. \tag{4.3.37}$$

### 4.3.5 Structure of the parent Hamiltonian

The expressions for the parent Hamiltonians (4.2.20)-(4.2.23), projected onto their scalar component as detailed in Section 4.3.3, will now be written out explicitly.

To shorten notation, we define for one-dimensional systems

$$w_{\alpha\mu\nu} := \bar{M}_{\alpha\mu} M_{\alpha\nu}, \tag{4.3.38}$$

and for two-dimensional systems

$$w_{\alpha\mu\nu}^{ab} := \bar{M}_{\alpha\mu}^{ab} M_{\alpha\nu}^{ab}. \tag{4.3.39}$$

The factors  $M_{\alpha\nu}$  and  $M_{\alpha\nu}^{ab}$  are defined in (4.2.4) and (4.2.7).

The first two-dimensional spin  $s$  system we investigate has the parent Hamiltonian

$$H_0^{s,2} = \sum_{\langle \alpha, \beta \rangle} \left[ \sum_{\substack{\mu \neq \nu \\ (\mu, \nu \neq \alpha, \beta)}} w_{\alpha\mu\nu}^{ab} w_{\beta\mu\nu}^{ab} \mathcal{H}_{\alpha\beta\mu\nu}^{s, \neq} + \sum_{\substack{\mu \\ (\mu \neq \alpha, \beta)}} w_{\alpha\mu\mu}^{ab} w_{\beta\mu\mu}^{ab} \mathcal{H}_{\alpha\beta\mu}^{s, =} \right]. \tag{4.3.40}$$

Such a system is labeled a “two-site” Hamiltonian, since two neighboring sites  $\alpha, \beta$  interact with one ( $\mu$ ) or two ( $\mu, \nu$ ) external sites. For a one-dimensional system, the prefactors  $w_{\alpha\mu\nu}^{ab}$  simply have to be replaced by  $w_{\alpha\mu\nu}$ . The Hamiltonian consists of two summands: In the first summand, the two neighboring sites  $\alpha$  and  $\beta$  interact with two distinct external sites  $\mu$  and  $\nu$ , which can be anywhere on the lattice. The second

summand treats the special case, in which the two external sites coincide,  $\mu = \nu$ . We call the expressions  $\mathcal{H}_{\alpha\beta\mu\nu}^{s,\neq}$  and  $\mathcal{H}_{\alpha\beta\mu}^{s,=}$  “small Hamiltonians”, since they describe a subsystem of only four ( $\mu \neq \nu$ ) or three interacting sites ( $\mu = \nu$ ). Explicitly written out, they read

$$\mathcal{H}_{\alpha\beta\mu\nu}^{s,\neq} = \{T_{\alpha\beta\nu}^3 T_{\alpha\beta\mu}^{-3}\}_0 = \{(S_\alpha^+)^{2s} (S_\beta^+)^{2s} S_\nu^+ (S_\alpha^-)^{2s} (S_\beta^-)^{2s} S_\mu^-\}_0, \quad (4.3.41)$$

and

$$\mathcal{H}_{\alpha\beta\mu}^{s,=} = \{T_{\alpha\beta\mu}^3 T_{\alpha\beta\mu}^{-3}\}_0 = \{(S_\alpha^+)^{2s} (S_\beta^+)^{2s} S_\mu^+ (S_\alpha^-)^{2s} (S_\beta^-)^{2s} S_\mu^-\}_0. \quad (4.3.42)$$

In case of a three-site interaction, three neighboring sites  $\alpha, \beta, \gamma$  interact with one or two external sites. The general form of the parent Hamiltonian for a two-dimensional spin  $s$  system is

$$H_0^{s,3} = \sum_{\langle \alpha, \beta, \gamma \rangle} \left[ \sum_{\substack{\mu \neq \nu \\ (\mu, \nu \neq \alpha, \beta, \gamma)}} w_{\alpha\mu\nu}^{ab} w_{\beta\mu\nu}^{a'b'} w_{\gamma\mu\nu}^{a''b''} \mathcal{H}_{\alpha\beta\gamma\mu\nu}^{s,\neq} + \sum_{\substack{\mu \\ (\mu \neq \alpha, \beta, \gamma)}} w_{\alpha\mu\mu}^{ab} w_{\beta\mu\mu}^{a'b'} w_{\gamma\mu\mu}^{a''b''} \mathcal{H}_{\alpha\beta\gamma\mu}^{s,=} \right]. \quad (4.3.43)$$

with the parameter choice given in (4.2.27),

$$(a, b) = (0, 0), \quad (a', b') = \left(\frac{1}{2}, 0\right) \quad \text{and} \quad (a'', b'') = \left(0, \frac{1}{2}\right).$$

The small Hamiltonians are

$$\mathcal{H}_{\alpha\beta\gamma\mu\nu}^{s,\neq} = \{T_{\alpha\beta\gamma\nu}^4 T_{\alpha\beta\gamma\mu}^{-4}\}_0 = \{(S_\alpha^+)^{2s} (S_\beta^+)^{2s} (S_\gamma^+)^{2s} S_\nu^+ (S_\alpha^-)^{2s} (S_\beta^-)^{2s} (S_\gamma^-)^{2s} S_\mu^-\}_0, \quad (4.3.44)$$

and

$$\mathcal{H}_{\alpha\beta\gamma\mu}^{s,=} = \{T_{\alpha\beta\gamma\mu}^4 T_{\alpha\beta\gamma\mu}^{-4}\}_0 = \{(S_\alpha^+)^{2s} (S_\beta^+)^{2s} (S_\gamma^+)^{2s} S_\mu^+ (S_\alpha^-)^{2s} (S_\beta^-)^{2s} (S_\gamma^-)^{2s} S_\mu^-\}_0. \quad (4.3.45)$$

Finally, for a four-site interaction, the general form of the parent Hamiltonian in a two-dimensional system with spin  $s$  is

$$H_0^{s,4} = \sum_{\langle \alpha, \beta, \gamma, \delta \rangle} \left[ \sum_{\substack{\mu \neq \nu \\ (\mu, \nu \neq \alpha, \beta, \gamma, \delta)}} w_{\alpha\mu\nu}^{ab} w_{\beta\mu\nu}^{ab} w_{\gamma\mu\nu}^{ab} w_{\delta\mu\nu}^{ab} \mathcal{H}_s^{\mu \neq \nu} + \sum_{\substack{\mu \\ (\mu \neq \alpha, \beta, \gamma, \delta)}} w_{\alpha\mu\mu}^{ab} w_{\beta\mu\mu}^{ab} w_{\gamma\mu\mu}^{ab} w_{\delta\mu\mu}^{ab} \mathcal{H}_s^{\mu = \nu} \right]. \quad (4.3.46)$$

The small Hamiltonians are

$$\begin{aligned} \mathcal{H}_{\alpha\beta\gamma\delta\mu\nu}^{s,\neq} &= \{T_{\alpha\beta\gamma\delta\nu}^5 T_{\alpha\beta\gamma\delta\mu}^{-5}\}_0 \\ &= \{(S_\alpha^+)^{2s} (S_\beta^+)^{2s} (S_\gamma^+)^{2s} (S_\delta^+)^{2s} S_\nu^+ (S_\alpha^-)^{2s} (S_\beta^-)^{2s} (S_\gamma^-)^{2s} (S_\delta^-)^{2s} S_\mu^-\}_0, \end{aligned} \quad (4.3.47)$$

and

$$\begin{aligned} \mathcal{H}_{\alpha\beta\gamma\delta\mu}^{s,=} &= \{T_{\alpha\beta\gamma\delta\mu}^5 T_{\alpha\beta\gamma\delta\mu}^{-5}\}_0 \\ &= \{(S_\alpha^+)^{2s} (S_\beta^+)^{2s} (S_\gamma^+)^{2s} (S_\delta^+)^{2s} S_\mu^+ (S_\alpha^-)^{2s} (S_\beta^-)^{2s} (S_\gamma^-)^{2s} (S_\delta^-)^{2s} S_\mu^-\}_0. \end{aligned} \quad (4.3.48)$$

We numerically derive explicit expressions for the small Hamiltonians in Section 4.5, consisting of simple scalar spin terms. This allows to develop a better intuition about the underlying models. In Section 4.6, we calculate the eigenspectra of these Hamiltonians in order to check whether they are local parent Hamiltonians for the Abelian and non-Abelian CSL.

## 4.4 Implementation details

We wish to demonstrate numerically, that the suggested Hamiltonians in Section 4.5 are indeed the parent Hamiltonians for the CSLs for a two-dimensional system with spin  $s$ . To achieve this, three numerical tasks are accomplished: First, the small Hamiltonians  $\mathcal{H}^{s,\neq}$  and  $\mathcal{H}^{s,=}$ , listed in Section 4.3.5, are decomposed into simple scalar spin products. This allows to have a better intuition about the underlying model, since we can analyze its constituent scalar spin interaction terms. We detail the numerical challenges in Section 4.4.1 and present results in Section 4.5. Second, the parent Hamiltonians (4.3.40)-(4.3.46) are constructed from the small Hamiltonians we obtained in the first step by choosing a lattice geometry and system size, then summing over all possible site configurations. This is explained in Section 4.4.2. In the third and final step, explained in Section 4.4.3, these Hamiltonians are diagonalized to obtain their eigenspectrum. We present our results in Section 4.6.

### 4.4.1 Numerical decomposition of tensor operators

Section 4.3.4 demonstrates the analytical decomposition of generic tensor expressions into simple spin products. Performing this task by hand is intricate and becomes unfeasible for more complex tensor expressions. We now present an exact numerical technique which resolves this problem. The essential idea is to gather all possible scalar spin terms which can possibly contribute to the tensor product we wish to decompose. We then determine the coefficients of the linear combination of these scalar terms which equals the tensor product.

We have implemented a program in Wolfram *Mathematica*<sup>®</sup> [153] which can decompose tensor products consisting of up to fourteen spin operators in total. Larger products can be decomposed in theory, though the computation time becomes excessively large. Our numerical method enables us to calculate the parent Hamiltonian for systems with spin 1/2, 1 and even 3/2. *Mathematica* uses the Wolfram Language. This high-level, dynamically typed, interactive programming language is symbolic and provides nearly 6000 built-in functions and algorithms.

For the interested reader, a copy of our program for the decomposition of the small Hamiltonian (4.3.44) of a spin-1 system with a three-site Hamiltonian is printed in Appendix D.

#### Finding all scalar spin terms

Before we can decompose a given tensor according to the linear equation (4.3.32), we have to find all spin products which possibly occur in the decomposition. With a few preliminary considerations, many spin terms can be excluded.

We illustrate how to find all scalar products with two examples: (1) A spin 1/2 system with a three-site interaction; (2) a spin 1 system with a two-site interaction. As a reminder, we define an “ $n$ -site” small Hamiltonian to describe an interaction of  $n$  neighboring sites with one or two external sites, as further explained in Section 4.3.5.

For a spin 1/2 system with a three-site interaction, the two small Hamiltonians (4.3.44) and (4.3.45) have to be decomposed. We start with

$$\mathcal{H}_{\alpha\beta\gamma\mu}^{1/2,=} = \{S_{\alpha}^{+} S_{\beta}^{+} S_{\gamma}^{+} S_{\mu}^{+} S_{\alpha}^{-} S_{\beta}^{-} S_{\gamma}^{-} S_{\mu}^{-}\}_0 =: \{T\}_0. \quad (4.4.1)$$

Using the identity for spin 1/2-systems,

$$S_i^{+} S_i^{-} = S_i^z + \frac{1}{2}, \quad (4.4.2)$$

tensor  $T$  can be rewritten as



$$\begin{aligned}
T &= (S_\alpha^z + \frac{1}{2})(S_\beta^z + \frac{1}{2})(S_\gamma^z + \frac{1}{2})(S_\mu^z + \frac{1}{2}) \\
&= \frac{1}{16} + \frac{1}{8}(S_\alpha^z + S_\beta^z + S_\gamma^z + S_\mu^z) \\
&\quad + \frac{1}{4}(S_\alpha^z S_\beta^z + S_\alpha^z S_\gamma^z + S_\beta^z S_\gamma^z + S_\alpha^z S_\mu^z + S_\beta^z S_\mu^z + S_\gamma^z S_\mu^z) \\
&\quad + \frac{1}{2}(S_\alpha^z S_\beta^z S_\gamma^z + S_\alpha^z S_\beta^z S_\mu^z + S_\alpha^z S_\gamma^z S_\mu^z + S_\beta^z S_\gamma^z S_\mu^z) + S_\alpha^z S_\beta^z S_\gamma^z S_\mu^z.
\end{aligned} \tag{4.4.3}$$

The projection on the scalar component for the individual terms in (4.4.3) is

$$\begin{aligned}
\{1\}_0 &= 1, \\
\{S_\alpha^z\}_0 &= 0, \\
\{S_\alpha^z S_\beta^z\}_0 &\propto (\mathbf{S}_\alpha \cdot \mathbf{S}_\beta), \\
\{S_\alpha^z S_\beta^z S_\gamma^z\}_0 &= 0, \\
\{S_\alpha^z S_\beta^z S_\gamma^z S_\mu^z\}_0 &\propto ((\mathbf{S}_\alpha \cdot \mathbf{S}_\beta)(\mathbf{S}_\gamma \cdot \mathbf{S}_\mu) + (\mathbf{S}_\alpha \cdot \mathbf{S}_\gamma)(\mathbf{S}_\beta \cdot \mathbf{S}_\mu) \\
&\quad + (\mathbf{S}_\beta \cdot \mathbf{S}_\gamma)(\mathbf{S}_\alpha \cdot \mathbf{S}_\mu)).
\end{aligned}$$

It is not necessary to calculate these projections explicitly as we do not need any prefactors for our numerical analysis.

In total, there can thus be four different types of scalar terms in  $\mathcal{H}_{\alpha\beta\mu}^{1/2,=}$ :

$$\begin{aligned}
(1) \quad & 1, & & \text{a constant,} \\
(2) \quad & (\mathbf{S}_i \cdot \mathbf{S}_j), & & (i, j) = (\alpha, \beta), (\alpha, \gamma), (\beta, \gamma), \\
(3) \quad & (\mathbf{S}_i \cdot \mathbf{S}_\mu), & & i = \alpha, \beta, \gamma, \\
(4) \quad & (\mathbf{S}_i \cdot \mathbf{S}_\mu)(\mathbf{S}_j \cdot \mathbf{S}_k), & & (i, j, k) = (\alpha, \beta, \gamma), (\beta, \gamma, \alpha), (\gamma, \alpha, \beta).
\end{aligned} \tag{4.4.4}$$

The second small Hamiltonian  $\mathcal{H}_{\alpha\beta\gamma\mu\nu}^{1/2,\neq} =: \{T'\}_0$  of the spin-1/2 system, (4.3.44), can be rewritten as

$$\begin{aligned}
T' &= (S_\alpha^z + \frac{1}{2})(S_\beta^z + \frac{1}{2})(S_\gamma^z + \frac{1}{2})S_\nu^+ S_\mu^- \\
&= \left[ \frac{1}{8} + \frac{1}{4}(S_\alpha^z + S_\beta^z + S_\gamma^z) + \frac{1}{2}(S_\alpha^z S_\beta^z + S_\alpha^z S_\gamma^z + S_\beta^z S_\gamma^z) + S_\alpha^z S_\beta^z S_\gamma^z \right] S_\nu^+ S_\mu^-.
\end{aligned} \tag{4.4.5}$$

We see that, when projecting  $T'$  onto its scalar component, no constant term can occur due to the factor  $S_\nu^+ S_\mu^-$ . Using Appendix B, we have

$$\begin{aligned}
\{S_\alpha^z S_\nu^+ S_\mu^-\}_0 &\propto i\mathbf{S}_\alpha \cdot (\mathbf{S}_\mu \times \mathbf{S}_\nu), \\
\{S_\alpha^z S_\beta^z S_\nu^+ S_\mu^-\}_0 &\propto (\mathbf{S}_\alpha \cdot \mathbf{S}_\mu)(\mathbf{S}_\beta \cdot \mathbf{S}_\nu) + (\mathbf{S}_\beta \cdot \mathbf{S}_\mu)(\mathbf{S}_\alpha \cdot \mathbf{S}_\nu) \\
&\quad + (\mathbf{S}_\alpha \cdot \mathbf{S}_\beta)(\mathbf{S}_\mu \cdot \mathbf{S}_\nu), \\
\{S_\alpha^z S_\beta^z S_\gamma^z S_\nu^+ S_\mu^-\}_0 &\propto i[(\mathbf{S}_\beta \cdot \mathbf{S}_\gamma)\mathbf{S}_\alpha + (\mathbf{S}_\alpha \cdot \mathbf{S}_\gamma)\mathbf{S}_\beta + (\mathbf{S}_\alpha \cdot \mathbf{S}_\beta)\mathbf{S}_\gamma] \cdot (\mathbf{S}_\mu \times \mathbf{S}_\nu).
\end{aligned}$$

The small Hamiltonian  $\mathcal{H}_{\alpha\beta\gamma\mu\nu}^{1/2,\neq}$  therefore can be decomposed into the terms

$$\begin{aligned}
(1) \quad & (\mathbf{S}_\mu \cdot \mathbf{S}_\nu), \\
(2) \quad & (\mathbf{S}_i \cdot \mathbf{S}_j)(\mathbf{S}_\mu \cdot \mathbf{S}_\nu), & & (i, j) = (\alpha, \beta), (\alpha, \gamma), (\beta, \gamma), \\
(3) \quad & i\mathbf{S}_i \cdot (\mathbf{S}_\mu \times \mathbf{S}_\nu), & & i = \alpha, \beta, \gamma, \\
(4) \quad & (\mathbf{S}_i \cdot \mathbf{S}_j)i\mathbf{S}_k \cdot (\mathbf{S}_\mu \times \mathbf{S}_\nu), & & (i, j, k) = (\alpha, \beta, \gamma), (\beta, \gamma, \alpha), (\gamma, \alpha, \beta),
\end{aligned} \tag{4.4.6}$$

$$(5) \quad (\mathbf{S}_i \cdot \mathbf{S}_\mu)(\mathbf{S}_j \cdot \mathbf{S}_\nu), \quad (i, j) = (\alpha, \beta), (\alpha, \gamma), (\beta, \gamma).$$

For a spin-1 system, the decomposition contains even more terms, as the small Hamiltonians are built out of more spin operators. For instance, given a two-site model, the small Hamiltonian with  $\mu = \nu$  is

$$\mathcal{H}_{\alpha\beta\mu}^{1,\pm} = \{(S_\alpha^+)^2(S_\beta^+)^2S_\mu^+(S_\alpha^-)^2(S_\beta^-)^2S_\mu^-\}_0 =: \{T\}_0. \quad (4.4.7)$$

This time, the identity

$$(S_i^+)^2(S_i^-)^2 = 2S_i^z(S_i^z + 1),$$

is useful. Applying the same method as for the spin-1/2 system, we see that the following scalar terms can occur:

$$\begin{aligned} (1) & \quad 1, \quad \text{a constant,} \\ (2) & \quad (\mathbf{S}_\alpha \cdot \mathbf{S}_\beta), \\ (3) & \quad (\mathbf{S}_\alpha \cdot \mathbf{S}_\beta)^2, \\ (4) & \quad (\mathbf{S}_\alpha + \mathbf{S}_\beta) \cdot \mathbf{S}_\mu, \\ (5) & \quad (\mathbf{S}_\alpha \cdot \mathbf{S}_\beta)(\mathbf{S}_\alpha + \mathbf{S}_\beta) \cdot \mathbf{S}_\mu, \\ (6) & \quad (\mathbf{S}_\alpha \cdot \mathbf{S}_\mu)^2 + (\mathbf{S}_\beta \cdot \mathbf{S}_\mu)^2, \\ (7) & \quad (\mathbf{S}_\alpha \cdot \mathbf{S}_\mu)(\mathbf{S}_\beta \cdot \mathbf{S}_\mu), \\ (8) & \quad (\mathbf{S}_\alpha \cdot \mathbf{S}_\beta)(\mathbf{S}_\alpha \cdot \mathbf{S}_\mu)(\mathbf{S}_\beta \cdot \mathbf{S}_\mu) + (\mathbf{S}_\alpha \cdot \mathbf{S}_\mu)(\mathbf{S}_\beta \cdot \mathbf{S}_\mu)(\mathbf{S}_\alpha \cdot \mathbf{S}_\beta). \end{aligned} \quad (4.4.8)$$

When constructing the scalar terms, we have to be aware that the order of the spin operators for systems with  $s > 1/2$  is relevant since repeated indices may occur in the tensors. The higher the number of neighboring sites in the parent Hamiltonian and the higher the spin  $s$ , the more scalar terms can occur in the decomposition. In practice, this makes a numerical approach necessary.

### Implementation of the scalar terms

At the beginning of the numerical implementation, a tensor representation for the spin operators acting on a single-site system has to be chosen. As outlined in Appendix A, we choose a  $SU(2)$ -matrix representation for the individual spin operators of each site. Given a spin  $s$ , the matrices have dimension  $(2s+1) \times (2s+1)$ .

If our system consists of  $N$  sites, the dimension of the Hilbert space is  $(2s+1)^N \times (2s+1)^N$ . A tensor operator  $T^N$  living in this many-site system can be created out of  $N$  single-site operators  $t_i$ ,  $i = 1, \dots, N$ , by taking the direct product,

$$T^N = t_1 \otimes t_2 \otimes \dots \otimes t_N. \quad (4.4.9)$$

For instance, the single-site spin operator  $\mathbf{S}_1$  becomes

$$\mathbf{S}_1 \otimes \underbrace{\mathbf{1} \otimes \dots \otimes \mathbf{1}}_{N-1 \text{ times}}. \quad (4.4.10)$$

The advantage of Mathematica's language for our purpose is, that it supports tensors as nested lists, where the nesting level corresponds to the rank of the tensor. The direct product in (4.4.9) can be taken by applying the built-in function

$$\text{TensorProduct}[\mathbf{t1}, \mathbf{t2}, \dots, \mathbf{tN}].$$

Since we are only calculating small Hamiltonians with Mathematica, the systems consist of only a few sites. For instance, for spin 1/2 and a three-site Hamiltonian (4.3.43), the total number of sites in the small Hamiltonian (4.3.44), including the external sites  $\mu$  and  $\nu$ , is  $N = 5$ . The Hilbert space has dimension  $2^5 \times 2^5$ , i. e. the Hamiltonian matrix has 1024 elements. The higher the spin and the more sites involved, the

larger the Hilbert space gets, for spin 3/2 and a two-site Hamiltonian, the small Hamiltonian (4.3.41) lives in a  $4^4 \times 4^4$ -Hilbert space, and the Hamiltonian matrix has 65,536 elements. This makes efficient programming necessary.

With the Hilbert space set-up, the scalar product of two spin operators can be implemented in a few lines of code. We have written the function

`ScalarProd[SiteList_],`

which takes as argument an occupation list, indicating which sites occur in the scalar product. An occupation list suffices since the site indices are always distinct, and therefore the spin operators commute in the scalar product. For instance, if our system consisted of the five sites  $\alpha, \beta, \gamma, \mu, \nu$  and we wanted to calculate  $\mathbf{S}_\alpha \cdot \mathbf{S}_\mu$ , the corresponding argument would be `SiteList = {1, 0, 0, 1, 0}`. Inside the function, the three direct products

$$\begin{aligned} S_\alpha^z \otimes \mathbb{1} \otimes \mathbb{1} \otimes S_\mu^z \otimes \mathbb{1}, \\ \frac{1}{2} S_\alpha^+ \otimes \mathbb{1} \otimes \mathbb{1} \otimes S_\mu^- \otimes \mathbb{1}, \\ \frac{1}{2} S_\alpha^- \otimes \mathbb{1} \otimes \mathbb{1} \otimes S_\mu^+ \otimes \mathbb{1} \end{aligned}$$

are calculated, added and flattened to a matrix which then is returned. A flattening becomes necessary since *Mathematica* can only treat matrix but not tensor equations, which we need to solve later in the program. On the level of implementation, flattening means nested lists are “unraveled” into a list of one-dimensional lists, which represents a matrix.

Since we wish to decompose a tensor into simple scalar spin products, we have written a function

`ArbTensor[P_, N_],`

which calculates arbitrary spin products, such as the products listed in (4.4.4), (4.4.6) and (4.4.8). The central insight is that all terms occurring in a scalar tensor decomposition are scalar products of an even number of sites. Even the vector product  $i\mathbf{S}_\alpha \cdot (\mathbf{S}_\mu \times \mathbf{S}_\nu)$  can be rewritten in terms of scalar products using the identity

$$i\mathbf{S}_\alpha \cdot (\mathbf{S}_\mu \times \mathbf{S}_\nu) = (\mathbf{S}_\alpha \cdot \mathbf{S}_\mu)(\mathbf{S}_\alpha \cdot \mathbf{S}_\nu) - (\mathbf{S}_\alpha \cdot \mathbf{S}_\nu)(\mathbf{S}_\alpha \cdot \mathbf{S}_\mu). \quad (4.4.11)$$

We encode such scalar product terms in two lists: A list `RR` of the indices, and a list `P` of the pairing of the indices. For instance, if the term

$$\sum_{p=x,y,z} \sum_{(i,j,k) \in \tilde{\mathcal{P}}_6^3} S_i^p (\mathbf{S}_j \cdot \mathbf{S}_\mu) (\mathbf{S}_i \cdot \mathbf{S}_\mu) S_j^p,$$

with

$$\tilde{\mathcal{P}}_6^3 := \{(\alpha, \beta, \gamma), (\alpha, \gamma, \beta), (\beta, \gamma, \alpha), (\beta, \alpha, \gamma), (\gamma, \alpha, \beta), (\gamma, \beta, \alpha)\}$$

shall be implemented, we have `RR = {i, j, μ, i, μ, j}` and `P = {1, 3, 4, 5, 6, 2}`. In contrast to the function `ScalarProd[SiteList]`, this function requires two lists, since the order of the spin indices matters.

Inside of our function `ArbTensor`, the sum over all permutations  $\tilde{\mathcal{P}}_6^3$  of the neighboring indices  $\alpha, \beta, \gamma$  is generated by a function

```
LL[x_, y_, z_, d_, N_] :=
  Which[N == 6, Permute[{x, y, z, d}, SymmetricGroup[4]],
        N == 5, Permute[{x, y, z}, SymmetricGroup[3]],
        N == 4, Permute[{x, y}, SymmetricGroup[2]]];
```

which works for systems with two ( $N = 4$ ), three ( $N = 5$ ) and four ( $N = 6$ ) neighboring sites and two external sites.

With all necessary spin operations set-up, we can generate and save all possible scalar terms  $U_k$ .

### Finding the coefficients of the scalar terms

The small Hamiltonian we wish to decompose can always be written as a product of two tensors,

$$\mathcal{H}^s =: \{T_{i_1, \dots, i_M}^M T_{j_1, \dots, j_M}^{-M}\}_0. \quad (4.4.12)$$

For the labeling of the indices, we use the convention introduced in (4.3.27).

To calculate (4.4.12), we first need a way to create tensors of the type  $T_{i_1, \dots, i_M}$ . For this purpose, we provide a function

**CreateTensor**[Tlist\_].

As an argument, it takes an occupation list of sites. For instance, in a Hilbert space with five sites  $\alpha, \beta, \gamma, \mu, \nu$ , the choice **Tlist** = {1, 1, 0, 1, 0} instructs **CreateTensor** to calculate  $T_{\alpha, \beta, \mu}$ . The function implements the method described in Appendix B, starting with (B.2.3). First, the highest order tensor component  $T_{i_1, \dots, i_M}^M$  is setup by taking the direct product of single-site spin operators and adding them up. For the aforementioned example, this means

$$\begin{aligned} T_{\alpha, \beta, \mu}^3 &= (S_\alpha^+)^{2s} (S_\beta^+)^{2s} S_\mu^+ \\ &\hat{=} ((S_\alpha^+)^{2s} \otimes \mathbb{1} \otimes \mathbb{1}) \cdot (\mathbb{1} \otimes (S_\beta^+)^{2s} \otimes \mathbb{1}) \cdot (\mathbb{1} \otimes \mathbb{1} \otimes S_\mu^+). \end{aligned}$$

Then, the ladder operator

$$S_{tot}^- = S_{i_1}^- + S_{i_2}^- + \dots + S_{i_M}^-, \quad (4.4.13)$$

is implemented (in this example for spin 1/2) via

```
sm := {{0, 0}, {1, 0}}
SpinIndex = Flatten[Position[Tlist, x_/; x > 0]];
Smtemp = 0;
SmArgs = Table[IdentityMatrix[2], {i, N}];
For[j = 1, j < (M + 1), SmArgs[[SpinIndex[[j]]]] = sm;
  Smtemp+ = (TensorProduct@@@SmArgs)[[1]];
  SmArgs = Table[IdentityMatrix[2], {i, N}]; j++;
Smtot := Flatten[Smtemp, {Table[2 * i - 1, {i, N}], Table[2 * i, {i, N}]}];
```

The first line defines a single-site ladder operator  $S_i^-$ . The second line lists the indices which contribute to the tensor. Taking the above example, where **Tlist** = {1, 1, 0, 1, 0}, **SpinIndex** evaluates to {1, 2, 4}, meaning that sites  $\alpha, \beta, \mu$  contribute. With a for-loop, the single-site ladder operators  $S_i^-$  are transformed into the  $N$ -site basis and summed up, yielding the total ladder operator (4.4.13). Applying this operator recursively to our tensor, beginning with its highest component, we obtain the return expression of the function, a list of all tensor components in decreasing order,  $\{T_{i_1, \dots, i_M}^M, T_{i_1, \dots, i_M}^{M-1}, \dots, T_{i_1, \dots, i_M}^{-M}\}$ .

Our program is generic enough to project onto an arbitrary component of the tensor. Here, however, we only project onto the scalar component. To project the tensor product  $T_{i_1, \dots, i_M}^M T_{j_1, \dots, j_M}^{-M}$  of (4.4.12) onto its scalar component, we directly implement (4.3.26) via a function

**TProject**[Tm1List\_, Tm2List\_, m1\_, m2\_, jres\_],

where `Tm1List` is the list of all components of tensor  $T_{i_1, \dots, i_M}$ , created via the function `CreateTensor` and similarly, `Tm2List` is the list of all components of  $T_{j_1, \dots, j_M}$ . Projection onto the scalar component is achieved by setting `jres = 1`, and the components `m1 = M` and `m2 = -M`.

To calculate the coefficient  $\{a_k\}$  of the contribution of each scalar term  $U_k$  to the tensor product, the system of linear equations

$$\{T_{i_1, \dots, i_M}^M T_{j_1, \dots, j_N}^{-M}\}_0 = \sum_{k=1}^r a_k U_k \quad (4.4.14)$$

has to be solved, where  $r$  is the number of scalar terms. This system is highly overdetermined, since we have in total  $t := (2s + 1)^{2N}$  equations, which is significantly larger than the number of coefficients,  $t \gg r$ . However, the matrices are sparse, effectively reducing the number of equations, since many equations are fulfilled trivially.

In our *Mathematica*-program, we have automated all previous steps into a single function

```
ResStructure[Tm1List_, Tm2List_, m1_, m2_, jres_, ResTerms_],
```

which takes as arguments the two tensors `Tm1List` and `Tm2List` contributing to the tensor product (4.4.12), their components `m1 = M` and `m2 = -M`, the component onto which we wish to project, `jres = 0`, and the list of scalar terms `ResTerms`  $\hat{=}$   $\{U_k\}$ , which can occur in the result. It returns a list of the coefficients  $\{a_1, \dots, a_r\}$ .

Using this *Mathematica*-program, we construct the small Hamiltonians for spin-1/2, spin-1 and spin-3/2 systems. The results are presented in Section 4.5.

Especially for higher spin systems, it is useful to reduce the number of coefficients by considering which scalar terms have equal coefficients due to the incorporated symmetries to save computation time.

Apart from its benefits for the decomposition into scalar spin products, the above described numerical method to write out arbitrary tensor products has one major advantage for the implementation of Hamiltonians for the CSL: It provides a user-friendly and efficient framework to obtain the matrix of the parent Hamiltonian without having to implement all individual spin products. This is especially relevant for systems with a higher spin  $s$  or with many-body interactions of three or more sites, since the number of spin terms increases decisively. In the *Mathematica*-program, we simply have to evaluate the function

```
TProject[Tm1List_, Tm2List_, m1_, m2_, jres_]
```

for a given system to obtain its Hamiltonian matrix for further numerical studies.

#### 4.4.2 From a small Hamiltonian to a parent Hamiltonian

With the small Hamiltonians set up, the complete parent Hamiltonians can now be calculated. We have chosen a 16-site lattice with periodic boundary conditions, which allows to numerically analyze the eigenspectra of our suggested parent Hamiltonians. Due to the exponential growth of the Hilbert space with system size, this is also the maximal site number accessible to our technical equipment in a decent amount of computation time.

Two different lattice geometries are implemented to analyze how they influence the eigenspectra: the square and triangular lattice. The choice of parameters  $(a, b)$  for the  $\vartheta$ -functions in the prefactors of the small Hamiltonians decides upon the conservation of rotational invariance. This will be explained in Section 4.6.

In what we refer to as an  $n$ -site term in the construction of the parent Hamiltonians, (4.3.40)-(4.3.46), we sum over  $n$  neighboring sites. Obviously, there are, depending on the lattice geometry, multiple possibilities to choose a subset  $\mathcal{C}$  of nearest-neighboring sites. In some cases, it even turns out to be useful to include next-nearest neighbor configurations.

As summarized in Figure 4.2, we thus have two different versions of the parent Hamiltonian for the square (triangular) lattice: One Hamiltonian has a  $90^\circ$  ( $60^\circ$ ) rotational invariance, commensurate with the

lattice rotational symmetry, and is from now on labeled the “full version”. The other Hamiltonian does not have such a rotational invariance, and it will be labeled the “minimal version”. Depending on the set  $\mathcal{C}$  of configurations chosen, the quality of the resulting eigenvalue spectrum differs dramatically, which will be analyzed in detail in Section 4.6.

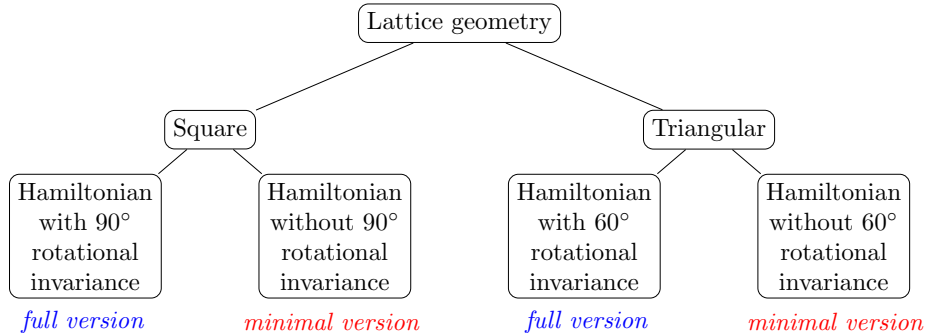


**Fig. 4.2** Two different lattice geometries are numerically analyzed: the square and the triangular lattice. For each lattice type, two different Hamiltonians are implemented: The so-called “full version” has the full rotational lattice symmetries. The “minimal” version does not have this rotational lattice invariance.

While the small Hamiltonians were calculated with *Mathematica*, we now switch gears. Since the systems investigated are growing exponentially with system size, an interpreted programming language such as *Mathematica*’s Wolfram Language would be too slow. Hence, the parent Hamiltonians are set up and diagonalized using the imperative programming language Fortran (2003 standard). Fortran is well suited to high performance computing and scientific computation and provides a huge number of libraries, e.g. LAPACK [2] for numerical linear algebra.

With the small Hamiltonians previously calculated and a set  $\mathcal{C}$  of configurations chosen, the next step is to take the sum

$$\sum_{\langle \alpha, \beta, \dots \rangle} \sum_{\substack{\mu \neq \nu \\ (\mu, \nu \neq \alpha, \beta, \dots)}} \quad (4.4.15)$$

in (4.3.40)-(4.3.46) over all lattice sites by applying the small Hamiltonians to all possible configurations of two, three or four neighboring sites, communicating with one or two external sites,  $\mu$  or  $\nu$ . In this process, the prefactors  $w_{\alpha\mu\nu}^{ab}$  have to be calculated, which involves computing multiple  $\vartheta$ -functions. As explained in Appendix C, these functions are defined by infinite sums. For instance, the odd  $\vartheta$ -function can be expressed as

$$\vartheta_{\frac{1}{2}, \frac{1}{2}}(z|\tau) = \sum_{n \in \mathbb{Z} + \frac{1}{2}} e^{\pi i n^2 \tau} e^{\pi i n z} e^{2\pi i n z}, \quad (4.4.16)$$

where we have shifted  $n$  by  $1/2$  as compared to the expression in (C.0.1). The convergence properties of the above sum can be visualized by rewriting  $\tau = \tau' + i\tau''$ , with  $\tau' \in \mathbb{R}$  and  $\tau'' \in \mathbb{R}^+$ . Obviously, convergence increases with larger  $\tau''$ . Under modular transformations

$$T : \tau \rightarrow \tau + 1, \quad \text{and} \quad S : \tau \rightarrow -\frac{1}{\tau}, \quad (4.4.17)$$

our system is invariant. Hence, it is always possible to choose a unit cell with  $\tau'' \geq \frac{\sqrt{3}}{2}$ . Even for the worst case of convergence in (4.4.16),  $\Im(z) = -\tau''$ , the series decays as  $e^{-\pi(n-2)n\tau''}$ , which is for  $\tau'' = 1$  of order 1 for  $n = \frac{1}{2}$  and of order  $10^{-27}$  for  $n = \frac{11}{2}$ . In contrast, the sum of all terms with  $n > \frac{11}{2}$  is below machine precision. Therefore, to calculate the  $\vartheta$ -functions, it is sufficient to only compute the 12 terms from  $n = -\frac{11}{2}$  to  $n = \frac{11}{2}$ .

Using translational symmetry, the Hilbert space can be reduced significantly, in our case by a factor of 16. The largest Hilbert spaces we analyzed were of order  $10^5 \times 10^5$ . To save memory, the Hamiltonians are therefore saved in a sparse matrix format.

#### 4.4.3 Calculation of the eigenspectra

With the Hamiltonian now numerically set up, the last step is to calculate the eigenspectrum by implementing an exact diagonalization algorithm [16; 109; 107]. After having obtained the eigenvectors of the true ground state, their overlaps with the CSL are calculated to determine the accuracy of the parent Hamiltonian.

A number of software libraries provide complete diagonalization routines. Examples are the NAGlibrary [3], the LAPACK library [2] or the algorithms published in *Numerical Recipes* [113]. In principle, these routines can be used to diagonalize the Hamiltonian matrix of a finite spin system. For large system sizes, however, it is generally much more efficient to use an iterative algorithm such as the Davidson algorithm [107] or the Lanczos algorithm [107; 82; 142].

The approach of the diagonalization routines is to transform first the matrix into tridiagonal form using a series of Householder transformations or Givens rotations. The resulting tridiagonal matrix is then diagonalized with the QR algorithm, which factorizes the matrix  $\mathbf{T} = \mathbf{QR}$  into an orthogonal  $\mathbf{Q}$  and an upper triangular matrix  $\mathbf{R}$ . Calculating eigenvalues and eigenvectors, the computational cost is  $\mathcal{O}(3n^3)$ . The drawback of this approach is obvious: The whole matrix has to be stored and the cost scales exponentially with system size.

For smaller systems, such as the spin-1/2 models with a Hilbert space of order  $10^4 \times 10^4$ , we have implemented an exact diagonalization routine from the LAPACK library, since it allows to analyze the degeneracy of the eigenstates easily. For larger systems, where execution time becomes critical, a Lanczos algorithm from the numerical software library ARPACK [91] is utilized.

Basis creation and matrix-vector multiplications are one of the most time-consuming parts of the program. By parallelizing these parts, we are able to reduce execution time by a factor of  $> 10$ . To do so, OpenMP is used, which is a standard for thread-memory multiprocessing [1]. It consists of a set of OpenMP directives (`!$omp parallel` in Fortran) and a run-time library. One of its advantages over other parallelization standards is that it requires only small changes in the source code. The programming paradigm is the so-called fork-join model which means that in the main code, there is only one master thread working through the serial code. Once the thread reaches a parallelized section, it forks into multiple threads and the work is shared equally. After finishing the parallel part, the threads join again, and the master thread continues with the serial code.

The eigenspectra of our parent Hamiltonians are analyzed in Section 4.6.

## 4.5 Results for a local parent Hamiltonian of the chiral spin liquid

In the previous Sections 4.2 and 4.3, we have outlined an analytical method to construct a parent Hamiltonian for a chiral spin liquid for systems with arbitrary spin. Section 4.4.1 details how to decompose a tensor operator into its scalar components numerically. We use this numerical technique to reformulate the small Hamiltonians  $\mathcal{H}^{s,\neq}$  and  $\mathcal{H}^{s,=}$  in (4.3.40)-(4.3.46) in terms of simple scalar spin products.

We have shown in (4.2.25) and (4.2.26) that locality in a two-dimensional system can be achieved by realizing a many-body interaction of three or more neighboring sites in the Hamiltonian. As mentioned above, in our method, the most intricate step is the final one, in which the Hamiltonian is projected onto its scalar component and decomposed into simple spin products. Since the Hilbert space grows exponentially for increasing spin  $s$ , the construction of a local Hamiltonian becomes computationally challenging. We have created parent Hamiltonians for systems with three different spin values: spin 1/2 systems with a two-, three- and four-site interaction, spin 1 systems with a two- and three-site interaction, as well as spin 3/2 systems with a two-site interaction.

In the following subsections, the small Hamiltonians decomposed into their scalar components for systems with spin 1/2, 1 and 3/2 are listed. In Sections 4.6 and 4.7, we numerically diagonalize the Hamiltonians for all spin-1/2 and spin-1 systems and successfully find that, indeed, these are parent Hamiltonians for the Abelian and non-Abelian CSLs.

### 4.5.1 Spin 1/2, two-site interaction

We start with the fermionic spin 1/2-system with a two-site interaction, the parent Hamiltonian consists of only a few terms. The small Hamiltonian for the case  $\mu \neq \nu$  of (4.3.40) is given by

$$\begin{aligned} \mathcal{H}_{\alpha\beta\mu\nu}^{1/2,\neq} &= \mathbf{S}_\mu \cdot \mathbf{S}_\nu + \frac{8}{5}(\mathbf{S}_\alpha \cdot \mathbf{S}_\beta)(\mathbf{S}_\mu \cdot \mathbf{S}_\nu) - i\mathbf{S}_\alpha \cdot (\mathbf{S}_\mu \times \mathbf{S}_\nu) \\ &\quad - \frac{4}{5}[(\mathbf{S}_\alpha \cdot \mathbf{S}_\mu)(\mathbf{S}_\beta \cdot \mathbf{S}_\nu) + (\mathbf{S}_\alpha \cdot \mathbf{S}_\nu)(\mathbf{S}_\beta \cdot \mathbf{S}_\mu)], \end{aligned} \quad (4.5.1)$$

and the small Hamiltonian for  $\mu = \nu$  is

$$\mathcal{H}_{\alpha\beta\mu}^{1/2,=} = \frac{3}{4} + \mathbf{S}_\alpha \cdot \mathbf{S}_\beta + (\mathbf{S}_\alpha + \mathbf{S}_\beta) \cdot \mathbf{S}_\mu. \quad (4.5.2)$$

### 4.5.2 Spin 1/2, three-site interaction

The small Hamiltonian for the case  $\mu \neq \nu$  for a spin 1/2 system with a three-site interaction (4.3.43) is

$$\begin{aligned} \mathcal{H}_{\alpha\beta\gamma\mu\nu}^{1/2,\neq} &= 5 \mathbf{S}_\mu \cdot \mathbf{S}_\nu + 8 (\mathbf{S}_\mu \cdot \mathbf{S}_\nu) [(\mathbf{S}_\alpha \cdot \mathbf{S}_\beta) + (\mathbf{S}_\alpha \cdot \mathbf{S}_\gamma) + (\mathbf{S}_\beta \cdot \mathbf{S}_\gamma)] \\ &\quad - 5i (\mathbf{S}_\alpha + \mathbf{S}_\beta + \mathbf{S}_\gamma) \cdot (\mathbf{S}_\mu \times \mathbf{S}_\nu) \\ &\quad - 2i [(\mathbf{S}_\beta \cdot \mathbf{S}_\gamma)\mathbf{S}_\alpha + (\mathbf{S}_\gamma \cdot \mathbf{S}_\alpha)\mathbf{S}_\beta + (\mathbf{S}_\alpha \cdot \mathbf{S}_\beta)\mathbf{S}_\gamma] \cdot (\mathbf{S}_\mu \times \mathbf{S}_\nu) \\ &\quad - 2 [(\mathbf{S}_\alpha \cdot \mathbf{S}_\mu)(\mathbf{S}_\beta \cdot \mathbf{S}_\nu) + (\mathbf{S}_\beta \cdot \mathbf{S}_\mu)(\mathbf{S}_\alpha \cdot \mathbf{S}_\nu) \\ &\quad \quad + (\mathbf{S}_\alpha \cdot \mathbf{S}_\mu)(\mathbf{S}_\gamma \cdot \mathbf{S}_\nu) + (\mathbf{S}_\gamma \cdot \mathbf{S}_\mu)(\mathbf{S}_\alpha \cdot \mathbf{S}_\nu) \\ &\quad \quad + (\mathbf{S}_\beta \cdot \mathbf{S}_\mu)(\mathbf{S}_\gamma \cdot \mathbf{S}_\nu) + (\mathbf{S}_\gamma \cdot \mathbf{S}_\mu)(\mathbf{S}_\beta \cdot \mathbf{S}_\nu)], \end{aligned} \quad (4.5.3)$$

and the small Hamiltonian for  $\mu = \nu$  is



$$\begin{aligned} \mathcal{H}_{\alpha\beta\gamma\mu}^{1/2,=} &= \frac{15}{4} + 5 [\mathbf{S}_\alpha + \mathbf{S}_\beta + \mathbf{S}_\gamma] \cdot \mathbf{S}_\mu + 5 [\mathbf{S}_\alpha \cdot \mathbf{S}_\beta + \mathbf{S}_\alpha \cdot \mathbf{S}_\gamma + \mathbf{S}_\beta \cdot \mathbf{S}_\gamma] \\ &+ 4 [(\mathbf{S}_\alpha \cdot \mathbf{S}_\beta) + (\mathbf{S}_\alpha \cdot \mathbf{S}_\gamma) + (\mathbf{S}_\beta \cdot \mathbf{S}_\gamma)] (\mathbf{S}_\gamma \cdot \mathbf{S}_\mu). \end{aligned} \quad (4.5.4)$$

### 4.5.3 Spin 1/2, four-site interaction

In case of a spin 1/2-system with a four-site interaction, the small Hamiltonian for  $\mu \neq \nu$  of (4.3.46) is

$$\begin{aligned} \mathcal{H}_{\alpha\beta\gamma\delta\mu\nu}^{1/2,\neq} &= 5 \mathbf{S}_\mu \cdot \mathbf{S}_\nu + 8 (\mathbf{S}_\mu \cdot \mathbf{S}_\nu) \sum_{(i,j) \in \mathcal{P}_6^2} (\mathbf{S}_i \cdot \mathbf{S}_j) \\ &+ \frac{12}{7} \sum_{(i,j,k,l) \in \mathcal{P}_6^4} (\mathbf{S}_i \cdot \mathbf{S}_j) (\mathbf{S}_k \cdot \mathbf{S}_l) (\mathbf{S}_\mu \cdot \mathbf{S}_\nu) \\ &- 5i (\mathbf{S}_\alpha + \mathbf{S}_\beta + \mathbf{S}_\gamma + \mathbf{S}_\delta) \cdot (\mathbf{S}_\mu \times \mathbf{S}_\nu) \\ &- 4i \sum_{(i,j,k) \in \mathcal{P}_{12}^3} (\mathbf{S}_i \cdot \mathbf{S}_j) \mathbf{S}_k \cdot (\mathbf{S}_\mu \times \mathbf{S}_\nu) \\ &- 2 \sum_{(i,j) \in \mathcal{P}_{12}^2} (\mathbf{S}_i \cdot \mathbf{S}_\mu) (\mathbf{S}_j \cdot \mathbf{S}_\nu) \\ &- \frac{8}{7} \sum_{(i,j,k,l) \in \mathcal{P}_{12}^4} (\mathbf{S}_i \cdot \mathbf{S}_j) (\mathbf{S}_k \cdot \mathbf{S}_\mu) (\mathbf{S}_l \cdot \mathbf{S}_\nu). \end{aligned} \quad (4.5.5)$$

To shorten the expression in (4.5.5), we sum over sets  $\mathcal{P}_n^m$ , which consist of  $n$   $m$ -tuples of indices. The first set  $\mathcal{P}_6^2$  consists of all possible unordered permutations of two of the four indices  $\alpha, \beta, \gamma, \delta$ ,

$$\mathcal{P}_6^2 = \{(\alpha, \beta), (\alpha, \gamma), (\alpha, \delta), (\beta, \gamma), (\beta, \delta)\}. \quad (4.5.6)$$

The total number of tuples in  $\mathcal{P}_6^2$  is  $4 \cdot 3/2 = 6$ . The other sets of permutations in (4.5.5) are defined as follows:

$$\mathcal{P}_6^4 = \{(\alpha, \beta, \gamma, \delta), (\alpha, \gamma, \beta, \delta), (\alpha, \delta, \beta, \gamma), (\beta, \gamma, \alpha, \delta), (\beta, \delta, \alpha, \gamma)\}, \quad (4.5.7)$$

$$\begin{aligned} \mathcal{P}_{12}^3 &= \{(\beta, \gamma, \alpha), (\beta, \gamma, \delta), (\alpha, \beta, \gamma), (\alpha, \beta, \delta), (\alpha, \gamma, \beta), (\alpha, \gamma, \delta), \\ &(\alpha, \delta, \beta), (\alpha, \delta, \gamma), (\beta, \delta, \alpha), (\beta, \delta, \gamma), (\gamma, \delta, \alpha), (\gamma, \delta, \beta)\}, \end{aligned} \quad (4.5.8)$$

$$\begin{aligned} \mathcal{P}_{12}^2 &= \{(\alpha, \beta), (\beta, \alpha), (\alpha, \gamma), (\gamma, \alpha), (\alpha, \delta), (\delta, \alpha), (\beta, \gamma), (\gamma, \beta), \\ &(\beta, \delta), (\delta, \beta)\}, \end{aligned} \quad (4.5.9)$$

$$\begin{aligned} \mathcal{P}_{12}^4 &= \{(\gamma, \delta, \alpha, \beta), (\gamma, \delta, \beta, \alpha), (\beta, \delta, \alpha, \gamma), (\beta, \delta, \gamma, \alpha), \\ &(\beta, \gamma, \alpha, \delta), (\beta, \delta, \delta, \alpha), (\alpha, \delta, \beta, \gamma), (\alpha, \delta, \gamma, \beta), \\ &(\alpha, \gamma, \beta, \delta), (\alpha, \gamma, \delta, \beta), (\alpha, \beta, \gamma, \delta), (\alpha, \beta, \delta, \gamma)\}. \end{aligned} \quad (4.5.10)$$

The small Hamiltonian for  $\mu = \nu$  is

$$\begin{aligned} \mathcal{H}_{\alpha\beta\gamma\delta\mu}^{1/2,=} &= \frac{15}{4} + 5 \sum_{(i,j) \in \mathcal{P}_6^2} (\mathbf{S}_i \cdot \mathbf{S}_j) + 4 \sum_{(i,j,k,l) \in \mathcal{P}_6^4} (\mathbf{S}_i \cdot \mathbf{S}_j) (\mathbf{S}_k \cdot \mathbf{S}_l) \\ &+ 5 [\mathbf{S}_\alpha + \mathbf{S}_\beta + \mathbf{S}_\gamma + \mathbf{S}_\delta] \cdot \mathbf{S}_\mu + 4 \sum_{(i,j,k) \in \mathcal{P}_{12}^3} (\mathbf{S}_i \cdot \mathbf{S}_j) (\mathbf{S}_k \cdot \mathbf{S}_\mu). \end{aligned} \quad (4.5.11)$$

#### 4.5.4 Spin 1, two-site interaction

Given a bosonic spin 1 system with a two-site interaction, the small Hamiltonian for  $\mu \neq \nu$  of (4.3.40) is

$$\begin{aligned}
\mathcal{H}_{\alpha\beta\mu\nu}^{1,\neq} = & 96 \mathbf{S}_\mu \cdot \mathbf{S}_\nu + 128 (\mathbf{S}_\alpha \cdot \mathbf{S}_\beta)(\mathbf{S}_\mu \cdot \mathbf{S}_\nu) + 54 (\mathbf{S}_\alpha \cdot \mathbf{S}_\beta)^2(\mathbf{S}_\mu \cdot \mathbf{S}_\nu) \\
& - 24 [(\mathbf{S}_\alpha \cdot \mathbf{S}_\mu)(\mathbf{S}_\beta \cdot \mathbf{S}_\nu) + (\mathbf{S}_\alpha \cdot \mathbf{S}_\nu)(\mathbf{S}_\beta \cdot \mathbf{S}_\mu)] \\
& - 8 (\mathbf{S}_\alpha \cdot \mathbf{S}_\beta) [(\mathbf{S}_\alpha \cdot \mathbf{S}_\mu)(\mathbf{S}_\beta \cdot \mathbf{S}_\nu) + (\mathbf{S}_\alpha \cdot \mathbf{S}_\nu)(\mathbf{S}_\beta \cdot \mathbf{S}_\mu)] \\
& - 8 [(\mathbf{S}_\alpha \cdot \mathbf{S}_\mu)(\mathbf{S}_\beta \cdot \mathbf{S}_\nu) + (\mathbf{S}_\alpha \cdot \mathbf{S}_\nu)(\mathbf{S}_\beta \cdot \mathbf{S}_\mu)] (\mathbf{S}_\alpha \cdot \mathbf{S}_\beta) \\
& - 8 [(\mathbf{S}_\alpha \cdot \mathbf{S}_\mu)(\mathbf{S}_\alpha \cdot \mathbf{S}_\nu) + (\mathbf{S}_\beta \cdot \mathbf{S}_\mu)(\mathbf{S}_\beta \cdot \mathbf{S}_\nu)] \\
& - 56i (\mathbf{S}_\alpha + \mathbf{S}_\beta) \cdot (\mathbf{S}_\mu \times \mathbf{S}_\nu) \\
& - 56i (\mathbf{S}_\alpha \cdot \mathbf{S}_\beta)(\mathbf{S}_\alpha + \mathbf{S}_\beta) \cdot (\mathbf{S}_\mu \times \mathbf{S}_\nu),
\end{aligned} \tag{4.5.12}$$

and for the small Hamiltonian with  $\mu = \nu$ , we get

$$\begin{aligned}
\mathcal{H}_{\alpha\beta\mu}^{1,=} = & 192 + 256 \mathbf{S}_\alpha \cdot \mathbf{S}_\beta + 96(\mathbf{S}_\alpha \cdot \mathbf{S}_\beta)^2 \\
& + 48(\mathbf{S}_\alpha + \mathbf{S}_\beta) \cdot \mathbf{S}_\mu + 56(\mathbf{S}_\alpha \cdot \mathbf{S}_\beta)(\mathbf{S}_\alpha + \mathbf{S}_\beta) \cdot \mathbf{S}_\mu \\
& + 16 [(\mathbf{S}_\alpha \cdot \mathbf{S}_\mu)^2 + (\mathbf{S}_\beta \cdot \mathbf{S}_\mu)^2] - 24(\mathbf{S}_\alpha \cdot \mathbf{S}_\mu)(\mathbf{S}_\beta \cdot \mathbf{S}_\mu) \\
& - 8(\mathbf{S}_\alpha \cdot \mathbf{S}_\beta)(\mathbf{S}_\alpha \cdot \mathbf{S}_\mu)(\mathbf{S}_\beta \cdot \mathbf{S}_\mu) \\
& - 8(\mathbf{S}_\alpha \cdot \mathbf{S}_\mu)(\mathbf{S}_\beta \cdot \mathbf{S}_\mu)(\mathbf{S}_\alpha \cdot \mathbf{S}_\beta).
\end{aligned} \tag{4.5.13}$$

#### 4.5.5 Spin 1, three-site interaction

For a spin 1 system with a three-site interaction, the small Hamiltonian for  $\mu \neq \nu$  of (4.3.43) is

$$\begin{aligned}
\mathcal{H}_{\alpha\beta\gamma\mu\nu}^{1,\neq} = & 128 \mathbf{S}_\mu \cdot \mathbf{S}_\nu + 256 [(\mathbf{S}_\alpha \cdot \mathbf{S}_\beta) + (\mathbf{S}_\alpha \cdot \mathbf{S}_\gamma) + (\mathbf{S}_\beta \cdot \mathbf{S}_\gamma)] (\mathbf{S}_\mu \cdot \mathbf{S}_\nu) \\
& + 96 [(\mathbf{S}_\alpha \cdot \mathbf{S}_\beta)^2 + (\mathbf{S}_\alpha \cdot \mathbf{S}_\gamma)^2 + (\mathbf{S}_\beta \cdot \mathbf{S}_\gamma)^2] (\mathbf{S}_\mu \cdot \mathbf{S}_\nu) \\
& + 160 \sum_{(i,j,k) \in \tilde{\mathcal{P}}_6^3} (\mathbf{S}_i \cdot \mathbf{S}_j)(\mathbf{S}_j \cdot \mathbf{S}_k)(\mathbf{S}_\mu \cdot \mathbf{S}_\nu) \\
& + \frac{80}{3} \sum_{p,q=x,y,z} \sum_{(i,j,k) \in \tilde{\mathcal{P}}_6^3} S_i^p S_j^q (\mathbf{S}_i \cdot \mathbf{S}_k) S_j^p S_k^q (\mathbf{S}_\mu \cdot \mathbf{S}_\nu) \\
& - (\mathbf{S}_\beta \cdot \mathbf{S}_\gamma) [40 + 8(\mathbf{S}_\beta \cdot \mathbf{S}_\gamma)] [(\mathbf{S}_\alpha \cdot \mathbf{S}_\mu)(\mathbf{S}_\alpha \cdot \mathbf{S}_\nu) + (\mathbf{S}_\alpha \cdot \mathbf{S}_\nu)(\mathbf{S}_\alpha \cdot \mathbf{S}_\mu)] \\
& - (\mathbf{S}_\alpha \cdot \mathbf{S}_\gamma) [40 + 8(\mathbf{S}_\alpha \cdot \mathbf{S}_\gamma)] [(\mathbf{S}_\beta \cdot \mathbf{S}_\mu)(\mathbf{S}_\beta \cdot \mathbf{S}_\nu) + (\mathbf{S}_\beta \cdot \mathbf{S}_\nu)(\mathbf{S}_\beta \cdot \mathbf{S}_\mu)] \\
& - (\mathbf{S}_\alpha \cdot \mathbf{S}_\beta) [40 + 8(\mathbf{S}_\alpha \cdot \mathbf{S}_\beta)] [(\mathbf{S}_\gamma \cdot \mathbf{S}_\mu)(\mathbf{S}_\gamma \cdot \mathbf{S}_\nu) + (\mathbf{S}_\gamma \cdot \mathbf{S}_\nu)(\mathbf{S}_\gamma \cdot \mathbf{S}_\mu)] \\
& - 8 \sum_{(i,j,k) \in \tilde{\mathcal{P}}_6^3} (\mathbf{S}_i \cdot \mathbf{S}_k)(\mathbf{S}_j \cdot \mathbf{S}_\nu)(\mathbf{S}_i \cdot \mathbf{S}_\mu)(\mathbf{S}_j \cdot \mathbf{S}_k) \\
& - 16 \sum_{(i,j,k) \in \tilde{\mathcal{P}}_6^3} (\mathbf{S}_i \cdot \mathbf{S}_\mu)(\mathbf{S}_j \cdot \mathbf{S}_\nu)(\mathbf{S}_i \cdot \mathbf{S}_j) \\
& - 16 \sum_{(i,j,k) \in \tilde{\mathcal{P}}_6^3} (\mathbf{S}_i \cdot \mathbf{S}_j)(\mathbf{S}_i \cdot \mathbf{S}_\mu)(\mathbf{S}_j \cdot \mathbf{S}_\nu) \\
& - 40 \sum_{(i,j,k) \in \tilde{\mathcal{P}}_6^3} (\mathbf{S}_i \cdot \mathbf{S}_k)(\mathbf{S}_j \cdot \mathbf{S}_\nu)(\mathbf{S}_i \cdot \mathbf{S}_\mu)
\end{aligned}$$

$$\begin{aligned}
& - 48 \sum_{(i,j,k) \in \tilde{\mathcal{P}}_6^3} (\mathbf{S}_i \cdot \mathbf{S}_\mu)(\mathbf{S}_j \cdot \mathbf{S}_\nu) \\
& - 96i (\mathbf{S}_\alpha + \mathbf{S}_\beta + \mathbf{S}_\gamma) \cdot (\mathbf{S}_\mu \times \mathbf{S}_\nu) \\
& - 192i [(\mathbf{S}_\beta \cdot \mathbf{S}_\gamma)\mathbf{S}_\alpha + (\mathbf{S}_\alpha \cdot \mathbf{S}_\gamma)\mathbf{S}_\beta + (\mathbf{S}_\alpha \cdot \mathbf{S}_\beta)\mathbf{S}_\gamma] \cdot (\mathbf{S}_\mu \times \mathbf{S}_\nu) \\
& - 48i [(\mathbf{S}_\beta \cdot \mathbf{S}_\gamma)^2\mathbf{S}_\alpha + (\mathbf{S}_\gamma \cdot \mathbf{S}_\alpha)^2\mathbf{S}_\beta + (\mathbf{S}_\alpha \cdot \mathbf{S}_\beta)^2\mathbf{S}_\gamma] \cdot (\mathbf{S}_\mu \times \mathbf{S}_\nu) \\
& - 96i \sum_{(i,j,k) \in \tilde{\mathcal{P}}_6^3} (\mathbf{S}_i \cdot \mathbf{S}_j)\mathbf{S}_i \cdot (\mathbf{S}_\mu \times \mathbf{S}_\nu) \\
& - 48i \sum_{(i,j,k) \in \tilde{\mathcal{P}}_6^3} \mathbf{S}_i \cdot (\mathbf{S}_\mu \times \mathbf{S}_\nu)(\mathbf{S}_j \cdot \mathbf{S}_k)(\mathbf{S}_i \cdot \mathbf{S}_j) \\
& - 48i \sum_{(i,j,k) \in \tilde{\mathcal{P}}_6^3} (\mathbf{S}_i \cdot \mathbf{S}_j)(\mathbf{S}_j \cdot \mathbf{S}_k)\mathbf{S}_i \cdot (\mathbf{S}_\mu \times \mathbf{S}_\nu), \tag{4.5.14}
\end{aligned}$$

The set of all permutations over three sites is defined as

$$\tilde{\mathcal{P}}_6^3 = \{(\alpha, \beta, \gamma), (\alpha, \gamma, \beta), (\beta, \gamma, \alpha), (\beta, \alpha, \gamma), (\gamma, \alpha, \beta), (\gamma, \beta, \alpha)\}. \tag{4.5.15}$$

The small Hamiltonian for  $\mu = \nu$  is

$$\begin{aligned}
\mathcal{H}_{\alpha\beta\gamma\mu}^{1,=} &= 1024 + \frac{256}{3} \sum_{(i,j,k) \in \tilde{\mathcal{P}}_6^3} (\mathbf{S}_i \cdot \mathbf{S}_j)(\mathbf{S}_j \cdot \mathbf{S}_k)(\mathbf{S}_k \cdot \mathbf{S}_i) \\
&+ 32 [(\mathbf{S}_\beta \cdot \mathbf{S}_\gamma)^2(\mathbf{S}_\alpha \cdot \mathbf{S}_\mu)^2 + (\mathbf{S}_\alpha \cdot \mathbf{S}_\gamma)^2(\mathbf{S}_\beta \cdot \mathbf{S}_\mu)^2 \\
&\quad + (\mathbf{S}_\alpha \cdot \mathbf{S}_\beta)^2(\mathbf{S}_\gamma \cdot \mathbf{S}_\mu)^2] \\
&- 192 [(\mathbf{S}_\alpha \cdot \mathbf{S}_\mu)^2 + (\mathbf{S}_\beta \cdot \mathbf{S}_\mu)^2 + (\mathbf{S}_\gamma \cdot \mathbf{S}_\mu)^2] \\
&+ \frac{512}{189}(\mathbf{S}_\alpha + \mathbf{S}_\beta + \mathbf{S}_\gamma) \cdot \mathbf{S}_\mu \\
&+ \frac{32}{3} \sum_{(i,j,k) \in \tilde{\mathcal{P}}_6^3} (\mathbf{S}_i \cdot \mathbf{S}_j)(\mathbf{S}_j \cdot \mathbf{S}_k)(\mathbf{S}_i \cdot \mathbf{S}_\mu) \\
&+ \frac{352}{3} \sum_{(i,j,k) \in \tilde{\mathcal{P}}_6^3} (\mathbf{S}_i \cdot \mathbf{S}_j)(\mathbf{S}_i \cdot \mathbf{S}_\mu) \\
&+ 128 [(\mathbf{S}_\beta \cdot \mathbf{S}_\gamma)(\mathbf{S}_\alpha \cdot \mathbf{S}_\mu) + (\mathbf{S}_\alpha \cdot \mathbf{S}_\gamma)(\mathbf{S}_\beta \cdot \mathbf{S}_\mu) + (\mathbf{S}_\alpha \cdot \mathbf{S}_\beta)(\mathbf{S}_\gamma \cdot \mathbf{S}_\mu)] \\
&+ \frac{352}{3} \sum_{p=x,y,z} \sum_{(i,j,k) \in \tilde{\mathcal{P}}_6^3} (\mathbf{S}_i \cdot \mathbf{S}_\mu)S_k^p(\mathbf{S}_j \cdot \mathbf{S}_\mu)(\mathbf{S}_i \cdot \mathbf{S}_k)S_j^p \\
&+ \frac{256}{3} \sum_{p=x,y,z} \sum_{(i,j,k) \in \tilde{\mathcal{P}}_6^3} S_i^p(\mathbf{S}_j \cdot \mathbf{S}_k)(\mathbf{S}_i \cdot \mathbf{S}_\mu)S_k^p(\mathbf{S}_j \cdot \mathbf{S}_\mu) \\
&+ 32 \sum_{p=x,y,z} \sum_{(i,j,k) \in \tilde{\mathcal{P}}_6^3} (\mathbf{S}_i \cdot \mathbf{S}_k)S_j^p(\mathbf{S}_i \cdot \mathbf{S}_\mu)S_k^i(\mathbf{S}_j \cdot \mathbf{S}_\mu) \\
&- 128 \sum_{p,q=x,y,z} \sum_{(i,j,k) \in \tilde{\mathcal{P}}_6^3} S_i^p S_k^q(\mathbf{S}_j \cdot \mathbf{S}_\mu)(\mathbf{S}_i \cdot \mathbf{S}_\mu)S_k^p S_j^q \\
&- 832 [(\mathbf{S}_\alpha \cdot \mathbf{S}_\mu)(\mathbf{S}_\beta \cdot \mathbf{S}_\mu)(\mathbf{S}_\alpha \cdot \mathbf{S}_\beta) + (\mathbf{S}_\alpha \cdot \mathbf{S}_\beta)(\mathbf{S}_\alpha \cdot \mathbf{S}_\mu)(\mathbf{S}_\beta \cdot \mathbf{S}_\mu) \\
&\quad + (\mathbf{S}_\alpha \cdot \mathbf{S}_\mu)(\mathbf{S}_\gamma \cdot \mathbf{S}_\mu)(\mathbf{S}_\alpha \cdot \mathbf{S}_\gamma) + (\mathbf{S}_\alpha \cdot \mathbf{S}_\gamma)(\mathbf{S}_\alpha \cdot \mathbf{S}_\mu)(\mathbf{S}_\gamma \cdot \mathbf{S}_\mu) \\
&\quad + (\mathbf{S}_\beta \cdot \mathbf{S}_\mu)(\mathbf{S}_\gamma \cdot \mathbf{S}_\mu)(\mathbf{S}_\beta \cdot \mathbf{S}_\gamma) + (\mathbf{S}_\beta \cdot \mathbf{S}_\gamma)(\mathbf{S}_\beta \cdot \mathbf{S}_\mu)(\mathbf{S}_\gamma \cdot \mathbf{S}_\mu)]
\end{aligned}$$

$$\begin{aligned}
& + 896 \sum_{p=x,y,z} \sum_{(i,j,k) \in \tilde{\mathcal{P}}_6^3} S_i^p (\mathbf{S}_j \cdot \mathbf{S}_\mu) (\mathbf{S}_i \cdot \mathbf{S}_\mu) S_j^p \\
& + \frac{352}{3} \sum_{(i,j,k) \in \tilde{\mathcal{P}}_6^3} (\mathbf{S}_i \cdot \mathbf{S}_\mu) (\mathbf{S}_j \cdot \mathbf{S}_\mu) \\
& + \frac{64}{3} \sum_{(i,j,k) \in \tilde{\mathcal{P}}_6^3} (\mathbf{S}_i \cdot \mathbf{S}_\mu) (\mathbf{S}_k \cdot \mathbf{S}_i) (\mathbf{S}_j \cdot \mathbf{S}_\mu).
\end{aligned} \tag{4.5.16}$$

#### 4.5.6 Spin 3/2, two-site interaction

We also managed to compute the parent Hamiltonian for a spin 3/2 system with a two-site interaction. Its small Hamiltonian for  $\mu \neq \nu$  of (4.3.40) is given by

$$\begin{aligned}
\mathcal{H}_{\alpha\beta\mu\nu}^{3/2,\neq} & = 990 \mathbf{S}_\mu \cdot \mathbf{S}_\nu + 1944 (\mathbf{S}_\alpha \cdot \mathbf{S}_\beta) (\mathbf{S}_\mu \cdot \mathbf{S}_\nu) \\
& + 928 (\mathbf{S}_\alpha \cdot \mathbf{S}_\beta)^2 (\mathbf{S}_\mu \cdot \mathbf{S}_\nu) + 128 (\mathbf{S}_\alpha \cdot \mathbf{S}_\beta)^3 (\mathbf{S}_\mu \cdot \mathbf{S}_\nu) \\
& - \frac{99}{2} \sum_{i=\alpha,\beta} [(\mathbf{S}_i \cdot \mathbf{S}_\mu) (\mathbf{S}_i \cdot \mathbf{S}_\nu) + (\mathbf{S}_i \cdot \mathbf{S}_\nu) (\mathbf{S}_i \cdot \mathbf{S}_\mu)] \\
& - 84 (\mathbf{S}_\alpha \cdot \mathbf{S}_\beta) \sum_{i=\alpha,\beta} [(\mathbf{S}_i \cdot \mathbf{S}_\mu) (\mathbf{S}_i \cdot \mathbf{S}_\nu) + (\mathbf{S}_i \cdot \mathbf{S}_\nu) (\mathbf{S}_i \cdot \mathbf{S}_\mu)] \\
& - 24 (\mathbf{S}_\alpha \cdot \mathbf{S}_\beta)^2 \sum_{i=\alpha,\beta} [(\mathbf{S}_i \cdot \mathbf{S}_\mu) (\mathbf{S}_i \cdot \mathbf{S}_\nu) + (\mathbf{S}_i \cdot \mathbf{S}_\nu) (\mathbf{S}_i \cdot \mathbf{S}_\mu)] \\
& - 99 [(\mathbf{S}_\alpha \cdot \mathbf{S}_\mu) (\mathbf{S}_\beta \cdot \mathbf{S}_\nu) + (\mathbf{S}_\beta \cdot \mathbf{S}_\mu) (\mathbf{S}_\alpha \cdot \mathbf{S}_\nu)] \\
& - 168 (\mathbf{S}_\alpha \cdot \mathbf{S}_\beta) [(\mathbf{S}_\alpha \cdot \mathbf{S}_\mu) (\mathbf{S}_\beta \cdot \mathbf{S}_\nu) + (\mathbf{S}_\beta \cdot \mathbf{S}_\mu) (\mathbf{S}_\alpha \cdot \mathbf{S}_\nu)] \\
& - 48 (\mathbf{S}_\alpha \cdot \mathbf{S}_\beta)^2 [(\mathbf{S}_\alpha \cdot \mathbf{S}_\mu) (\mathbf{S}_\beta \cdot \mathbf{S}_\nu) + (\mathbf{S}_\beta \cdot \mathbf{S}_\mu) (\mathbf{S}_\alpha \cdot \mathbf{S}_\nu)] \\
& - \frac{891}{2} i (\mathbf{S}_\alpha + \mathbf{S}_\beta) \cdot (\mathbf{S}_\mu \times \mathbf{S}_\nu) \\
& - 756i (\mathbf{S}_\alpha \cdot \mathbf{S}_\beta) (\mathbf{S}_\alpha + \mathbf{S}_\beta) \cdot (\mathbf{S}_\mu \times \mathbf{S}_\nu) \\
& - 216i (\mathbf{S}_\alpha \cdot \mathbf{S}_\beta)^2 (\mathbf{S}_\alpha + \mathbf{S}_\beta) \cdot (\mathbf{S}_\mu \times \mathbf{S}_\nu),
\end{aligned} \tag{4.5.17}$$

and the small Hamiltonian for  $\mu = \nu$  is

$$\begin{aligned}
\mathcal{H}_{\alpha\beta\mu}^{3/2,=} & = \frac{7425}{2} + 7290 (\mathbf{S}_\alpha \cdot \mathbf{S}_\beta) + 3480 (\mathbf{S}_\alpha \cdot \mathbf{S}_\beta)^2 \\
& + 480 (\mathbf{S}_\alpha \cdot \mathbf{S}_\beta)^3 - 99 [(\mathbf{S}_\alpha \cdot \mathbf{S}_\mu)^2 + (\mathbf{S}_\beta \cdot \mathbf{S}_\mu)^2] \\
& - 168 (\mathbf{S}_\alpha \cdot \mathbf{S}_\beta) [(\mathbf{S}_\alpha \cdot \mathbf{S}_\mu)^2 + (\mathbf{S}_\beta \cdot \mathbf{S}_\mu)^2] \\
& - 48 (\mathbf{S}_\alpha \cdot \mathbf{S}_\beta)^2 [(\mathbf{S}_\alpha \cdot \mathbf{S}_\mu)^2 + (\mathbf{S}_\beta \cdot \mathbf{S}_\mu)^2] \\
& - 336 (\mathbf{S}_\alpha \cdot \mathbf{S}_\beta) (\mathbf{S}_\alpha \cdot \mathbf{S}_\mu) (\mathbf{S}_\beta \cdot \mathbf{S}_\mu) \\
& - 96 (\mathbf{S}_\alpha \cdot \mathbf{S}_\beta)^2 (\mathbf{S}_\alpha \cdot \mathbf{S}_\mu) (\mathbf{S}_\beta \cdot \mathbf{S}_\mu) \\
& - 198 (\mathbf{S}_\alpha \cdot \mathbf{S}_\mu) (\mathbf{S}_\beta \cdot \mathbf{S}_\mu) + 396 \mathbf{S}_\alpha \cdot \mathbf{S}_\mu \\
& + 672 (\mathbf{S}_\alpha \cdot \mathbf{S}_\beta) (\mathbf{S}_\alpha \cdot \mathbf{S}_\mu) + 192 (\mathbf{S}_\alpha \cdot \mathbf{S}_\beta)^2 (\mathbf{S}_\alpha \cdot \mathbf{S}_\mu).
\end{aligned} \tag{4.5.18}$$

## 4.6 Numerical validation of spin 1/2 systems

Applying the numerical techniques detailed in Section 4.4.3, we calculate and analyze the eigenspectra of our parent Hamiltonians for the Abelian CSL.

### 4.6.1 Two-site interaction

We start with the simplest model, a spin-1/2 system with a two-site interaction. The parent Hamiltonian is presented in (4.3.40), with the small Hamiltonians (4.5.1) and (4.5.2).

As pointed out in Section 4.2.5, this Hamiltonian is not local. Still, it is useful to analyze the model since it is closely related to its local counterparts and only consists of a few terms (eight in total) as compared to the three-site (26 terms) and four-site Hamiltonians (82 terms), simplifying the numerical analysis decisively.

The numerical results confirm that, independent of the lattice geometry, our Hamiltonian is the parent Hamiltonian of the Abelian CSL with a largely gapped eigenspectrum, robust to finite size effects. In the following, the results for each lattice type are documented.

#### Square lattice, full version

The 16-site square lattice is set up as depicted in Figure 4.3 on the left side. Now, in the two-site Hamiltonian (4.3.40), we have to choose which one of the three even  $\vartheta$ -functions shall occur in the prefactors  $w_{ijk}^{ab}$ . Our aim is to provide a parent Hamiltonian with the smallest possible number of terms. As explained in Appendix C, among the even  $\vartheta$ -functions, only  $\vartheta_{0,0}(z|\tau)$  is invariant under a rotation by  $\pi/2$  around the origin in real space. Therefore, we choose  $(a, b) = (0, 0)$  for our prefactor.

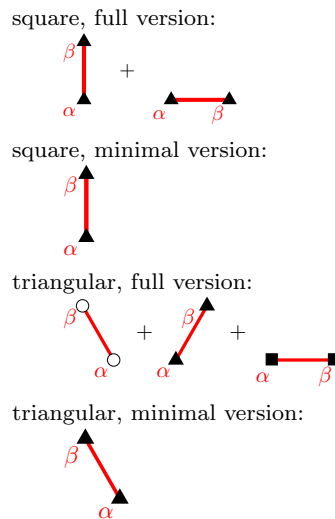


**Table 4.1** Nearest-neighbor configurations occurring in the parent Hamiltonians with a two-site interaction. The two neighboring sites are labeled  $\alpha$  and  $\beta$ . The symbol at the lattice site depicts which even  $\vartheta$ -function, with the distance from this lattice point to  $\mu$  and  $\nu$  as its argument, is chosen for the prefactor of the Hamiltonian:  $\blacktriangle$  is  $\vartheta_{0,0}(z|\tau)$ ,  $\blacksquare$  is  $\vartheta_{\frac{1}{2},0}(z|\tau)$ , and  $\circ$  is  $\vartheta_{0,\frac{1}{2}}(z|\tau)$ . A minimal and a full version of the Hamiltonian, each for the square and triangular lattice, are created.

In the sum over neighboring lattice sites,  $\sum_{\langle a,b \rangle}$ , we include the two NN configurations illustrated in the first row of Table 4.6.1: For instance, for site 1, we sum over the two configurations  $\alpha = 1, \beta = 2$  and  $\alpha = 1, \beta = 5$ .

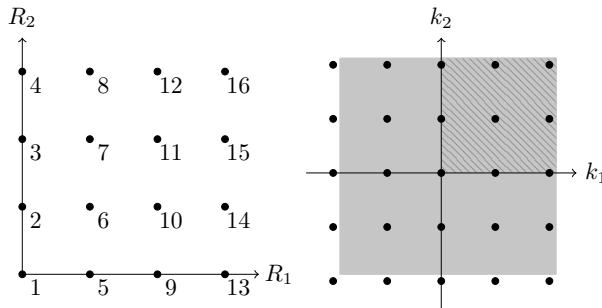


**Fig. 4.3** Left: Indexing of the lattice sites in the 16-site square lattice. Right: The light-gray region marks the corresponding Brillouin zone, consisting of 16 momentum points. Due to reflection symmetry, only the momenta in the shaded-gray region have unique eigenvalues.

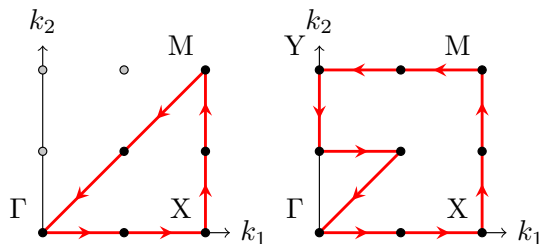


**Fig. 4.4** A plot of the symmetry points in the Brillouin zone of the square lattice for a system with  $90^\circ$  rotational invariance (left) and without  $90^\circ$  rotational invariance (right). The arrows indicate the path taken for the energy spectra in Figure 4.5 and 4.6, starting at the  $\Gamma$ -point.

The corresponding Brillouin zone consists of sixteen momentum points. As it turns out, the eigenspectrum is reflection symmetric while the state is not, as it transforms as  $\Psi \rightarrow \Psi^*$ . Hence, for our eigenspectrum analysis, we only have to calculate at most nine eigenvalues for  $k_x \geq 0$  and  $k_y \geq 0$ . This region is shaded dark-gray in the right panel of Figure 4.3. Combined with the four-fold rotational symmetry of the lattice, only six momentum points are distinct. Thus, for the calculation of the eigenspectrum, the system has to be diagonalized numerically at six different points in momentum space.

The resulting eigenspectrum is presented in Figure 4.5, with the path taken in the Brillouin zone displayed in the left panel of Figure 4.4. The spectrum is positive semidefinite and its zero-energy state at the  $\Gamma$ -point is two-fold degenerate. For an analysis of the ground state, we numerically construct the CSL state (3.2.3) and find a two-dimensional subspace of functions. The subspace of the exact ground state of our Hamiltonian is numerically identical to the CSL subspace. Since we obtain *only* two zero-energy states, the Abelian CSL state is the only ground state of our parent Hamiltonian. This conclusion could not have been drawn analytically. We also confirmed numerically, that the ground state is a singlet, as its the case for the CSL.

The spectrum exhibits a large gap between the ground state and the remainder of the spectrum. We believe that this gap is substantial and does not stem from finite size effects, since a comparison with a twelve-site lattice reveals that the gap is decisively larger than any finite size effect. The presence of a gap is expected since the CSL ground state is energetically separated from what should be two-spinon excitations. The nature of those states is not be addressed in this work.

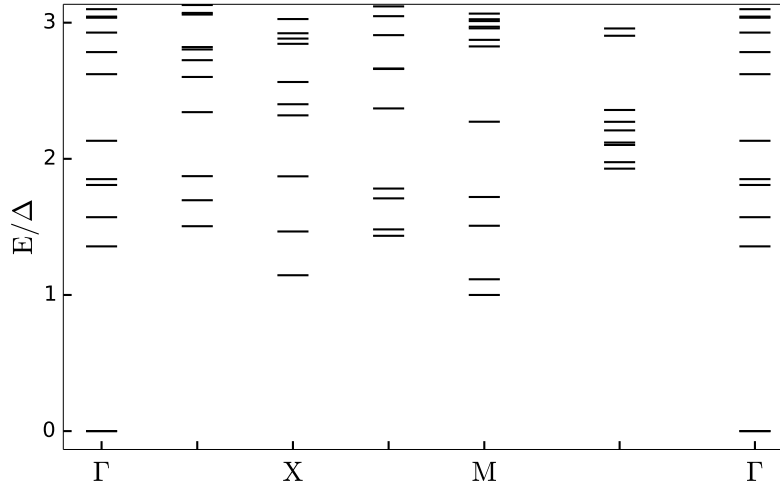


**Fig. 4.5** Low-energy spectrum of the rotationally invariant parent Hamiltonian for a spin-1/2 system with a two-site interaction on a square lattice with 16 sites. The  $E = 0$  eigenvalue at the  $\Gamma$  point is doubly-degenerate.

#### Square lattice, minimal version

Next, the minimal version of the two-site parent Hamiltonian on the square lattice is analyzed. This model is not rotationally invariant, so that we have to consider nine points in momentum space, as illustrated in the right panel of Figure 4.4. As  $\vartheta$ -function for the prefactor of the Hamiltonian (4.3.40), similar to the full version on the square lattice, we choose  $\vartheta_{0,0}(z|\tau)$  and sum over the nearest-neighbor configurations in  $y$ -direction, as depicted in the second row of Table 4.6.1.

The eigenspectrum is presented in Figure 4.6, the corresponding path in the Brillouin zone is illustrated in the right panel of Figure 4.4.

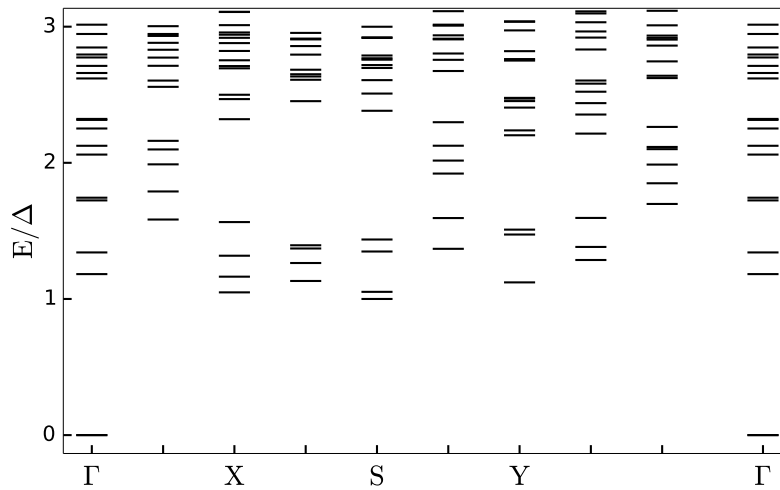


**Fig. 4.6** Low-energy spectrum of the parent Hamiltonian without rotational invariance for a spin-1/2 system with a two-site interaction on a square lattice with 16 sites. The  $E = 0$  eigenvalue at the  $\Gamma$  point is doubly-degenerate.

As for the full version, the zero-energy state is two-fold degenerate and the calculation of the overlap confirms that it is identical to the Abelian CSL. Above the excitation gap, the spectrum is denser than for the full version.

### Triangular lattice, full version

In the triangular lattice, Figure 4.7, each site has six nearest neighbors, as compared to four in the square lattice. This also increases the possible numbers of nearest-neighbor configurations we can choose to construct the parent Hamiltonian. In Appendix C, it is explained that, under a rotation by  $\pi/3$  around the origin in real space, the even  $\vartheta$ -functions map into each other via  $(0,0) \rightarrow (0, \frac{1}{2}) \rightarrow (\frac{1}{2}, 0) \rightarrow (0,0)$ . Thus, to obtain a rotationally invariant system, we need at least three configurations, depicted in the third row of Table 4.6.1.

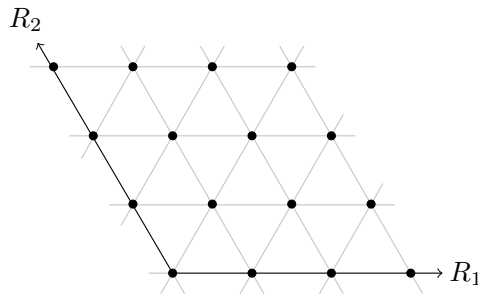


**Fig. 4.7** The 16-site triangular lattice in real space.

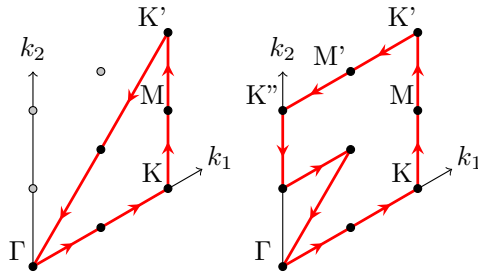


**Fig. 4.8** A plot of the symmetry points in the Brillouin zone of the triangular lattice for a system with  $60^\circ$  rotational invariance (left) and without  $60^\circ$  rotational invariance (right). The arrows indicate the path taken for the energy spectra in Figure 4.9 and 4.10, starting at the  $\Gamma$ -point.

Similar to the square lattice, in the full version, there are six distinct momentum points in the Brillouin zone. For the eigenspectrum, Figure 4.9, we have chosen the path depicted in the left panel of Figure 4.8. Also for this lattice geometry, the gapped spectrum is positive semidefinite and its zero-energy state at the  $\Gamma$ -point is doubly degenerate. Calculating the overlap with the Abelian CSL confirms that both states are numerically identical.



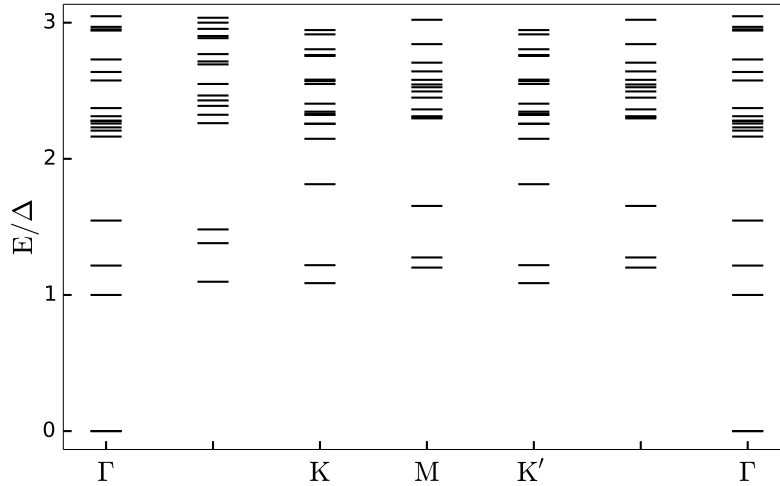


**Fig. 4.9** Low-energy spectrum of the rotationally invariant parent Hamiltonian for a spin-1/2 system with a two-site interaction on a triangular lattice with 16 sites. The  $E = 0$  eigenvalue at the  $\Gamma$  point is doubly-degenerate.

#### Triangular lattice, minimal version

The minimal version on the triangular lattice is the non-rotational invariant counterpart of the full version. For the eigenspectrum, Figure 4.10, we have to consider a path along nine points in momentum space, as depicted in the right panel of Figure 4.8. As  $\vartheta$ -function for the prefactor of the Hamiltonian (4.3.40), we choose  $\vartheta_{0,0}(z|\tau)$  and sum over the nearest-neighbor configurations in  $y$ -direction, as depicted in the fourth row of Table 4.6.1.

Again, the Abelian CSL is the doubly degenerate ground state. Above the excitation gap, the spectrum is denser than for the full version.

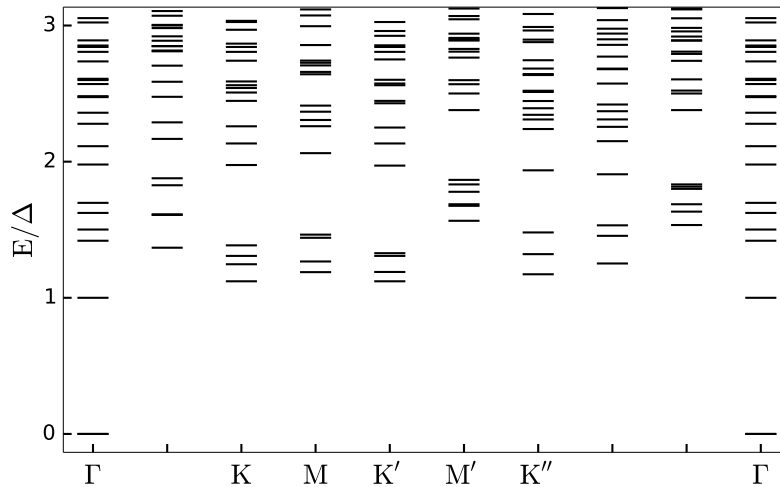


**Fig. 4.10** Low-energy spectrum of the parent Hamiltonian without rotational invariance for a spin-1/2 system with a two-site interaction on a triangular lattice with 16 sites. The  $E = 0$  eigenvalue at the  $\Gamma$  point is doubly-degenerate.

### 4.6.2 Three-site interaction

The parent Hamiltonian is presented in (4.3.43), with the small Hamiltonians (4.5.3) and (4.5.4). As explained in Section 4.2.5, this model is local in two spatial dimensions.

Independently of the lattice geometry, the eigenspectrum of the three-site Hamiltonian is largely gapped with a doubly degenerate ground state. Calculating the overlap with the exact Abelian CSL confirms that both states are numerically identical. We have thus found a *local* parent Hamiltonian for the CSL. In the following, the results for the individual lattices for the full and minimal versions of the parent Hamiltonians are presented.

#### Square lattice, full version

For the square lattice, we construct two different realizations of the parent Hamiltonian: In the first realization, we sum only over the four nearest-neighbor configurations illustrated in the first row of Table 4.6.2. The  $\vartheta$ -functions are assigned to the respective sites such that the resulting Hamiltonian is rotationally invariant. For the second realization, we add to the four nearest-neighbor terms four next-nearest neighbor configurations, as specified in the second row of Table 4.6.2.

The eigenspectra for the realization with only nearest-neighbor configurations, Figure 4.11, and for the realization with additional next-nearest neighbor interactions, Figure 4.12, differ decisively in the density of the excited states. For a denser spectrum, the excitation gap becomes larger relative to the separation between adjacent excited states. Thus, it is worth the computational effort to include next-nearest neighbor interactions into the parent Hamiltonian.

#### Square lattice, minimal version

The minimal version is the non-rotational invariant counterpart of the full version. Here, it is sufficient to consider only one configuration per site, as illustrated in the third row of Table 4.6.2. As explained for the two-site Hamiltonian, nine momentum points have to be considered in the eigenspectrum, Figure 4.13. Obviously, the spectrum is less dense as compared to the full version.

#### Triangular lattice, full version

For the triangular lattice, at least six nearest-neighbor configurations are necessary to create a rotationally invariant model. They are listed in the fourth row of Table 4.6.2. The fifth row presents an alternative version, in which also next-nearest neighbor configurations are considered. The resulting spectra are displayed in Figure 4.14 and 4.15. Similar to the square lattice, the excitation spectrum for the model including next-nearest neighbor interactions is much denser.

#### Triangular lattice, minimal version

For the minimal version on the triangular lattice, nine momentum points in the Brillouin zone are distinct, see Figure 4.8. In the construction of the parent Hamiltonian, one configuration per lattice site is sufficient, as illustrated in the last row of Table 4.6.2. The eigenspectrum, Figure 4.16, is less dense as compared to the full version.

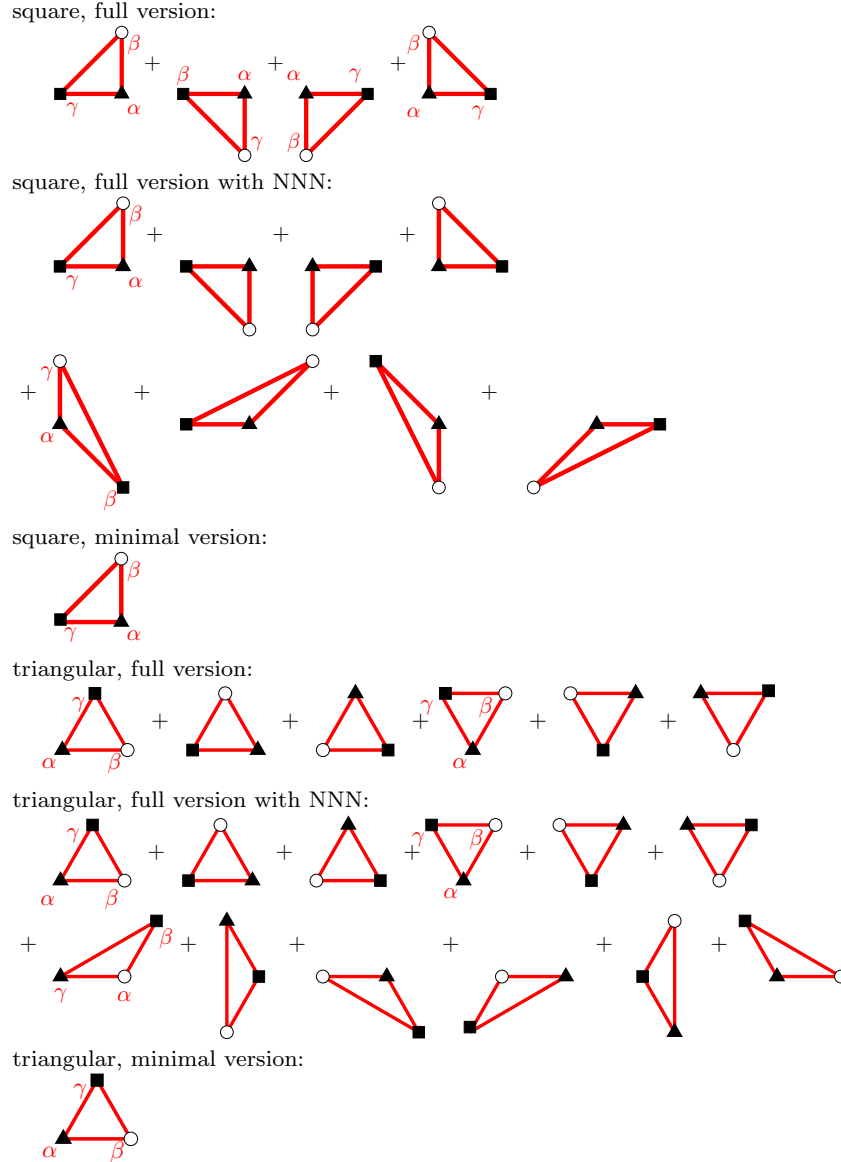


**Table 4.2** Configurations, including nearest neighbors, and in two cases also next-nearest neighbors (NNN), occurring in the parent Hamiltonian with a three-site interaction. The three neighboring sites are labeled  $\alpha$ ,  $\beta$  and  $\gamma$ . The symbol at the lattice site depicts which even  $\vartheta$ -function, with the distance from this lattice point to  $\mu$  and  $\nu$  as its argument, is chosen for the prefactor of the Hamiltonian:  $\blacktriangle$  is  $\vartheta_{0,0}(z|\tau)$ ,  $\blacksquare$  is  $\vartheta_{\frac{1}{2},0}(z|\tau)$ , and  $\circ$  is  $\vartheta_{0,\frac{1}{2}}(z|\tau)$ . Configurations on the square and triangular lattice are created, for models with (full version) and without (minimal version) rotational invariance.

### 4.6.3 Four-site interaction

The parent Hamiltonian is presented in (4.3.46), with the small Hamiltonians (4.5.5) and (4.5.11). Here, the interaction drops off as  $1/r^4$  with the distance, so that this model is even more local than the three-site version.

Also for this parent Hamiltonian, we find that, independently of the lattice geometry and the rotational symmetry, the eigenspectrum is largely gapped with a doubly degenerate ground state. Calculating the

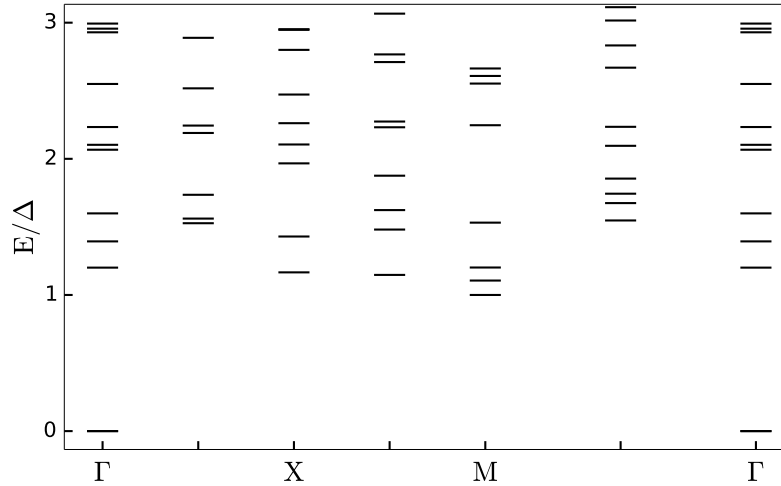


**Fig. 4.11** Low-energy spectrum of the rotationally invariant parent Hamiltonian for a spin-1/2 system with a three-site interaction on a square lattice with 16 sites, summing only over nearest-neighbor configurations. The  $E = 0$  eigenvalue at the  $\Gamma$  point is doubly-degenerate.

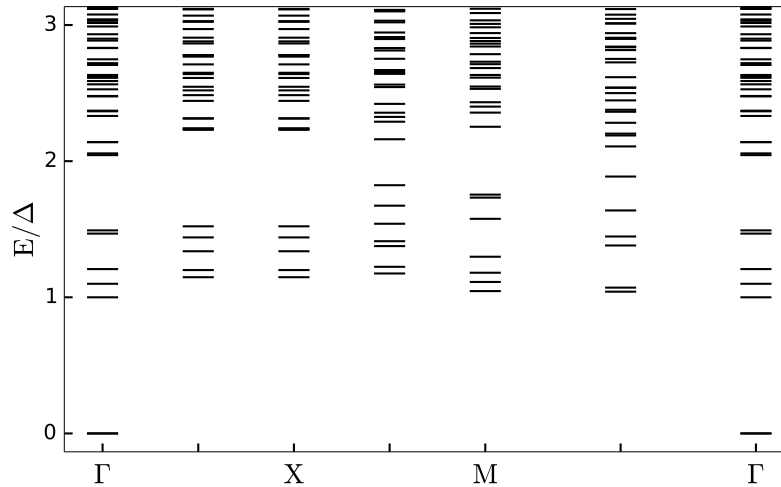


**Fig. 4.12** Low-energy spectrum of the rotationally invariant parent Hamiltonian for a spin-1/2 system with a three-site interaction on a square lattice with 16 sites, including nearest and next-nearest neighbor interactions. The  $E = 0$  eigenvalue at the  $\Gamma$  point is doubly-degenerate.

overlap with the exact Abelian CSL confirms that both states are numerically identical. We have thus found another *local* parent Hamiltonian for the CSL. Compared to the eigenspectra for a two- and three-site interaction, the following spectra are the least dense. Still, a robust gap is discernible.

#### Square lattice, full version

The eigenspectrum is presented in Figure 4.17.

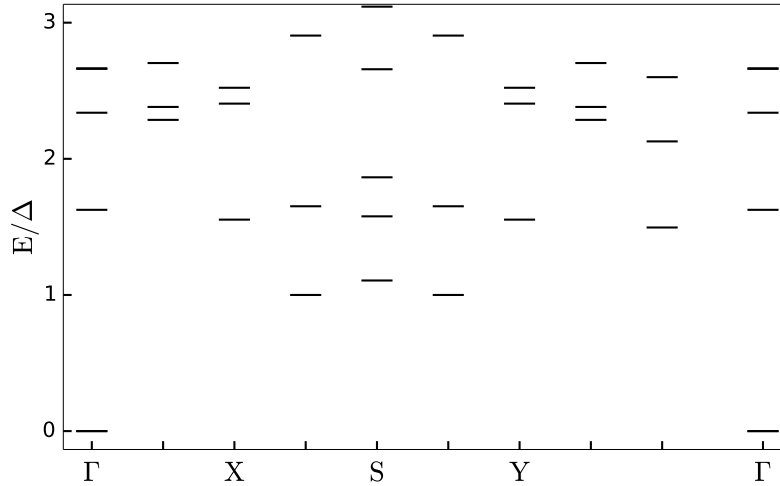


**Fig. 4.13** Low-energy spectrum of the non-rotationally invariant parent Hamiltonian for a spin-1/2 system with a three-site interaction on a square lattice with 16 sites. The  $E = 0$  eigenvalue at the  $\Gamma$  point is doubly-degenerate.

#### Square lattice, minimal version

The eigenspectrum is presented in Figure 4.18.

#### Triangular lattice, full version

The eigenspectrum is presented in Figure 4.19.

#### Triangular lattice, minimal version

The eigenspectrum is presented in Figure 4.20.

## 4.7 Numerical validation of spin 1 systems

Applying the numerical techniques detailed in Section 4.4.3, we calculate and analyze the eigenspectra of our parent Hamiltonians for the non-Abelian CSL.

### 4.7.1 Two-site interaction

Now, we turn to the parent Hamiltonians for the non-Abelian CSL. The model with a two-site interaction is presented in (4.3.40), with the small Hamiltonians (4.5.12) and (4.5.13). For a two-dimensional system, this Hamiltonian is not local. We nevertheless analyzed the system for pedagogical purposes.

As compared to spin-1/2 systems, the numerical calculation becomes much more challenging since the Hilbert space for a  $N$ -site lattice is of size  $3^N$  (43, 046, 721 for  $N = 16$ ), instead of  $2^N$  (65, 536 for  $N = 16$ ) for the spin-1/2 system.

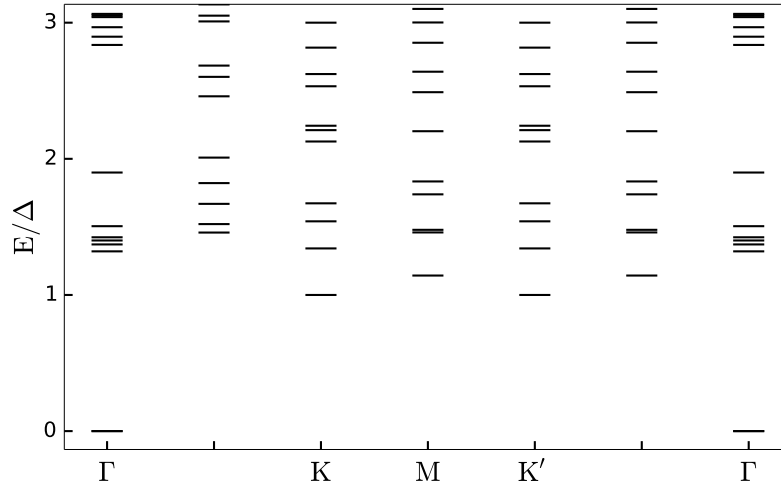


**Fig. 4.14** Low-energy spectrum of the rotationally invariant parent Hamiltonian for a spin-1/2 system with a three-site interaction on a triangular lattice with 16 sites, summing only over nearest-neighbor configurations. The  $E = 0$  eigenvalue at the  $\Gamma$  point is doubly-degenerate.

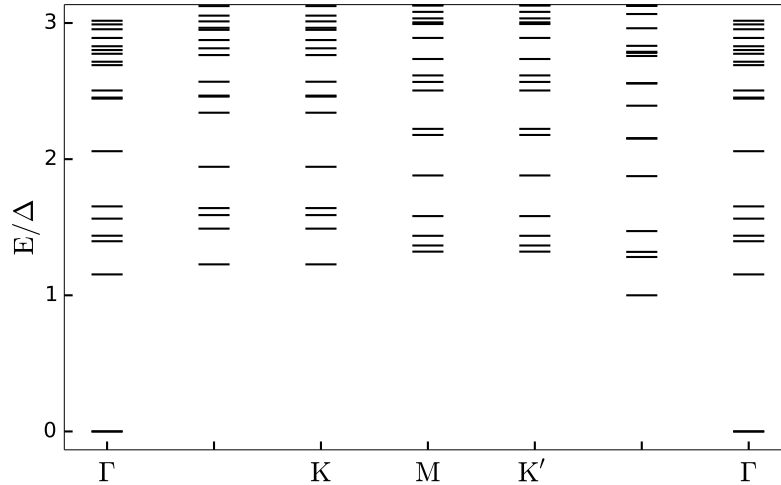


**Fig. 4.15** Low-energy spectrum of the rotationally invariant parent Hamiltonian for a spin-1/2 system with a three-site interaction on a triangular lattice with 16 sites, including nearest and next-nearest neighbor interactions. The  $E = 0$  eigenvalue at the  $\Gamma$  point is doubly-degenerate.

As expected, the eigenspectrum is largely gapped with a three-fold degenerate ground state at the  $\Gamma$ -point. The overlap with the non-Abelian CSL confirms that both states are numerically identical. The results for the different lattice geometries for systems with and without rotational invariance are presented below. The choice of lattice site configurations occurring in the parent Hamiltonian is similar to the spin-1/2 case and listed in Table 4.6.1.

#### Square lattice, full version

The eigenspectrum is presented in Figure 4.21.

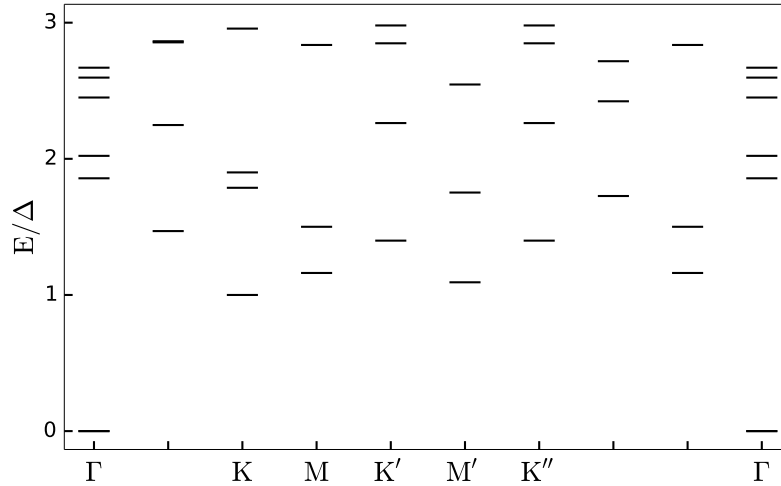


**Fig. 4.16** Low-energy spectrum of the non-rotationally invariant parent Hamiltonian for a spin-1/2 system with a three-site interaction on a triangular lattice with 16 sites. The  $E = 0$  eigenvalue at the  $\Gamma$  point is doubly-degenerate.

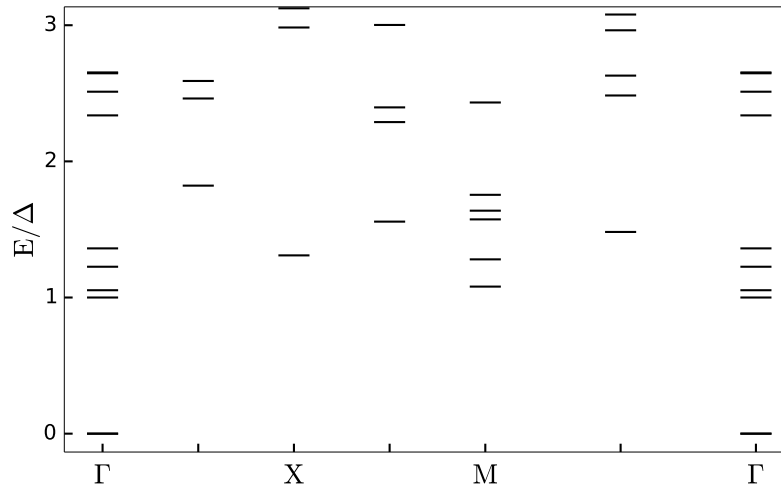


**Fig. 4.17** Low-energy spectrum of the rotationally invariant parent Hamiltonian for a spin-1/2 system with a four-site interaction on a square lattice with 16 sites. The  $E = 0$  eigenvalue at the  $\Gamma$  point is doubly-degenerate.

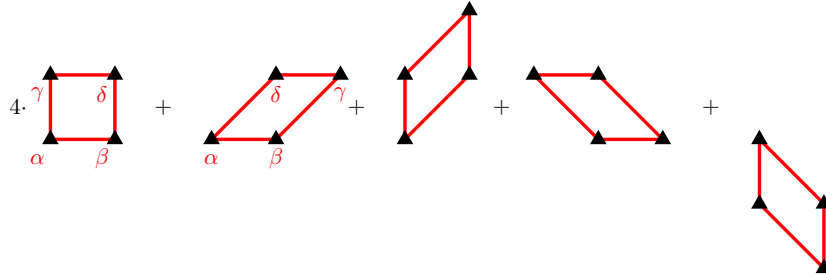
#### Square lattice, minimal version

The eigenspectrum is presented in Figure 4.22.

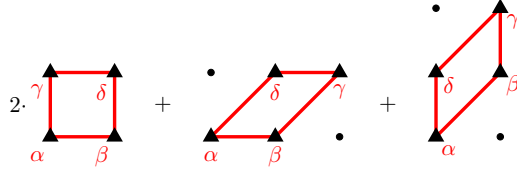
#### Triangular lattice, full version

The eigenspectrum is presented in Figure 4.23. Since this spectrum is much denser than for the square and rectangular lattice, this geometry seems to be more suitable.

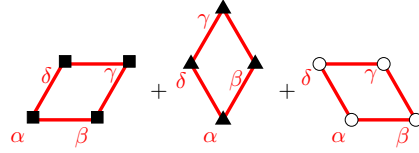
square, full version:



square, minimal version:



triangular, full version:



triangular, minimal version:

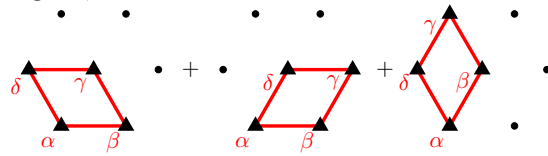


**Table 4.3** Nearest-neighbor configurations occurring in the parent Hamiltonian with a four-site interaction. The four neighboring sites are labeled  $\alpha$ ,  $\beta$ ,  $\gamma$  and  $\delta$ . The symbol at the lattice site depicts which even  $\vartheta$ -function is chosen for the prefactor of the Hamiltonian:  $\blacktriangle$  is  $\vartheta_{0,0}(z|\tau)$ ,  $\blacksquare$  is  $\vartheta_{\frac{1}{2},0}(z|\tau)$ , and  $\circ$  is  $\vartheta_{0,\frac{1}{2}}(z|\tau)$ . Configurations on the square and triangular lattice are created, for models with (full version) and without (minimal version) rotational invariance.

### Triangular lattice, minimal version

The eigenspectrum is presented in Figure 4.24.

### 4.7.2 Three-site interaction

The parent Hamiltonian is presented in (4.3.43), with the small Hamiltonians (4.5.14) and (4.5.16). As explained in Section 4.2.5, this model is local in two dimensions.

We find that, independent of the lattice geometry, our model is a *local* parent Hamiltonian of the non-Abelian CSL. Due to the size of the Hilbert space and the convincing quality of the previous results, we only tested the full version of this model on the square and triangular lattice.

### Square lattice, full version

The eigenspectrum is presented in Figure 4.25.



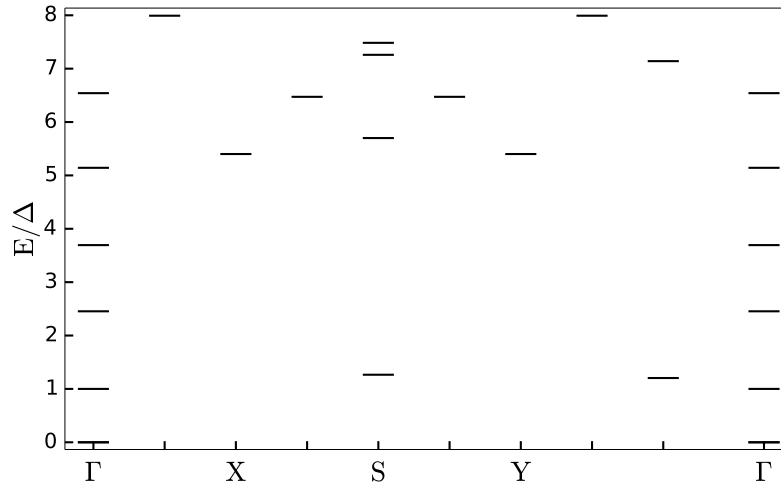


**Fig. 4.18** Low-energy spectrum of the non-rotationally invariant parent Hamiltonian for a spin-1/2 system with a four-site interaction on a square lattice with 16 sites. The  $E = 0$  eigenvalue at the  $\Gamma$  point is doubly-degenerate.

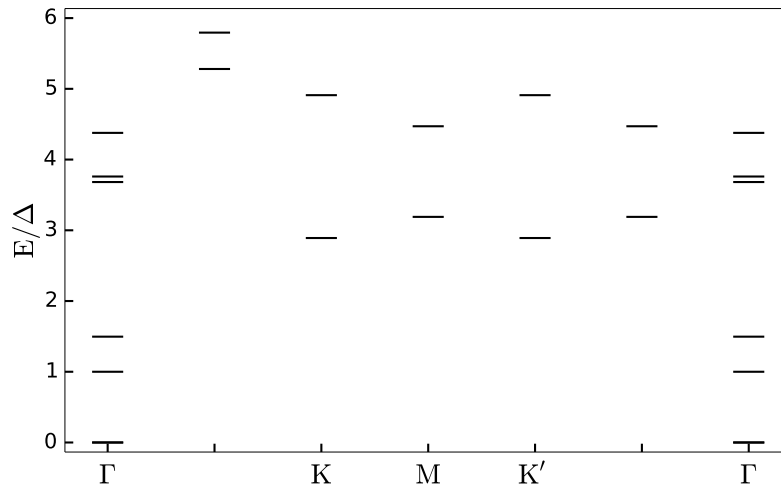


**Fig. 4.19** Low-energy spectrum of the rotationally invariant parent Hamiltonian for a spin-1/2 system with a four-site interaction on a triangular lattice with 16 sites. The  $E = 0$  eigenvalue at the  $\Gamma$  point is doubly-degenerate.

### Triangular lattice, full version

The eigenspectrum is presented in Figure 4.26.

Since the numerical calculation for arbitrary spin  $s$  represents a proof of concept, a detailed finite size analysis is left for future research. Also, a numerical study of the parent Hamiltonian for the spin-3/2 system, (4.5.17) and (4.5.18), will be subject of future work.

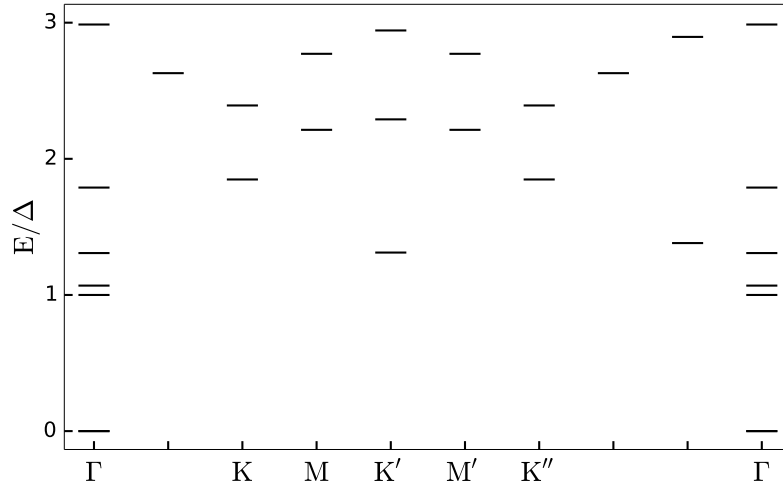


**Fig. 4.20** Low-energy spectrum of the non-rotationally invariant parent Hamiltonian for a spin-1/2 system with a four-site interaction on a triangular lattice with 16 sites. The  $E = 0$  eigenvalue at the  $\Gamma$  point is doubly-degenerate.

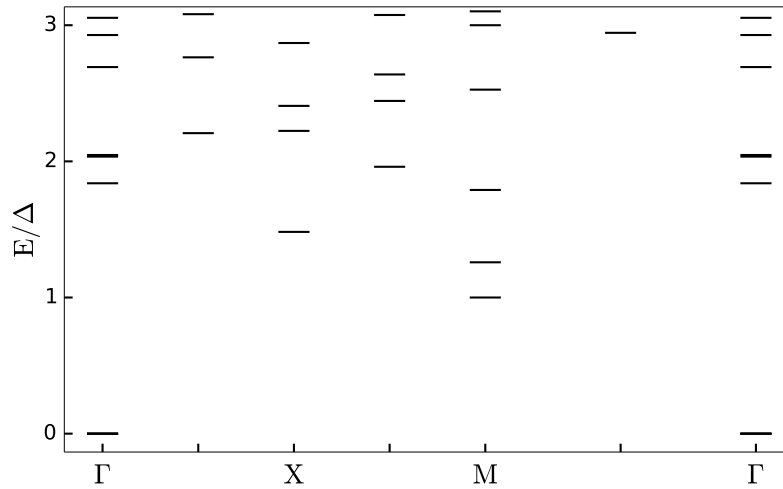


**Fig. 4.21** Low-energy spectrum of the rotationally invariant parent Hamiltonian for a spin-1 system with a two-site interaction on a square lattice with 16 sites. The  $E = 0$  eigenvalue at the  $\Gamma$  point is three-fold degenerate.

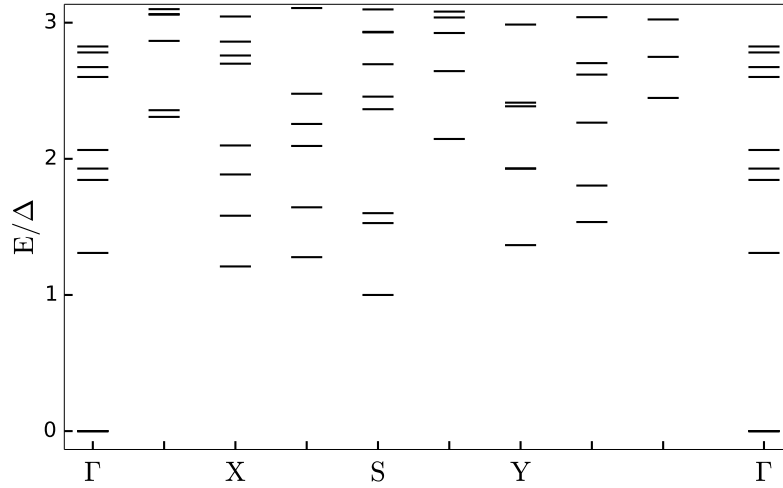


**Fig. 4.22** Low-energy spectrum of the non-rotationally invariant parent Hamiltonian for a spin-1 system with a two-site interaction on a square lattice with 16 sites. The  $E = 0$  eigenvalue at the  $\Gamma$  point is three-fold degenerate.

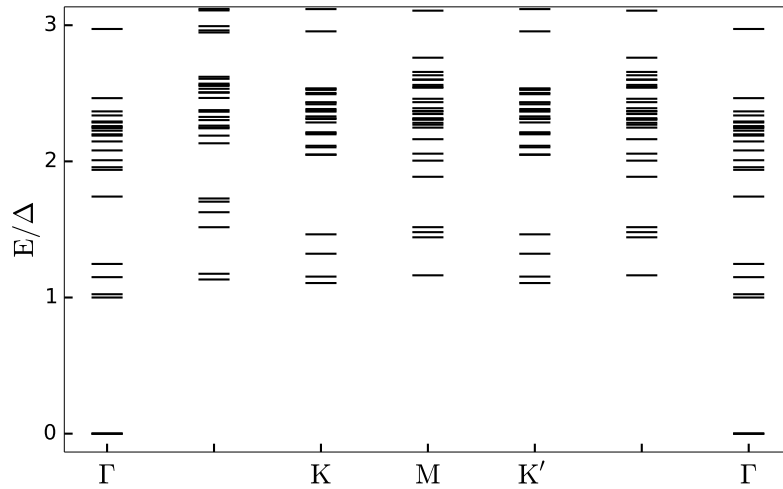


**Fig. 4.23** Low-energy spectrum of the rotationally invariant parent Hamiltonian for a spin-1 system with a two-site interaction on a triangular lattice with 16 sites. The  $E = 0$  eigenvalue at the  $\Gamma$  point is three-fold degenerate.

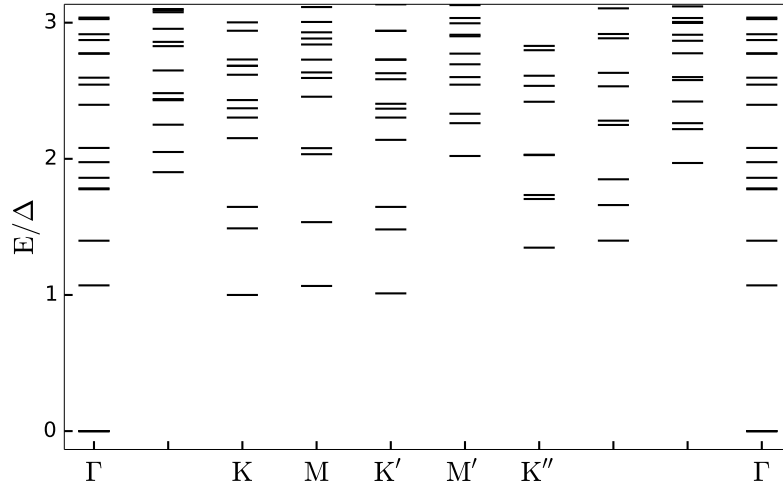


**Fig. 4.24** Low-energy spectrum of the non-rotationally invariant parent Hamiltonian for a spin-1 system with a two-site interaction on a triangular lattice with 16 sites. The  $E = 0$  eigenvalue at the  $\Gamma$  point is three-fold degenerate.

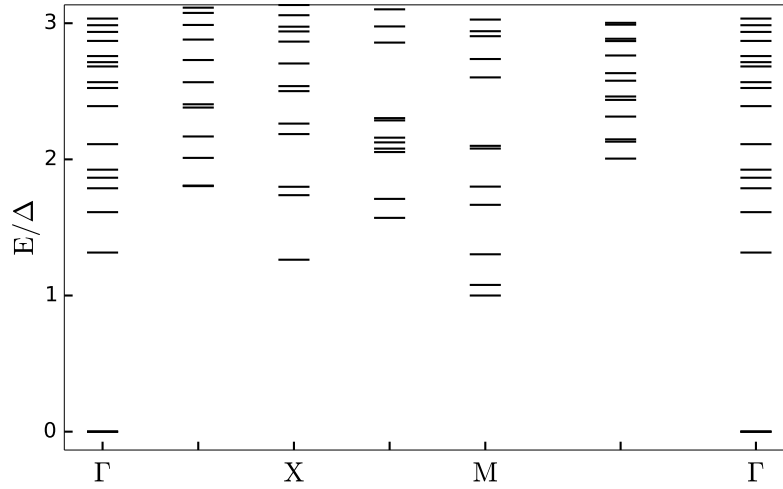


**Fig. 4.25** Low-energy spectrum of the rotationally invariant parent Hamiltonian for a spin-1 system with a three-site interaction on a square lattice with 16 sites, including nearest and next-nearest neighbor interactions. The  $E = 0$  eigenvalue at the  $\Gamma$  point is three-fold degenerate.

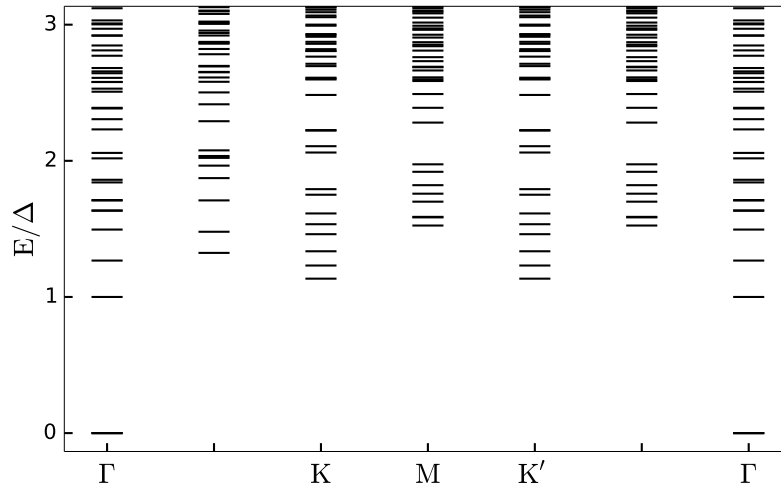


**Fig. 4.26** Low-energy spectrum of the rotationally invariant parent Hamiltonian for a spin-1 system with a three-site interaction on a triangular lattice with 16 sites, including nearest and next-nearest neighbor interactions. The  $E = 0$  eigenvalue at the  $\Gamma$  point is three-fold degenerate.



# Chapter 5

## Topological insulators

### 5.1 Overview

Currently, topological insulators [64; 116; 9] are one of the most fashionable topics in condensed matter physics, with currently about 3000 publications per year with the words “topological insulators” in the title and about 30,000 references made to this topic.

For a long time in condensed matter physics, different states of matter could be classified by the symmetries they spontaneously break. With the discovery of the integer quantum Hall effect (IQHE) in 1980 [80], however, a new quantum state without any broken symmetry entered the stage, a so-called topological state of quantum matter. Klaus von Klitzing was investigating the Hall conductance of a 2D electron gas at low temperatures, when he observed that the Hall conductance  $\sigma_{xy}$  exhibited a sequence of wide plateaus as a function of the strength of the magnetic field applied perpendicularly to the sample. More astonishingly, each plateau occurred at a precise integer multiple of a fundamental natural constant, the so-called von Klitzing constant  $h/e^2$ ,

$$\sigma_{xy} = n \frac{e^2}{h}, \quad n \in \mathbb{N}. \quad (5.1.1)$$

It was a big surprise when, in 1982, Tsui and Störmer measured an additional plateau at a fractional value,  $n = 1/3$  [140], discovering the fractional quantum Hall effect (FQHE). Since then, a plethora of additional plateaus at fractional values have been discovered. However, not all fractions appear.

The quantum Hall effect (QHE) occurs when a strong magnetic field is applied perpendicular to the plane of a 2D electron gas. As a result, bulk electrons become localized, turning the bulk into an insulator. Electrons near the edge of the sample, however, form extended, gapless 1D channels with a quantized Hall conductance. The electrons’ counterflows are separated spatially, top and bottom edge of the QH sample each contains only half the degrees of freedom: One edge has only right-moving electrons, the other edge only left-moving electrons. Thus, the channels are said to be chiral. In literature, this behavior is represented by the symbolic equation  $2 = 1(\text{forward mover}) + 1(\text{backward mover})$  [115]. As electrons on one edge cannot reverse their direction of propagation, backscattering is completely suppressed, making the QH state robust to disorder. Unlike other 1D systems, the QH channels completely evade Anderson localization.

The bulk of a QH state does not break any symmetries except for time reversal ( $T$ ). Therefore, there is no local order parameter to characterize the state. Nonetheless, QH states with different Hall conductances are distinct phases of matter, their ground states cannot be connected adiabatically, i.e. without closing an energy gap. Instead, a topological invariant is needed to characterize this state: The TKNN-invariant [139] or first Chern number [129]. For the IQHE, the Chern number equals the number of edge states which are stable against local perturbations, which is equal to the quantized Hall conductance in units of  $e^2/h$ . The connection of the Hall conductance of the edge and the topological index (Chern number) of the bulk establishes a so-called bulk-edge correspondence.

Microscopically, the IQHE can be understood using one-particle physics. In the presence of a magnetic field, the single particle energy spectrum splits up into equally spaced levels, the Landau levels (LL). Their

gap is proportional to the magnetic field. The LL quantization for different geometries has been reviewed in Chapter 2. Each LL can accommodate a finite number of electrons, its degeneracy is proportional to the magnetic field  $B$ . Thus by increasing  $B$ , electrons from higher LLs drop to lower levels until they are completely filled again. If by further increasing  $B$ , the highest Landau level is depleted, the Fermi energy drops suddenly, causing a change in the number of extended states in the sample. According to Laughlin's gauge argument [85], the Hall conductance is quantized in exact multiples of  $e^2/h$ , and it is carried by the extended states, as pointed out by Halperin [61]. Thus, with increasing  $B$ , at some point, a jump of the Hall conductivity is observed.

The finite width of the conductivity plateaus owes its existence to disorder in the physical sample, giving rise to localized states. As they cannot contribute to the current, the conductivity remains unchanged until a new Fermi level is populated.

For a theory of the FQHE, we need to take into account interactions between electrons, making the problem much harder and richer. This gives rise to a plethora of exotic properties, for instance the emergence of gauge fields, fractional charges and non-Abelian statistics in the Moore-Read state [100] and higher states of the Read-Rezayi series [120]. Laughlin was the first to formulate a theory for plateaus with  $n = 1/m$ ,  $m$  odd [86]. He illustrated that the fractionalization occurs due to the formation of a correlated incompressible electron liquid with exotic properties. In such a state, a LL of the electronic system is only partially filled, making the Coulomb interaction relevant. The quantity  $n$  in the Hall conductance (5.1.1) also determines the filling fraction of the LL. Laughlin's formalism to explain the FQHE was further discussed in Section 2.

Another series of plateaus occurs at filling fractions  $p/(2sp \pm 1)$ ,  $s, p \in \mathbb{Z}$ . This type of FQH states has been explained by a hierarchy theory, which views the FQH effect as an IQH effect of a novel quasiparticle, which is an electron with an even number of flux quanta attached to it [53; 63; 49]. A third type of FQH states was discovered at filling fractions  $n = 5/2$  and  $7/2$  [151], being in so far surprising as up to that time, only odd denominator filling fractions had been observed. In 1991, a theoretical explanation was attempted by Greiter, Wilczek and Wen [47], demonstrating that this type of FQH effect could be described by a Pfaffian wave function. Having anyonic excitations and non-Abelian statistics, these states are more than ever of high interest as they might play a role in quantum computing.

The FQH effect is the first physical system, in which fractional statistics have been discovered. Let us shortly mention that a cousin of this state with fractionalized quasiparticle excitations is the chiral spin liquid (CSL), which emerges in frustrated magnetic systems. The CSL is a state with strong, local anti-ferromagnetic correlations but without long range order, which breaks time reversal ( $T$ ) and parity ( $P$ ) symmetry. Kalmeyer and Laughlin proposed that a FQH wave function for bosons can describe the amplitudes for spin-flips in a two-dimensional frustrated Heisenberg antiferromagnet via a Holstein-Primakoff transformation [73; 74]. The bosons then form a  $1/2$  FQH state.

Unfortunately, the prerequisite of strong magnetic fields makes the broad scale application of the QHE unfeasible. Early on, it was therefore asked: Is it possible to have dissipationless edge modes without any magnetic field? A first step in this direction was achieved in 1988 by Haldane [55] with the theoretical proposal of a lattice analog to the IQH state without an orbital magnetic field: Analogously to the classical effect, this was labeled quantum anomalous Hall effect (QAHE). For the effect to arise, the system needs an energy band with non-zero Chern number, which is achieved by breaking  $T$  symmetry. Haldane proposed a tight-binding model on a periodic 2D honeycomb lattice with real nearest neighbor hopping and complex next-nearest neighbor hopping, where the (net zero) flux is distributed inhomogeneously over the unit cell. Consequently, certain materials, other than the 2D electron gas with external magnetic field, can have topologically non-trivial band structures, nowadays labeled Chern insulators (CI).

Although Haldane demonstrated the existence of a QAH state, an experimental realization remained unachieved for another two decades. In the end, it was discovered via a detour by realizing first a cousin of this effect protected by  $T$  symmetry: In 2005, Kane and Mele theoretically proposed a system exhibiting a so-called quantum spin Hall (QSH) state [75]. Based on the spin-orbit coupling of graphene, they combined two copies of the Haldane model such that the  $\uparrow$ -spin electrons manifest a chiral QHE, while the  $\downarrow$ -spin electrons manifest an anti-chiral QHE. The QSH effect is deeply related to the QAH effect as the state of each spin component can be either an IQH state or a QAH state.



Independently, Bernevig and Zhang proposed a realization of the QSHE [13] in a strained GaAs system, which engineers, due to spin-orbit coupling, a magnetic field pointing upwards for spin up electrons and a magnetic field pointing downwards for spin down electrons. Mostly due to the small spin-orbit coupling in the proposed systems, so far, neither theory has been realized experimentally.

As an experimentally more attainable system, in 2006, Bernevig et al. [12] followed up an idea by Molenkamp et al. [111; 108] and theoretically investigated semiconductors with an inverted band structure, predicting a quantum phase transition in type-III HgTe/CdTe quantum wells between a trivial insulator phase and QSH phase beyond a critical thickness of the well. Only one year later, in 2007, this prediction could be confirmed experimentally [81]. While for most semiconductors, the conduction band is formed by electrons in s-orbitals and the valence band by electrons in p-orbitals, in HgTe, the bands are inverted due to spin orbit coupling. Sandwiched with the normal ordered semiconductor CdTe, having a similar lattice constant as compared to HgTe, the band structure can be varied with the thickness of the quantum well.

A system exhibiting the QSHE, also called a topological insulator (TI), is a new topological state of matter, characterized by a bulk insulating gap and a pair of gapless edge states protected by  $T$  symmetry. It can be symbolically summarized by  $(2D\ TI)=IQHE+\overline{IQHE}$ . The edge states are labeled “helical states”, since spin is correlated with the direction of propagation. The traffic lanes for the electrons can be split into four channels in a  $T$  invariant manner as follows: On the top edge of the sample, there is a  $\uparrow$ -spin forward and a  $\downarrow$ -spin backward mover, the other two channels are on the bottom edge. This behavior is represented by the symbolic equation  $4 = 2 + 2$ . Thus, there is a net transport of spin forward along the top edge and backward along the bottom edge - similar to the separated charge transport in the QH state. On a given edge, the two states with opposite chirality transform into each other under  $T$ . This is called a “Kramers pair”. The helical edge states are robust to nonmagnetic disorder (meaning impurities that preserve  $T$  symmetry), as backscattering would require a spin flip which is prohibited by  $T$  symmetry. Furthermore, the helical states consist of a single massless Dirac fermion, which is “holographic”, as it can only live on the boundary of a two-dimensional system, but not in a purely 1D system [154].

Hall conductivity violates  $T$  symmetry, so it must vanish in the QSH state. In a realistic system, the spin  $s_z$  is not a good quantum number, for instance due to the existence of spin-orbit coupling. Therefore, there is no quantized SH conductance  $\sigma_{xy}^\uparrow - \sigma_{xy}^\downarrow$  in the QSHE. This is the reason why it would be incorrect to label this effect *quantized* spin-Hall effect instead of quantum spin-Hall effect. Unlike for the QH effect, the Chern number thus cannot provide a useful classification for  $T$ -invariant systems. The actual topological invariant is in the  $\mathbb{Z}_2$  group, containing only the elements 0 and 1 [75]. Here, 1 corresponds to the nontrivial QSH state, while 0 labels the topologically trivial insulator. This invariant therefore counts the number of stable helical states modulo 2. A nontrivial QSH state indeed requires an odd number of edge states. If the number was even, an electron on one edge could be scattered from a forward- to a backward-moving channel without changing spin, making the system dissipative and thus giving a trivial insulator.

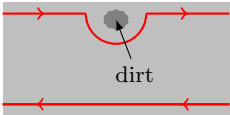
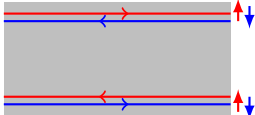
The two-dimensional model for the QSH effect offers a template for a generalization to three dimensions. Initial theories turned out to be extremely complex [28]. A much simpler model has been provided for the  $\text{Bi}_2\text{Se}_3$ -,  $\text{Bi}_2\text{Te}_3$ - and  $\text{Sb}_2\text{Te}_3$ -class of materials [159; 156], for which angle-resolved photoemission spectroscopy (ARPES) experiments could confirm the existence of 3D TIs [156; 20; 67]. Again, spin orbit coupling provokes a band inversion at the  $\Gamma$ -point, giving rise to a topologically protected surface state, which consists of a two-dimensional massless Dirac fermion. Its dispersion forms a single Dirac cone on the surface. Similarly to the 2D case, the fermion is “holographic”, as it can only exist at the boundary of a 3D system. Its spin lies in the surface plane and is always perpendicular to the propagation direction of the electrons, thus forming a helical state.

The following brief summary on topological insulators is an extension of a lecture held by Martin Greiter during a winter school at Galileo Galilei Institute for Theoretical Physics in Florence, 2014.

## 5.2 Basic properties of topological insulators

Topological insulators (TIs) can be realized in two or three spatial dimensions. For most of this chapter, we will limit the explanations to two dimensions. In the last section, a brief overview of three-dimensional TIs will be presented.

For a first understanding of TIs, it is instructive to compare the quantum spin Hall (QSH) effect to the integer quantum Hall (IQH) effect, as summarized in Table 5.2. Equivalently, a 2D TI can be compared to a Chern insulator (CI), which is in the same universality class as the IQH effect, but without an external magnetic field. CIs can be understood as an IQH effect on a lattice commensurate with the magnetic field such that the flux per unit cell is one Dirac flux quantum.

IQH effect ( $\mathbf{B} \neq 0$ ) or Chern insulator (no external $\mathbf{B}$ )	QSH effect = 2D TI
	
<ul style="list-style-type: none"> <li>• chiral edge states</li> <li>• violates time reversal (<math>T</math>)</li> <li>• Hall conductivity <math>\sigma_{xy}</math> quantized</li> <li>• edge state protected by the TKNN invariant</li> </ul>	<ul style="list-style-type: none"> <li>• helical edge states</li> <li>• <math>T</math> is restored</li> <li>• spin Hall conductivity <math>\sigma_{xy}^S</math> not quantized</li> <li>• edge states protected by <math>T</math></li> </ul>

**Table 5.1** Comparison of the IQH effect and the QSH effect.

For a two-dimensional system displaying the IQH effect, as depicted in the left figure of Table 5.2, the bulk violates  $T$  invariance. The edge states (red lines in the figure) are chiral and thus protected from backscattering. This leads to a quantized Hall conductivity

$$\sigma_{xy} = n \frac{e^2}{h} \quad (5.2.1)$$

with the topological quantum number  $n \in \mathbb{Z}$ , which is related to the TKNN invariant in band structures. For the CI,  $n$  is exactly the TKNN invariant, and it counts the number of chiral modes.

In the QSH effect, the bulk is gapped, similar to a conventional insulator, but gapless edge states exist and are protected by time reversal ( $T$ ) symmetry. The effect is driven by spin-orbit coupling (SOC). To a naive interpretation, there are two copies, one for  $\uparrow$ -spins and one for  $\downarrow$ -spins, of a Chern insulator with opposite Hall conductivity for the two layers. As illustrated in the right figure of Table 5.2,  $T$ -symmetry is restored. Importantly, the spin Hall conductance

$$\sigma_{xy}^s = \frac{J_x^\uparrow - J_x^\downarrow}{E_y}, \quad (5.2.2)$$

which is the difference of the  $\uparrow$ -spin current and the  $\downarrow$ -spin current divided by the electric field, is not quantized. Nevertheless, there is a topological invariant  $\nu$  which can take the values 0 for a trivial insulator or 1 for a TI. We define a “trivial insulator” as an insulator which can be adiabatically deformed into an

atomic insulator, in which the orbitals are isolated and do not form bands. The invariant  $\nu$  is the number of Kramers pairs of edge states modulo 2. The edge states come in Kramers pairs since the system is  $T$ -invariant. The topological invariant will be further explained in the following Sections 5.3 and 5.4.

### 5.3 Time reversal and Kramers pairs

Under time reversal  $T$ , the position operator remains unaltered while the momentum changes sign,

$$TxT^{-1} = x, \quad TpT^{-1} = -p. \quad (5.3.1)$$

It therefore follows that

$$T[x, p]T^{-1} = -[x, p], \quad \text{with} \quad [x, p] = i\hbar. \quad (5.3.2)$$

Thus,  $T$  is a combination of a unitary transformation  $U$  and a complex conjugation  $K$ ,  $T = U \cdot K$ . The square of  $T$  then is

$$\begin{aligned} T^2 &= UKUK = UU^* = U(U^\dagger)^\dagger = U(U^\dagger)^{-1} \stackrel{!}{=} e^{i\phi} \\ \Rightarrow U &= e^{i\phi}U^\dagger = e^{i\phi}(e^{i\phi}U^\dagger)^\dagger = e^{2i\phi}U \\ \Rightarrow \phi &= 0 \text{ or } \pi \\ \Rightarrow T^2 &= \pm 1. \end{aligned}$$

The spin operator reverses under  $T$ ,

$$TST = -S. \quad (5.3.3)$$

If we choose a basis where  $S^\pm = S^x \pm iS^y$  and  $S^z$  are real, then

$$T = e^{-i\pi S^y} K. \quad (5.3.4)$$

For  $S = 1/2$ , we have

$$\begin{aligned} T &= e^{-i\frac{\pi}{2}\sigma_y} K = -i\sigma_y K = \begin{pmatrix} 0 & -1 \\ 1 & 0 \end{pmatrix} \cdot K \\ \Rightarrow T|\uparrow\rangle &= |\downarrow\rangle, \quad T|\downarrow\rangle = -|\uparrow\rangle, \end{aligned}$$

so that  $T$  leaves a singlet unaltered. In general,

$$T^2 = (-1)^{2s} = \begin{cases} +1, & \text{integer } s \\ -1, & \text{half-integer } s. \end{cases} \quad (5.3.5)$$

Kramers theorem states that for a system with  $T^2 = -1$  and a  $T$ -invariant Hamiltonian  $H$ , the single particle states come in pairs of  $T$ -conjugates.

*Proof.* We define  $|T\psi\rangle = T|\psi\rangle$ . The overlap of two arbitrary states is

$$\begin{aligned} \langle T\phi|T\psi\rangle &= \sum_{m,n,p} (U_{nm}K\phi_m)^* (U_{np}K\psi_p) \\ &= \sum_{m,p} \psi_p^* \sum_n (U^\dagger)_{mn} U_{np} \phi_m \\ &= \sum_{m,p} \psi_p^* \delta_{mp} \phi_m = \langle \psi|\phi\rangle. \end{aligned}$$

First, we take  $\phi = T\psi$ . Then, (5.3.6) becomes

$$\begin{aligned} \langle T^2\psi|T\psi\rangle &= \langle\psi|T\psi\rangle \\ \Rightarrow \langle\psi|T\psi\rangle &= 0 \quad \text{for } T^2 = -1. \end{aligned} \quad (5.3.6)$$

Thus,  $|\psi\rangle$  and  $|T\psi\rangle$  are orthogonal.

Second, we take  $\phi = HT\psi$  and assume  $THT = H$ . Then, from (5.3.6), we get

$$\langle THT\psi|T\psi\rangle = \langle\psi|HT\psi\rangle. \quad (5.3.7)$$

This can be rewritten to

$$\langle T^2\psi|H|T\psi\rangle = \langle\psi|H|T\psi\rangle = 0 \quad \text{for } T^2 = -1, \quad (5.3.8)$$

meaning that a  $T$ -invariant Hamiltonian does not scatter between members of a Kramers pair, which is the essence of TIs.

□

## 5.4 Absence of backscattering in 2D topological insulators

In the previous section, we already encountered the absence of backscattering in TIs. An intuitive understanding of the effect can be conveyed by Figure 5.1: Let us assume we have a forward and a backward moving edge mode and a non-magnetic impurity. There are two possible scattering paths, depicted by the black solid and dotted lines in the figure. The relative phase of the rotation of the spin between the two paths is  $2\pi$ , which gives a minus-sign for spin  $s = 1/2$ . Thus, the two paths cancel each other, destructive interference annihilates backscattering.

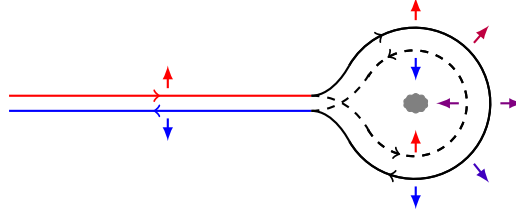


**Fig. 5.1** Intuitive understanding of the absence of backscattering in a 2D TI. The destructive interference of the two scattering paths of a Kramers pair annihilates backscattering.

Mathematically, the absence of backscattering can also be easily derived. The Hamiltonian for a single edge state is

$$\begin{aligned} H_{\text{edge}} &= -iv\sigma^z\partial_x - \mu \\ &= \int \frac{dk}{2\pi} \left( \psi_{\uparrow}^{\dagger}(k), \psi_{\downarrow}^{\dagger}(k) \right) (vk\sigma^z - \mu) \begin{pmatrix} \psi_{\uparrow}(k) \\ \psi_{\downarrow}(k) \end{pmatrix}. \end{aligned} \quad (5.4.1)$$

This expression simply means that  $\uparrow$ -spins ( $\downarrow$ -spins) travel to the right (left).

Let us consider a mass term to gap the spectrum,

$$H_{\text{mass}} = m \int \frac{dk}{2\pi} (\psi_{\uparrow}^{\dagger}(k)\psi_{\downarrow}(k) + \text{h.c.}), \quad (5.4.2)$$

which scatters between  $\uparrow$ - and  $\downarrow$ -spins. Since

$$TH_{\text{mass}}T^{-1} = -H_{\text{mass}}, \quad (5.4.3)$$

such a term (5.4.2) cancels out and is thus forbidden by  $T$ -invariance.

However, for a system with two edge modes, two forward and two backward movers,

$$H_{\text{edge}} = \sum_{j=1,2} \int \frac{dk}{2\pi} \left( \psi_{\uparrow j}^\dagger(k), \psi_{\downarrow j}^\dagger(k) \right) (vk\sigma^z - \mu) \begin{pmatrix} \psi_{\uparrow j}(k) \\ \psi_{\downarrow j}(k) \end{pmatrix}, \quad (5.4.4)$$

the total spin of one mode is 1 and Kramers theorem does not apply anymore. It is now possible to construct a  $T$ -invariant mass term,

$$H_{\text{mass}} = m \int \frac{dk}{2\pi} (\psi_{\uparrow 1}^\dagger(k)\psi_{\downarrow 2}(k) - \psi_{\downarrow 1}^\dagger(k)\psi_{\uparrow 2}(k) + \text{h.c.}). \quad (5.4.5)$$

Thus, the two edge states gap each other out, making backscattering possible. Any impurity thus can eliminate the modes. This is the reason why the topological invariant of the TI is only a  $\mathbb{Z}_2$ -invariant, since backscattering is only absent for single modes with half-integer spin.

## 5.5 TKNN and Chern invariants

We consider a 2D lattice Hamiltonian,

$$H(\mathbf{k}) |u_n(\mathbf{k})\rangle = \epsilon_n(\mathbf{k}) |u_n(\mathbf{k})\rangle, \quad (5.5.1)$$

where  $|u_n(\mathbf{k})\rangle$  are the Bloch states and  $n$  is the band index. If a Bloch state is transported around a closed loop in  $\mathbf{k}$ -space, it will acquire a Berry phase

$$\begin{aligned} \gamma_n(C) &= \oint_C d\mathbf{k} \cdot i \underbrace{\langle u_n(\mathbf{k}) | \nabla_{\mathbf{k}} | u_n(\mathbf{k}) \rangle}_{\substack{=: \mathcal{A}_n(\mathbf{k}), \\ \text{Berry connection}}} \\ &= \iint_{BZ} d^2k \hat{e}_z \cdot \underbrace{(\nabla_{\mathbf{k}} \times \mathcal{A}_n(\mathbf{k}))}_{\substack{=: -\mathcal{V}_n(\mathbf{k}), \\ \text{Berry curvature}}}, \end{aligned} \quad (5.5.2)$$

where  $BZ$  is short for Brillouin zone. After a few steps of algebra [14], we have

$$\mathcal{V}_n = \Im \left( \sum_{\substack{m \\ (m \neq n)}} \frac{\langle u_n | \nabla_{\mathbf{k}} H | u_m \rangle \times \langle u_m | \nabla_{\mathbf{k}} H | u_n \rangle}{(\epsilon_m(\mathbf{k}) - \epsilon_n(\mathbf{k}))^2} \right) = \mathcal{V}_n \hat{e}_z. \quad (5.5.3)$$

The Chern number  $C_n$  of each band is the total Berry flux through the Brillouin zone in units of  $2\pi$ ,

$$C_n = \frac{1}{2\pi} \gamma_n(C) = -\frac{1}{2\pi} \iint_{BZ} d^2k \mathcal{V}_n(\mathbf{k}) \in \mathbb{Z}. \quad (5.5.4)$$

In a seminal paper in 1982, Thouless, Kohmoto, Nightingale and den Nijs (TKNN) [139] proved that the IQH conductivity is precisely the Chern number times natural constants,

$$\sigma_{xy} = \sum_n C_n \frac{e^2}{h}. \quad (5.5.5)$$

In the following, we explain why the Chern number is an integer. To do so, it is sufficient to consider a two-level system. The lattice Hamiltonian can always be written as

$$H = \epsilon(\mathbf{k}) + \mathbf{h}(\mathbf{k}) \cdot \boldsymbol{\sigma}, \quad (5.5.6)$$

since this is the most general form of a Hermitian  $2 \times 2$ -matrix. Here,  $\boldsymbol{\sigma} = (\sigma_x, \sigma_y, \sigma_z)$  is the vector of Pauli matrices. We introduce the unit vector  $\hat{\mathbf{h}} := \mathbf{h}/|\mathbf{h}|$ , which simply maps the Brillouin zone (BZ) to a unit sphere. Due to its periodic boundary conditions in the  $k_x$ - and  $k_y$ -direction, the BZ has the topology of a torus. For the Chern number of the lower band, we get

$$C_- = \frac{1}{4\pi} \iint_{BZ} dk_x dk_y \left( \frac{\partial \hat{\mathbf{h}}}{\partial k_x} \times \frac{\partial \hat{\mathbf{h}}}{\partial k_y} \right) \cdot \hat{\mathbf{h}}. \quad (5.5.7)$$

When mapping the system from a torus to a unit sphere, the infinitesimal space element  $dk_x dk_y$  maps into the solid angle on the unit sphere, which is given by the first part of the integrand,

$$dk_x dk_y \left( \frac{\partial \hat{\mathbf{h}}}{\partial k_x} \times \frac{\partial \hat{\mathbf{h}}}{\partial k_y} \right). \quad (5.5.8)$$

By multiplying this expression with  $\hat{\mathbf{h}}$  in (5.5.7), we keep track of the sign of the solid angle. The torus is a compact surface and we map it to a sphere, which is compact itself. The Chern number has a simple geometric interpretation, since it counts the number of times the vector  $\hat{\mathbf{h}}(\mathbf{k})$  covers the unit sphere for  $\mathbf{k}$  in the first Brillouin zone.

## 5.6 Graphene band structure and the Haldane model

Graphene is a single layer of carbon atoms arranged in a honeycomb lattice. It is a hexagonal lattice with two atoms,  $A$  and  $B$ , per unit cell, as depicted in Figure 5.2. The  $A$  and  $B$  sublattices are triangular Bravais lattices, and the honeycomb lattice may be viewed as a triangular lattice with a two-atom basis  $A$  and  $B$ . The Brillouin zone is a hexagon featuring two Dirac cones  $Q_+$  and  $Q_-$ .

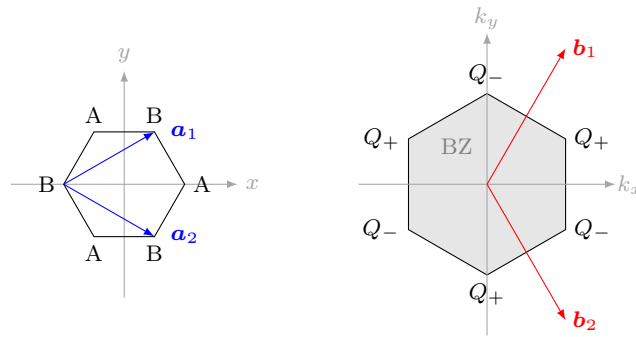


**Fig. 5.2** The unit cell (left) of graphene consists of two sites inequivalent sites  $A$  and  $B$ . The unit vectors in real space are  $\mathbf{a}_1$  and  $\mathbf{a}_2$ . The Brillouin zone (right) is hexagonal with two Dirac points  $Q_+$  and  $Q_-$ . The unit vectors in reciprocal space are  $\mathbf{b}_1$  and  $\mathbf{b}_2$ .

Its Hamiltonian is

$$H = \sum_k (c_{Ak}^\dagger, c_{Bk}^\dagger) \mathcal{H}(\mathbf{k}) \begin{pmatrix} c_{Ak} \\ c_{Bk} \end{pmatrix}, \quad (5.6.1)$$

with

$$\mathcal{H}(\mathbf{k}) = \mathbf{h}(\mathbf{k}) \cdot \boldsymbol{\sigma}. \quad (5.6.2)$$

and  $c_{Ak}^\dagger$  ( $c_{Bk}^\dagger$ ) the creation operator for an electron on the A (B) sublattice. We expand  $\mathcal{H}$  around the two Dirac points  $Q_\pm$  to first order,

$$\mathcal{H}(Q_\pm + \mathbf{p}) \approx \frac{a}{2}(\mp\sigma_x p_y - \sigma_y p_x) =: \mathcal{H}_\pm(\mathbf{p}) \quad (5.6.3)$$

Time reversal maps the Hamiltonian matrix into

$$T\mathcal{H}(\mathbf{k})T^{-1} = \mathcal{H}^*(-\mathbf{k}). \quad (5.6.4)$$

Under inversion symmetry,  $(x, y) \rightarrow (-x, -y)$ , the sublattices  $A$  and  $B$  are interchanged, with the Hamiltonian matrix transforming as

$$I\mathcal{H}(\mathbf{k})I^{-1} = \sigma_x \mathcal{H}(-\mathbf{k})\sigma_x. \quad (5.6.5)$$

Since under inversion  $I$ ,  $Q_\pm \rightarrow Q_\mp$ ,  $\sigma_y \rightarrow -\sigma_y$ ,  $\sigma_x \rightarrow \sigma_x$  and  $p_{x/y} \rightarrow -p_{x/y}$ ,  $\mathcal{H}$  is inversion invariant at the Dirac points  $Q_\pm$ .

Time reversal and inversion symmetry together protect the Dirac points locally. To demonstrate this, consider adding a mass term

$$\mathcal{H}_{\pm, m} = m_\pm \sigma_z. \quad (5.6.6)$$

Its transformation properties are dictated by the Pauli matrix,

$$T\sigma_z T^{-1} = \sigma_z, \quad I\sigma_z I^{-1} = -\sigma_z, \quad (5.6.7)$$

If we impose both time reversal and inversion symmetry, it follows  $m_+ = m_- = 0$ . Thus, the Dirac cones are protected.

To open a gap in the spectrum of graphene, we have to break at least one symmetry. The first possibility is to keep time reversal symmetry intact but break inversion symmetry. Then,  $m_+ = m_- = M$ , which is equivalent to an on-site potential of  $\pm M$  at the A/B sites. The resulting system is a trivial insulator, since the Chern number  $C_- = 0$  vanishes due to the equal sign of the masses at both Dirac points.

The second possibility is to keep inversion symmetry intact but break time reversal symmetry. It follows that  $m_+ = -m_- = m$ , and  $\mathcal{H}(Q_\pm) = \pm m\sigma_z$  at the Dirac points. Since  $\hat{\mathbf{h}}(Q_\pm) = \text{sgn}(m_\pm)\hat{e}_z$ , the sphere is covered once when calculating the Chern number, yielding  $C_- = \nu$  and a Hall conductance  $\sigma_{xy} = \nu e^2/h$ , with  $\nu = \frac{1}{2}(\text{sgn}(m_+) - \text{sgn}(m_-))$  [55]. Thus, in this phase, we have a topologically non-trivial insulator.

A way to accomplish this was first proposed by F.D.M. Haldane in 1988 [55]. This so-called Haldane model is a paradigmatic example of a Hamiltonian featuring topologically distinct phases of matter, having provided the conceptual basis for theoretical as well as experimental research of TIs and superconductors [18; 75; 81; 65; 64]. This model is the realization of the integer quantum Hall effect without Landau levels. It features a chiral edge spectrum without a net external magnetic field, being the prototype for the quantum anomalous Hall insulator [147; 94]. This is achieved with a periodic magnetic field with a zero net flux per plaquette.

Time reversal symmetry is broken by introducing a complex next-nearest neighbor hopping with an amplitude  $t'e^{i\phi}$ , additionally to a real nearest-neighbor hopping. If both mass terms are present, the insulator is non-trivial for  $|M/t'| < |3\sqrt{3}\sin(\phi)|$ , and the Chern number is  $\pm 1$ . Its sign equals the sign of the phase  $\phi$ ,  $-\pi < \phi < \pi$ . The phase diagram of the Haldane model is displayed in Figure 5.3.

## 5.7 Edge states of Chern insulators

A simple theory for a chiral edge state was first proposed by Jackiw and Rebbi in 1976 [71]. They considered a system in which the mass at one Dirac point is fixed  $m_+ > 0$ , while the other mass  $m_-$  changes as a

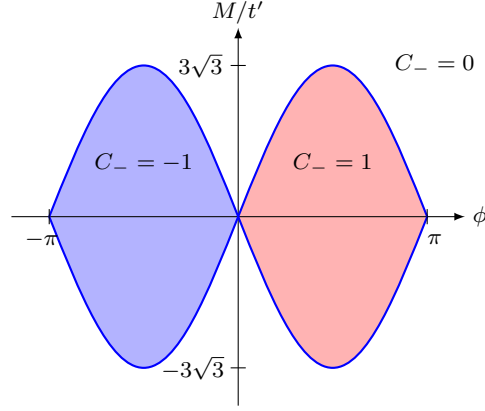


**Fig. 5.3** Phase diagram of the Haldane model. The Chern number  $C_-$  of the bottom band is plotted as a function of the hopping parameters  $\phi$  and  $M/t'$ . As compared to the original work by Haldane [55], the sign of the Chern number is reversed here.

function of  $x$ , vanishing at  $x = 0$ , as depicted in Figure 5.4. Thus, for  $x > 0$  ( $x < 0$ ), the system is a trivial (topological) insulator.

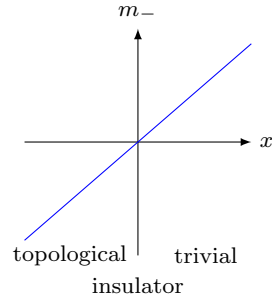


**Fig. 5.4** In the system studied here, the mass  $m_-$  changes linearly as a function of  $x$ , changing sign at  $x = 0$ .

Taking  $\mathbf{p} = -i\nabla$  and  $v_0 := a/2$ , the Hamiltonian (5.6.3) at the Dirac point  $\mathbf{Q}_-$  takes the form of a massive Dirac Hamiltonian,

$$\begin{aligned} \mathcal{H}_-(x, y) &= v_0 (\sigma_x(-i\partial_y) - \sigma_y(-i\partial_x)) + m_-(x)\sigma_z \\ &= \begin{pmatrix} m_- & v_0(\partial_x - i\partial_y) \\ v_0(-\partial_x - i\partial_y) & -m_- \end{pmatrix} \end{aligned} \quad (5.7.1)$$

The function

$$\psi_{p_y}(x, y) = \begin{pmatrix} 1 \\ 1 \end{pmatrix} e^{ip_y y} e^{-\frac{1}{v_0} \int_0^x dx' m_-(x')}. \quad (5.7.2)$$

is an eigenstate of  $\mathcal{H}_-$ . This can be easily proven by acting with the Hamiltonian on the state. Since

$$v_0(\pm i\partial_x - i\partial_y) \left( e^{ip_y y} e^{-\frac{1}{v_0} \int_0^x dx' m_-(x')} \right) = (\mp m_- + v_0 p_y) \left( e^{ip_y y} e^{-\frac{1}{v_0} \int_0^x dx' m_-(x')} \right), \quad (5.7.3)$$

we have

$$\mathcal{H}_- \psi_{p_y} = \begin{pmatrix} m_- & -m_- + v_0 p_y \\ m_- + v_0 p_y & -m_- \end{pmatrix} \begin{pmatrix} 1 \\ 1 \end{pmatrix} e^{ip_y y} e^{-\frac{1}{v_0} \int_0^x dx' m_-(x')} = v_0 p_y \psi_{p_y}. \quad (5.7.4)$$



This state is exponentially localized at the boundary  $x = 0$ , is extended in the  $y$ -direction, and has the dispersion  $E(p_y) = v_0 p_y$ . With a positive group velocity of  $dE/dp_y = v_0$ , the state (5.7.2) describes a right-moving gapless chiral edge mode.

The occurrence of such a gapless edge mode at the interface where the topological invariant changes is a fundamental consequence of the topological classification of gapped band structures. A low energy electronic state has to be bound to the region where the energy gap vanishes, since otherwise it would be impossible for the topological invariant to change.

## 5.8 2D Topological insulators in HgTe/CdTe quantum wells

Since graphene is made out of carbon, which is a light element with weak spin-orbit coupling, its energy gap is small, although its absolute magnitude remains controversial [69; 99; 15; 157; 31]. This makes an experimental measurement of the topological effects challenging. A more promising approach is to look for materials with strong spin-orbit coupling. Bernevig, Hughes and Zhang followed up on an idea by Molenkamp to investigate semiconductor quantum well structures of HgCdTe [12]. A few months later, the first signature of the quantum spin Hall insulator was measured by the Molenkamp group in Würzburg [81].

CdTe is a semiconductor with a GaAs-type band structure near the  $\Gamma$ -point, which is depicted on the left in Figure 5.5. Due to spin-orbit coupling, the total angular momentum  $J$  becomes a good quantum number. At the  $\Gamma$ -point with in-plane momentum  $k_{\parallel} = 0$ , also the angular momentum component  $m_J$  remains a good quantum number. The conduction band  $\Gamma_6$  has an  $s$ -type symmetry, while the valence band  $\Gamma_8$ , which splits into two bands with  $m = \pm 3/2$  and  $m = \pm 1/2$ , has a  $p$ -like symmetry.

The band structure of HgTe exhibits a band inversion at the  $\Gamma$ -point. Figure 5.5 on the right displays that the  $\Gamma_8$ -band lies energetically higher than the  $\Gamma_6$ -band. Since the chemical potential  $\mu$  coincides with the bottom of the  $\Gamma_8$ -band, HgTe is a zero gap semiconductor [64].

In both materials, the gap is smallest near the  $\Gamma$ -point in the Brillouin zone. Other bands, such as the bulk split-off  $\Gamma_7$ -band, have a negligible effect on the band structure around the Fermi level [108; 111], so that the system can be constricted to a six band model with the states

$$\begin{aligned} &|\Gamma_6, 1/2\rangle, |\Gamma_6, -1/2\rangle, |\Gamma_8, 3/2\rangle, \\ &|\Gamma_8, -3/2\rangle, |\Gamma_8, 1/2\rangle, |\Gamma_8, -1/2\rangle. \end{aligned} \quad (5.8.1)$$

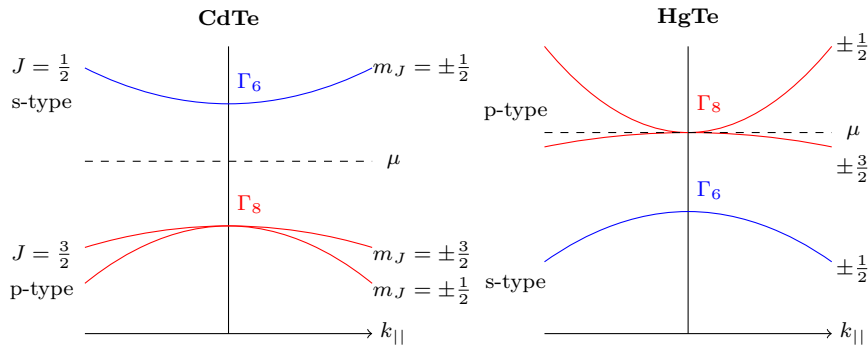


**Fig. 5.5** Bulk band structure near the  $\Gamma$ -point of CdTe and HgTe. The angular momentum  $J$  and its  $z$ -component of the bands are specified. Here and in the following Figures,  $\Gamma_8$ - ( $\Gamma_6$ -) symmetry is indicated in red (blue).

Following [111], Bernevig et al. considered a quantum well structure with CdTe as barrier material in between which a layer of HgTe is sandwiched. In the quantum well, the system is confined in  $z$ -direction and the six states (5.8.1) hybridize to form three subbands, each with a  $\uparrow$ -spin and a  $\downarrow$ -spin component:  $E_1$ ,  $H_1$  and  $L_1$ . The  $L_1$ -subband can be neglected due to a large separation from the other two bands [111]. Hence, the quantum well is effectively described by a four-band model. At the  $\Gamma$ -point, the  $E_1$ -subband is formed by a linear combination of the  $|\Gamma_6, \pm 1/2\rangle$  and  $|\Gamma_8, \pm 1/2\rangle$  states,

$$\begin{aligned} |E_1, +\rangle &= \alpha |\Gamma_6, 1/2\rangle + \beta |\Gamma_8, 1/2\rangle, \\ |E_1, -\rangle &= \alpha^* |\Gamma_6, -1/2\rangle + \beta^* |\Gamma_8, -1/2\rangle. \end{aligned}$$

The  $H_1$  band is formed by the  $\Gamma_8, \pm 3/2$  states,

$$|H_1, \pm\rangle = |\Gamma_8, \pm 3/2\rangle.$$

Since away from the  $\Gamma$ -point,  $m_J$  is not a good quantum number, the bands  $E_1$  and  $H_1$  can mix.

The states  $|H_1, \pm\rangle$  ( $|E_1, \pm\rangle$ ) have odd (even) parity under two-dimensional spatial reflections [12]. Thus, the coupling matrix element between these states has odd parity. Since the states  $|E_1, +\rangle$  and  $|E_1, -\rangle$  are Kramers pairs, there are no matrix elements coupling these states. The same holds for  $|H_1, +\rangle$  and  $|H_1, -\rangle$ . There is also no coupling between  $|E_1, +\rangle$  and  $|H_1, -\rangle$  or  $|E_1, -\rangle$  and  $|H_1, +\rangle$  due to inversion symmetry.

With the above considerations, the general form of the effective Hamiltonian around the  $\Gamma$ -point can be deduced. In the basis

$$\{|E_1, +\rangle, |H_1, +\rangle, |E_1, -\rangle, |H_1, -\rangle\}, \quad (5.8.2)$$

it is block-diagonal,

$$\mathcal{H} = \begin{pmatrix} H(\mathbf{k}) & 0 \\ 0 & H^*(-\mathbf{k}) \end{pmatrix}, \quad (5.8.3)$$

with

$$H(\mathbf{k}) = \epsilon(\mathbf{k})\mathbb{1} + \mathbf{h}(\mathbf{k}) \cdot \boldsymbol{\sigma}. \quad (5.8.4)$$

The above parity symmetry arguments imply that  $\epsilon(\mathbf{k})$  and  $h_z(\mathbf{k})$  are an even function of  $\mathbf{k}$ , while  $h_{x/y}(\mathbf{k})$  is an odd functions of  $\mathbf{k}$ ,

$$\mathbf{h}(\mathbf{k}) = \begin{pmatrix} Ak_x \\ -Ak_y \\ M + B(k_x^2 + k_y^2) \end{pmatrix}, \quad \epsilon(\mathbf{k}) = C - D(k_x^2 + k_y^2), \quad (5.8.5)$$

where  $A$ ,  $B$ ,  $C$  and  $D$  are expansion parameters, depending on the heterostructure. The effective Hamiltonian thus has the form of a  $(2 + 1)$ -dimensional Dirac Hamiltonian with an additional diagonal term  $\epsilon(\mathbf{k})$ . The sign of the gap parameter  $M$  determines the topology of the problem. It is the energy difference between the  $E_1$  and  $H_1$  levels at the  $\Gamma$ -point.

Now, due to the band inversion in HgTe, there exists a level crossing at a critical thickness  $d_c$  of the HgTe-layer. The system undergoes a phase transition as a function of the HgTe-layer thickness  $d$ . If  $d < d_c = 6.3\text{nm}$  [111; 81], the 2D electronic states bound to the quantum well have normal band order, meaning that the  $\Gamma_6$ -band lies energetically higher than the  $\Gamma_8$ -band, resulting in a trivial insulator (Figure 5.6). For  $d > d_c$ , the bands invert, so that the electron-like band  $E_1$  lies below the heavy hole band  $H_1$ . As a consequence, the system becomes a topological insulator. Thus, at  $d = d_c$ , the energy gap vanishes.

The energy levels  $E_1$  and  $H_1$  as a function of the HgTe-layer thickness  $d$  are plotted in Figure 5.7.

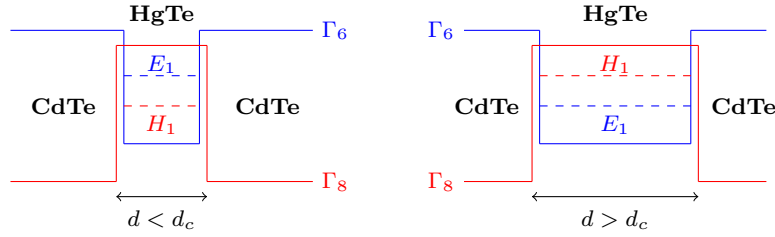


**Fig. 5.6** The CdTe/HgTe/CdTe quantum well in the normal band order regime  $E_1 > H_1$  with  $d < d_c$  (left) and the band inversion regime  $H_1 > E_1$  with  $d > d_c$  (right).

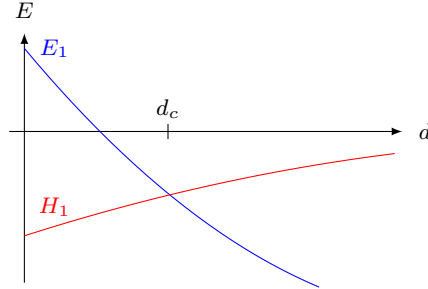


**Fig. 5.7** Energy of the  $E_1$  and  $H_1$  bands at  $k_{||}$  as a function of the quantum well thickness  $d$ .

## 5.9 $\mathbb{Z}_2$ -invariant

We assume an inversion-symmetric band structure. Under an inversion  $I$ , the momentum transforms as  $\mathbf{k} \rightarrow -\mathbf{k}$ . Then, the four points  $\Lambda_a$ ,  $a = 1, 2, 3, 4$  in the Brillouin zone, marked in Figure 5.8, are inversion invariant. The Bloch state  $|u_m(\mathbf{k})\rangle$  therefore is an eigenstate of the inversion operator,

$$I |u_m(\Lambda_a)\rangle = \xi_m(\Lambda_a) |u_m(\Lambda_a)\rangle \quad (5.9.1)$$

with eigenvalues  $\xi_m(\Lambda_a) = \pm 1$ .

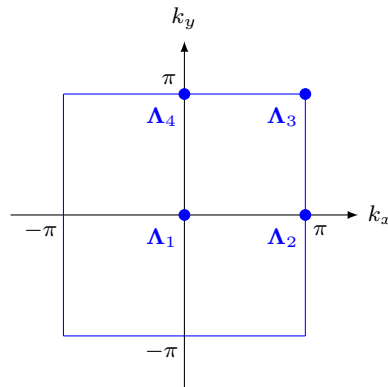


**Fig. 5.8** Brillouin zone of a system with inversion symmetry, the points  $\Lambda_a$ ,  $a = 1, 2, 3, 4$ , are inversion invariant.

It turns out that it is not necessary to explicitly calculate the TKNN invariant to determine the topological phase of the system. The eigenvalues  $\xi_m$  are sufficient for this purpose [27], since the topological

invariant  $\nu$  is determined by

$$(-1)^\nu = \prod_{a=1}^4 \prod_{m \text{ (filled bands)}} \xi_m(\mathbf{\Lambda}_a). \quad (5.9.2)$$

This relation has proven useful for the identification of topological insulators from band structure calculations [27; 135].

## 5.10 3D topological insulators

In 2006, three theoretical groups independently discovered that the quantum spin Hall insulator can be extended to three dimensions [28; 101; 122]. It took only a year to discover the first realizations such as  $\text{Bi}_{1-x}\text{Sb}_x$  [66] and  $\text{Bi}_2\text{Se}_3$  [156] via ARPES measurements.

There are two types of 3D TIs: weak and strong TIs. They are defined by four independent topological  $\mathbb{Z}_2$ -invariants,  $\nu_x, \nu_y, \nu_z$  and  $\nu_0$ . A weak 3D TI can be constructed by stacking several 2D TIs on top of each other in  $y$ -direction. The Brillouin zone of the 3D system is a cube with eight inversion invariant points  $\mathbf{\Lambda}_a$ ,  $a = 1, \dots, 8$ , as presented in Figure 5.9. Now, equation (5.9.2) for  $\nu_z$  is fulfilled for each set of four points  $\mathbf{\Lambda}_a$  in the  $k_y = 0$  and  $k_y = \pi$  plane.

The helical edge states of the 2D TI-layers become anisotropic surface states. The Fermi surface for a system of weakly coupled layers stacked along the  $y$ -direction is depicted in the left panel of Figure 5.10. However, since there are always multiple edge states from the individual 2D TI-layers, they gap each other out, since the surface states are not protected by inversion symmetry. The same holds for the topological invariants  $\nu_x$  and  $\nu_z$ . Therefore, such systems are labeled “weak” TIs.

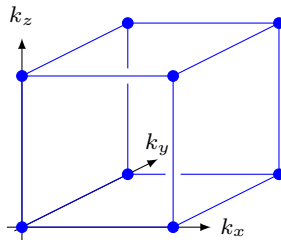


**Fig. 5.9** The Brillouin zone of a 3D TI is a cube with eight inversion invariant points  $\mathbf{\Lambda}_a$  (marked as blue circles).

The fourth topological invariant can be determined via equation (5.9.2), summing over all eight inversion invariant points,

$$(-1)^{\nu_0} = \prod_{a=1}^8 \prod_{m \text{ (filled bands)}} \xi_m(\mathbf{\Lambda}_a). \quad (5.10.1)$$

For the weak TI, we have  $\nu_0 = 0$ , since the two planes with four points each give the same result.

A strong TI has  $\nu_0 = 1$  and cannot be interpreted as a descendant of a 2D TI. Its surface state is protected and consists of a single two-dimensional massless Dirac fermion, with the physical spin tied to its momentum. As depicted in Figure 5.11 and in the right panel of Figure 5.10, the spin is always perpendicular to the momentum.

Its effective field theory is

$$H = v_F \hat{\mathbf{n}} \cdot (\boldsymbol{\sigma} \times \mathbf{k}), \quad (5.10.2)$$

with  $\hat{\mathbf{n}}$  the surface normal,  $\boldsymbol{\sigma}$  the electron spin and  $\mathbf{k}$  the surface momentum [64].

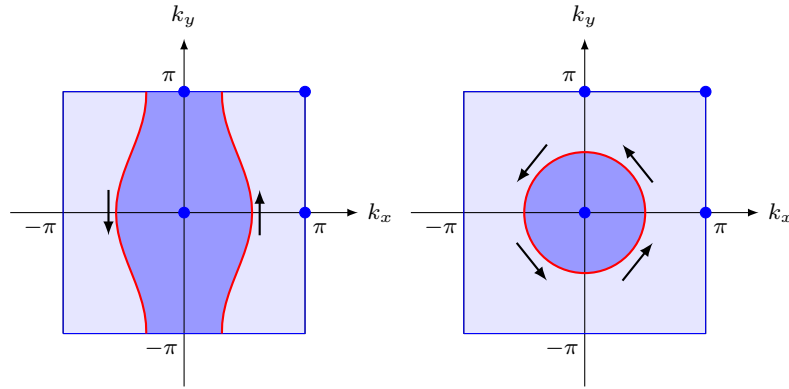


**Fig. 5.10** Fermi circles in the surface Brillouin zone of a weak TI (left) and a strong TI (right).

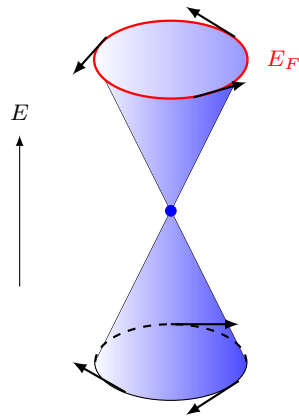


**Fig. 5.11** Dispersion of the surface state of a strong 3D TI. The Fermi circle encloses a single Dirac point. The spin (black arrows) of the surface state is tied to its momentum.



## Chapter 6

# Fractional insulators

In this work, we introduce a novel microscopic state describing a fractional insulator in which different spin species are interlocked without loss of locality. In the following, this state will be called the “311-state”, a nomenclature which will be explained later on.

After a brief review of the advancements in fractional quantum Hall (FQH) systems and topological insulators in Section 6.1, the 311-state is constructed in Section 6.2, based on Laughlin’s wave function. In Sections 6.3.1-6.3.4, an efficient numerical technique is introduced to find the exact or approximate parent Hamiltonian of a specified wave function. This technique makes use of pseudopotential coefficients, which are derived in Section 6.3.1, and we label it “Hamiltonian Finder method”. Furthermore, in Section 6.3.5, we introduce the relative angular momentum resolved correlators, which allow to analyze the correlation properties of our 311-state. Section 6.3.6 explains how to obtain the real space interaction potential from a Hamiltonian specified by angular momentum resolved pseudopotentials. Our numerical results are presented in Section 6.4: After succeeding the numerically challenging task of implementing the 311-state for sufficiently large systems in Section 6.4.1, its correlation properties including a finite size analysis are investigated in Sections 6.4.2 and 6.4.3. Applying the Hamiltonian Finder method in Section 6.4.4 and some manual fine tuning returns an approximate parent Hamiltonian with a large overlap of the exact ground state with our 311-state even for larger systems. The corresponding real space interactions, presented in Section 6.4.5, show, that the 311-state can be stabilized for a reasonable, local interaction profile among the electrons.

The results presented in this chapter are product of a joint collaboration of Martin Greiter, Ronny Thomale and the author of this thesis [123].

### 6.1 Introduction

As detailed in Chapter 5, the quantum Hall effect (QHE) and quantum spin-Hall effect (QSHE) share many similarities. For the former, an integer version and a fractional version have been discovered. Therefore, the question arises: Is there an interaction-driven set of fractionalized phases with time reversal (T) symmetry? From now on, we will call such phases “fractional topological insulators” (FTIs).

Inspired by the construction of a topological insulator (TI) by the combination of two Haldane models, one for each spin species, a first step in answering this question is to look for a lattice realization of the fractional quantum Hall effect (FQHE). Due to particle interactions, this quest is much more intricate, but highly important if we recall that it is experimentally enormously challenging to achieve the settings needed to realize a FQH state: First, the electrons must be confined to a two-dimensional plane maintaining high electron mobility, as too much disorder destroys the FQHE. Second, a very strong magnetic field is needed for the Landau level quantization to be measurable. And third, only at low temperatures ( $<10\text{K}$ ), the FQH physics become manifest. Even nowadays, it remains tremendously intricate to reproduce all FQH states. Per contra, in lattice models, the interaction energy scale is at the order of ten or even one-hundred

Kelvin, and each unit cell usually sees a large effective magnetic field. This opens the possibility to stabilize exotic topological phases without large cooling units and external magnetic fields. Moreover, the interplay of topological order with lattice symmetries gives rise to a plethora of new physics beyond the continuum realization of the FQHE. One example are topological crystalline insulators, in which lattice symmetries protect the edge states [26].

The basic idea of the lattice realization of the QHE is that a single LL may be identified with an infinitely flat band of two-dimensional electrons with a non-trivial Chern number, as the electrons' energy is completely quenched due to LL quantization. For the IQHE, it was realized that a filled Chern band is equivalent to a filled LL. The extension to fractionally filled Chern bands holds as well: Fractional Chern insulators (FCIs) are the lattice analog of the FQHE [106; 128; 141; 121; 114; 155]. Microscopically, these flat band models create a (nearly) degenerate low-energy subspace. To generate an exact degeneracy, the electron hopping would have to span infinitely large distances. Instead, an approximately flat band is created by an exponential decay of the hopping amplitude. A relatively flat band can thus be created with a small number of hopping amplitudes. As a quantitative measure for this property, the flatness parameter equals the ratio of the band gap to the bandwidth. We actually do not need an exactly flat band, but a band which is so flat that the dependence of the energy on the different momenta is sub-dominant to the potential energy of the Coulomb interaction, meaning that the bandwidth is small compared to the Coulomb energy scale. If the kinetic energy was dominant, the electrons would arrange themselves in a Fermi sea, being the starting point for a perturbative analysis of weakly coupled systems.

Let us return to the question whether FTIs exist. At present, no such system could be realized experimentally, as most theoretical proposals so far are based on idealized models without relation to any existing material. One intuitive approach, in analogy to the construction of TIs, would be to take two copies of a FCI, one for each partner of the Kramers pairs [93; 13], resulting in a T-invariant system<sup>1</sup>:  $(\text{FTI}) = \text{FQHE} + \overline{\text{FQHE}}$ . Without any interaction between electrons of opposite spin, the corresponding ground state is a direct product of wave functions for both spin species. These states are from now on labeled fractional topological insulators (FTI). Several wave functions and model interactions for such FTIs have been constructed [114; 95; 130].

However, the FTIs investigated so far have two shortcomings. First, in order to stabilize a FQH fluid in a lattice model, electron-electron interaction energies on neighboring lattice sites of at least the order of the bandwidth are needed, which is only possible for extremely flat bands. In our project, we do not address this problem. Second, and more importantly, such states are well studied conceptually and do not lead to new physics, as the idea of taking a state and its mirror image together without any interaction between the states has been well understood in the context of TIs. So effectively replacing the IQH state (for the TI) by a FQH state (for the FTI) does not give rise to profoundly new physics, since the topological order (the fractionalization) and the symmetry protection do not entangle. Additionally, in real-life electronic systems, interactions between T-conjugate particles, for instance  $\uparrow$ -spin and  $\downarrow$ -spin particles, are present. Therefore, the community has been looking for ways to implement some topological entanglement between different spin species [137]. For all practical purposes so far, however, T symmetry has appeared to limit the set of possible fractional states to those with no interlocking between both "layers" of up- and down-spins [133]. Up to now, this is just an empirical observation, but it may be due to a theorem which has not yet been formulated or verified. Thus, the quest for a state beyond a FTI, a state where different spin species are entangled, ideally via topological order, remains open.

Our proposal is based on the idea that demanding T as protecting symmetry might be too restrictive. The concepts of protection of edge states via T and fractionalization are orthogonal. We found that, given two FQH-layers and looking for a way to interlock up- and down-spins, we do not necessarily need T as a protecting symmetry. Rather, the protection can be established through topological interlocking. Moreover, experience tells that it is difficult to realize both topological interlocking and protection by T [95; 130; 133],

---

<sup>1</sup> An alternative approach is presented in [158]: The authors apply a slave-rotor mean-field approach to study a bilayer honeycomb lattice with spin-orbit coupling and short-range electron-electron repulsion. A FQSH phase occurs, carried by fractionalized spinons



and, as alluded to above, it may well be that for reasons we presently do not know, both ways of protection cannot coexist.

In this chapter, we propose the very first example of a microscopic state where a topological entanglement is present, and hence introduce a new universality class of fractionally quantized, topologically ordered insulators. While  $T$  is no longer an exact symmetry, it is only violated in a subtle way, making it an “approximate symmetry”. By this, we mean that locally observable quantities such as the filling factors and quasi-particle charges in both layers are time reversal symmetry invariant. We refer to this situation as “topological time reversal symmetry breaking”. Our new universality class of FIs includes the previously established FTI as a trivial case. For our novel state, the meaning of “approximate” becomes clearer as we formulate our proposal in the upcoming sections. We choose a state in which the energetic cost of non-conservation of  $T$  is minimal: The interlayer interaction energies are similar to the  $T$ -symmetric case for non-interacting systems, while a significant interaction between the layers is present. Incidentally, if  $T$  was not even an approximate symmetry, we could still have an interesting state for further research.

The challenge in our work is not to find an energetically optimal state for our system. It is a proof-of-concept, in which we want to demonstrate that interlayer correlation through topological interlocking can be energetically advantageous. This opens the door for a possible generalization of the conceptual framework, investigating FIs which are not symmetry-protected but topologically protected.

As we know from recent discoveries, the protecting symmetry for TIs does not necessarily need to be  $T$ : For instance, topological crystalline insulators are protected by an interplay of  $T$ - and lattice symmetries [26; 68]. So far, there is a whole class of symmetry protected TIs, but we found the first topological phase protected by topology, meaning that the topological properties are not protected by a symmetry but by a topological entanglement itself. The step, we propose, from a conventional TI to a topologically stabilized TI is loosely comparable to the conceptual difference between conventional order and topological order, even though there are crucial differences. In a conventionally ordered system, a symmetry is violated and an order parameter can be defined, while in a topologically ordered system, the order manifests itself only through topological properties including fractional quantum numbers of excitations, emergent gauge fields, edge states and topological degeneracies on higher genus Riemann surfaces.

Another perspective on the problem is that, while the exact restoration of a symmetry like time reversal in a TI takes place on the level of single particle physics, the approximate restoration of a symmetry (for us  $T$ ) in a state as we propose here is intrinsically a many body effect. For our state, time reversal is violated by topological order, meaning that local quantities such as the filling factor and charge are the same in both layers. One has to employ a non-local probe to see the difference to a time reversal symmetric system, for instance by measuring the quasiparticle statistics, which is a non-local quantity. It is noteworthy that the spontaneous time reversal symmetry breaking by topological order, which amounts to a global symmetry breaking of a locally conserved symmetry, does not affect the dynamics of the edge states. The chiral edge states still form Kramers pairs, and are protected from backscattering by the local time reversal symmetry.

One important point to address is the issue of locality. We have developed and employed a method to formulate wave functions where topological interlocking is possible without the loss of locality. The locality of our state follows from the locality of the quasihole and quasiparticle excitations of the wave functions for FQH states. Their locality, on the other hand, stems from Laughlin’s gauge argument [85]: He created a quasihole by piercing a droplet of the Hall fluid with a magnetic flux tube, turning the flux adiabatically from  $\Phi = 0$  to  $\Phi = 2\pi$ . By the end of the process, the Hamiltonian of the state has evolved back to its initial form modulo a singular gauge transformation. We hence assume that the changes in the density of the Hall fluid occur locally in a region around the flux tube. The length scale determining the size of this region has to be the only available length scale in this problem, that is, the so-called magnetic length. The difference between quasihole and quasiparticle excitation lies merely in the direction, in which the flux is applied. The locality of the excitations has been amply confirmed by numerical studies [103].

So far, we have analyzed the 311-state only in a spherical geometry. For many purposes, however, it is highly desirable to embed the state into a system without rotational symmetry, such as a torus or cylinder. For instance, only on higher genus manifolds, quantum Hall states exhibit a topological ground state degeneracy. The framework of the parent Hamiltonian construction of Chapter 6.3 would have to be modified to accommodate cylindrical and toroidal geometries as indicated in [90], since it relies on the relative

angular momentum as an exact quantum number, which only applies for rotationally invariant systems. Pseudopotentials for systems without rotational symmetry would have to be defined, which is possible as outlined in [90].

## 6.2 Properties of the 311-state

### 6.2.1 Construction of the 311-state

To investigate the feasibility to stabilize a fractional insulator (FI), we construct a quantized Hall wave function, describing electrons in a two dimensional continuum subject to a perpendicular magnetic field. More precisely, we need a wave function for  $\uparrow$ - and  $\downarrow$ -spin electrons, which move in magnetic fields of equal magnitude but pointing in opposite directions, since we wish to describe a topological insulator with chiral edge modes protected by time reversal symmetry.

Our wave function for an FI is inspired by the explicit form of the Haldane-Halperin hierarchy states (2.6.1) [38] and a coupled-wire construction in [97]. In the plane, we have

$$\begin{aligned} \Psi_{m_\uparrow, m_\downarrow, n}[z, \bar{w}] &= \prod_{i=1}^{N_\uparrow} e^{-\frac{1}{4}|z_i|^2} \prod_{k=1}^{N_\downarrow} e^{-\frac{1}{4}|\bar{w}_k|^2} \\ &\cdot \frac{1}{\mathcal{N}} \prod_{k<l}^{N_\downarrow} (\bar{w}_k - \bar{w}_l)^{m_\downarrow} \prod_k^{N_\downarrow} \prod_i^{N_\uparrow} (\bar{w}_k - 2\frac{\partial}{\partial z_i})^n \prod_{i<j}^{N_\uparrow} (z_i - z_j)^{m_\uparrow}, \end{aligned} \quad (6.2.1)$$

where  $\mathcal{N}$  is the overall normalization of the state, and  $z_1, \dots, z_{N_\uparrow}$  and  $w_1, \dots, w_{N_\downarrow}$  denote the coordinates of the  $\uparrow$  and  $\downarrow$  electrons, respectively, in complex coordinate notation. The bars above the  $w$ -coordinates indicate complex conjugation. The exponents  $m_\uparrow$  and  $m_\downarrow$  are positive, odd integers and  $n \in \mathbb{Z}$ .

A translational invariant version is derived by placing the wave function on a unit sphere, as explained in Section 2.4, yielding the wave function

$$\begin{aligned} \Psi_{m_\uparrow, m_\downarrow, n}[u, v, \bar{a}, \bar{b}] &= \\ \frac{1}{\mathcal{N}} \prod_{k<l}^{N_\downarrow} (\bar{a}_k \bar{b}_l - \bar{a}_l \bar{b}_k)^{m_\downarrow} \prod_k^{N_\downarrow} \prod_i^{N_\uparrow} \left( \bar{b}_k \frac{\partial}{\partial u_i} - \bar{a}_k \frac{\partial}{\partial v_i} \right)^n \prod_{i<j}^{N_\uparrow} (u_i v_j - u_j v_i)^{m_\uparrow}. \end{aligned} \quad (6.2.2)$$

This state realizes a system of  $N_\uparrow$  particles of flavor  $\uparrow$  and  $N_\downarrow$  particles of flavor  $\downarrow$ , which are described by the spinor coordinates  $(u, v)$  and  $(\bar{a}, \bar{b})$ , respectively. It can be visualized as a two-layered system, one for flavor  $\uparrow$  and one for flavor  $\downarrow$ . As formally reflected in the complex conjugation, the  $\downarrow$ -particles experience a magnetic field  $B_\downarrow$  with opposite direction as compared to the magnetic field  $B_\uparrow$  for the  $\uparrow$ -particles.

The flux quanta seen in each layer are

$$2s_\uparrow = N_{\Phi, \uparrow} = m_\uparrow(N_\uparrow - 1) - nN_\downarrow \quad (6.2.3)$$

and

$$2s_\downarrow = N_{\Phi, \downarrow} = m_\downarrow(N_\downarrow - 1) + nN_\uparrow. \quad (6.2.4)$$

We assume that the magnetic field in both layers is of equal strength,  $N_{\Phi, \uparrow} = N_{\Phi, \downarrow} = N_\Phi$ . The filling fraction is defined by

$$\frac{1}{\nu} := \left. \frac{\partial N_\Phi}{\partial N} \right|_{N \rightarrow \infty}, \quad (6.2.5)$$

such that the filling fractions in both layers are given by

$$\begin{pmatrix} \nu_\uparrow \\ \nu_\downarrow \end{pmatrix} = \frac{1}{m_\uparrow m_\downarrow + n^2} \begin{pmatrix} m_\downarrow + n \\ m_\uparrow - n \end{pmatrix}. \quad (6.2.6)$$

In our numerical analysis, however, we assume an unpolarized ground state, i.e. equal particle numbers  $N_\uparrow = N_\downarrow$ . The filling fractions in both layers then are

$$\nu_{\uparrow} = \frac{1}{m_{\uparrow} - n} \quad \text{and} \quad \nu_{\downarrow} = \frac{1}{m_{\downarrow} + n}. \quad (6.2.7)$$

In general, (6.2.6) and (6.2.7) give different results. For our state, we choose  $m_{\uparrow} = 3$ ,  $m_{\downarrow} = 1$  and  $n = 1$ , to which we from now on refer to as the “311-state”. This is the simplest applicable choice for which the filling fractions are identical,  $\nu_{\uparrow} = \nu_{\downarrow} = 1/2$ . This guarantees that time reversal symmetry is locally valid. Another possible choice preserving time-reversal symmetry locally is  $m_{\uparrow} = 5$ ,  $m_{\downarrow} = 1$  and  $n = 2$ . In this 512-state, it is  $\nu_{\uparrow} = \nu_{\downarrow} = 1/3$ .

The state (6.2.2) starts with a Laughlin state of filling fraction  $1/m_{\uparrow}$  for the  $\uparrow$ -particles and a completely filled lowest Landau level for the  $\downarrow$ -particles. The effect of the interflavor term

$$\prod_r \prod_s \left( \bar{b}_s \frac{\partial}{\partial u_r} - \bar{a}_s \frac{\partial}{\partial v_r} \right)^n$$

can be understood by comparing our state to the Laughlin state with a quasielectron (2.3.5): The  $\uparrow$ -particles see quasielectrons at the positions of the  $\downarrow$ -particles. The quasiparticles decrease the flux through the  $\uparrow$ -sphere by  $nN_{\downarrow}$ . This implies that the degree of the polynomial for the  $\downarrow$ -particles increases by  $nN_{\uparrow}$ , while the total flux seen by the  $\downarrow$ -particles increases by  $nN_{\uparrow}$ . The interflavor term thus shifts zeros from the  $\uparrow$ -layer to the  $\downarrow$ -layer. As far as the filling factors are concerned, increasing  $n$  thereby effectively increases  $\nu_{\uparrow}$  while decreasing  $\nu_{\downarrow}$ . Since quasiparticles correspond to a surplus of electron charge, we see that the density of  $\uparrow$ -particles is increased at the position of the  $\downarrow$ -particles. In other words, the interlayer correlation is attractive. When both fillings factors are equal, the quasiparticle excitations in both groups carry opposite charges which are equal in magnitude.

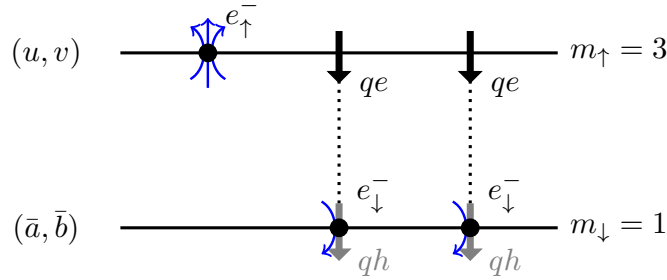


**Fig. 6.1** Illustration of the 311-state. In the  $\uparrow$ -layer, the particles  $e_{\uparrow}^{-}$  have spherical coordinates  $(u, v)$  and live in a Laughlin state with filling fraction  $1/m_{\uparrow} = 1/3$  before the interlayer interaction is turned on. In the  $\downarrow$ -layer, the particles  $e_{\downarrow}^{-}$ , have coordinates  $(\bar{a}, \bar{b})$  and start off in a filled lowest Landau level,  $m_{\downarrow} = 1$ . The  $\uparrow$ -particles see quasielectrons (qe) at the positions of the  $\downarrow$ -particles, which remove one zero each in the  $\uparrow$ -layer. This corresponds to quasiholes (qh) adding zeros in the  $\downarrow$ -layer, yielding one extra zero per electron. Finally, the number of zeros in each layer is two per electron, which implies  $\nu_{\uparrow} = \nu_{\downarrow} = \frac{1}{2}$ .

## 6.2.2 Angular momentum calculation and rotational invariance

As we are dealing with a two-layer system in which the magnetic fields point in opposite directions, the calculation of angular momenta is somewhat more subtle. Remembering the formalism leading to (2.4.10), in the lowest Landau level, the angular momentum  $\mathbf{L}$  is

$$\mathbf{L} = \frac{1}{2}(u, v)\boldsymbol{\sigma} \begin{pmatrix} \partial_u \\ \partial_v \end{pmatrix}.$$

This formalism is applicable for the  $\uparrow$ -layer, where we describe the particles by spinor coordinates

$$\begin{aligned} u &= \cos\left(\frac{\theta}{2}\right) e^{i\frac{\varphi}{2}}, \\ v &= \sin\left(\frac{\theta}{2}\right) e^{-i\frac{\varphi}{2}}. \end{aligned} \quad (6.2.8)$$

The angular momentum components are

$$\begin{aligned} L_{\uparrow}^z &= \frac{1}{2}(u\partial_u - v\partial_v), \\ L_{\uparrow}^+ &= u\partial_v, \\ L_{\uparrow}^- &= v\partial_u. \end{aligned} \quad (6.2.9)$$

The spinor coordinates  $u$  and  $v$  can also be viewed as independent boson creation operators, and their derivative operators  $\partial_u$  and  $\partial_v$  as the conjugate destruction operators.

As detailed in Section 2.4, the states

$$\psi_{m,0}^s(u, v) = \sqrt{\frac{(2s+1)!}{(s+m)!(s-m)!}} u^{s+m} v^{s-m} \quad (6.2.10)$$

form a complete orthogonal basis,  $m = -s, -s+1, \dots, s$ . A single particle state localized at position  $\mathbf{\Omega}(\alpha, \beta)$ , defined in (2.4.14), is given by

$$\Psi_{(\alpha,\beta)}(u, v) = (\bar{\alpha}u + \bar{\beta}v)^{2s}. \quad (6.2.11)$$

Its angular momentum along  $\mathbf{\Omega}$  is  $s$ , since

$$(\mathbf{\Omega} \cdot \mathbf{L}_{\uparrow}) \Psi_{(\alpha,\beta)}(u, v) = s \Psi_{(\alpha,\beta)}(u, v) \quad (6.2.12)$$

and, according to [36],

$$(\mathbf{\Omega} \cdot \mathbf{L}_{\uparrow}) = (u, v) \begin{pmatrix} \bar{\alpha} \\ \bar{\beta} \end{pmatrix} (\alpha, \beta) \begin{pmatrix} \partial_u \\ \partial_v \end{pmatrix} - \frac{1}{2}(\alpha\bar{\alpha} + \beta\bar{\beta})(u\partial_u + v\partial_v). \quad (6.2.13)$$

In Figure 6.2,  $\mathbf{\Omega}$  is chosen to point towards the north pole, so that  $\alpha = 1$  and  $\beta = 0$ . Then,  $\uparrow$ -particles with maximal angular momentum  $s$  along  $\mathbf{\Omega}$ , described by (6.2.11), are located at the north pole, while particles at the south pole have angular momentum  $-s$ .

A more intuitive understanding of the state (6.2.11) can be achieved by the following considerations: The chord distance between two points on the unit sphere is given by

$$|\mathbf{\Omega}(u_1, v_1) - \mathbf{\Omega}(u_2, v_2)| = 2|u_1v_2 - u_2v_1|. \quad (6.2.14)$$

Given a point  $\mathbf{\Omega}(\alpha, \beta)$  on the sphere, the point antipodal to it is  $-\mathbf{\Omega}(\alpha, \beta) = \mathbf{\Omega}(\bar{\beta}, -\bar{\alpha})$ , since insertion into (6.2.14) gives

$$|\mathbf{\Omega}(\alpha, \beta) - \mathbf{\Omega}(\bar{\beta}, -\bar{\alpha})| = 2(|\alpha|^2 + |\beta|^2) = 2.$$

Then the absolute value of state (6.2.11) is proportional to the distance of point  $(u, v)$  to the point  $P'$  antipodal to  $(\alpha, \beta)$  taken to the power  $2s$ , since the distance is

$$|\mathbf{\Omega}(u, v) - \mathbf{\Omega}(\bar{\beta}, -\bar{\alpha})| = 2|\bar{\alpha}u + \bar{\beta}v|.$$

For the  $\downarrow$ -layer, however, the sign of the magnetic field is reversed. Thus, the spinor coordinates are

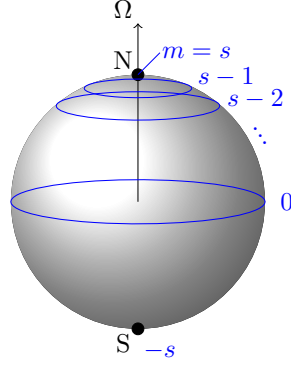


**Fig. 6.2** Localization of a single-particle state on the  $\uparrow$ -sphere for an angular momentum component along  $\Omega$  of  $m$ . For maximum angular momentum  $m = s$ , the state is localized at the north pole.

$$\begin{aligned}\bar{a} &= \cos\left(\frac{\theta}{2}\right) e^{-i\frac{\varphi}{2}}, \\ \bar{b} &= \sin\left(\frac{\theta}{2}\right) e^{i\frac{\varphi}{2}}.\end{aligned}\tag{6.2.15}$$

The states

$$\psi_{m',0}^{s'}(\bar{a}, \bar{b}) = \sqrt{\frac{(2s'+1)!}{(s'+m')!(s'-m')!}} \bar{a}^{s'-m'} \bar{b}^{s'+m'}\tag{6.2.16}$$

form a complete orthogonal basis,  $m' = -s', -s'+1, \dots, s'$ .

Since  $\Psi_{(\alpha,\beta)}(u, v)$  is located around  $\Omega(\alpha, \beta)$  on the sphere, the same holds for

$$\Psi'_{(\alpha,\beta)}(\bar{a}, \bar{b}) = (\alpha\bar{a} + \beta\bar{b})^{2s'}.\tag{6.2.17}$$

In this case, however, the angular momentum points to the antipodal point  $-\Omega(\alpha, \beta)$ , as we will explain now.

At the north pole,  $\alpha = e^{i\xi}$  and  $\beta = 0$ , where  $\xi$  is a pure phase. Since the complex-valuedness of  $\alpha$  only adds a phase  $\xi$  to the wave function  $\Psi'$ , we can set it to 0, such that  $\alpha = 1$ . Then  $\Psi'$  becomes

$$\Psi'_{(1,0)}(\bar{a}, \bar{b}) = \bar{a}^{2s'} = e^{-is'\varphi}.\tag{6.2.18}$$

Thus, the  $z$ -component of the angular momentum operator

$$L_{\downarrow}^z = -i\frac{\partial}{\partial\varphi}\tag{6.2.19}$$

is  $L_{\downarrow}^z = -s'$ . We therefore need to construct an angular momentum operator for the  $\downarrow$ -particle which fulfills

$$(\Omega \cdot \mathbf{L}_{\downarrow})\Psi'_{(\alpha,\beta)}(\bar{a}, \bar{b}) = -s'\Psi'_{(\alpha,\beta)}(\bar{a}, \bar{b}),\tag{6.2.20}$$

with

$$\Omega(\alpha, \beta) = (\alpha, \beta)\boldsymbol{\sigma} \begin{pmatrix} \bar{\alpha} \\ \bar{\beta} \end{pmatrix} = (\bar{\alpha}, \bar{\beta})\boldsymbol{\sigma}^{\top} \begin{pmatrix} \alpha \\ \beta \end{pmatrix}.\tag{6.2.21}$$

The previous expression (6.2.21) can be proven by explicitly writing out  $\Omega$ ,

$$\begin{aligned}
\Omega_z &= \alpha\bar{\alpha} - \beta\bar{\beta} = \cos^2\left(\frac{\theta}{2}\right) - \sin^2\left(\frac{\theta}{2}\right) = \cos(\theta), \\
\Omega_x &= \alpha\bar{\beta} + \bar{\alpha}\beta = \cos\left(\frac{\theta}{2}\right)\sin\left(\frac{\theta}{2}\right)(e^{i\varphi} + e^{-i\varphi}) = \sin(\theta)\cos(\varphi), \\
\Omega_y &= -i(\alpha\bar{\beta} - \bar{\alpha}\beta) = \dots = \sin(\theta)\sin(\varphi).
\end{aligned} \tag{6.2.22}$$

The operator

$$\mathbf{L}_\downarrow = -\frac{1}{2}(\bar{a}, \bar{b})\boldsymbol{\sigma}^\top \begin{pmatrix} \partial_{\bar{a}} \\ \partial_{\bar{b}} \end{pmatrix}. \tag{6.2.23}$$

fulfills the Lie algebra and the above requirement (6.2.20). It is thus the total angular momentum for the  $\downarrow$ -layer.

We then have

$$(\boldsymbol{\Omega} \cdot \mathbf{L}_\downarrow) = -(\bar{a}, \bar{b}) \begin{pmatrix} \alpha \\ \beta \end{pmatrix} (\bar{\alpha}, \bar{\beta}) \begin{pmatrix} \partial_{\bar{a}} \\ \partial_{\bar{b}} \end{pmatrix} + \frac{1}{2}(\bar{\alpha}\alpha + \bar{\beta}\beta)(\bar{a}\partial_{\bar{a}} + \bar{b}\partial_{\bar{b}}). \tag{6.2.24}$$

The components of the angular momentum are

$$\begin{aligned}
L_\downarrow^z &= -\frac{1}{2}(\bar{a}\partial_{\bar{a}} - \bar{b}\partial_{\bar{b}}), \\
L_\downarrow^+ &= -\bar{b}\partial_{\bar{a}}, \\
L_\downarrow^- &= -\bar{a}\partial_{\bar{b}}.
\end{aligned} \tag{6.2.25}$$

Obviously, the  $\downarrow$ -layer components have a minus sign as compared to the  $\uparrow$ -components (6.2.9). Thus, for maximum  $L_\downarrow^z$ -eigenvalue  $s'$ , the single-particle state is located at the south pole of the  $\downarrow$ -sphere. This state is maximally separated from a single-particle state on the  $\uparrow$ -sphere with maximum  $L_\uparrow^z$ -eigenvalue, which sits at the north pole.

The 311-state is invariant under spacial rotations around the sphere, i.e., it is a singlet state with respect to the total angular momentum:  $\mathbf{L}_{\text{tot}}^2 |\Psi_{311}\rangle = 0$ , with

$$\begin{aligned}
\mathbf{L}_{\text{tot}} &= \mathbf{L}_{\text{tot}}^\uparrow + \mathbf{L}_{\text{tot}}^\downarrow, \\
\mathbf{L}_{\text{tot}}^\alpha &= \sum_{i=1}^{N_\alpha} \mathbf{L}_i^\alpha, \quad \alpha = \uparrow, \downarrow.
\end{aligned} \tag{6.2.26}$$

The singlet nature of the 311-state can be verified both analytically and numerically for finite systems. The easiest way to do this is to verify  $L_{\text{tot}}^z |\Psi_{311}\rangle = 0$  and to check if the ladder operator  $L_{\text{tot}}^+$  annihilates the state,

$$L_{\text{tot}}^+ |\Psi_{311}\rangle = 0, \tag{6.2.27}$$

as only rotationally invariant states fulfill this requirement. The total ladder operator is

$$L_{\text{tot}}^+ = \sum_{i=1}^{N_\uparrow} L_{\uparrow,i}^+ + \sum_{j=1}^{N_\downarrow} L_{\downarrow,j}^+ \tag{6.2.28}$$

$$= \sum_i u_i \partial_{v_i} - \sum_j \bar{b}_j \partial_{\bar{a}_j}. \tag{6.2.29}$$

The above statement (6.2.27) can be easily proven, since  $L_{\text{tot}}^+$  commutes with each of the three factors of the 311-state (6.2.2). For instance, for the interlayer term, we have

$$\begin{aligned} \left[ L_{\text{tot}}^+, \left( \bar{b}_k \frac{\partial}{\partial u_i} - \bar{a}_k \frac{\partial}{\partial v_i} \right) \right] &= \left[ \sum_l u_l \frac{\partial}{\partial v_l}, \bar{b}_k \frac{\partial}{\partial u_i} \right] + \left[ \sum_l \bar{b}_l \frac{\partial}{\partial \bar{a}_l}, \bar{a}_k \frac{\partial}{\partial v_i} \right] \\ &= -\frac{\partial}{\partial v_i} \bar{b}_k + \bar{b}_k \frac{\partial}{\partial v_i} = 0. \end{aligned} \quad (6.2.30)$$

We have also confirmed the singlet nature of the wave function for all available system sizes.

### 6.2.3 Effective field theory of the 311-state

An effective field theory of the 311-state can be formulated, and we will summarize the main results here. A detailed derivation will be subject of a future publication by our research group.

For the Lagrangian, we get

$$\mathcal{L} = -\frac{1}{4\pi} \varepsilon^{\mu\nu\rho} \mathbf{a}_\mu^\top K \partial_\nu \mathbf{a}_\rho - \frac{1}{2\pi} \varepsilon^{\mu\nu\rho} (\mathbf{a}_\mu^\top \mathbf{q}) \partial_\nu A_\rho + (\mathbf{a}_\mu^\top \mathbf{l}) J_{\text{QP}}^\mu, \quad (6.2.31)$$

where we sum over repeated indices. The  $K$ -matrix, charge vector  $\mathbf{q}$  and vector  $\mathbf{l}$  are specified by

$$K = \begin{pmatrix} 3 & -1 \\ -1 & -1 \end{pmatrix}, \quad \mathbf{q} = \begin{pmatrix} 1 \\ -1 \end{pmatrix}, \quad \mathbf{l} = \begin{pmatrix} l_\uparrow \\ l_\downarrow \end{pmatrix} \quad (6.2.32)$$

In terms of the above quantities, the quantum Hall conductivity  $\sigma_{xy}$ , the quasiparticle charge  $Q_{\text{QP}}$  and the exchange phase  $\theta$  can be expressed as

$$\sigma_{xy} = \frac{e^2}{h} \mathbf{q}^\top K^{-1} \mathbf{q}, \quad Q_{\text{QP}} = \mathbf{q}^\top K^{-1} \mathbf{l}, \quad \theta = \pi \mathbf{l}^\top K^{-1} \mathbf{l}. \quad (6.2.33)$$

For the 311-state, we have

$$\sigma_{xy} = 0, \quad Q_\uparrow = Q_\downarrow = \frac{1}{2}, \quad \theta_\uparrow = \frac{\pi}{4}, \quad \theta_\downarrow = -\frac{3\pi}{4}. \quad (6.2.34)$$

Comparing this result to the state proposed by Meng et al. [97], we see that both systems are equivalent: After interchanging the labels of the first and second layer ( $K \rightarrow \tilde{K}$ ,  $q \rightarrow \tilde{q}$ ), the two systems can be transformed into each other via a simple transformation matrix [145],  $W \in SL(n, Z)$ , according to

$$K' = W \tilde{K} W^T, \quad q' = W \tilde{q}, \quad W = \begin{pmatrix} 0 & 1 \\ 1 & 0 \end{pmatrix}. \quad (6.2.35)$$

### 6.2.4 Pair correlation function

The pair correlation function  $g(\mathbf{r})$  of a many particle system describes how its particle density varies as a function of distance to a reference particle [7]. Loosely speaking, it is related to the probability of finding a particle at a specified distance from a reference particle. In order to link microscopic details to macroscopic properties, this function is of fundamental interest. In this section, the analytical construction of the pair correlation function is presented. In Section 6.4.2, the numerical results for our 311-state are discussed.

In case of a two-flavor system, as for the 311-state, there are three different types of pair correlation functions: two intraflavor correlations  $g_{\uparrow\uparrow}$  and  $g_{\downarrow\downarrow}$ , and one interflavor correlation  $g_{\uparrow\downarrow}$ . On the sphere, for a system with  $N_\uparrow$  ( $N_\downarrow$ ) spin-up (spin-down) particles with spinor coordinates  $(u_i, v_i)$  ( $(\bar{a}_i, \bar{b}_i)$ ), they are



$$\begin{aligned}
N_\uparrow(N_\uparrow - 1)g_{\uparrow\uparrow}(u_1, v_1, u_2, v_2) &= \prod_{i=3}^{N_\uparrow} \int D(u_i, v_i) \\
&\cdot \prod_{k=1}^{N_\downarrow} \int D(\bar{a}_k, \bar{b}_k) \bar{\Psi}_{311}(\{u_i, v_i\}_i, \{\bar{a}_k, \bar{b}_k\}_k) \Psi_{311}(\{u_i, v_i\}_i, \{\bar{a}_k, \bar{b}_k\}_k),
\end{aligned} \tag{6.2.36}$$

$$\begin{aligned}
N_\downarrow(N_\downarrow - 1)g_{\downarrow\downarrow}(\bar{a}_1, \bar{b}_1, \bar{a}_2, \bar{b}_2) &= \prod_{i=1}^{N_\uparrow} \int D(u_i, v_i) \\
&\cdot \prod_{k=3}^{N_\downarrow} \int D(\bar{a}_k, \bar{b}_k) \bar{\Psi}_{311}(\{u_i, v_i\}_i, \{\bar{a}_k, \bar{b}_k\}_k) \Psi_{311}(\{u_i, v_i\}_i, \{\bar{a}_k, \bar{b}_k\}_k),
\end{aligned} \tag{6.2.37}$$

$$\begin{aligned}
N_\downarrow N_\uparrow g_{\downarrow\uparrow}(u_1, v_1, \bar{a}_1, \bar{b}_1) &= \prod_{i=2}^{N_\uparrow} \int D(u_i, v_i) \\
&\cdot \prod_{k=2}^{N_\downarrow} \int D(\bar{a}_k, \bar{b}_k) \bar{\Psi}_{311}(\{u_i, v_i\}_i, \{\bar{a}_k, \bar{b}_k\}_k) \Psi_{311}(\{u_i, v_i\}_i, \{\bar{a}_k, \bar{b}_k\}_k).
\end{aligned} \tag{6.2.38}$$

We integrate out all particle coordinates except for two.

To numerically calculate these quantities, we write out the correlation functions in terms of creation and annihilation operators. To begin with, we take a system with only one particle flavor. Extending this feature to a two flavor-system is straightforward. A normalized single particle state with spinor coordinates  $(u_1, v_1)$  is

$$|u_1, v_1\rangle = \Psi^\dagger(u_1, v_1) |0\rangle = \sum_{\beta=0}^{2s} \frac{1}{\mathcal{N}_\beta} \bar{u}_1^\beta \bar{v}_1^{2s-\beta} c_\beta^\dagger |0\rangle, \tag{6.2.39}$$

with the normalization  $\mathcal{N}_\beta^2 = \frac{\beta!(2s-\beta)!}{(2s+1)!}$ . The single-particle state fulfills the completeness relation

$$\int D(u_1, v_1) |u_1, v_1\rangle \langle u_1, v_1| = \mathbb{1}. \tag{6.2.40}$$

A many particle state in second quantization, consisting of  $M$  configurations, is

$$\begin{aligned}
|\alpha\rangle &= \sum_{n=1}^M \alpha_n |\alpha_n\rangle = \sum_n \alpha_n |n_0, n_1, \dots, n_{2s}\rangle \\
&= \sum_{n=1}^M \alpha_n \frac{(c_0^\dagger)^{n_0}}{\sqrt{n_0!}} \frac{(c_1^\dagger)^{n_1}}{\sqrt{n_1!}} \dots \frac{(c_{2s}^\dagger)^{n_{2s}}}{\sqrt{n_{2s}!}} |0\rangle_N,
\end{aligned} \tag{6.2.41}$$

with  $|n_0, n_1, \dots, n_{2s}\rangle$  being the occupation number basis, id est  $n_i$  indicates the number of particles in orbital  $i$  and  $2s + 1$  is the number of orbitals in the state. For a fermionic system, the orbitals can be at most singly occupied,  $n_i = 0, 1$ . Each configuration is labelled by its orbital occupation  $n = n_0, n_1, \dots, n_{2s}$ .

To calculate the pair correlation function, we integrate out all but two particles

$$\begin{aligned}
N(N-1)g(u_1, v_1, u_2, v_2) &= \langle \alpha | u_1, v_1 \rangle |u_2, v_2\rangle \langle u_2, v_2 | \langle u_1, v_1 | \alpha \rangle \\
&= \sum_{n=1}^M \sum_{n'=1}^M \sum_{\beta, \gamma} \sum_{\beta', \gamma'} \bar{\alpha}_{n'} \alpha_n \frac{1}{\mathcal{N}_\beta} \frac{1}{\mathcal{N}_\gamma} \frac{1}{\mathcal{N}_{\beta'}} \frac{1}{\mathcal{N}_{\gamma'}} \bar{u}_1^{\beta'} \bar{v}_1^{-2s-\beta'} \bar{u}_2^{-\gamma'} \bar{v}_2^{-2s-\gamma'} u_1^\beta v_1^{2s-\beta} u_2^\gamma v_2^{2s-\gamma} \\
&\cdot {}_N \langle 0 | \frac{(c_{2s})^{n_{2s}}}{\sqrt{n_{2s}!}} \dots \frac{(c_1)^{n_1}}{\sqrt{n_1!}} c_\beta^\dagger c_\gamma^\dagger c_{\gamma'} c_{\beta'} \frac{(c_1^\dagger)^{n_1}}{\sqrt{n_1!}} \dots \frac{(c_{2s}^\dagger)^{n_{2s}}}{\sqrt{n_{2s}!}} |0\rangle_N.
\end{aligned} \tag{6.2.42}$$

In general, all matrix elements, diagonal ( $n = n'$ ) as well as off-diagonal ( $n \neq n'$ ), contribute to the pair correlation function. However, if we pin the first particle at the south pole,  $(u_1, v_1) = (0, 1)$ , only those configurations with the first particle in the orbital 0 contribute, which imposes  $\beta = \beta' = 0$ . As a reminder, according to Haldane's definition [53] of a set of spinor coordinates  $(a, b)$ , they correspond to a point  $\Omega(a, b)$  with

$$\Omega(a, b) = (a, b)\sigma\left(\frac{\bar{a}}{\bar{b}}\right), \quad (6.2.43)$$

where  $\sigma$  is the Pauli matrix vector. Thus, the above values correspond to real space positions  $\Omega(0, 1) = (0, 0, -1)$  and  $\Omega(\sin(\theta/2), \cos(\theta/2)) = (\sin(\theta), 0, -\cos(\theta))$ .

Now, if we fix one particle to a specific orbital, only diagonal matrix elements can contribute to the pair correlation function as the total angular momentum in  $z$ -direction is conserved for each configuration. This decisively simplifies the above equation (6.2.42) to

$$\begin{aligned} N(N-1)g(u_1, v_1, u_2, v_2) &= \sum_n |\alpha_n|^2 \langle \alpha_n | u_1, v_1 \rangle |u_2, v_2\rangle \langle u_2, v_2 | \langle u_1, v_1 | \alpha_n \rangle \\ &= \sum_{n=1}^M \sum_{\beta, \gamma=0}^{2s} \sum_{\beta', \gamma'=0}^{2s} |\alpha_n|^2 \frac{1}{\mathcal{N}_\beta} \frac{1}{\mathcal{N}_\gamma} \frac{1}{\mathcal{N}_{\beta'}} \frac{1}{\mathcal{N}_{\gamma'}} \bar{u}_1^{\beta'} \bar{v}_1^{2s-\beta'} \bar{u}_2^{\gamma'} \bar{v}_2^{2s-\gamma'} u_1^\beta v_1^{2s-\beta} u_2^\gamma v_2^{2s-\gamma} \langle \alpha_n | c_\beta^\dagger c_\gamma^\dagger c_{\gamma'} c_{\beta'} | \alpha_n \rangle. \end{aligned} \quad (6.2.44)$$

We can further simplify

$$\langle \alpha_n | c_\beta^\dagger c_\gamma^\dagger c_{\gamma'} c_{\beta'} | \alpha_n \rangle = -\delta_{\beta, \gamma'} \delta_{\gamma, \beta'} \langle \alpha_n | n_\beta n_\gamma | \alpha_n \rangle + \delta_{\beta, \beta'} \delta_{\gamma, \gamma'} \langle \alpha_n | n_\beta n_\gamma | \alpha_n \rangle \quad (6.2.45)$$

with the number operator  $n_\beta = c_\beta^\dagger c_\beta$ . Inserting (6.2.45) into (6.2.44) yields

$$\begin{aligned} N(N-1)g(u_1, v_1, u_2, v_2) &= \sum_n \sum_{\beta, \gamma} |\alpha_n|^2 \frac{1}{\mathcal{N}_\beta^2 \mathcal{N}_\gamma^2} n_\beta n_\gamma \\ &\cdot \left( \bar{u}_1^\beta \bar{v}_1^{2s-\beta} \bar{u}_2^\gamma \bar{v}_2^{2s-\gamma} u_1^\beta v_1^{2s-\beta} u_2^\gamma v_2^{2s-\gamma} - \bar{u}_1^\beta \bar{v}_1^{2s-\beta} \bar{u}_2^\gamma \bar{v}_2^{2s-\gamma} u_1^\gamma v_1^{2s-\gamma} u_2^\beta v_2^{2s-\beta} \right). \end{aligned} \quad (6.2.46)$$

The pair correlation function of particles with different flavor, e.g. spin-up particles with coordinates  $(u_1, v_1)$  and spin-down particles with coordinates  $(\bar{a}_1, \bar{b}_1)$ , with the spin-down particle pinned at the south pole, is

$$N_\uparrow N_\downarrow g(\bar{a}_1, \bar{b}_1, u_1, v_1) = \sum_n \sum_{\beta=0}^{2s_\uparrow} \sum_{\gamma=0}^{2s_\downarrow} |\alpha_n|^2 \frac{1}{\mathcal{N}_\beta^2 \mathcal{N}_\gamma^2} n_\beta n_\gamma \cdot a_1^{\gamma \uparrow} \bar{a}_1^{2s_\downarrow - \gamma} \bar{u}_1^\beta \bar{v}_1^{2s_\uparrow - \beta} \bar{a}_1^{\gamma \uparrow} \bar{a}_1^{2s_\downarrow - \gamma} u_1^\beta v_1^{2s_\uparrow - \beta}. \quad (6.2.47)$$

For a bosonic system with  $N$  particles, the pair correlation function with one particle pinned at the south pole  $((u_1, v_1) = (0, 1))$  simplifies accordingly. However, we get an additional term in expression (6.2.45) for the case  $\beta = \gamma = \beta' = \gamma'$  which is excluded in the fermionic case. It is

$$\begin{aligned} N(N-1)g(u_1, v_1, u_2, v_2) &= \\ &\sum_n \sum_{\beta, \gamma} |\alpha_n|^2 \left( (1 - \delta_{\beta, \gamma}) \frac{1}{\mathcal{N}_\beta^2 \mathcal{N}_\gamma^2} n_\beta n_\gamma \right. \\ &\cdot (\bar{u}_1^\beta \bar{v}_1^{2s-\beta} \bar{u}_2^\gamma \bar{v}_2^{2s-\gamma} u_1^\beta v_1^{2s-\beta} u_2^\gamma v_2^{2s-\gamma} + \bar{u}_1^\beta \bar{v}_1^{2s-\beta} \bar{u}_2^\gamma \bar{v}_2^{2s-\gamma} u_1^\gamma v_1^{2s-\gamma} u_2^\beta v_2^{2s-\beta}) \\ &\left. + \delta_{\beta, \gamma} \frac{1}{\mathcal{N}_\beta^4} n_\beta (n_\beta - 1) \bar{u}_1^\beta \bar{v}_1^{2s-\beta} \bar{u}_2^\beta \bar{v}_2^{2s-\beta} u_1^\beta v_1^{2s-\beta} u_2^\beta v_2^{2s-\beta} \right). \end{aligned} \quad (6.2.48)$$

To check the correctness of the correlation functions, the particle density  $\rho(u_1, v_1)$  can be calculated by integrating out one particle degree of freedom of the correlation function  $g(u_1, v_1, u_2, v_2)$ ,

$$\rho(u_1, v_1) = \int D(u_1, v_1) g(u_1, v_1, u_2, v_2). \quad (6.2.49)$$

We expect a constant particle density over the whole sphere, as the particles spread over it evenly.

### 6.3 Construction of a parent Hamiltonian

The knowledge of a parent Hamiltonian is crucial for the characterization of a specified state. Therefore, we wish to derive a parent Hamiltonian for our 311-state. For the system to be experimentally viable, this Hamiltonian optimally contains only short-range interactions. In the following chapter, we introduce a numerical method to construct an approximate parent Hamiltonian for any specified state.

#### 6.3.1 Pseudopotentials

Initially, pair pseudopotentials were developed by Haldane in the context of the FQHE [53], expressing the interaction energy of a pair of particles in terms of their relative angular momentum. The formalism applies to QH systems in the infinite plane or on the surface of a sphere. In such cases, the system is invariant under transformations around at least one axis, so that the Wigner-Eckart theorem (4.2.15) applies.

According to the Wigner-Eckart theorem, any long range interaction  $V$  in a spherically symmetric system decomposes into a discrete set of components depending only on the relative angular momentum, the so-called pseudopotential coefficients. These are partial wave expansion coefficients of  $N$ -body interactions. For two particle-scattering, the pseudopotential is a quantitative measure of the interaction energy in terms of the relative angular momentum. Generalizations to more than two bodies allow the expansion of a wider range of interaction types [131]. For instance, the ‘‘Pfaffian’’ state [100] has a parent Hamiltonian which is the shortest-range repulsion potential acting on three particles at a time [47; 48; 119]. The pseudopotential formalism has proven to be very useful to universally classify different interaction profiles, to provide an adequate description of FQHE phase diagrams, and to find a parent Hamiltonian to a specified FQH wave function. In the following, we will restrict our analysis to pair pseudopotentials.

Let us consider a sphere of radius  $R$  with a magnetic monopole placed at the center of the sphere, resulting in a radial magnetic field  $B$ . Due to Dirac’s quantization condition, the total flux  $4\pi R^2 B$  equals an integer  $2s$  of the elementary flux quantum  $h/e$ . Taking  $c = 1$ , we have

$$B = \frac{\hbar s}{eR^2} \iff s = \frac{R^2}{a_0^2}, \quad (6.3.1)$$

with  $a_0 = (\hbar/eB)^{1/2}$  the magnetic length. In the following, we again set  $\hbar = 1$ . The kinetic energy within a single LL is effectively constant. Thus, the remaining effective Hamiltonian is rotationally invariant, which equals translational invariance on the sphere. The Hamiltonian depends solely on particle interactions (e.g. the Coulomb potential) projected to the LL.

Assuming a two-body interaction, the projection  $\Pi_n$  of the Hamiltonian  $H$  on the  $n$ -th LL can be expressed in second quantized form as

$$H_{\text{eff}} = \Pi_n H \Pi_n = \sum_{m_1=-s}^s \sum_{m_2=-s}^s \sum_{m_3=-s}^s \sum_{m_4=-s}^s c_{m_1}^\dagger c_{m_2}^\dagger c_{m_4} c_{m_3} \cdot \delta_{m_1+m_2, m_3+m_4} V_{m_1 m_2 m_3 m_4}, \quad (6.3.2)$$

where  $c_m^\dagger$  ( $c_m$ ) creates (annihilates) a particle with  $L^z$  quantum number  $m$  in the properly normalized single particle state

$$\psi_{m,0}^s(u, v) = \sqrt{\frac{(2s+1)!}{4\pi(s+m)!(s-m)!}} u^{s+m} v^{s-m}. \quad (6.3.3)$$

The Kronecker-delta assures angular momentum conservation throughout the scattering process. Due to rotational invariance, the matrix element  $V_{m_1 m_2 m_3 m_4}$  factorizes into

$$V_{m_1 m_2 m_3 m_4} = \sum_{l=0}^{2s} \langle s, m_1; s, m_2 | 2s - l, m_1 + m_2 \rangle V_l^{2s} \langle 2s - l, m_3 + m_4 | s, m_3; s, m_4 \rangle, \quad (6.3.4)$$

which is a product of the Haldane pair pseudopotential  $V_l^{2s}$  and a geometrical factor involving the Clebsch-Gordon coefficients  $\langle s, m_1; s, m_2 | j, m_1 + m_2 \rangle$ . The relative angular momentum  $l$  of two particles with angular momenta  $\mathbf{L}_1$  and  $\mathbf{L}_2$ ,  $\mathbf{L}_1^2 = \mathbf{L}_2^2 = s(s+1)$ , fulfills  $0 \leq l \leq 2s$ ,  $l \in \mathbb{N}$ . For fermions (bosons), the sum is restricted to  $l$  odd (even). The coefficient  $V_l^{2s}$  then equals the energy cost of two particles having relative angular momentum  $l$ . Basically, in (6.3.4), a basis transformation is performed from an uncoupled tensor product basis to a total angular momentum basis, the result is multiplied with a pseudopotential coefficient and then transformed back into the original uncoupled basis. The finite set of pseudopotentials contains the information about the interaction projected to the specified LL.

To understand pseudopotentials in more detail, it is instructive to expand the effective Hamiltonian in terms of projection operators, with the pseudopotentials as expansion coefficients. In the following, we restrict our analysis to two-body interactions and the lowest LL. However, the pseudopotential formalism can be expanded to higher-order interactions [131] and higher LLs [36]. The simple generalization to higher LLs is based on the fact that there is in every LL a one-to-one mapping to a system confined to the lowest LL with a modified interparticle interaction.

To derive the pseudopotential expansion, we first need to define an orthonormal basis for the space of magnetic translation invariant QH states. A convenient choice are the two-particle coherent lowest LL states introduced by Haldane [53], which are defined by

$$\{\Omega(\alpha, \beta) \cdot (\mathbf{L}_1 + \mathbf{L}_2)\} \psi_{(\alpha, \beta), 0}^{s, j}[u, v] = j \psi_{(\alpha, \beta), 0}^{s, j}[u, v], \quad (6.3.5)$$

with  $[u, v] := (u_1, u_2, v_1, v_2)$  the particle coordinates on the sphere and  $j$  the total angular momentum,

$$(\mathbf{L}_1 + \mathbf{L}_2)^2 \psi_{(\alpha, \beta), 0}^{s, j}[u, v] = j(j+1) \psi_{(\alpha, \beta), 0}^{s, j}[u, v]. \quad (6.3.6)$$

(6.3.5) is solved by

$$\psi_{(\alpha, \beta), 0}^{s, j}[u, v] = (u_1 v_2 - u_2 v_1)^{2s-j} \prod_{i=1,2} (\bar{\alpha} u_i + \bar{\beta} v_i)^j, \quad (6.3.7)$$

describing two particles with relative angular momentum  $l = 2s - j$  precessing around their common center of mass at  $\Omega(\alpha, \beta)$ . As above,  $l$  has to be odd (even) for fermions (bosons). The total angular momentum can take  $2s+1$  values  $j = 0, 1, \dots, 2s$ , and the relative angular momentum accordingly  $l = 2s, 2s-1, \dots, 0$ . Properly orthogonalized, the states  $\{\psi_{(\alpha, \beta), 0}^{s, j}\}_j$  form an orthogonal basis in the subspace of two-particle interactions.

Analogously to the localization of the single-particle state, illustrated in Figure 6.2 of Section 6.2.2, the two-particle state has its two particles localized at the north pole for  $j = 2s$ . For  $j = 0$ , the state is rotationally invariant. However, the two particles are not located at opposite sides of the sphere. This can be seen mathematically by multiplying out (6.3.7), yielding

$$\psi_{(\alpha, \beta), 0}^{s, 0}[u, v] = \sum_{k=0}^{2s} \binom{2s}{k} (-1)^k u_1^{2s-k} v_2^{2s-k} u_2^k v_1^k. \quad (6.3.8)$$

The terms with  $k = 0$  and  $k = 2s$  describes a state with the two particles localized at opposite sides of the sphere. Modulo the antisymmetrization, these terms correspond to the state

$$|j_1, m_1; j_2, m_2\rangle = |s, s; s, -s\rangle$$

in Clebsch-Gordon notation. All other terms occurring in the sum (6.3.8), however, describe states in which the two particles are not maximally separated.

Projected onto the lowest Landau level via  $\Pi_0$ , every rotationally invariant two-body operator  $V(\mathbf{r}_1 \cdot \mathbf{r}_2)$  can be expanded as

$$\Pi_0 V(\boldsymbol{\Omega}(u_1, v_1) \cdot \boldsymbol{\Omega}(u_2, v_2)) \Pi_0 = \sum_{l=0}^{2s} V_l^{2s} P_{2s-l}(\mathbf{L}_1 + \mathbf{L}_2), \quad (6.3.9)$$

and the pseudopotential coefficients  $V_l^{2s}$ , similar to those in (6.3.4), can be evaluated using the coherent states (6.3.7), yielding

$$V_l^{2s} = \frac{\langle \psi_{(\alpha, \beta), 0}^{s, j} | V(\boldsymbol{\Omega}(u_1, v_1) \cdot \boldsymbol{\Omega}(u_2, v_2)) | \psi_{(\alpha, \beta), 0}^{s, j} \rangle}{\langle \psi_{(\alpha, \beta), 0}^{s, j} | \psi_{(\alpha, \beta), 0}^{s, j} \rangle}. \quad (6.3.10)$$

The relative angular momentum quantum number  $l = 2j - 1$  is restricted to odd (even) integers, depending on the fermionic (bosonic) character of the system. The projection operator  $P_j(\mathbf{L})$  projects onto states with total angular momentum  $\mathbf{L}^2 = (\mathbf{L}_1 + \mathbf{L}_2)^2 = j(j + 1)$ .

The most general two-particle interaction Hamiltonian for a system of  $N$  particles in terms of pseudopotential coefficients thus is

$$H_{\text{int}} = \sum_{i < j}^N \sum_l^{2s} V_l^{2s} P_{2s-l}(\mathbf{L}_i + \mathbf{L}_j) =: \sum_l^{2s} V_l^{2s} H^{(l)}. \quad (6.3.11)$$

The pseudopotential expansion has proven to be highly useful to describe FQH states. For instance, the Laughlin state with a filling fraction of  $\nu = 1/3$  is the unique zero mode of the  $V_1^{2s}$  pseudopotential ( $V_l^{2s} = 0 \forall l > 1$ ). For a filling of  $1/m$ , the Laughlin state emerges as the densest ground state of a Hamiltonian  $H = \sum_{l' < m} V_{l'}^{2s} H^{(l')}$ , with arbitrary, but positive coefficients  $V_{l'}^{2s}$ . The requirement of being the densest zero mode is necessary to obtain non-trivial results, since it is easy to construct additional zero modes by increasing the flux and thus creating quasihole states.

A pseudopotential of the form  $V_l^{2s} = a + bl(l + 1)$ , with  $a, b \in \mathbb{R}$ , is called harmonic. The parameter  $a$  adds a constant potential, while  $b$  adds a term  $\propto \mathbf{L}_{\text{tot}}^2$ . It can be proven that it does not break the degeneracy of  $n$ -particle angular momentum multiplets and thus does not introduce correlations into the QH system [152; 117]. Correlations in the system then can be introduced by deviations from the harmonic pseudopotential.

### 6.3.1.1 Intralayer pseudopotentials for the Coulomb potential

For the Coulomb potential, the pseudopotential coefficients can be expressed in a compact form. We first consider an intralayer interaction, meaning a single-flavor system of  $N$  electrons on the sphere interacting with each other and a positive background via the Coulomb potential. In Section 6.3.1.3, we will derive an expression for the more complicated system of an interlayer interaction, described by a Coulomb potential. Assuming the magnetic length  $a_0$  as the unit length and  $e^2/4\pi\epsilon a_0$  the unit of energy,  $\epsilon$  being the dielectric constant, (6.3.1) simplifies to  $S = R^2$ . The Coulomb potential then simplifies to  $V(r) = 1/r$ , where  $r$  is the distance between two interacting particles. On the unit sphere, the chord distance between two particles is given by (6.2.14).

Inserting the Coulomb potential into (6.3.2), we get

$$V_{\text{Coul}} = \frac{1}{2} \sum_{m_1=-s}^s \sum_{m_2=-s}^s \sum_{m_3=-s}^s \sum_{m_4=-s}^s c_{m_1}^\dagger c_{m_2}^\dagger c_{m_4} c_{m_3} \cdot \langle s, m_1; s, m_2 | \frac{1}{r} | s, m_3; s, m_4 \rangle. \quad (6.3.12)$$

The coefficient can be written as

$$\langle s, m_1; s, m_2 | \frac{1}{r} | s, m_3; s, m_4 \rangle = \sum_{l=0}^{2s} V_l^{2s} \sum_{M=-l}^l \langle s, m_1; s, m_2 | l, M \rangle \langle l, M | s, m_3; s, m_4 \rangle R^{-1}. \quad (6.3.13)$$

As derived by Fano et al. [25], the pseudopotential coefficients are given by

$$V_l^{2s} = 2 \frac{\binom{2l}{l} \binom{2(4s-l+1)}{4s-l+1}}{\binom{2(2s+1)}{2s+1}^2}, \quad (6.3.14)$$

for a relative angular momentum  $0 \leq l \leq 2s$ . The pseudopotential coefficients for different total fluxes  $2s$  through the sphere are depicted in Figure 6.3. For large values of  $2s$ ,  $l$  and  $2s - l$ , the asymptotic behavior is

$$V_l^{2s} \sim \frac{1}{2} \frac{s}{\sqrt{l(s-l/4)}}. \quad (6.3.15)$$

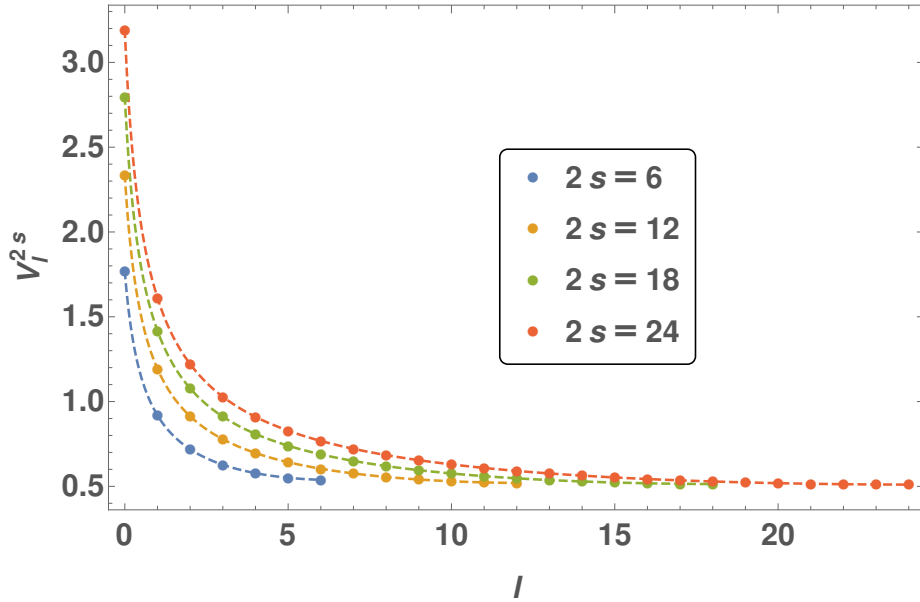


**Fig. 6.3** Plot of the pseudopotential coefficients  $V_l^{2s}$  of the Coulomb potential, as a function of the relative angular momentum  $l$  for different total fluxes  $2s$  through the sphere, according to (6.3.14). The relative angular momentum can only take values  $0 \leq l \leq 2s$ . In case of a fermionic (bosonic) system, only the pseudopotential coefficients with  $l$  odd (even) are non-zero.

### 6.3.1.2 Pseudopotentials for the total angular momentum

It is further useful to calculate the pseudopotentials of the total angular momentum of our two-layer system in order to compare them to the parent Hamiltonian we propose below.

Given a single layer system of  $N$  particles living on a sphere, pierced by  $2s$  Dirac flux quanta, the total angular momentum can be rewritten in the form of (6.3.9) as a two-body scattering part and some constant

$$\mathbf{L}_{\text{tot}}^2 = \sum_{i < j}^N \sum_{l=0}^{2s} V_l^{2s} P_{2s-l}(\mathbf{L}_i + \mathbf{L}_j) + C. \quad (6.3.16)$$

The operator  $P_{2s-l}(\mathbf{L}_i + \mathbf{L}_j)$  projects onto a two-particle state with total angular momentum  $(\mathbf{L}_i + \mathbf{L}_j)^2 = (2s-l)(2s-l+1)$ , such that

$$\mathbf{L}_{\text{tot}}^2 = \sum_{i < j}^N \sum_{l=0}^{2s} (2s-l)(2s-l+1) P_{2s-l}(\mathbf{L}_i + \mathbf{L}_j) + C. \quad (6.3.17)$$

The constant  $C$  can be determined by expanding the total angular momentum,

$$\begin{aligned} \mathbf{L}_{\text{tot}}^2 &= \left( \sum_{i=1}^N \mathbf{L}_i \right)^2 = \sum_i \mathbf{L}_i^2 + 2 \sum_{i < j} \mathbf{L}_i \cdot \mathbf{L}_j \\ &= Ns(s+1) + \sum_{i < j} (\mathbf{L}_i + \mathbf{L}_j)^2 - 2 \sum_{i < j} \mathbf{L}_i^2 \\ &= Ns(s+1) + \sum_{i < j} (\mathbf{L}_i + \mathbf{L}_j)^2 - 2 \frac{N-1}{2} Ns(s+1) \\ &= \sum_{i < j} \sum_{l=0}^{2s} (2s-l)(2s-l+1) P_{2s-l}(\mathbf{L}_i + \mathbf{L}_j) - N(N-2)s(s+1), \end{aligned} \quad (6.3.18)$$

and therefore

$$V_l^{2s} = (2s-l)(2s-l+1) - 2 \frac{N-2}{N-1} s(s+1). \quad (6.3.19)$$

Now, for a two-layer system, the total angular momentum can be separated into an intralayer part for each sphere (first and second term) and an interlayer part (third term),

$$\begin{aligned} \mathbf{L}_{\text{tot}}^2 &= \left( \sum_{i=1}^{N_\uparrow} \mathbf{L}_i^\uparrow + \sum_{i=1}^{N_\downarrow} \mathbf{L}_i^\downarrow \right)^2 \\ &= (\mathbf{L}_{\text{tot}}^\uparrow)^2 + (\mathbf{L}_{\text{tot}}^\downarrow)^2 + 2 \mathbf{L}_{\text{tot}}^\uparrow \cdot \mathbf{L}_{\text{tot}}^\downarrow \\ &= \sum_{i < j}^{N_\uparrow} \sum_{l=1}^{2s'} V_l^{2s} P_{2s-l}(\mathbf{L}_i^\uparrow + \mathbf{L}_j^\uparrow) \\ &\quad + \sum_{k < l}^{N_\downarrow} \sum_{l=1}^{2s'} V_l^{2s'} P_{2s'-l}(\mathbf{L}_k^\downarrow + \mathbf{L}_l^\downarrow) \\ &\quad + \sum_i^{N_\uparrow} \sum_k^{N_\downarrow} \sum_{l=0}^{2s} V_l^{s+s'} P_{s+s'-l}(\mathbf{L}_i^\uparrow + \mathbf{L}_k^\downarrow). \end{aligned} \quad (6.3.20)$$

The primed summation in the first two terms includes only odd relative angular momenta due to the fermionic nature of the particles. The total angular momentum can take values in the interval  $|s' - s| < j < (s' + s)$ . Since  $l = (s + s' - j)$ , the relative angular momentum fulfills

$$0 \leq l \leq 2 \min(s, s').$$

According to the considerations for the one-layer system, the intralayer pseudopotentials are

$$\begin{aligned} V_l^{2s} &= (2s-l)(2s-l+1) - 2 \frac{N_\uparrow - 2}{N_\uparrow - 1} s(s+1), \\ V_l^{2s'} &= (2s'-l)(2s'-l+1) - 2 \frac{N_\downarrow - 2}{N_\downarrow - 1} s'(s'+1). \end{aligned} \quad (6.3.21)$$

Analogously to the intralayer case, an orthonormal basis for the space of two-particle coherent states has to be set up to derive the pseudopotential expansion for the interlayer case. The coherent states are



defined by

$$\{\mathbf{\Omega}(\alpha, \beta) \cdot (\mathbf{L}_\uparrow + \mathbf{L}_\downarrow)\} \psi_{(\alpha, \beta), 0}^{s+s', j}[u, v, \bar{a}, \bar{b}] = j \psi_{(\alpha, \beta), 0}^{s+s', j}[u, v, \bar{a}, \bar{b}], \quad (6.3.22)$$

with

$$(\mathbf{L}_\uparrow + \mathbf{L}_\downarrow)^2 \psi_{(\alpha, \beta), 0}^{s+s', j}[u, v, \bar{a}, \bar{b}] = j(j+1) \psi_{(\alpha, \beta), 0}^{s+s', j}[u, v, \bar{a}, \bar{b}]. \quad (6.3.23)$$

The expression

$$\psi_{(\alpha, \beta), 0}^{s+s', j}[u, v, \bar{a}, \bar{b}] = (\bar{a}u + \bar{b}v)^{s+s'-j} (\bar{\alpha}u + \bar{\beta}v)^{s-s'+j} (\bar{\alpha}\bar{b} - \bar{\beta}\bar{a})^{s'-s+j} \quad (6.3.24)$$

solves (6.3.22). The total angular momentum can have values  $|s - s'| \leq j \leq s + s'$  and the relative angular momentum  $l = s + s' - j$  has values  $l = 0, 1, \dots, \min(s, s')$ . For  $l = 0$ , the two particles are maximally separated, sitting on opposite points of the sphere. For  $l = s + s'$ , the particles are in a rotationally invariant state close to each other.

Similar to (6.3.10), the pseudopotential coefficients can be obtained from the coherent states (6.3.24),

$$V_l^{s+s'} = \frac{\langle \psi_{(\alpha, \beta), 0}^{s+s', j} | V(\mathbf{\Omega}(u, v) \cdot \mathbf{\Omega}(\bar{a}, \bar{b})) | \psi_{(\alpha, \beta), 0}^{s+s', j} \rangle}{\langle \psi_{(\alpha, \beta), 0}^{s+s', j} | \psi_{(\alpha, \beta), 0}^{s+s', j} \rangle}. \quad (6.3.25)$$

For the total angular momentum, the pseudopotential coefficients for the interlayer term are

$$V_l^{s+s'} = -(s + s' - l)(s + s' - l + 1) + [s(s + 1) + s'(s' + 1)], \quad (6.3.26)$$

since

$$\begin{aligned} -2\mathbf{L}_{\text{tot}}^\uparrow \cdot \mathbf{L}_{\text{tot}}^\downarrow &= -\sum_{i=1}^{N_\uparrow} \sum_{k=1}^{N_\downarrow} (\mathbf{L}_i^\uparrow + \mathbf{L}_k^\downarrow)^2 + N^\uparrow N^\downarrow \left[ \sum_{i=1}^{N_\uparrow} (\mathbf{L}_i^\uparrow)^2 + \sum_{k=1}^{N_\downarrow} (\mathbf{L}_k^\downarrow)^2 \right] \\ &= -\sum_{i=1}^{N_\uparrow} \sum_{i=k}^{N_\downarrow} \sum_{l=0}^{2s} (s + s' - l)(s + s' - l + 1) P_{s+s'-l}(\mathbf{L}_i^\uparrow + \mathbf{L}_k^\downarrow)^2 \\ &\quad + N^\uparrow N^\downarrow [s(s + 1) + s'(s' + 1)]. \end{aligned} \quad (6.3.27)$$

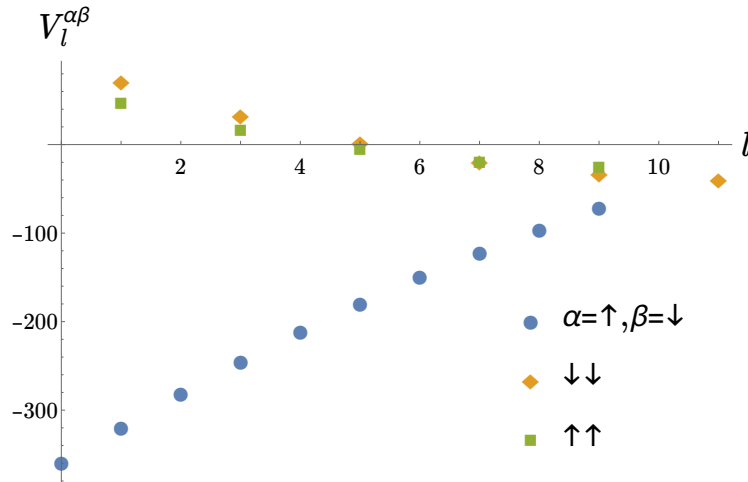


**Fig. 6.4** Plot of the pseudopotential coefficients  $V_l^{\alpha\beta}$  of the total angular momentum, as a function of the relative angular momentum  $l$  for a system of six  $\uparrow$  - and six  $\downarrow$  -particles. The intralayer angular momentum can only take odd values as each layer consists of indistinguishable fermions, and  $1 \leq l \leq 2s_\alpha$ . For the interlayer pseudopotentials, all values for  $l$  are allowed, and it is  $0 \leq l \leq (s + s') - |s - s'|$ .

### 6.3.1.3 Interlayer pseudopotentials for the Coulomb potential

The pseudopotentials  $V_l^{s+s'}$  for a two-flavor system are given in (6.3.25). Given a Coulomb interaction between the particles of the two layers, we wish to derive a compact expression by explicitly writing out the coefficients. The chord distance between two particles located at  $\mathbf{\Omega}(u, v)$  and  $\mathbf{\Omega}(\bar{a}, \bar{b})$  on the unit sphere is

$$|\mathbf{\Omega}(\bar{a}, \bar{b}) - \mathbf{\Omega}(u, v)| = 2|av - bu|, \quad (6.3.28)$$

so that the Coulomb potential reads

$$V(\mathbf{\Omega}(\bar{a}, \bar{b}) \cdot \mathbf{\Omega}(u, v)) = \frac{1}{2|av - bu|}. \quad (6.3.29)$$

Since our system is rotationally invariant, we may choose  $(\alpha, \beta) = (1, 0)$  in (6.3.25) without loss of generality. Then, the denominator of (6.3.25) written out explicitly is

$$N_0 := \int d\mathbf{\Omega}(u, v) \int d\mathbf{\Omega}(a, b) |u|^{2(2s-l)} |b|^{2(2s'-l)} |\bar{a}u + b\bar{v}|^{2l}, \quad (6.3.30)$$

the nominator is

$$I := \frac{1}{2} \int d\mathbf{\Omega}(u, v) \int d\mathbf{\Omega}(a, b) |u|^{2(2s-l)} |b|^{2(2s'-l)} \frac{|\bar{a}u + b\bar{v}|^{2l}}{|av - bu|}. \quad (6.3.31)$$

The integrals can be simplified by applying a unitary transformation

$$\begin{pmatrix} a' \\ b' \end{pmatrix} = \underbrace{\begin{pmatrix} \bar{u} & \bar{v} \\ -v & u \end{pmatrix}}_{=:T} \begin{pmatrix} a \\ b \end{pmatrix} \quad (6.3.32)$$

with

$$T^{-1} = \begin{pmatrix} u & -\bar{v} \\ v & \bar{u} \end{pmatrix}.$$

The spherical coordinates are defined as

$$\begin{aligned} u &= \cos\left(\frac{\theta}{2}\right) e^{i\varphi/2}, \\ v &= \sin\left(\frac{\theta}{2}\right) e^{-i\varphi/2}, \\ a' &= \cos\left(\frac{\theta'}{2}\right) e^{i\varphi'/2}, \\ b' &= \sin\left(\frac{\theta'}{2}\right) e^{-i\varphi'/2}. \end{aligned} \quad (6.3.33)$$

Inserting (6.3.32) into (6.3.31), we obtain

$$\begin{aligned} I &= \frac{1}{2} \int d\mathbf{\Omega}(u, v) \int d\mathbf{\Omega}(a', b') |u|^{2(2s-l)} |a'v + \bar{u}b'|^{2(2s'-l)} \frac{|a'|^{2l}}{|b'|} \\ &= \frac{1}{2} \int d\varphi \int d\varphi' \int d\theta \sin(\theta) \int d\theta' \sin(\theta') \frac{|\cos(\frac{\theta}{2})|^{2(2s-l)} |\cos(\frac{\theta'}{2})|^{2l}}{|\sin(\frac{\theta'}{2})|} \\ &\quad \cdot \left| \sin\left(\frac{\theta}{2}\right) \cos\left(\frac{\theta'}{2}\right) + \cos\left(\frac{\theta}{2}\right) \sin\left(\frac{\theta'}{2}\right) e^{-i\varphi'} \right|^{2(2s'-l)} \end{aligned}$$

Using the identity [33]

$$\int_0^{2\pi} d\varphi |\alpha + \beta e^{-i\varphi}|^{2n} = 2\pi \sum_{k=0}^n \binom{n}{k}^2 \alpha^{2k} \beta^{2n-2k}, \quad (6.3.34)$$

the nominator  $I$  can be simplified to

$$\begin{aligned} I &= 2\pi^2 \sum_{k=0}^{2s'-l} \binom{2s'-l}{k}^2 \int_0^\pi d\theta \sin(\theta) \int_0^\pi d\theta' \sin(\theta') \left| \cos\left(\frac{\theta}{2}\right) \right|^{2(2s-l)} \\ &\quad \cdot \frac{\left| \cos\left(\frac{\theta'}{2}\right) \right|^{2l}}{\left| \sin\left(\frac{\theta'}{2}\right) \right|^{2k}} \left| \sin\left(\frac{\theta}{2}\right) \cos\left(\frac{\theta'}{2}\right) \right|^{2k} \left| \cos\left(\frac{\theta}{2}\right) \sin\left(\frac{\theta'}{2}\right) \right|^{2(2s'-l)-2k} \\ &= 32\pi^2 \sum_{k=0}^{2s'-l} \binom{2s'-l}{k}^2 \\ &\quad \cdot \underbrace{\int_0^{\pi/2} d\theta \sin(\theta) (\cos(\theta))^{2(2s-l)+2(2s'-l)-2k+1} (\sin(\theta))^{2k+1}}_{=:I_1} \\ &\quad \cdot \underbrace{\int_0^{\pi/2} d\theta' \sin(\theta') (\cos(\theta'))^{2l+2k+1} (\sin(\theta'))^{2(2s'-l)-2k}}_{=:I_2}. \end{aligned}$$

To solve the integrals  $I_1$  and  $I_2$ , we need the identity [33]

$$\begin{aligned} \int_0^{\pi/2} (\sin(\theta))^{2\alpha+1} (\cos(\theta))^{2\beta+1} &= \frac{\Gamma(\alpha+1)\Gamma(\beta+1)}{2\Gamma(\alpha+\beta+2)} \\ &= \frac{\alpha!\beta!}{2(\alpha+\beta+1)!} \quad \text{for } \alpha, \beta \in \mathbb{N}_0. \end{aligned} \quad (6.3.35)$$

In  $I_1$ , we have

$$\alpha = k, \quad \beta = 2s - l + 2s' - l - k,$$

in  $I_2$ , we have

$$\alpha = 2s' - l - k - \frac{1}{2}, \quad \beta = l + k.$$

Inserting (6.3.35) into the integrals yields

$$I_1 = \frac{k!(2s + 2s' - 2l + k)!}{2(2s + 2s' - 2l + 1)!}$$

and

$$\begin{aligned} I_2 &= \frac{\Gamma(2s' - l - k + 1/2)\Gamma(l + k + 1)}{2\Gamma(2s' + 3/2)} \\ &= (l + k)! 2^{2(l+k+1)-1} \frac{[2(2s' - l - k)]! (2s' + 1)!}{(2s' - l - k)! [(2(2s' + 1))]} \end{aligned} \quad (6.3.36)$$

where we have used

$$\Gamma(n + 1/2) = \frac{(2n)! \sqrt{\pi}}{n! 2^{2n}}, \quad n \in \mathbb{N}_0.$$

Putting all results together, we obtain for the nominator of the pseudopotentials (6.3.25)

$$I = 8\pi^2 \sum_{k=0}^{2s'-l} \binom{2s'-l}{k}^2 k!(k+l)! 2^{2(l+k+1)} \cdot \frac{(2s+2s'-2l-k)! [2(2s'-l-k)]! (2s'+1)!}{(2s+2s'-2l+1)! (2s'-l-k)! [2(2s'+1)]!}. \quad (6.3.37)$$

Similar calculations for the denominator yield

$$N_0 = 16\pi^2 \frac{[(2s'-l)!]^2}{(2s+2s'-2l+1)!(2s'+1)!} \underbrace{\sum_{k=0}^{2s'-l} \frac{(2s+2s'-2l-k)!(l+k)!}{k!(2s'-l-k)!}}_{=:S_2}. \quad (6.3.38)$$

The sum  $S_2$  can be explicitly written out,

$$S_2 = \frac{(2s-l)! l! (2s+1+2s'-l)!}{(2s'-l)!(2s+1)!},$$

so that the final expression for the denominator is

$$N_0 = 16\pi^2 \frac{(2s'-l)!(2s-l)! l! (2s+2s'-l+1)!}{(2s'+1)!(2s+1)!(2s+2s'-2l+1)!}. \quad (6.3.39)$$

Combining both results, we get for the pseudopotential coefficients

$$\begin{aligned} V_l^{s+s'} &= \frac{I}{N_0} \\ &= 2 \frac{(2s'-l)! [(2s'+1)!]^2 (2s+1)!}{[2(2s'+1)]! (2s+2s'-l+1)! l! (2s-l)!} \\ &\quad \cdot \sum_{k=0}^{2s'-l} 4^{k+l} \frac{(k+l)! (2s+2s'-2l-k)! [2(2s'-l-k)]!}{k! [(2s'-l-k)!]^3} \\ &= 2^{1+4s'} \frac{(2s+1)! [(2s'+1)!]^2 (2s+2s-2l)! \Gamma\left(\frac{4s'-2l+1}{2}\right)}{\sqrt{\pi} (2s-l)! [2(2s'+1)]! (2s'-l)! (2s'+2s-l+1)!} \\ &\quad \cdot {}_pF_q\left(\{l+1, -2s'+l, -2s'+l\}, \{-2s'+l+\frac{1}{2}, -2s'-2s+2l\}, 1\right). \end{aligned}$$

While all previous steps of this derivation were calculated analytically, the last step (6.3.40) was obtained using the `FullSimplify`-routine in *Mathematica*. The generalized hypergeometric function  ${}_pF_q$  is defined by the series expansion

$${}_pF_q(\{a_1, \dots, a_p\}, \{b_1, \dots, b_q\}, z) := \sum_{k=0}^{\infty} \frac{(a_1)_k \dots (a_p)_k}{(b_1)_k \dots (b_q)_k} \frac{z^k}{k!},$$

which can be calculated in *Mathematica* using the function `HypergeometricPFQ`. The Pochhammer symbol  $(a)_k$ , also called the rising factorial, is defined by

$$(a)_k := \frac{\Gamma(a+k)}{\Gamma(a)} = a(a+1) \dots (a+k-1).$$

### 6.3.2 The Hamiltonian Finder - General method

In the following, we describe and employ a general method to identify exact, local parent Hamiltonians for trial states like quantum Hall or spin liquid states [41]. It can be used to identify exact parent Hamiltonians, either directly or via the construction of simpler annihilation operators from which a parent Hamiltonian respecting all the required symmetries can be constructed. Most remarkably, however, the method provides approximate parent Hamiltonians whenever an exact solution is not available within the space of presumed interaction terms.

The goal of the method is to determine the parent Hamiltonian of a trial ground state  $|\Psi\rangle$  for a finite system, of a system size amenable to exact diagonalization studies. We now wish to ask whether  $|\Psi\rangle$  is the exact ground state of a (local) model Hamiltonian specified by a finite number  $L$  of terms  $H^{(i)}$  with unknown coefficients  $a_i$ ,

$$H = \sum_{i=1}^L a_i H^{(i)}, \quad (6.3.40)$$

and determine the coefficients. To begin with, this requires that  $|\Psi\rangle$  is an exact eigenstate,

$$H |\Psi\rangle = E_0 |\Psi\rangle, \quad (6.3.41)$$

which we write as

$$(H + a_0) |\Psi\rangle = 0. \quad (6.3.42)$$

Clearly, the additional variational parameter  $a_0$  is to be interpreted as  $-E_0$ . Defining  $H^0 \equiv 1$ , we may write this compactly as

$$\sum_{i=0}^L a_i H^{(i)} |\Psi\rangle = 0. \quad (6.3.43)$$

Since we are interested in identifying parent Hamiltonians for highly correlated many body states, and the number of translationally invariant  $m$ -body terms  $H^{(i)}$  for a system with  $N$  sites, scales roughly as  $N^{m-1}$ , the dimension of the Hilbert space for system sizes with more than four particles will in general be larger than the number of terms  $L$ . This means that some special principle must be at work for each solution of (6.3.43). In most applications, there is one or several solutions due to conserved quantities (e.g. total spin in a spin system, total angular momentum for quantized Hall fluids on the sphere), and an additional one if an exact parent Hamiltonian exists.

To find these solutions, we define the state vectors  $|\Psi^i\rangle \equiv H^{(i)} |\Psi\rangle$ , and multiply (6.3.43) from the left with the corresponding dual  $\langle\Psi^j|$ . With  $M_{ji} \equiv \langle\Psi^j|\Psi^i\rangle$ , this yields<sup>2</sup>

$$\sum_{i=0}^L M_{ji} a_i = 0 \quad \text{for } j = 0, 1, \dots, L. \quad (6.3.45)$$

<sup>2</sup> In general, given a matrix  $\mathbf{A}$ , we have

$$\mathbf{A}\mathbf{v} = 0 \Leftrightarrow \mathbf{A}^\dagger \mathbf{A}\mathbf{v} = 0. \quad (6.3.44)$$

The corresponding proof is trivial,

$$\begin{aligned} \mathbf{A}\mathbf{v} = 0 &\Rightarrow \mathbf{A}^\dagger \mathbf{A}\mathbf{v} = 0 \\ &\Rightarrow \mathbf{v}^\dagger \mathbf{A}^\dagger \mathbf{A}\mathbf{v} = 0 = |\mathbf{A}\mathbf{v}|^2 \\ &\Rightarrow \mathbf{A}\mathbf{v} = 0. \end{aligned}$$

Obviously, there is one solution of (6.3.45) for each zero eigenvalue of the  $L + 1$  dimensional, Hermitian matrix  $M_{ji}$ . Substitution of the corresponding eigenvectors  $a_i$  into (6.3.43) yields operators annihilating the ground state, which enable us to extract the desired parent Hamiltonian (6.3.40). Even though this may come across as a trivial observation, the models one can obtain with this method are in general highly non-trivial.

Possibly the most outstanding feature is that, according to our longstanding experience, the method usually yields a highly non-trivial approximate parent Hamiltonian if no exact one exists within the operator space spanned by the  $H^{(i)}$ 's. In these cases, there are likewise one or several zero eigenvalues due to conserved quantities, and one small, nonzero eigenvalue. The eigenstate corresponding to this eigenvalue defines the approximate Hamiltonian.

An obvious drawback is that the method guarantees that  $|\Psi\rangle$  is an exact or approximate eigenstate of  $H$ , but not that it is the ground state. This has hence to be verified *a posteriori* by exact, numerical diagonalization of  $H$ . Our experience here is that whenever an exact parent Hamiltonian exists, it will have  $|\Psi\rangle$  as its unique ground state. In the case of approximate solutions, we have sometimes encountered situations where the method suggested operators for which  $|\Psi\rangle$  has only been an approximate eigenstate, not the ground state. In the cases we have studied, however, it was always possible to find a suitable set of operators  $H^{(i)}$  such that the method converged on an approximate parent Hamiltonian for the ground state.

For our 311-state, the system's behavior is dominated by particle interactions, since the kinetic term is effectively a constant. We can expand the Hamiltonian in terms of many-body pseudopotentials. For the sake of simplicity, we restrict our analysis to two-body interactions, i.e. two particles precessing about their common center of mass. As explained in the previous section, the model Hamiltonian can be written as a discrete, angular momentum resolved sum of projection operators, see (6.3.11), with pseudopotential coefficients  $V_l^{2s}$ , which have yet to be determined. The relative angular momentum is again  $l = 2s - j$ , The total angular momentum is  $j = 2s - l$ , and  $s$  is the maximum angular momentum for each particle. In case of charged particles on a sphere in a magnetic field,  $2s$  corresponds to the number of Dirac flux quanta through this sphere. As  $0 \leq j \leq 2s$ , the relative angular momentum quantum number fulfills  $l \geq 0$ . We now wish to ask whether  $|\Psi\rangle$  is the exact ground state of such a Hamiltonian,

$$H = \sum_{l=0}^{2s} V_l^{2s} H^{(l)} \quad \text{and} \quad H |\Psi\rangle = E_0 |\Psi\rangle. \quad (6.3.46)$$

It is easy to see that

$$V_l^{2s} = 1 \quad \forall l \quad \Rightarrow \quad H = \sum_l H^{(l)} \propto \mathbb{1}. \quad (6.3.47)$$

To eliminate this trivial solution from our eigenvalue equation (6.3.46), we note that a constant shift in the eigenenergy of  $|\Psi\rangle$ ,  $(H - E_0 \mathbb{1})\Psi = 0$ , can be absorbed into a shift of the pseudopotentials,  $V_l^{2s} + E_0 \quad \forall l$ . Therefore, we focus on the eigenvalue equation

$$H |\Psi\rangle = 0. \quad (6.3.48)$$

There is another trivial solution which we want to eliminate from the solution space. It is

$$\begin{aligned} V_l^{2s} &= (2s - l)(2s - l + 1) + \text{const.}, \quad l = 0, 1, 2, \dots, 2s \\ \Rightarrow H &= L_{\text{tot}}^2. \end{aligned} \quad (6.3.49)$$

One way of eliminating this solution is to add additional constraints such as  $V_{2s}^{2s} = V_{2s-1}^{2s}$  or  $V_1^{2s} = 0$ , depending on the properties of the physical system.

Our state lives in a finite Hilbert space of some dimension  $n_{\text{max}}$ ,

$$\{|\varphi_1\rangle, |\varphi_2\rangle, \dots, |\varphi_{n_{\text{max}}}\rangle\}. \quad (6.3.50)$$

Usually, for large systems,  $n_{\max} \gg (2s + 1)$  applies.

In this basis, our state is

$$|\Psi\rangle = (\Psi_1, \Psi_2, \dots, \Psi_{n_{\max}})^\top, \quad (6.3.51)$$

and we write

$$H^{(l)} |\Psi\rangle =: |\Psi^l\rangle =: \left( h_1^{(l)}, h_2^{(l)}, \dots, h_{n_{\max}}^{(l)} \right)^\top. \quad (6.3.52)$$

The eigenvalue equation (6.3.48) can then be written in matrix form as

$$0 = \sum_l V_l^{2s} |\Psi^l\rangle = \begin{pmatrix} h_1^{(0)} & h_1^{(1)} & \dots & h_1^{(2s)} \\ h_2^{(0)} & h_2^{(1)} & \dots & h_2^{(2s)} \\ \vdots & \vdots & \ddots & \vdots \\ h_{n_{\max}}^{(0)} & h_{n_{\max}}^{(1)} & \dots & h_{n_{\max}}^{(2s)} \end{pmatrix} \begin{pmatrix} V_0^{2s} \\ V_1^{2s} \\ \vdots \\ V_{2s}^{2s} \end{pmatrix} =: \mathbf{A} \mathbf{v}. \quad (6.3.53)$$

Thus, matrix  $\mathbf{A}$  has dimension  $n_{\max} \times (2s + 1)$ , whereas the eigenspace of our Hamiltonian has at most  $(2s + 1)$  solutions depending on how many columns  $|\Psi^l\rangle$  of matrix  $\mathbf{A}$  are linearly independent. These solutions determine a set of pseudopotential coefficients  $\{V_l^{2s}\}_{l=0}^{2s}$ , defining an exact parent Hamiltonian for the state  $|\Psi\rangle$ .

The product matrix  $\mathbf{M} := \mathbf{A}^\dagger \mathbf{A}$  has dimension  $(2s + 1) \times (2s + 1)$ , and as usually  $s \ll n_{\max}$ , this matrix is considerably smaller than  $\mathbf{A}$ , reducing computational costs when treating the system numerically. Diagonalizing the quadratic matrix  $\mathbf{M}$  yields its eigenspectrum. Its zero mode determines the sought parent Hamiltonian, and its entries are the pseudopotential coefficients.

### 6.3.3 The Hamiltonian Finder - Approximate parent Hamiltonians

Possibly the most important feature of our method is that it delivers approximate parent Hamiltonians whenever an exact parent Hamiltonian for the trial ground state is not available in the considered space spanned by the terms  $H^{(i)}$ . More often than not, this situation arises because no simple, local, analytically amenable parent Hamiltonian exists for the state in question. Examples for such a situation are provided by the hierarchy wave functions of the QH effect, which is also the instance where this method was first applied [34], or for the non-Abelian chiral spin liquid (NACSL) [45].

As explained in the context of the general method above, in situations where no exact, but an approximate, parent Hamiltonian can be constructed with the terms  $H^{(i)}$  included in (6.3.40), the eigenvector associated with the smallest non-zero eigenvalue of  $M_{ji}$  usually provides such an approximate Hamiltonian  $H$ . The result, however, will slightly depend on the relative normalizations  $w_i$  of the operators  $H^{(i)}$  used in the numerical procedure. In the following, we refer to these normalizations as precondition weights.

In this context, however, the optimal solution will depend on what one desires to optimize. This could be the relative variance of the ground state energy

$$\frac{\langle \Psi | H^2 | \Psi \rangle - \langle \Psi | H | \Psi \rangle^2}{\langle \Psi | H | \Psi \rangle^2}, \quad (6.3.54)$$

the overlap  $\langle GS | \Psi \rangle$  between the exact ground state  $|GS\rangle$  of  $H$  and the reference trial state  $|\Psi\rangle$ , or the similarity between the expectation values  $C_{GS,i} = \langle GS | H^{(i)} | GS \rangle$  and  $C_{\Psi,i} = \langle \Psi | H^{(i)} | \Psi \rangle$ . These quantities will be further explained in Section 6.3.5, and we label them ‘‘correlators’’. For the NACSL [45], the method was applied to demonstrate that a local, approximate Hamiltonian with a gap between the three (in the thermodynamic limit topologically degenerate) ground states and the remaining spectrum can be found. The size of this gap was hence a parameter considered as well.

In most applications studied so far with this method, its most naive application designed for the identification of an exact parent Hamiltonian provided us with remarkably accurate approximations whenever

no exact solutions were available. If one then desires to optimize the Hamiltonian specified by the set of parameters  $[a_i] \equiv (a_0, a_1, \dots, a_L)$  further, one may apply a Newton scheme, as follows.

We illustrate the method here for an optimization of the similarity in the correlators, as this usually optimizes variance and overlap as well. To begin with, we choose a set of weights  $[w_i]$ , and another set  $[w'_i]$ , where only a single weight  $w_j$  differs by a small parameter  $\delta_j$ . We then evaluate the corresponding coefficients  $[a_i]$  and  $[a'_i]$ , and from there  $[C_i]$  and  $[C'_i]$ . This yields the  $j$ -th row of the derivative matrix

$$\frac{\partial C_i}{\partial w_j} \equiv \frac{C'_i - C_i}{\delta_j}.$$

As a next step, we solve the linear equation

$$\sum_{j=0}^L \frac{\partial C_i}{\partial w_j} \Delta w_j = C_{0,i} - C_i$$

for the shifts  $\Delta w_j$  we would require if we assume a linear dependence. The procedure can then be repeated with the adjusted weights  $[w_i + \Delta w_i]$  until it has converged. In the examples we considered, however, a single iteration was sufficient. Whenever adjustments of the weights  $[w_i]$  are insufficient to induce the desired changes in the correlators, one possible route is to follow the same steps with infinitesimal variations in the coefficients  $[a_i]$ . Usually, one needs to adjust nuances of the method to the problem one is considering. For example, it is sometimes better to include  $w_0$  and  $a_0$  in the optimization, while in other situations it is better to take  $a_0$  constant, if not zero to start with.

Also, examples were encountered where the optimization worked better when we adjusted the weights not on a linear, but on a logarithmic scale, a change which is fully implemented by taking  $e^{w_i} H^{(i)}$  instead of  $w_i H^{(i)}$  for the re-normalized operators in  $H = \sum_i a_i w_i H^{(i)}$  and  $|\Psi_i\rangle = w_i H^{(i)} |\Psi\rangle$ . The procedure we have outlined here hence should be taken mostly as a guideline to find an adequate algorithm for the problem one is interested in.

The approximate method we just outlined is heuristic and crude, but has been highly successful in our experience. The reader might ask at this point whether a more scholarly approach does not offer itself. One possible avenue we have explored is to minimize the variance (6.3.54) by maximizing  $\langle \Psi | H | \Psi \rangle^2$  subject to the constraints  $\langle \Psi | \Psi \rangle = \langle \Psi | H^2 | \Psi \rangle = 1$  with  $H$  specified in (6.3.40). This yields

$$\sum_{i=1}^L M_{ji} a_i = -M_{j0} a_0 \quad \text{for } j = 1, \dots, L, \quad (6.3.55)$$

where  $a_0$  is now a normalization constant

$$a_0^{-2} = \sum_{i,j=1}^L M_{0i} (M^{-1})_{ij} M_{j0}. \quad (6.3.56)$$

Note that since  $a_0$  only affects the overall normalization of the parent Hamiltonian, we do not need to evaluate (6.3.56) in practical applications. Instead, we may set  $a_0 = 1$  in (6.3.55). In some of the examples we have investigated, the Hamiltonian corresponding to the solution of (6.3.55) for  $a_i$  was more accurate than the one obtained with the previous method, i.e., via the lowest non-zero eigenvalue of (6.3.45). In general, however, this method has not been as stable and robust as the previous one.

As an example of how the two methods (6.3.45) (from now on called method A) and (6.3.55) (from now on called method B) perform if only an approximate parent Hamiltonian can be determined, we have numerically investigated a system of  $N$  charged fermionic particles on a sphere, pierced by a flux of  $2s$  Dirac flux quanta, and interacting via a Coulomb potential. To do so, we first construct the Coulomb Hamiltonian using the pseudopotential coefficients (6.3.14). Via exact diagonalization, the exact ground state  $|\Psi_0\rangle$  is determined. For this state, now, we want to see how accurately a parent Hamiltonian in both methods can



be constructed. As we want to check the approximate version of the Hamiltonian Finder, we artificially restrict our Hilbert space by setting all pseudopotentials  $V_l^{2s}$  with  $l > 5$  to zero. For this fermionic system, only three pseudopotential coefficients  $V_1^{2s}$ ,  $V_3^{2s}$  and  $V_5^{2s}$  are non-zero.

Three different system sizes were considered: (1)  $N = 7$ ,  $2s = 18$ , (2)  $N = 8$ ,  $2s = 18$  and (3)  $N = 8$ ,  $2s = 20$ . In case (1), the system setup is similar to a Laughlin state with filling fraction  $\nu = 1/3$ . As a measure to compare the accuracy of the resulting Hamiltonian  $H_{\text{res}}$ , we calculated the overlap of the initial state  $|\Psi_0\rangle$  with the exact ground state  $|GS\rangle$  of  $H_{\text{res}}$ , and the relative variance (6.3.54). The results are presented in Table 6.1.

	$N = 7, 2s = 18$		$N = 8, 2s = 18$		$N = 8, 2s = 20$	
	A	B	A	B	A	B
<i>overlap</i>	0.9999	0.9529	0.0000	0.0000	0.9990	0.9815
<i>rel. variance</i>	$0.9151 \cdot 10^4$	0.5171	$0.1871 \cdot 10^4$	0.0009	$0.290 \cdot 10^4$	0.0008

**Table 6.1** Results of the two methods A and B of the Hamiltonian Finder for three different system sizes. As indicators for the accuracy of the approximate parent Hamiltonian, the overlap of the initial state  $|\Psi_0\rangle$  with the exact, zero energy ground state  $|GS\rangle$ , and the relative variance are calculated.

For systems (1) and (3), both methods A and B find a ground state. The original method A, however, reaches a higher overlap. In contrast, for system (2), both methods fail to determine a zero mode. Obviously, method B minimizes the relative variance as its value is by orders of magnitude smaller than that of method A. Yet, as we can see, this does not necessitate a higher overlap.

### 6.3.4 Finding an approximate parent Hamiltonian for the 311-state

So far, we have only considered systems with one particle-flavor. If there are particles of two flavors in the system, as is the case for the 311-state, the Hilbert space extends, and also additional constraints have to be formulated to eliminate trivial solutions from the solution space.

Consider a system with particles of two flavors,  $\uparrow$  and  $\downarrow$  (for instance spin  $\pm 1/2$ ). All states then live in a product Hilbert space  $\mathcal{H}_\uparrow \otimes \mathcal{H}_\downarrow$  and the Hamiltonian consists of three parts: two intraflavor interactions  $H^{(\downarrow, \downarrow)}$  and  $H^{(\uparrow, \uparrow)}$  and one interflavor interaction  $H^{(\uparrow, \downarrow)}$ . The angular momentum of a  $\uparrow$ -particle ( $\downarrow$ -particle) is  $s$  ( $s'$ ). For a system of charged particles which live on different spheres according to their flavor,  $2s$  ( $2s'$ ) is the number of Dirac flux quanta through the  $\uparrow$ -sphere ( $\downarrow$ -sphere). We will only consider fermionic particles, therefore, the intraflavor pseudopotential coefficients for even relative angular momenta are zero,

$$V_l^{2s} = V_l^{2s'} = 0 \quad \forall l \in 2\mathbb{Z}. \quad (6.3.57)$$

The total Hamiltonian is the sum of all three contributions,

$$\begin{aligned}
H &= \sum_{i < j}^{N_\uparrow} \sum_{l=1}^{2s-1} V_l^{2s} P_{2s-l}(\mathbf{L}_i^\uparrow + \mathbf{L}_j^\uparrow) + \sum_{i < j}^{N_\downarrow} \sum_{l=1}^{2s'-1} V_l^{2s'} P_{2s'-l}(\mathbf{L}_i^\downarrow + \mathbf{L}_j^\downarrow) \\
&\quad + \sum_{i=1}^{N_\uparrow} \sum_{j=1}^{N_\downarrow} \sum_{l=0}^{2s} V_l^{s+s'} P_{s+s'-l}(\mathbf{L}_i^\uparrow + \mathbf{L}_j^\downarrow) \\
&= \sum_{l=1}^{2s'-1} V_l^{2s'} H^{(\downarrow, \downarrow, l)} + \sum_{l=1}^{2s-1} V_l^{2s} H^{(\uparrow, \uparrow, l)} + \sum_{l=0}^{2s} V_l^{s+s'} H^{(\uparrow, \downarrow, l)}.
\end{aligned} \quad (6.3.58)$$

The primed summation in the first two terms includes only odd relative angular momenta. We assume  $s \leq s'$ . For  $s \geq s'$ , the sum of  $l$  in the interflavor term would range from 0 to  $2s'$ .

Using (6.3.52), the eigenvalue equation can therefore be written as

$$\begin{aligned}
 H |\Psi\rangle &= E_0 |\Psi\rangle = \mathbf{A} \mathbf{v}, \\
 \mathbf{A} &:= \begin{pmatrix} h_1^{(\uparrow\uparrow,1)} & \dots & h_1^{(\uparrow\uparrow,2s-1)} & h_1^{(\downarrow\downarrow,1)} & \dots & h_1^{(\downarrow\downarrow,2s'-1)} & h_1^{(\uparrow\downarrow,0)} & \dots & h_1^{(\uparrow\downarrow,2s)} \\ h_2^{(\uparrow\uparrow,1)} & \dots & h_2^{(\uparrow\uparrow,2s-1)} & h_2^{(\downarrow\downarrow,1)} & \dots & h_2^{(\downarrow\downarrow,2s'-1)} & h_2^{(\uparrow\downarrow,0)} & \dots & h_2^{(\uparrow\downarrow,2s)} \\ \vdots & \ddots & \vdots & \vdots & \ddots & \vdots & \vdots & \ddots & \vdots \\ h_{n_{\max}}^{(\uparrow\uparrow,1)} & \dots & h_{n_{\max}}^{(\uparrow\uparrow,2s-1)} & h_{n_{\max}}^{(\downarrow\downarrow,1)} & \dots & h_{n_{\max}}^{(\downarrow\downarrow,2s'-1)} & h_{n_{\max}}^{(\uparrow\downarrow,0)} & \dots & h_{n_{\max}}^{(\uparrow\downarrow,2s)} \end{pmatrix}, \\
 \mathbf{v} &:= \left( V_1^{2s} \dots V_{2s-1}^{2s} V_1^{2s'} \dots V_{2s'-1}^{2s'} V_0^{s+s'} \dots V_{2s}^{s+s'} \right)^\top.
 \end{aligned} \tag{6.3.59}$$

Matrix  $\mathbf{A}$  has dimension  $(3s + s' + 1) \times n_{\max}$ . The column size of the interflavor block is determined by the range in which the relative angular momentum between two particles of different flavor lies,  $|s - s'| \leq s + s' - l \leq s + s'$ .

For many physical realizations, the matrix dimension is decreased due to additional constraints on the choice of pseudopotential coefficients. In the case of the 311-state, we have four trivial solutions to (6.3.59) we wish to eliminate. Three of the four trivial solutions arise from setting all pseudopotential coefficients to zero except for one type of interaction,

1.  $V_l^{2s} = 1, V_l^{2s'} = 0, V_l^{s+s'} = 0 \quad \forall l,$
2.  $V_l^{2s} = 0, V_l^{2s'} = 1, V_l^{s+s'} = 0 \quad \forall l,$
3.  $V_l^{2s} = 0, V_l^{2s'} = 0, V_l^{s+s'} = 1 \quad \forall l.$

The resulting Hamiltonian is proportional to the identity in the respective Hilbert subspace. The fourth trivial solution is specified by the choice

$$\begin{aligned}
 V_l^{2s} &= 0 = V_l^{2s'} \quad \forall l, \\
 V_l^{s+s'} &= (s + s' - l)(s + s' + 1 - l) + \text{const.}
 \end{aligned} \tag{6.3.60}$$

One of these four solutions can be eliminated by choosing  $E_0 = 0$  in (6.3.59). For the remaining trivial solutions to be eliminated, we have to further introduce three constraints. Assuming the pseudopotentials to decrease with increasing distance, a first guess could be

$$V_{2s-3}^{2s} = V_{2s-1}^{2s}, \quad V_{2s'-3}^{2s'} = V_{2s'-1}^{2s'}, \quad V_0^{s+s'} = V_1^{s+s'}. \tag{6.3.61}$$

For the intralayer interactions, large distances translate into large relative angular momentum  $l$ . However, for the interlayer interaction, a large distance results into a small relative angular momentum due to the opposite magnetic fields in the two layers.

The numerical implementation of the Hamiltonian finder yields one or even several sets of pseudopotential coefficients, each forming an interaction Hamiltonian  $H_{\text{res}}$ , whose ground state is approximately the specified state  $|\Psi\rangle$ . To investigate which of these sets of coefficients is the best approximation, we calculate two quantities: the overlap of the exact ground state  $|GS\rangle$  of  $H_{\text{res}}$  with our initial state  $|\Psi\rangle$ , and the relative variance, defined by (6.3.54).

As we are dealing with finite size systems, a high overlap, however, is not a quantitative indication of a good approximate parent Hamiltonian. For instance, in non-interacting Fermi gases perturbed by a finite-range scattering potential, the so-called Anderson orthogonality catastrophe is observed [4]. Given a system of  $N$  fermions living in a box of length  $L$ , it manifests itself in the asymptotic vanishing of the overlap of the ground state of the unperturbed system with the ground state of the same system with a finite range perturbation,

$$\langle \Psi_L^N | \Phi_L^N \rangle \sim L^{\gamma/2}, \tag{6.3.62}$$

in the thermodynamic limit,  $N \rightarrow \infty$ ,  $L \rightarrow \infty$  and  $N/L^d = \text{const.} > 0$ . Here,  $d \in \mathbb{N}$  is the spatial dimension. The decay exponent  $\gamma$  is derived from the scattering phases associated with the perturbation. Nonetheless, for our system, a high overlap indicates that the approximate parent Hamiltonian lies in the same equivalence class as the unknown exact parent Hamiltonian.

A far better way of determining the accuracy of the approximate parent Hamiltonian is to make a spectral analysis of our 311-state  $|\Psi\rangle$  and the exact ground state  $|GS\rangle$ . To do so, relative angular momentum resolved pseudopotential expectation values for both states must be calculated. This procedure is explained in further detail in the following Section 6.3.5. In Section 6.4, we will apply these quantities to determine the best approximate parent Hamiltonian for our 311-state.

### 6.3.5 Relative angular momentum resolved analysis

Since we are interested in a system exhibiting rotational symmetry, the  $z$ -component of the relative angular momentum of two particles is a good quantum number. Thus, it makes sense to analyze relative angular momentum resolved properties of our system. For instance, we can calculate the expectation value of the relative angular momentum resolved projection operators in (6.3.58) with respect to the system's ground state  $\psi$ ,

$$C_{\psi,l}^{\alpha\alpha'} := \langle \psi | H^{(\alpha\alpha',l)} | \psi \rangle, \quad \text{where } \alpha, \beta = \uparrow, \downarrow, \quad (6.3.63)$$

which we will from now on label relative angular momentum resolved correlators, or short ‘‘correlators’’.

For implementation purposes, the Hamiltonian is rewritten in terms of creation and annihilation operators as in (6.3.2),

$$\begin{aligned} H^{(\alpha\alpha',l)} = & \sum_{m_1=-s}^s \sum_{m_2=-s'}^{s'} \sum_{m_3=-s}^s \sum_{m_4=-s'}^{s'} c_{m_2,\alpha}^\dagger c_{m_1,\beta}^\dagger c_{m_3,\alpha} c_{m_4,\beta} \delta_{m_1+m_2,m_3+m_4} \\ & \cdot \langle s, m_1; s', m_2 | s + s' - l, m_1 + m_2 \rangle V_l^{\alpha\alpha'} \langle s + s' - l, m_3 + m_4 | s, m_3; s', m_4 \rangle, \end{aligned} \quad (6.3.64)$$

where  $\langle s, m_1; s', m_2 | j, m_1 + m_2 \rangle$  are Clebsch-Gordan coefficients and  $c_{m,\alpha}$  annihilates a particle with flavor  $\alpha$  in the properly normalized single particle state (6.3.3), which is further explained in Section 2.4.

It can be used to compare two states  $\psi_1$  and  $\psi_2$  by analyzing how much the correlators  $C_{\psi_1}$  and  $C_{\psi_2}$  differ for a specific angular momentum. In Section 6.4, we will do exactly this to compare the 311-state to the exact ground state of the approximate parent Hamiltonian.

Given two states  $\psi_1$  and  $\psi_2$ , the calculation of the correlators  $C_{\psi_1,l}^{\alpha\alpha'}$  and  $C_{\psi_2,l}^{\alpha\alpha'}$  for a specific relative angular momentum  $l$  allows us to compare the scattering properties of the two states. In Section 6.4, we then use this to compare the 311-state to the exact ground state of the approximate parent Hamiltonian. Based on this information, we will manually alter the pseudopotential coefficients  $V_l^{s+s'}$  of our parent Hamiltonian in such a way that the new interaction Hamiltonian represents a better approximate parent Hamiltonian of our state  $\Psi$ .

As an illustration of the information being provided by the correlators, the single particle Laughlin state with filling factor  $\nu = 1/m = 1/3$  is calculated for a single flavor-system of seven fermions. The results are presented in Figure 6.5. Due to the system's fermionic character, all correlators with even momentum must vanish. Moreover, they equal zero for relative angular momenta  $l < m$  due to the construction of the Laughlin state, minimizing the energetical cost of the state living in a potential  $\sum_{l < m} V_l^{2s} H^{(\uparrow\uparrow,l)}$ , in which all pseudopotential coefficients with  $l \geq m$  vanish. The maximum relative angular momentum of the system is  $m(N - 1)$ . Thus, in Figure 6.5, all correlators for  $l > 18$  vanish. The absolute values of the correlators does not convey any physical information, as it is given in arbitrary units. Due to the locality of the correlations, the correlators decay with increasing angular momentum.

### 6.3.6 Real space potentials

We assume a spherical two-layer system of  $N$   $\uparrow$ -spin particles living on a  $\uparrow$ -sphere pierced by  $2s$  Dirac flux quanta, and  $N$   $\downarrow$ -spin particles living on a  $\downarrow$ -sphere pierced by  $2s'$  Dirac flux quanta. Given a set of pseudopotential coefficients  $\{\tilde{V}_l\}_l$ , we wish to obtain the real space potential  $\tilde{V}(\theta) = f(\{\tilde{V}_l\}_l)$ , where  $f$  is some analytic function of the pseudopotentials.

To fulfill this task, we first have to set up a basis of real space potentials

$$V_n(\theta) = \mathcal{N}_n \left( \cos \frac{\theta}{2} \right)^{2(2s-n)} \left( \sin \frac{\theta}{2} \right)^{2n}, \quad n = 0, 1, \dots, 2s, \quad (6.3.65)$$

with their normalization

$$\mathcal{N}_n = \int_0^\pi d\theta \, 2\pi \sin \theta \, V_n(\theta). \quad (6.3.66)$$

There are two types of potentials for a two-layer system: The intralayer interactions in one sphere, and the interlayer interactions between  $\uparrow$ - and  $\downarrow$ -particles on different spheres. In the first case,  $\theta$  is the angle between two interacting particles of the same flavor, in the second case, it is the angle between an  $\uparrow$ - and a  $\downarrow$ -particle. Since the system is rotationally invariant, we can pin one of the two particles to the north pole. Then,  $\theta = 0$  ( $\theta = \pi$ ) corresponds to the north (south) pole.

In Figures 6.6 and 6.7, the real space basis potentials (6.3.65) are shown for  $2s = 9$  and  $2s = 11$ , respectively. For  $n = 0$  ( $n = 2s$ ), the maximum of the potential is at the north (south) pole. Since we have pinned one particle at the north pole,  $V_0$  describes an interaction which yields a maximal separation between the two particles, while they move closer together for increasing  $n$ .

With the help of (6.3.10) for the intralayer case and (6.3.25) for the interlayer case, the basis of pseudopotentials  $\tilde{V}_{l,n}$ ,  $l = 0, 1, \dots, 2s$ , corresponding to the real space basis potentials  $V_n(\theta)$  can be calculated. Explicit expressions for the pseudopotential basis will be derived below. Since the calculations are similar to the calculation in Section 6.3.1.3, only the starting equations and the final result are given.

With the potential basis set up, we get the real space potential from a set of pseudopotentials  $\{\tilde{V}_l\}_l$  by solving the system of linear equations

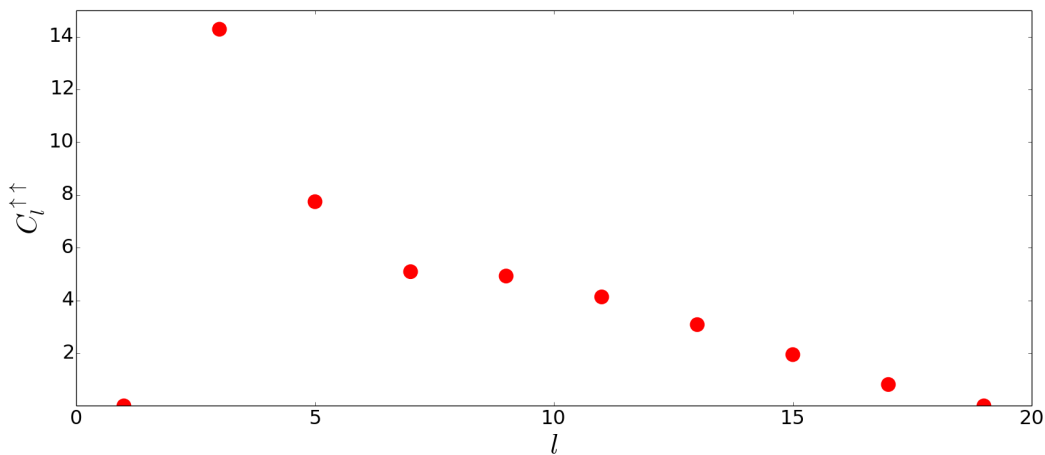


**Fig. 6.5** Angular momentum resolved correlators for the single particle Laughlin state with filling factor  $\nu = 1/3$  in a single flavor-system of seven fermions.

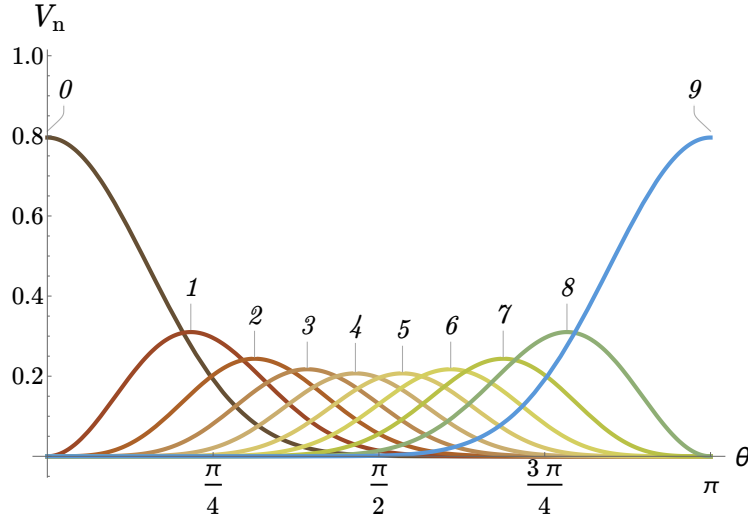


**Fig. 6.6** Real space basis potentials  $V_n(\theta)$  in arbitrary units for a sphere pierced by  $2s = 9$  flux quanta. The italic label indicates the index  $n$ . The north (south) pole corresponds to  $\theta = 0$  ( $\theta = \pi$ ).

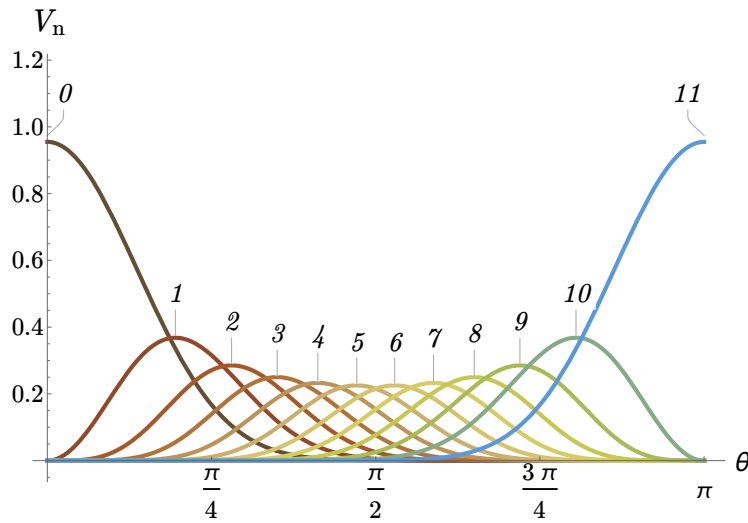


**Fig. 6.7** Real space basis potentials  $V_n(\theta)$  in arbitrary units for a sphere pierced by  $2s = 11$  flux quanta. The italic label indicates the index  $n$ . The north (south) pole corresponds to  $\theta = 0$  ( $\theta = \pi$ ).

$$\begin{aligned}
 \sum_n a_n V_{l,n} &= \tilde{V}_l, \quad \forall l, n, \\
 \sum_n b_n V_{l,n} &= \mathbb{1}, \\
 \sum_n c_n V_{l,n} &= V_l^{\text{ang}},
 \end{aligned} \tag{6.3.67}$$

where  $V_l^{\text{ang}}$  are the pseudopotentials for the total angular momentum, corresponding to (6.3.21) for the intralayer case and (6.3.26) for the interlayer case. The real space potential is given by

$$\tilde{V}^{\alpha\beta}(\theta) = \sum_n (a_n^{\alpha\beta} + \gamma^{\alpha\beta} b_n + \mu c_n^{\alpha\beta}) V_n(\theta), \quad (6.3.68)$$

with  $\alpha = \beta = \uparrow$  or  $\alpha = \beta = \downarrow$  for the intralayer case, and  $\alpha = \uparrow, \beta = \downarrow$  for the interlayer case. The second and third term in (6.3.68) only add a constant to the potential, so that their coefficients  $\gamma$  and  $\mu$  can be used as tuning parameters to create the experimentally most realistic potential possible. While the coefficient  $\gamma$  can be chosen arbitrarily for the intra- and interlayer case, the coefficient  $\mu$  has to be equal in both real space potentials. In summary, we can thus visualize the potential in real space with this method, given a set of pseudopotential coefficients. We can fine-tune the shape of the potential, adjusting it to possible experimental needs.

### Intralayer pseudopotentials

Given two particles of the same flavor at positions  $\mathbf{\Omega}(u_1, v_1)$  and  $\mathbf{\Omega}(u_2, v_2)$  on the sphere, the pseudopotential coefficients are evaluated via

$$V_l^{2s} = \frac{\langle \psi_{(\alpha,\beta),0}^{s,j} | V_n(\theta) | \psi_{(\alpha,\beta),0}^{s,j} \rangle}{\langle \psi_{(\alpha,\beta),0}^{s,j} | \psi_{(\alpha,\beta),0}^{s,j} \rangle} =: \frac{I}{N_0}, \quad (6.3.69)$$

with the basis wave functions defined in (6.3.7). Written out explicitly, the denominator is

$$N_0 = \int d\mathbf{\Omega}(u_1, v_1) \int d\mathbf{\Omega}(u_2, v_2) |u_1|^{2(2s-l)} |u_2|^{2(2s-l)} |u_1 v_2 - u_2 v_1|^{2l}, \quad (6.3.70)$$

the nominator is

$$I = \int d\mathbf{\Omega}(u_1, v_1) \int d\mathbf{\Omega}(u_2, v_2) |u_1|^{2(2s-l)} |u_2|^{2(2s-l)} |u_1 v_2 - u_2 v_1|^{2l} \cdot \mathcal{N} \left( \cos \frac{\theta}{2} \right)^{2(2s-n)} \left( \sin \frac{\theta}{2} \right)^{2n}. \quad (6.3.71)$$

The chord distance between the two particles reads

$$d := |\mathbf{\Omega}(u_1, v_1) - \mathbf{\Omega}(u_2, v_2)| = |u_1 v_2 - u_2 v_1| = 2 \sin \frac{\theta}{2}. \quad (6.3.72)$$

To solve the above expressions, it is useful to perform the unitary transformation

$$\begin{pmatrix} u'_2 \\ v'_2 \end{pmatrix} = \underbrace{\begin{pmatrix} \bar{u}_1 & \bar{v}_1 \\ -v_1 & u_1 \end{pmatrix}}_{=:T} \begin{pmatrix} u_2 \\ v_2 \end{pmatrix}, \quad (6.3.73)$$

with

$$u_i = \cos \frac{\theta_i}{2} e^{i\varphi_i/2},$$

$$v_i = \sin \frac{\theta_i}{2} e^{-i\varphi_i/2}.$$

Applying this transformation,  $\theta \xrightarrow{T} \theta'_2$ , yields

$$N_0 = \int d\mathbf{\Omega}(u_1, v_1) \int d\mathbf{\Omega}(u'_2, v'_2) |u_1|^{2(2s-l)} |u_1 u'_2 - \bar{v}_1 v'_2|^{2(2s-l)} |v'_2|^{2l}, \quad (6.3.74)$$

and

$$\begin{aligned}
I &= \int d\Omega(u_1, v_1) \int d\Omega(u'_2, v'_2) |u_1|^{2(2s-l)} |u_1 u'_2 - \bar{v}_1 v'_2|^{2(2s-l)} |v'_2|^{2l} \\
&\quad \cdot \mathcal{N} \left( \cos \frac{\theta'_2}{2} \right)^{2(2s-n)} \left( \sin \frac{\theta'_2}{2} \right)^{2n}.
\end{aligned} \tag{6.3.75}$$

Applying similar steps as in Section 6.3.1.3, we finally obtain

$$\begin{aligned}
V_{l,n} &= \frac{1}{4\pi} \frac{[(2s+1)!]^3 (2s+n)!}{n! l! (4s+1)! (4s-l+1)!} \\
&\quad \cdot {}_pF_q(\{l-2s, 2s-l+1, 2s-n+1\}, \{1, -2s-n\}, 1).
\end{aligned} \tag{6.3.76}$$

The pseudopotentials for all possible values of  $l$  and  $n$  are shown in Figure 6.8 for a sphere pierced by  $2s = 9$  flux quanta and in Figure 6.9 for a sphere pierced by  $2s = 11$  flux quanta.

### Interlayer pseudopotentials

For the interlayer pseudopotentials, given the choice (6.3.65) of the real space basis potentials, the fluxes through the  $\uparrow$ - and  $\downarrow$ -sphere have to fulfill  $s \leq s'$ . Similar to the intralayer case, the pseudopotential coefficients are evaluated via (6.3.69). This time, the basis wave functions are specified by (6.3.24). The denominator of (6.3.69) is identical to the denominator for the Coulomb potential, given in (6.3.39). The nominator in explicit form is

$$I = \frac{1}{2} \int d\Omega(u, v) \int d\Omega(a, b) |u|^{2(2s-l)} |b|^{2(2s'-l)} |\bar{a}u + b\bar{v}|^{2l} \mathcal{N} \left( \cos \frac{\theta}{2} \right)^{2(2s-n)} \left( \sin \frac{\theta}{2} \right)^{2n}.$$

Under the unitary transformation (6.3.32), the angle  $\theta$  transforms as  $\theta \xrightarrow{T} \theta'_2$ , allowing to simplify the above integral. The spherical coordinates are defined in (6.3.33). Applying similar steps as in Section 6.3.1.3, we finally obtain

$$\begin{aligned}
V_{l,n} &= \frac{1}{4\pi} \frac{[(2s+1)!]^2 (2s'+1)! (2s+l-n)! (2s'-l+n)! (2s+2s'-2l)!}{n! l! (2s-n)! (2s-l)! (2s'-l)! (2s+2s'-l+1)! (2s+2s'+1)!} \\
&\quad \cdot {}_pF_q(\{2s+l-n+1, l-2s', l-2s'\}, \{l-n-2s', 2l-2s'-2s\}, 1).
\end{aligned} \tag{6.3.77}$$

The pseudopotentials for all possible values of  $l$  and  $n$  are shown in Figure 6.10 for the interlayer interaction in a two-layer system, consisting of an  $\uparrow$ -sphere pierced by  $2s = 9$  flux quanta and a  $\downarrow$ -sphere pierced by  $2s' = 11$  flux quanta, which, according to (6.2.3), corresponds to a system of six  $\uparrow$ -spin particles and six  $\downarrow$ -spin particles for the 311-state. For  $n = 0$ , the maximum of the pseudopotential is at maximal relative angular momentum  $l = 2s$ . In contrast, for the intralayer pseudopotential at  $n = 0$ , the maximum is at minimal relative angular momentum  $l = 0$ . This is a consequence of the fact that the magnetic field on the  $\downarrow$ -sphere points in the opposite direction than the magnetic field on the  $\uparrow$ -sphere.

Having obtained explicit expressions for the intra- and interlayer basis pseudopotentials, we can calculate the real space potential given a set of pseudopotential coefficients. This method will be applied in Section 6.4.5 to create a real space potential for the 311-state with the pseudopotential coefficients obtained by our Hamiltonian Finder method.

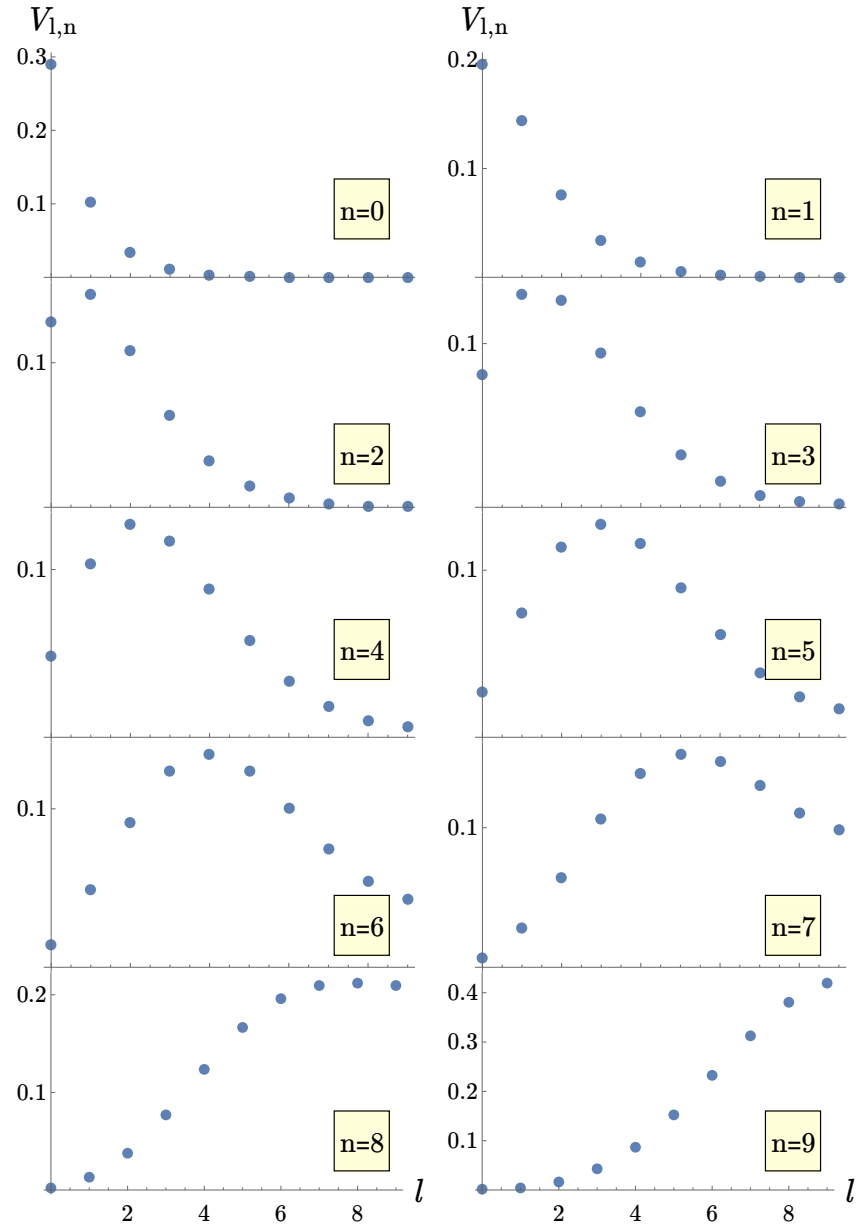


**Fig. 6.8** Basis pseudopotentials  $V_{l,n}$  for the intralayer interaction on a sphere pierced by  $2s = 9$  flux quanta. The index  $n$  can take values  $0, 1, \dots, 2s$ .



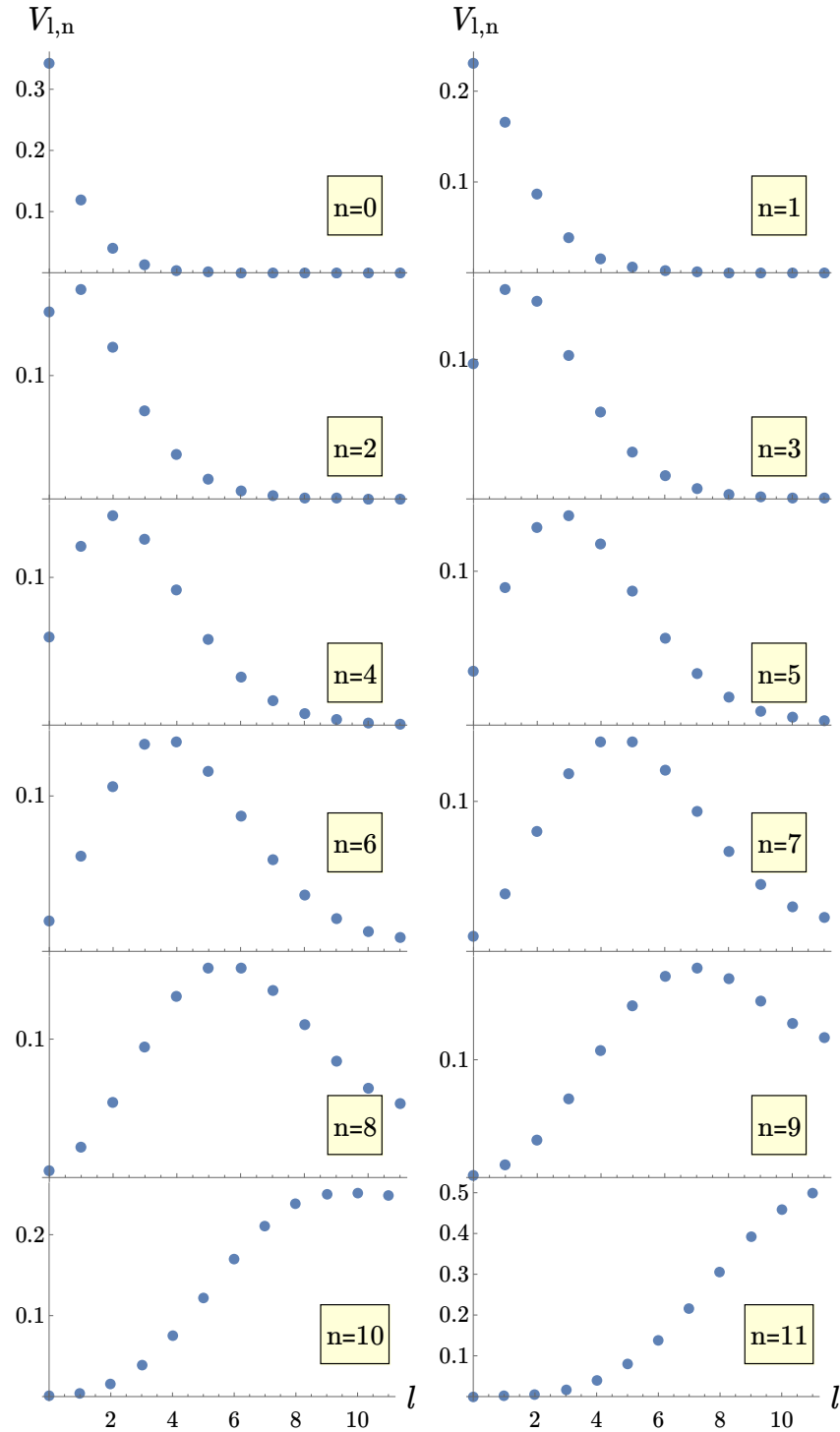


**Fig. 6.9** Basis pseudopotentials  $V_{l,n}$  for the intralayer interaction on a sphere pierced by  $2s = 11$  flux quanta. The index  $n$  can take values  $0, 1, \dots, 2s$ .

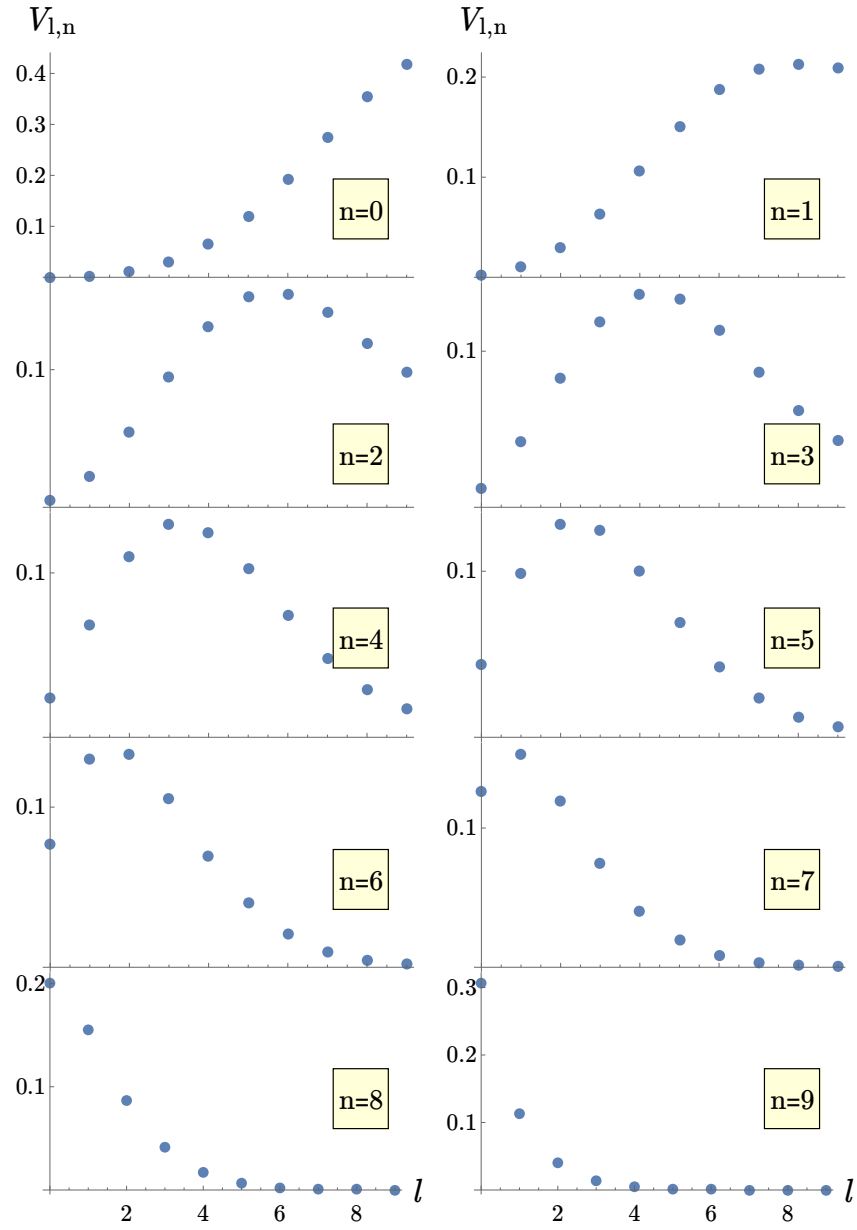


**Fig. 6.10** Basis pseudopotentials  $V_{l,n}$  for the interlayer interaction in a two-layer system, consisting of an  $\uparrow$ -sphere pierced by  $2s = 9$  flux quanta and a  $\downarrow$ -sphere pierced by  $2s' = 11$  flux quanta. The index  $n$  can take values  $0, 1, \dots, 2s$ .

## 6.4 Numerical results for the 311-state

With the analytical background of the previous chapters, we now wish to analyze the properties of the 311-state numerically. One challenge is to set up the state for large enough systems, as the size of the Hilbert space grows exponentially with system size. For the present application, we managed to treat two-layer systems with up to fourteen particles, corresponding to seven particles per layer. We use the imperative programming language Fortran (2003 standard) for the numerical analysis, which provides an efficient framework for high-performance scientific programming.

The first numerical task is to implement the 311-state. Section 6.4.1 details how this can be achieved. Given the numerical 311-state, we calculate the pair correlation function in Section 6.4.2, which provides a measure of how the particles are distributed on the sphere. In Section 6.4.3, we calculate the relative angular momentum correlation of the 311-state and compare it to other uncorrelated quantum Hall states. Using the Hamiltonian Finder method, which is explained in detail in Section 6.3.3, we manage to construct an approximate parent Hamiltonian of the 311-state for different system sizes in Section 6.4.4. Out of the pseudopotential coefficients specifying the parent Hamiltonian, we finally construct a physically realistic real space potential in Section 6.4.5.

To eliminate possible *programming errors* in our program, we have extensively run test cases by studying various systems documented in literature. For instance, we have tested our Hamiltonian Finder method by calculating the parent Hamiltonian of the Laughlin state. Additionally, such tests help to determine the influence of finite size effects on the results.

In contrast to *programming errors*, numerical errors cannot be eliminated entirely. One type of numerical error is the *roundoff error*, which is due to the finite number precision of computers, which depends on the choice of data type. For example, for 64-bit double precision values, the exponent is represented by 11 bits, and the mantissa by 52 bits. One bit is reserved for the sign of the number. The resulting machine precision<sup>3</sup> is  $\epsilon_m = 2.22 \cdot 10^{-16}$ . Non-representable numbers are rounded to the next representable value and the roundoff error accumulates with the number of arithmetic operations.

*Truncation errors* are independent of the computer hardware. They occur when, for instance, an originally continuous mathematical operation is discretized. While roundoff errors can hardly be eliminated, truncation errors can be decisively decreased by a careful choice of the discretization method and system resolution. If, as for the present case, a naturally discrete system is analyzed, this type of error does not occur.

Another important aspect is the numerical stability of the algorithms used. In a stable algorithm, small fluctuations of the input values lead to only small fluctuations of the output data. If there is an instability, roundoff and/or truncation errors build up unboundedly and yield unphysical results. Here, a thorough understanding of the numerical background is necessary to circumvent possible instabilities.

### 6.4.1 Numerical construction of the wave function

To write out the microscopic 311-state (6.2.2) numerically, we start by expanding its first quantized form. We assume a two-layer system of  $N_\uparrow$   $\uparrow$ -spin particles and  $N_\downarrow$   $\downarrow$ -spin particles, living on an  $\uparrow$ -sphere pierced by  $2s$  Dirac flux quanta and a  $\downarrow$ -sphere pierced by  $2s'$  Dirac flux quanta, respectively. Then, the 311-state can be written as

$$\Psi_{311}[u, v, \bar{a}, \bar{b}] = \frac{1}{\mathcal{N}} \sum_{(c_\uparrow, c_\downarrow)} \frac{a_{2, (c_\uparrow, c_\downarrow)}}{\sqrt{N_\uparrow! N_\downarrow!}} \sum_{\mathcal{P}} \text{sign}(\mathcal{P}) \Psi_{(c_\uparrow, c_\downarrow)}^{\mathcal{P}}[u, v, \bar{a}, \bar{b}], \quad (6.4.1)$$

with

---

<sup>3</sup> The machine precision is defined as the smallest floating point number which, when added to 1.0, yields a result other than 1.0.

$$\Psi_{(c_\uparrow, c_\downarrow)}^{\mathcal{P}}[u, v, \bar{a}, \bar{b}] := \prod_{i=1}^{N_\uparrow} \prod_{k=1}^{N_\downarrow} u_i^{c_\uparrow(\mathcal{P}(i))} v_i^{2s - c_\uparrow(\mathcal{P}(i))} \bar{a}_k^{c_\downarrow(\mathcal{P}(k))} \bar{b}_k^{2s' - c_\downarrow(\mathcal{P}(k))}, \quad (6.4.2)$$

$\mathcal{N}$  being the overall normalization of the wave function. Similar to (6.3.5), we define  $[u, v, \bar{a}, \bar{b}] := (\{u_i, v_i\}_i, \{\bar{a}_k, \bar{b}_k\}_k)$  as the list of all particle coordinates in both layers. Each monomial occurring in the sum in (6.4.1) is a product of a coefficient  $a_{2, (c_\downarrow, c_\uparrow)} \in \mathbb{C}$ , all  $\uparrow$ -spin coordinates

$$(u_1, v_1, u_2, v_2, \dots, u_{N_\uparrow}, v_{N_\uparrow})$$

with corresponding exponents

$$(\beta_1, 2s - \beta_1, \beta_2, 2s - \beta_2, \dots, \beta_{N_\uparrow}, 2s - \beta_{N_\uparrow}) \quad (6.4.3)$$

and all  $\downarrow$ -spin coordinates

$$(\bar{a}_1, \bar{b}_1, \bar{a}_2, \bar{b}_2, \dots, \bar{a}_{N_\downarrow}, \bar{b}_{N_\downarrow})$$

with corresponding coordinates

$$(\gamma_1, 2s' - \gamma_1, \gamma_2, 2s' - \gamma_2, \dots, \gamma_{N_\downarrow}, 2s' - \gamma_{N_\downarrow}). \quad (6.4.4)$$

For each monomial,  $c_\uparrow$  is the list of ordered exponents of the spinor components  $u_i$ , corresponding to the  $\uparrow$ -spin particles, with

$$c_\uparrow := (\beta_1, \beta_2, \dots, \beta_{N_\uparrow}). \quad (6.4.5)$$

Similarly, the list of ordered exponents of the spinor components  $\bar{a}_k$  corresponding to the  $\downarrow$ -spin particles is  $c_\downarrow$ , with

$$c_\downarrow := (\gamma_1, \gamma_2, \dots, \gamma_{N_\downarrow}). \quad (6.4.6)$$

We label  $a_{2, (c_\downarrow, c_\uparrow)}$  the ‘‘geometrical coefficients’’, as they result from expanding the factorized expression of the 311-state (6.2.2). In (6.4.1), we sum over all possible permutations  $\mathcal{P}$  of the elements of lists  $c_\uparrow$  and  $c_\downarrow$ . For even permutations, it is  $\text{sign}(\mathcal{P}) = 1$ , for odd permutations, it is  $\text{sign}(\mathcal{P}) = -1$ .

The idea of our numerical construction of the 311-state (6.2.2) is to first create parent states for the  $\uparrow$ -spin and  $\downarrow$ -spin particles, which are the Laughlin-3 state and the Laughlin-1 state, respectively. Then, we take the direct product of the two parent states to create a two-layer system. Finally, the interlayer derivative term is applied to the Laughlin-3 term, yielding our 311-state.

In the program, the state is saved in second quantization, (6.2.41), as a list of normalized coefficients  $a_{1, (c_\uparrow, c_\downarrow)} / \mathcal{N}_\beta := \alpha_{(c_\uparrow, c_\downarrow)}$  and their corresponding orbital configurations

$$|\Psi_{(c_\uparrow, c_\downarrow)}\rangle := |c_\uparrow(0), c_\uparrow(1), \dots, c_\uparrow(2s); c_\downarrow(0), c_\downarrow(1), \dots, c_\downarrow(2s')\rangle,$$

yielding

$$|\Psi\rangle = \frac{1}{\mathcal{N}_\beta} \sum_{(c_\uparrow, c_\downarrow)} a_{1, (c_\uparrow, c_\downarrow)} |\Psi_{(c_\uparrow, c_\downarrow)}\rangle. \quad (6.4.7)$$

The orbital number basis is orthonormal,  $\langle \Psi_n | \Psi_m \rangle = \delta_{n, m}$ . The overall normalization is  $\mathcal{N}_\beta$ , which we determine via

$$\begin{aligned} 1 &\stackrel{!}{=} \langle \Psi | \Psi \rangle = \frac{1}{\mathcal{N}_\beta^2} \sum_{(c'_\uparrow, c'_\downarrow)} \sum_{(c_\uparrow, c_\downarrow)} a_{1, (c'_\uparrow, c'_\downarrow)}^* a_{1, (c_\uparrow, c_\downarrow)} \langle \Psi_{(c'_\uparrow, c'_\downarrow)} | \Psi_{(c_\uparrow, c_\downarrow)} \rangle \\ &= \frac{1}{\mathcal{N}_\beta^2} \sum_{(c_\uparrow, c_\downarrow)} |a_{1, (c_\uparrow, c_\downarrow)}|^2. \end{aligned} \quad (6.4.8)$$

One challenging part of the numerical implementation is the correct calculation of the orbital coefficients. To do so, we have to keep track of how often every possible permutation of exponents can appear and which sign is associated to it. A sign can occur when permuting particles due to their fermionic character. The orbital coefficients then have to be rescaled in order for the wave function to be normalized. In the following, we demonstrate how to obtain the normalization factor as well as the final coefficients.

Using the first quantized form (6.4.1) of the wave function, the normalization constraint (6.4.8) can be rewritten as

$$1 \stackrel{!}{=} \frac{1}{\mathcal{N}^2} \sum_{(c_\uparrow, c_\downarrow)} |a_{2, (c_\uparrow, c_\downarrow)}|^2 \sum_{\mathcal{P}} \frac{1}{N_\uparrow!} \frac{1}{N_\downarrow!} \int DuDv \int D\bar{a}D\bar{b} (\Psi_{(c_\uparrow, c_\downarrow)}^{\mathcal{P}}[u, v, \bar{a}, \bar{b}])^* \Psi_{(c_\uparrow, c_\downarrow)}^{\mathcal{P}}[u, v, \bar{a}, \bar{b}], \quad (6.4.9)$$

where we have used the orthogonality of the basis states. The two integrals denote an integration over the entire sphere of  $\uparrow$ -spin and  $\downarrow$ -spin electrons,

$$\begin{aligned} \int DuDv &= \prod_{i=1}^{N_\uparrow} \int du_i dv_i = \prod_i \frac{1}{4\pi} \int d\Omega_{\uparrow, i} = \left(\frac{1}{4\pi}\right)^{N_\uparrow} \int d\Omega_\uparrow, \\ \int D\bar{a}D\bar{b} &= \prod_{i=1}^{N_\downarrow} \int d\bar{a}_i d\bar{b}_i = \prod_i \frac{1}{4\pi} \int d\Omega_{\downarrow, i} = \left(\frac{1}{4\pi}\right)^{N_\downarrow} \int d\Omega_\downarrow, \end{aligned} \quad (6.4.10)$$

with  $d\Omega = \sin\theta d\theta d\phi$ . Using the integration relations

$$\frac{1}{4\pi} \int d\Omega_\uparrow \bar{u}^{m'} \bar{v}^{2s-m'} u^m v^{2s-m} = \frac{m!(2s-m)!}{(2s+1)!} \delta_{m, m'} \quad (6.4.11)$$

and

$$\frac{1}{4\pi} \int d\Omega_\downarrow \bar{a}^{m'} \bar{b}^{2s'-m'} a^m b^{2s'-m} = \frac{m!(2s'-m)!}{(2s'+1)!} \delta_{m, m'}, \quad (6.4.12)$$

we get

$$1 \stackrel{!}{=} \frac{1}{\mathcal{N}^2} \sum_{(c_\uparrow, c_\downarrow)} |a_{2, (c_\uparrow, c_\downarrow)}|^2 \prod_{i=1}^{N_\uparrow} \prod_{j=1}^{N_\downarrow} \frac{c_\uparrow(i)!(2s-c_\uparrow(i))!}{(2s+1)!} \frac{c_\downarrow(j)!(2s'-c_\downarrow(j))!}{(2s'+1)!} \quad (6.4.13)$$

The factor  $1/N!$  cancels out as there are  $N!$  permutations  $\mathcal{P}$ , and their integration gives always the same result. The expression can be rewritten into

$$\frac{1}{\mathcal{N}_\beta} \sum_{(c_\uparrow, c_\downarrow)} |a_{1, (c_\uparrow, c_\downarrow)}|^2 \stackrel{!}{=} 1 \stackrel{!}{=} \frac{1}{\beta_\uparrow \beta_\downarrow \mathcal{N}^2} \sum_{(c_\uparrow, c_\downarrow)} |a_{2, (c_\uparrow, c_\downarrow)}|^2 a_{3, (c_\uparrow, c_\downarrow)}, \quad (6.4.14)$$

where we have introduced the quantities

$$\begin{aligned} a_{3, (c_\uparrow, c_\downarrow)} &:= \prod_{i=1}^{N_\uparrow} \frac{c_\uparrow(i)!(2s-c_\uparrow(i))!}{(2s+1)!} \frac{(2s+1)!}{c_{\uparrow,1}(i)!(2s-c_{\uparrow,1}(i))!} \\ &\quad \cdot \prod_{j=1}^{N_\downarrow} \frac{c_\downarrow(j)!(2s'-c_\downarrow(j))!}{(2s'+1)!} \frac{(2s'+1)!}{c_{\downarrow,1}(j)!(2s'-c_{\downarrow,1}(j))!}, \\ \beta_\uparrow &:= \prod_{i=1}^{N_\uparrow} \frac{(2s+1)!}{c_{\uparrow,1}(i)!(2s-c_{\uparrow,1}(i))!} \quad \text{and} \\ \beta_\downarrow &:= \prod_{j=1}^{N_\downarrow} \frac{(2s'+1)!}{c_{\downarrow,1}(j)!(2s'-c_{\downarrow,1}(j))!}. \end{aligned} \quad (6.4.15)$$

In the first expression, the factors

$$\frac{(2s+1)!}{c_{\uparrow,1}(i)!(2s-c_{\uparrow,1}(i))!} \quad \text{and} \quad \frac{(2s'+1)!}{c_{\downarrow,1}(i)!(2s'-c_{\downarrow,1}(i))!}$$

are introduced to limit the size of the resulting decimal numbers, since large values can cause numerical instabilities. In the normalization process, the factor cancels out. Hence, we arbitrarily choose the normalization factor of the first basis configuration to be  $a_{3,(c_{\uparrow,1},c_{\downarrow,1})} = 1$ .

For the normalization, we get  $\mathcal{N}_{\beta} = \sqrt{\beta_{\uparrow}\beta_{\downarrow}}\mathcal{N}$ . The phase of the normalization is free to choose, and we set it to zero. We get for the orbital coefficients

$$a_{1,(c_{\uparrow},c_{\downarrow})} = a_{2,(c_{\uparrow},c_{\downarrow})}\sqrt{a_{3,(c_{\uparrow},c_{\downarrow})}} \quad (6.4.16)$$

To numerically implement the 311-state, we compute the necessary parameters in second quantization via the geometrical coefficients  $a_{2,(c_{\uparrow},c_{\downarrow})}$  of the first quantized wave function.

Table 6.2 displays for different system sizes the dimension of the Hilbert space,  $\dim(\mathcal{H})$ , as well as the total number of possible orbital configurations  $N_{\text{config}}$ . Given the product Hilbert space with  $N_{\uparrow}$  ( $N_{\downarrow}$ ) particles in the first (second) layer pierced by  $2s$  ( $2s'$ ) flux quanta, this total number is simply the stochastic quantity

$$N_{\text{config}} = \binom{2s+1}{N_{\uparrow}} \binom{2s'+1}{N_{\downarrow}}. \quad (6.4.17)$$

The dimension of the Hilbert space is much smaller than the total number of configurations, as the 311-state is rotationally invariant, thus living in the singlet subspace. Nevertheless, the dimension grows rapidly with increasing particle number. The largest system we are able to treat numerically is a two-layer system with seven  $\uparrow$ -spin and seven  $\downarrow$ -spin particles.

$N_{\uparrow} + N_{\downarrow}$	$(2s, 2s')$	$N_{\text{config}}$	$\dim(\mathcal{H})$
2+2	(1,3)	6	2
3+3	(3,5)	80	12
4+4	(5,7)	1050	100
5+5	(7,9)	14,112	936
6+6	(9,11)	194,040	9697
7+7	(11,13)	2,718,144	106,872

**Table 6.2** For different system sizes, the total number of possible orbital configurations  $N_{\text{config}}$ , specified in (6.4.17), and the dimension of the Hilbert space  $\dim(\mathcal{H})$  of the 311-state are listed.

## 6.4.2 Pair correlation function

The pair correlation function introduced in Section 6.2.4 is a measure of the correlation properties of a many-particle system. It returns the probability of finding a particle at a specified distance from a reference particle. Since we only investigate rotationally invariant systems, we pin the reference particle to the north pole of the sphere. Since the 311-state is a two-layer system, we calculate the intra- and interlayer pair correlations.

To develop an intuition for the pair correlation function, it is useful to first calculate the quantity for a well-studied system, such as the Laughlin state. In Figure 6.11, the pair correlation function  $g(r)$  of a fermionic Laughlin state with filling fraction  $\nu = 1/m = 1/3$  for a system of eight particles is plotted. Figure 6.12 shows the pair correlation function of the bosonic Laughlin state with  $\nu = 1/2$  for eight particles. In both systems, the reference particle sits at the north pole with spinor coordinates  $(0, 1)$ , and  $\theta$  is the angle

between the two particle positions. The spinor coordinates of the second particle are  $(\sin(\theta/2), \cos(\theta/2))$ . The largest distance between the two particles is reached for  $\theta = \pi$ , when the second particle is located at the south pole. For small distances  $r$  between two particles, the correlation function is proportional to  $|\mathbf{r}|^m$ , which is in terms of angle  $\theta$

$$|\mathbf{r}|^m = \sqrt{2(1 - \cos \theta)}^m. \quad (6.4.18)$$

Fermionic statistics requires  $g \rightarrow 0$  for  $r \rightarrow 0$ . Incompressibility implies suppressed long range correlations, so that the pair correlation function is constant for large distances. The pair correlation functions are mirror symmetric around the south pole,  $g(\pi + x) = g(\pi - x)$ . The wiggles observed in both figures appear due to finite size effects.

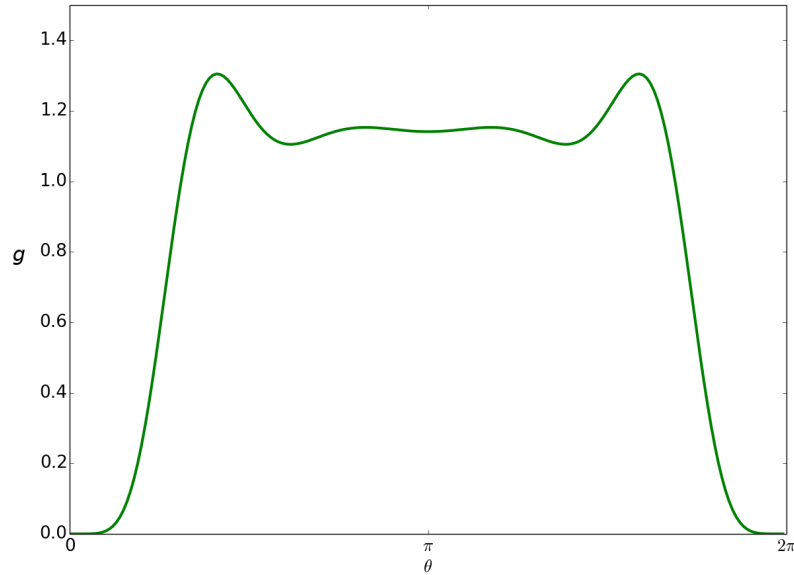


**Fig. 6.11** Pair correlation function for the fermionic Laughlin state with filling fraction  $\nu = 1/3$  for a system with  $N = 8$  particles living on a sphere. One particle is pinned at the north pole corresponding to  $\theta = 0$ .

For the 311-state, the pair correlation functions for 6+6 (meaning six  $\uparrow$ -spin particles on a sphere with flux  $2s$  and six  $\downarrow$ -spin particles on a sphere with flux  $2s'$ ) and 7+7 particles are presented in Figures 6.13 and 6.14. The first particle sits at the north pole, and the second particle is at  $(\sin(\theta/2), \cos(\theta/2))$ . The correlation functions  $g_r(\theta) = g(\theta)/N_r$  are renormalized with a renormalization constant  $N_r$  in such a way, that the integration over the sphere,  $\theta \in [0, \pi]$  equals 1,

$$\int_0^\pi d\left(\frac{\theta}{2}\right) \frac{1}{N_r} g(0, 1, u_2(\theta/2), v_2(\theta/2)) = 1. \quad (6.4.19)$$

The intraspin pair correlation functions are qualitatively similar to those for the fermionic Laughlin state: For small distances, the particles avoid each other, for large distances, the function reaches a constant value. Also, for increasing system size, the intraspin correlation functions for both spin flavors become increasingly similar.

As the Pauli exclusion principle does not hold for distinguishable particles, the interspin pair correlation function does not vanish for  $\theta \rightarrow 0$ . The wavy structure indicates some degree of correlation between the layers.

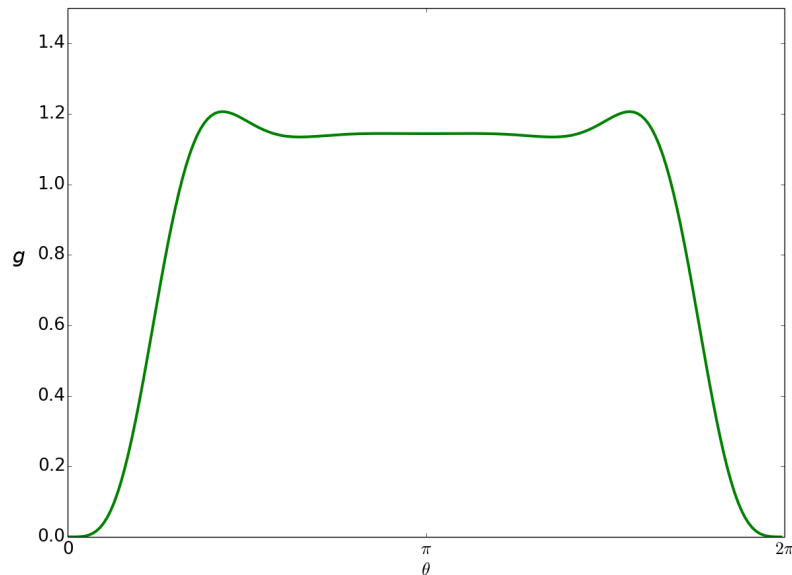


**Fig. 6.12** Pair correlation function for the bosonic Laughlin state with filling fraction  $\nu = 1/2$  for a system with  $N = 8$  particles living on a sphere. One particle is pinned at the north pole corresponding to  $\theta = 0$ .

In Figure 6.15, we have compared the interlayer pair correlation function for different system sizes. This finite size analysis shows that the shape of the correlation function indicates some correlation between the two layers. However, a quantitative measure cannot be deduced, since also finite size effects influence the wavy structure of the function. This leads us to the conclusion that, although the pair correlation function delivers some information about our wave function, we need to calculate different quantities for a more detailed analysis. As the relative angular momentum is a good quantum number in the given system, essential information lies in its relative angular momentum resolved correlation values, introduced in Section 6.3.5. This information gets lost in the pair correlation function by integrating over all angular momenta.

### 6.4.3 Relative angular momentum resolved correlators

For our 311-state in a system with up to 7  $\uparrow$ -spin and 7  $\downarrow$ -spin particles, we calculate the relative angular momentum resolved correlators  $C_l^{\uparrow\uparrow}$ ,  $C_l^{\uparrow\downarrow}$  and  $C_l^{\downarrow\downarrow}$ , which are specified in Section 6.3.5. As compared to the pair correlation function of the previous section, these quantities convey much more information on the correlation properties of the state.

In Figures 6.16 and 6.17, the correlators for the 311-state with 5+5 and 6+6 particles are plotted. Since the particles for the intralayer correlators are indistinguishable and fermionic, the relative angular momentum can only take odd values, and  $0 \leq l \leq 2s$  for  $C_l^{\uparrow\uparrow}$ ,  $0 \leq l \leq 2s'$  for  $C_l^{\downarrow\downarrow}$ . For the interspin correlators, all values with  $0 \leq l \leq 2s$  for  $s \leq s'$  are possible. The difference between the dots and crosses in the figures will be explained in Section 6.4.4.

The dashed lines show the value of the correlators for an uncorrelated system, which equals the average relative angular momentum density of the particles being distributed homogeneously over the sphere, which is



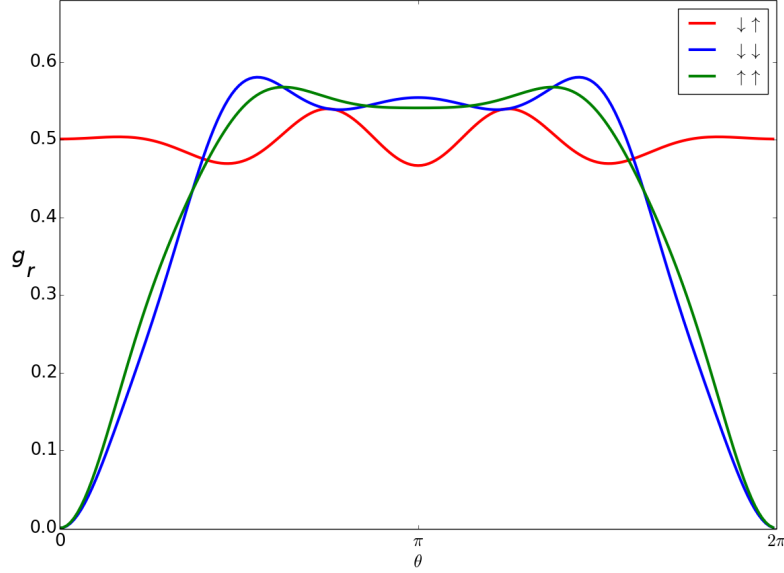


**Fig. 6.13** Intra- and interflavor pair correlation functions of the 311-state for a system of six  $\uparrow$ -spin and six  $\downarrow$ -spin particles living on a sphere.

$$\bar{C}^{\uparrow\downarrow} = \frac{N_{\uparrow}N_{\downarrow}}{(s+s'+1)^2}, \quad \bar{C}^{\uparrow\uparrow} = \frac{N_{\uparrow}^2}{(2s+1)^2}, \quad \bar{C}^{\downarrow\downarrow} = \frac{N_{\downarrow}^2}{(2s'+1)^2}. \quad (6.4.20)$$

These expressions can be derived as follows: With the steps yielding (6.3.11), we have constructed our pseudopotentials such that by setting all pseudopotentials to 1, we have

$$\sum_{l=0}^{2s} \sum_{m_l=-l}^l H^{(l)} = \sum_{l=0}^{2s} (2l+1)H^{(l)} \stackrel{!}{=} N_{\uparrow}^2 \quad (6.4.21)$$

for particles on the  $\uparrow$ -sphere and

$$\sum_{l=0}^{2s'} \sum_{m_l=-l}^l H^{(l)} = \sum_{l=0}^{2s'} (2l+1)H^{(l)} \stackrel{!}{=} N_{\downarrow}^2 \quad (6.4.22)$$

for particles on the  $\downarrow$ -sphere as well as

$$\sum_{l=0}^{s+s'} \sum_{m_l=-l}^l H^{(l)} = \sum_{l=0}^{s+s'} (2l+1)H^{(l)} \stackrel{!}{=} N_{\uparrow}N_{\downarrow}, \quad (6.4.23)$$

where we sum over all possible relative angular momenta  $l$  and their  $z$ -components  $m_l$ . With the definition (6.3.63) of the correlators, we can rewrite (6.4.21)-(6.4.23) into

$$\sum_{l=0}^{s_{\alpha}+s_{\beta}} (2l+1)C_l^{\alpha\beta} = \langle \Psi | N_{\alpha}N_{\beta} | \Psi \rangle = N_{\alpha}N_{\beta}, \quad (6.4.24)$$

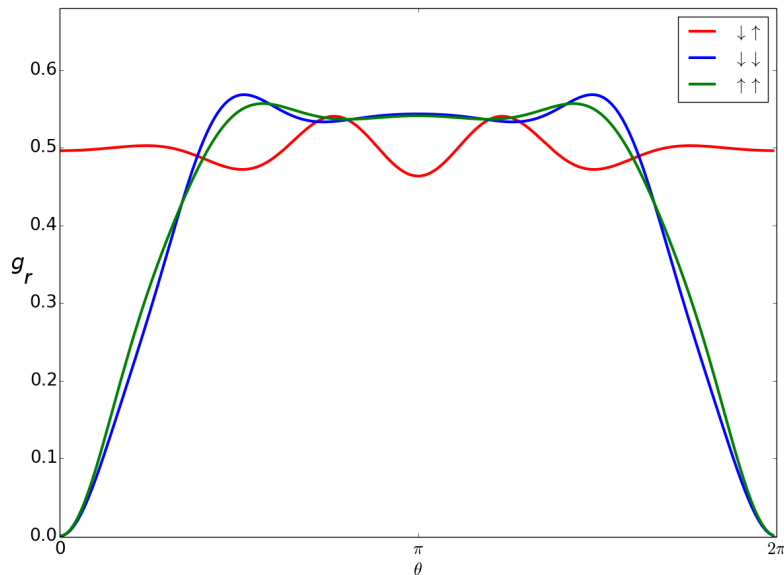


**Fig. 6.14** Intra- and interflavor pair correlation functions of the 311-state for a system of seven  $\uparrow$ -spin and seven  $\downarrow$ -spin particles living on a sphere.

with  $\alpha, \beta \in \{\uparrow, \downarrow\}$  and  $s_\uparrow := s$ ,  $s_\downarrow := s'$ . In a non-interacting system, all correlators are constant,  $C_l^{\alpha\beta} = \bar{C}^{\alpha\beta} \forall l$ . Then, (6.4.24) simplifies to

$$(s_\alpha + s_\beta + 1)^2 \bar{C}^{\alpha\beta} = N_\alpha N_\beta, \quad (6.4.25)$$

yielding the result (6.4.20).

For the 311-state, (6.4.20) can be further simplified by expressing the flux numbers in terms of particle numbers with (6.2.3) and setting  $N_\uparrow = N_\downarrow$ , so that

$$\bar{C}^{\uparrow\downarrow} = \frac{N^2}{4(N - \frac{1}{2})^2}, \quad \bar{C}^{\uparrow\uparrow} = \frac{N^2}{4(N - 1)^2}, \quad \bar{C}^{\downarrow\downarrow} = \frac{1}{4}. \quad (6.4.26)$$

The relative angular momentum density in the  $\downarrow$ -layer is independent of the system size, and all densities are equal in the thermodynamic limit.

For large relative angular momentum  $l$ , the intralayer correlators converge to  $\bar{C}^{\alpha\alpha}$ . Large values of  $l$  loosely translate into a large distance between the two particles of the same flavor. In contrast, for the interlayer interaction, the maximal distance of the two particles is reached at  $l = 0$ . For decreasing  $l$ , the interlayer correlators converge to  $\bar{C}^{\uparrow\downarrow}$ . Thus, for large distances, the 311-state resembles an uncorrelated system. For small distances, however, the 311-state shows high correlation of the particles.

To further analyze the correlations in the 311-state, we compare it to the correlators of the Laughlin product state, Figure 6.18. The Laughlin product state in spherical geometry is constructed by taking the direct product of two Laughlin states (2.5.1) with filling fraction  $\nu = 1/3$  and  $N = 5$  particles each, experiencing an opposite magnetic field. This yields a two layer system, and we label the particles of the first (second) Laughlin state in the product as  $\uparrow$ -spin ( $\downarrow$ -spin) particles. The flux through each sphere for this state is  $2s_\alpha = 3(N_\alpha - 1) = 12$ ,  $\alpha = \uparrow, \downarrow$ . The interlayer correlators for the Laughlin product state have a constant value independent of the relative angular momentum. Thus, the  $\uparrow$ - and  $\downarrow$ -layer are completely uncorrelated. In contrast, our 311-state shows a high deviation from the average angular momentum density, especially for high values of  $l$ . The intralayer correlators for all three states have a qualitatively similar shape.

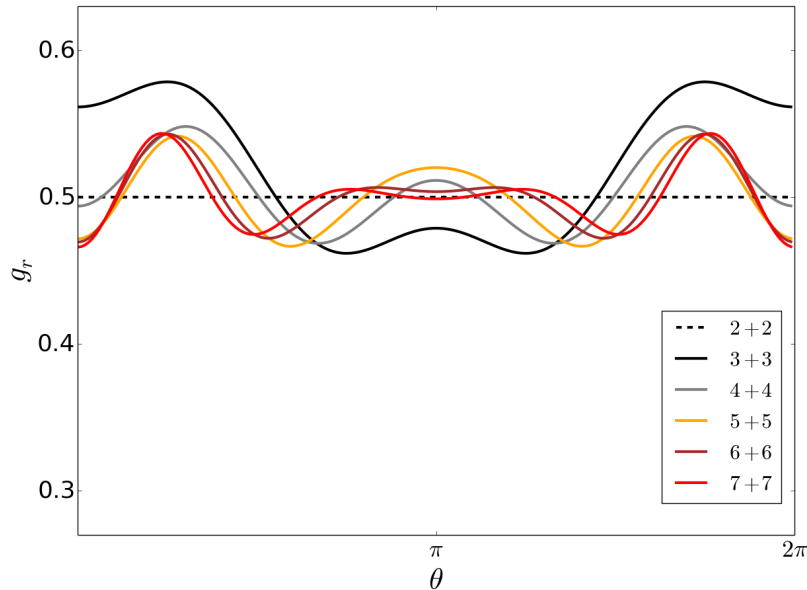


**Fig. 6.15** Finite size analysis of the interlayer pair correlation function for the 311-state for different system sizes. As compared to Figures 6.11-6.14, we have taken  $\theta \rightarrow \pi - \theta$ .

Since we can only treat finite systems, it is important to determine how the finite size of the system influences the computational results. For this purpose, we compare the correlators of the 311-state for 5+5, 6+6 and 7+7 particles. Figure 6.19 compares the intralayer correlators  $\bar{C}^{\uparrow\uparrow}$ , Figure 6.20 compares the intralayer correlators  $\bar{C}^{\downarrow\downarrow}$ , and Figure 6.21 compares the interlayer correlators  $\bar{C}^{\uparrow\downarrow}$ . One consequence of the finite system is that there is only a finite number of pseudopotential coefficients, since  $0 \leq l \leq 2s$  for  $\bar{C}^{\uparrow\uparrow}$  and  $\bar{C}^{\uparrow\downarrow}$ , and  $0 \leq l \leq 2s'$  for  $\bar{C}^{\downarrow\downarrow}$ . Only the absolute values slightly change. While the local extrema of the intralayer correlators remain at the same angular momentum for varying system size, they shift to higher momenta for the interlayer correlators. However, for all three correlator types, we see that the overall shape of the scatter plot does not alter with system size. It is therefore safe to assume that the 311-state shows a strong correlation not only between particles of the same flavor, but also between the  $\uparrow$ - and  $\downarrow$ -particles.

What about time-reversal (T) symmetry in a system described by the 311-state? For a finite system, T symmetry is broken. This can be seen analytically by observing that either the number of  $\uparrow$ -spin and  $\downarrow$ -spin particles differs ( $N_{\uparrow} \neq N_{\downarrow}$ ) or the number of flux quanta through the two spheres ( $2s \neq 2s'$ ) is unequal or both. Thus, the 311-state changes under a time-reversal operation,  $\Psi_{311} \neq T\Psi_{311}T^{-1}$ . Now, if we compare the intraspin correlators  $C_l^{\uparrow\uparrow}$  and  $C_l^{\downarrow\downarrow}$  numerically, their difference decreases with increasing system size.

#### 6.4.4 Construction and analysis of a parent Hamiltonian

The calculation of an approximate parent Hamiltonian has the highest computational cost as compared to the other numerical tasks performed in this chapter. The largest system we are able to treat, is a two-layer 311-state with six particles per layer. Our Hamiltonian Finder method is explained in detail in Section 6.3.3.

We first analyze a system of five  $\uparrow$ -spin and five  $\downarrow$ -spin particles, each living on a sphere with respectively  $2s = 9$  and  $2s' = 7$  Dirac flux quanta running through it. The Hilbert space is of the order  $\mathcal{O}(10^3)$ . With the choice of pseudopotential coefficients given in Table 6.3 and plotted in Figure 6.22, obtained by our Hamiltonian Finder method and further manual fine tuning, we obtain an overlap  $\langle \Psi_{311} | GS \rangle = 98.2\%$  of

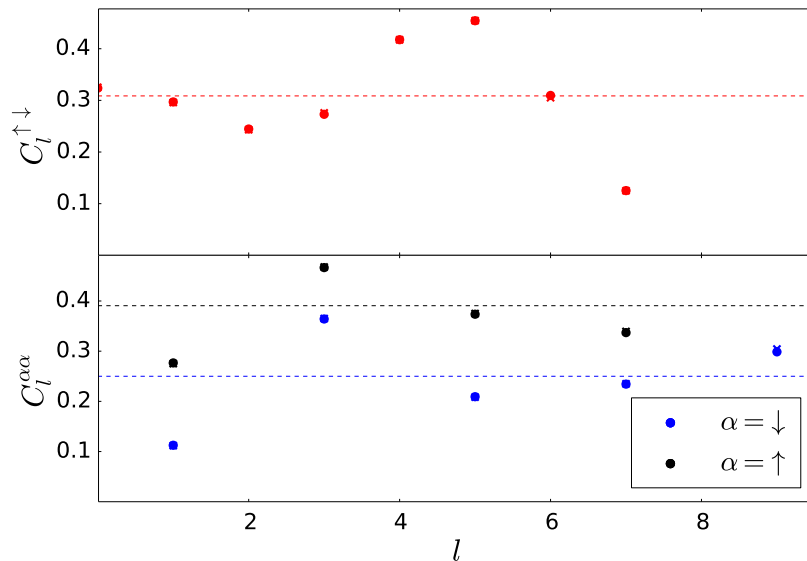


**Fig. 6.16** The relative angular momentum resolved correlators  $C_l^{\alpha\alpha'}$  of the 311-state (crosses) and the actual ground state (dots) of the parent Hamiltonian for the interlayer (red) and intralayer (black and blue) case. The system consists of five  $\uparrow$ -spin particles living on an  $\uparrow$ -sphere pierced by  $2s = 7$  flux quanta, and five  $\downarrow$ -spin particles living on a  $\downarrow$ -sphere pierced by  $2s' = 9$  flux quanta. The dashed lines show the value of the correlators for an uncorrelated system.

the 311-state with the actual ground state of the resulting Hamiltonian. The relative angular momentum of the intralayer pseudopotentials cannot exceed the number of Dirac flux quanta through the respective sphere: For the  $\uparrow$ -sphere ( $\downarrow$ -sphere), it is  $0 \leq l \leq 2s$  ( $0 \leq l \leq 2s'$ ). Since the particles inside one layer are indistinguishable and fermionic,  $l$  has to be odd. For the interlayer pseudopotentials, it is  $0 \leq l \leq 2s$  for  $s \leq s'$ . The corresponding relative angular momentum resolved correlators for both states are plotted in Figure 6.16. We see that both for interlayer and intralayer interactions, the correlators are almost identical. The pseudopotential coefficients  $V_l^{\alpha\beta}$  drop monotonously for increasing  $l$ . Only the interlayer pseudopotential coefficient  $V_7^{\uparrow\downarrow}$  is larger than the previous value. Since this anomaly does not reproduce in larger systems, we expect this to be a finite size effect.

$l$	$V_l^{\uparrow\downarrow}$	$V_l^{\uparrow\uparrow}$	$V_l^{\downarrow\downarrow}$
0	16.950		
1	8.453	10.16	18.50
2	0.868		
3	-5.50	-1.16	3.14
4	-10.74		
5	-15.07	-8.25	-7.97
6	-18.16		
7	-7.25	-11.28	-15.02
8			
9			-18.02

**Table 6.3** The interlayer and intralayer pseudopotential coefficients of our approximate parent Hamiltonian for the 311-state with five  $\uparrow$ -spin and five  $\downarrow$ -spin particles.

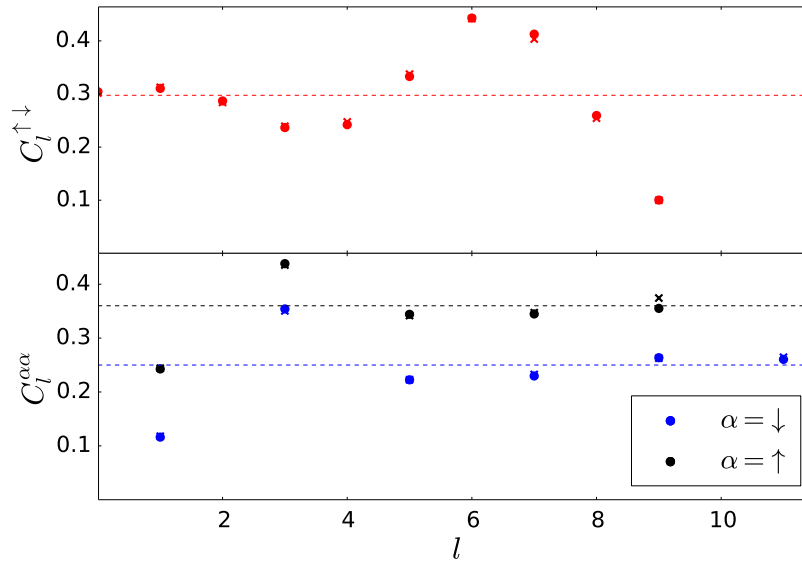


**Fig. 6.17** The relative angular momentum resolved correlators  $C_l^{\alpha\alpha'}$  of the 311-state (crosses) and the actual ground state (dots) of the parent Hamiltonian for the interlayer (red) and intralayer (black and blue) case. The system consists of six  $\uparrow$ -spin particles living on an  $\uparrow$ -sphere pierced by  $2s = 9$  flux quanta, and six  $\downarrow$ -spin particles living on a  $\downarrow$ -sphere pierced by  $2s' = 11$  flux quanta. The dashed lines show the value of the correlators for an uncorrelated system.

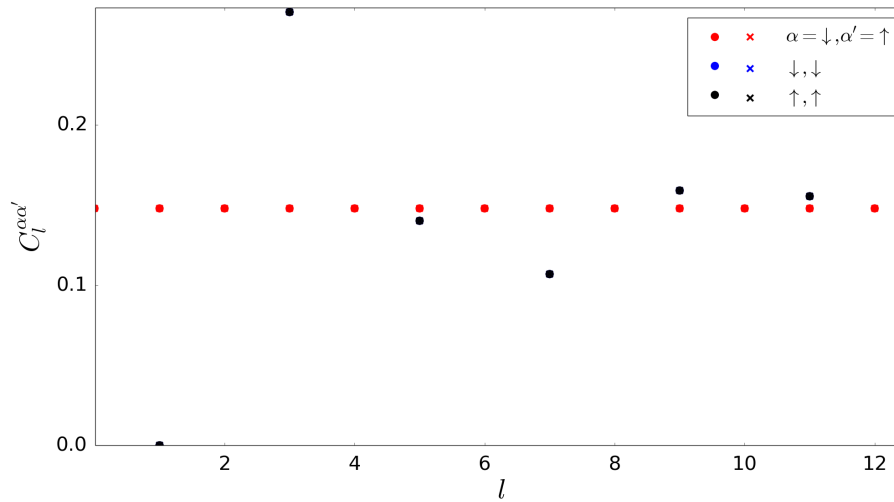


**Fig. 6.18** Relative angular momentum resolved correlators of the product Laughlin state with filling fraction  $\nu = 1/3$  of a system with five  $\uparrow$ -spin and five  $\downarrow$ -spin particles.

Increasing the system size, we investigate a state with six  $\uparrow$ -spin and six  $\downarrow$ -spin particles living on spheres with  $2s = 11$  and  $2s' = 9$  Dirac flux quanta respectively. The corresponding Hilbert space is of the order  $\mathcal{O}(10^4)$ . Assuming the pseudopotential coefficients listed in Table 6.4 and displayed in Figure 6.23, the overlap of our 311-state and the actual ground state of the Hamiltonian  $\langle \Psi_{311} | GS \rangle$  is 82.1%. The intralayer pseudopotentials are monotonously decreasing with increasing relative angular momentum  $l$ , meaning that the interaction is strongest for the particles being close to each other, which is physically realistic. The

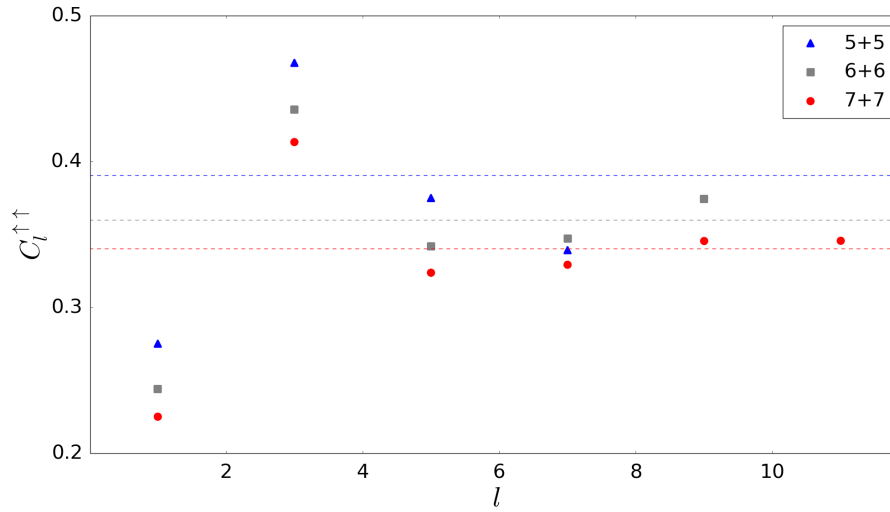


**Fig. 6.19** Finite size analysis of the intralayer correlators  $C_l^{\uparrow\uparrow}$  of the 311-state with 5+5 (blue triangles), 6+6 (gray squares) and 7+7 (red circles) particles. The dashed lines show the value of the correlators for an uncorrelated system.

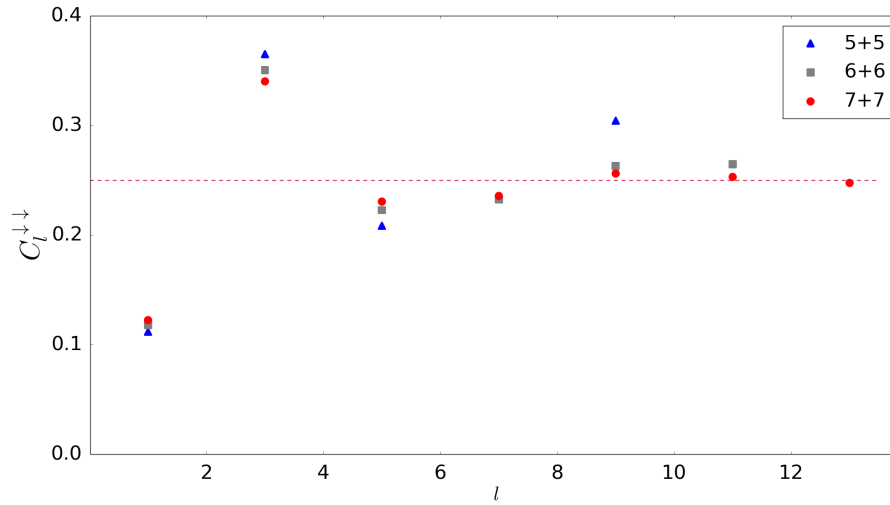


**Fig. 6.20** Finite size analysis of the intralayer correlators  $C_l^{\downarrow\downarrow}$  of the 311-state with 5+5 (blue triangles), 6+6 (gray squares) and 7+7 (red circles) particles. The dashed lines show the value of the correlators for an uncorrelated system.

two intralayer pseudopotentials are similar in shape, the difference arises only due to the different flux number. Thus, in the thermodynamic limit, we most likely have  $V_l^{\uparrow\uparrow} \approx V_l^{\downarrow\downarrow} \forall l$ . Figure 6.17 shows that the correlators of the 311-state and the ground state have qualitatively the same shape, the differences being marginal. Comparing to the smaller system with five  $\uparrow$ -spin and five  $\downarrow$ -spin particles, pseudopotential coefficients are of equivalent shape and magnitude, if we take into account that the range of permitted non-zero pseudopotentials is restricted by the system size.

In our Hamiltonian Finder method, we have only considered two-body interactions. To construct an exact parent Hamiltonian, it would be necessary to include many-body terms with three or more particles. This increases the numerical effort decisively. Since our two-body parent Hamiltonian turns out to be an

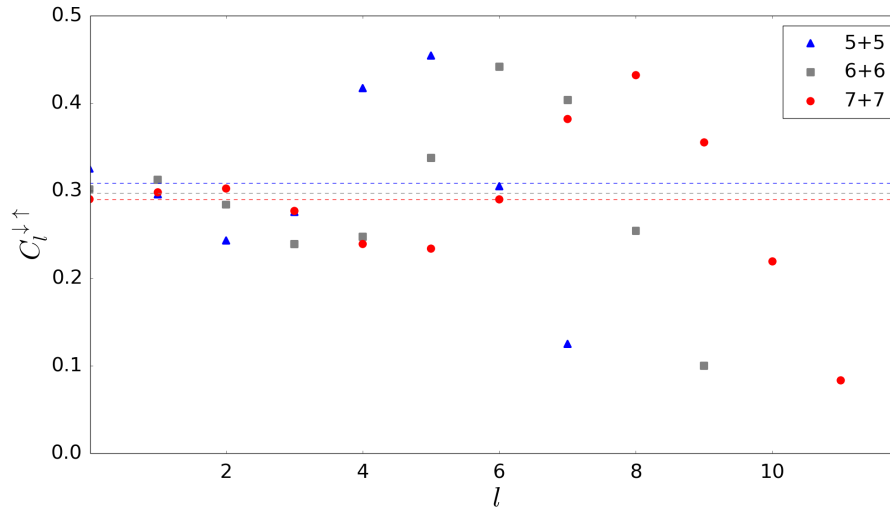


**Fig. 6.21** Finite size analysis of the interlayer correlators  $C_l^{\uparrow\downarrow}$  of the 311-state with 5+5 (blue triangles), 6+6 (gray squares) and 7+7 (red circles) particles. The dashed lines show the value of the correlators for an uncorrelated system.

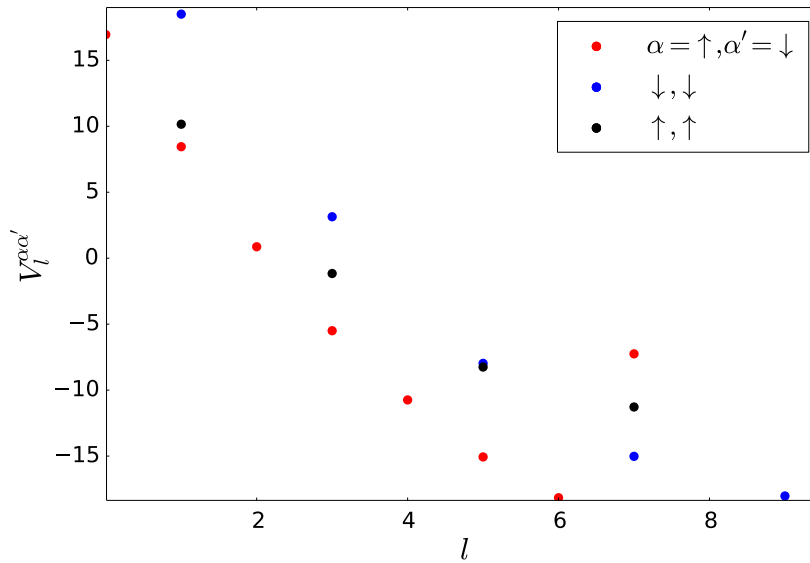


**Fig. 6.22** For a system of five  $\uparrow$ -spin and five  $\downarrow$ -spin particles, the best approximation of a parent Hamiltonian for our 311-state is specified by this choice of intralayer (black and blue dots) and interlayer (red dots) pseudopotential coefficients  $V_l^{\alpha\alpha'}$ .

accurate approximation, we leave the search for an exact parent Hamiltonian as well as the detailed analysis of the eigenspectrum of our approximate parent Hamiltonian for future research.

$l$	$V_l^{\uparrow\downarrow}$	$V_l^{\uparrow\uparrow}$	$V_l^{\downarrow\downarrow}$
0	3.24		
1	1.72	6.00	7.93
2	0.34		
3	-0.87	3.72	5.04
4	-1.93		
5	-2.84	2.05	2.76
6	-3.60		
7	-4.21	0.99	1.09
8	-4.67		
9	-4.97	0.53	0.03
10			
11			-0.43

**Table 6.4** The interlayer and intralayer pseudopotential coefficients of our approximate parent Hamiltonian for the 311-state with six  $\uparrow$ -spin and six  $\downarrow$ -spin particles.

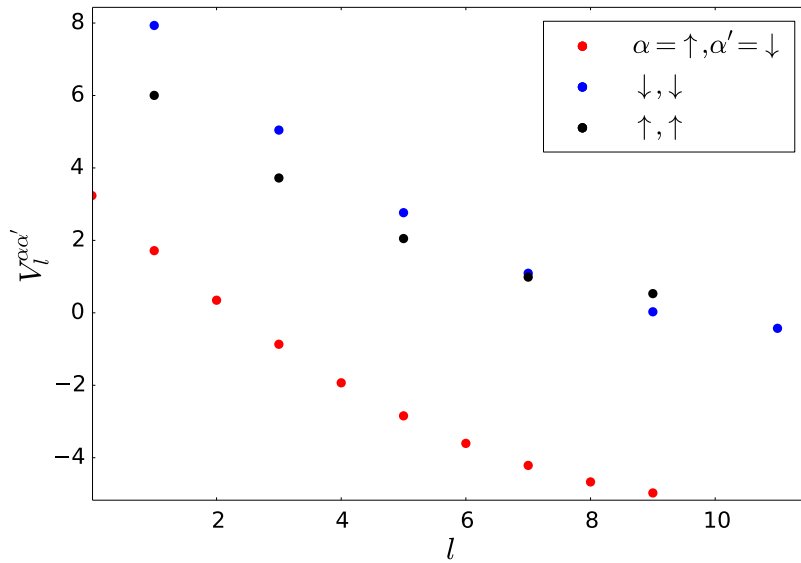


**Fig. 6.23** For a system of six  $\uparrow$ -spin and six  $\downarrow$ -spin particles, the best approximation of a parent Hamiltonian for our 311-state is specified by this choice of intralayer (black and blue dots) and interlayer (red dots) pseudopotential coefficients  $V_l^{\alpha\alpha'}$ .

#### 6.4.5 Real space potentials for the 311-state

For the 311-state with six  $\uparrow$ -spin particles and six  $\downarrow$ -spin particles, given the choice of pseudopotential coefficients  $\{\tilde{V}_l\}_l$  in Figure 6.23, the corresponding real space potentials  $V_{311}^{\alpha\beta}(\theta)$  for the intralayer ( $\alpha = \beta = \uparrow$  or  $\alpha = \beta = \downarrow$ ) and interlayer ( $\alpha = \uparrow$  and  $\beta = \downarrow$ ) interactions are derived by solving the system of linear equations (6.3.67). Details of this method are described in Section 6.3.6. The three real space potentials then are



$$\begin{aligned}
V_{311}^{\uparrow\uparrow}(\theta) &= \sum_{n=0}^{2s} (a_n^{\uparrow\uparrow} + \gamma^{\uparrow\uparrow} b_n + \mu c_n^{\uparrow\uparrow}) V_n(\theta), \\
V_{311}^{\downarrow\downarrow}(\theta) &= \sum_{n=0}^{2s'} (a_n^{\downarrow\downarrow} + \gamma^{\downarrow\downarrow} b_n + \mu c_n^{\downarrow\downarrow}) V_n(\theta), \\
V_{311}^{\uparrow\downarrow}(\theta) &= \sum_{n=0}^{2s} (a_n^{\uparrow\downarrow} + \gamma^{\uparrow\downarrow} b_n + \mu c_n^{\uparrow\downarrow}) V_n(\theta).
\end{aligned} \tag{6.4.27}$$

By manually fine-tuning the coefficients  $\gamma^{\alpha\beta}$  and  $\mu$ , we attempt to create the most realistic real space potentials possible. With “realistic”, we mean that the interaction drops to zero for large distances and is monotonous. The choice  $\gamma^{\uparrow\uparrow} = 3.54$ ,  $\gamma^{\downarrow\downarrow} = 3.92$  and  $\gamma^{\uparrow\downarrow} = -5.26$ ,  $\mu = 7.60$  gives the real space potentials shown in Figures 6.24 and 6.25. As expected, the intralayer potential is repulsive, differing slightly for the  $\uparrow$ - and  $\downarrow$ -sphere since they experience a different magnetic field. The interlayer interaction is attractive. This behavior is plausible since, as explained in 6.2.1, the  $\uparrow$ -spin particles see quasielectrons at the positions of the  $\downarrow$ -spin particles. The real space potentials presented here show, that the 311-state can be stabilized for a reasonable, local interaction profile among the electrons.

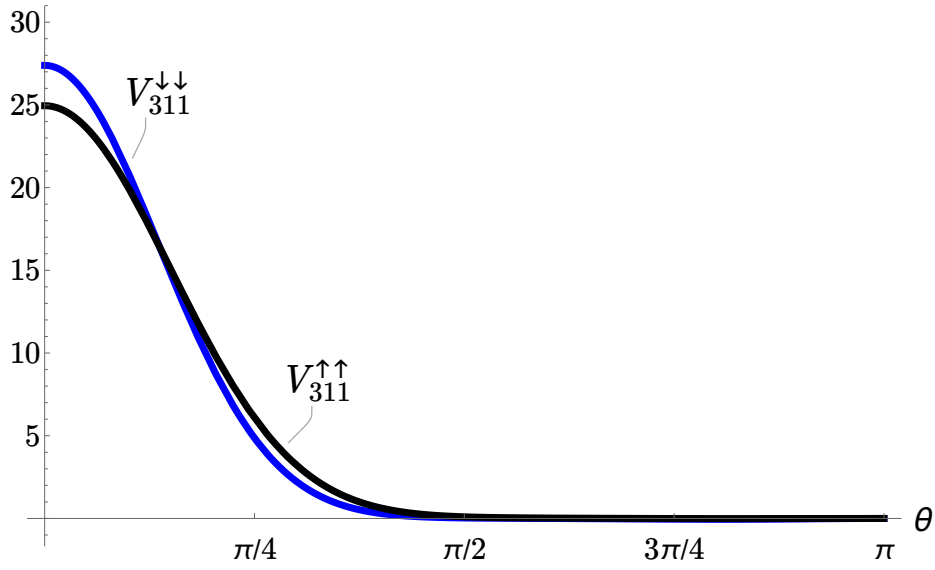


**Fig. 6.24** Repulsive real space potential for the intralayer interaction of the parent Hamiltonian of the 311-state for a two-layer system with six  $\uparrow$ -spin and six  $\downarrow$ -spin particles. One particle is pinned at the north pole ( $\theta = 0$ ). The orange (blue) curve shows the potential in the  $\uparrow$ -sphere ( $\downarrow$ -sphere).

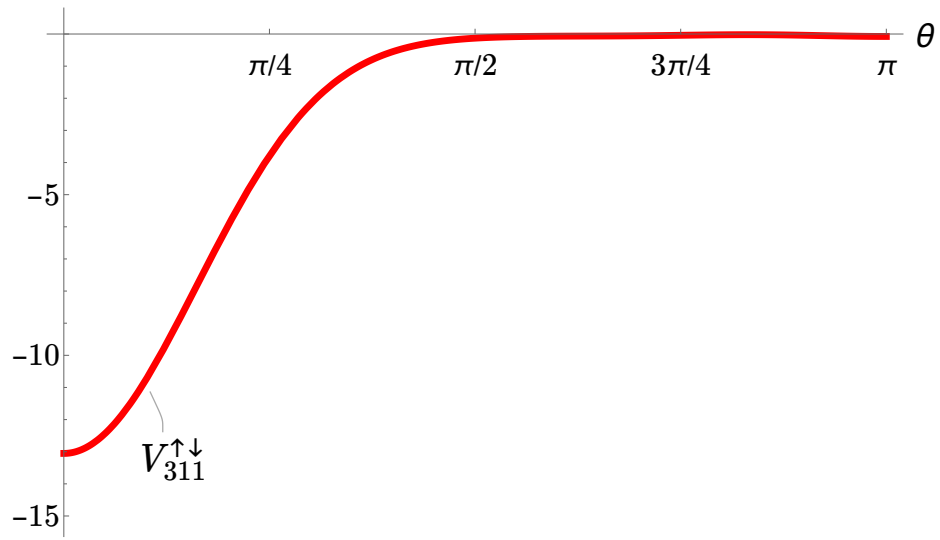


**Fig. 6.25** Attractive real space potential for the interlayer interaction of the parent Hamiltonian of the 311-state for a two-layer system with six  $\uparrow$ -spin and six  $\downarrow$ -spin particles. One particle is pinned at the north pole ( $\theta = 0$ ).

## Chapter 7

# Conclusion

In this thesis, we investigate known and new fractional quantum Hall states in two-dimensional spin systems. Our research pursues two different projects:

In the first project, we develop a method to construct parent Hamiltonians for the CSL, and present the first local spin Hamiltonians for which the Abelian or the non-Abelian CSLs are the exact and, modulo a topological degeneracy, unique ground states. These microscopic models are promising candidates for the study of elementary excitations and fractional statistics in the CSLs, since all parent Hamiltonians proposed so far have only non-local interactions. Our method relies on the singlet property of the CSLs, allowing for a spherical tensor decomposition of the introduced annihilation operator. We confirm numerically that the CSLs are the unique ground states of our Hamiltonians for the square lattice and the triangular lattice. Moreover, our numerical method to write out arbitrary tensor products provides a user-friendly and efficient framework to implement the parent Hamiltonian of a CSL for further numerical studies.

In the second project, we propose “fractional insulators” as a new universality class of fractionally quantized, topologically ordered insulators. We construct a wave function, which we label the “311-state”, and which exhibits topological order, but violates time reversal symmetry. Even though time reversal symmetry is broken, the state is designed in such a way, that all locally observable quantities remain time reversal invariant - a condition we label “topological time reversal symmetry breaking”. For the 311-state, this condition is achieved by coupling two Laughlin states for the  $\uparrow$ -spin and  $\downarrow$ -spin electrons through an interflavor term, which creates entanglement between the two spin species. Thereby we go beyond well-studied time reversal symmetric fractionalized phases, where the state is constructed as a direct product of a fractional quantum Hall state and its time reversal conjugate without any entanglement between the spin species.

In this context, we introduce a numerical technique to identify the exact or approximate parent Hamiltonian of a spin system. For the 311-state with up to six  $\uparrow$ -spin and six  $\downarrow$ -spin electrons, we manage to construct an approximate parent Hamiltonian with a physically realistic, local interaction. It might therefore be possible to find an experimental realization of such a state. Still, there are many tasks open for future research. A detailed analysis of the new class of insulators may reveal interesting physics. A concrete next step is to calculate and understand their excitation spectra and fractional statistics. By including many-body interactions of three- or more particles, it might also be possible to obtain an exact parent Hamiltonian for the 311-state.

In view of the rapid developments both theoretically and experimentally in the field of fractional quantization in recent years, its importance will even increase in the near future. We hope to contribute with the research presented here to a deeper understanding of fractionalization in two dimensional quantum systems.



## Appendix A

### Angular momentum algebra and spin operators

The group  $SU(2)$  corresponds to special unitary transformations on complex 2D vectors. Its natural representation is that of  $2 \times 2$ -matrices acting on 2D vectors. However, there are other representations, especially in higher dimension vector spaces, which will be detailed below. There are  $2^2 - 1$  parameters, thus 3 generators, which have to be traceless and Hermitian. They are given by the angular momentum components  $\{J^x, J^y, J^z\}$ . In the matrix representation, the generators have the form

$$\begin{pmatrix} a & b^* \\ b & -a \end{pmatrix}, \quad (\text{A.1})$$

with  $a \in \mathbb{R}$ . A suitable, but not unique, representation are the Pauli matrices with  $J^i = \sigma^i/2$  and

$$\sigma^x = \begin{pmatrix} 0 & 1 \\ 1 & 0 \end{pmatrix}, \quad \sigma^y = \begin{pmatrix} 0 & -i \\ i & 0 \end{pmatrix}, \quad \sigma^z = \begin{pmatrix} 1 & 0 \\ 0 & -1 \end{pmatrix}. \quad (\text{A.2})$$

It is  $\sigma^i \sigma^j = \delta^{ij} \mathbf{1} + i\epsilon^{ijk} \sigma^k$ , using Einstein's sum convention.

In the following, a few basic relations of the angular momentum algebra are reviewed [7; 32]. The components of the angular momentum operator  $\mathbf{J}$  obey the Lie algebra

$$[J^a, J^b] = i\epsilon^{abc} J^c \quad \text{for } a, b, c = x, y, z. \quad (\text{A.3})$$

A Casimir operator is one which commutes with all generators. In  $SU(2)$ , there is one Casimir, the square of the total angular momentum  $\mathbf{J}^2$ . The operators  $\mathbf{J}^2$  and  $J^z$  have a set of simultaneous eigenstates, since  $[\mathbf{J}^2, J^z] = 0$ . Their eigenvalues are

$$\begin{aligned} \mathbf{J}^2 |j, m\rangle &= j(j+1) |j, m\rangle, \\ J^z |j, m\rangle &= m |j, m\rangle, \end{aligned} \quad (\text{A.4})$$

where  $m = -j, \dots, j$ .

Defining the ladder operators with  $J^\pm \equiv J^x \pm iJ^y$ , we have

$$[J^z, J^\pm] = \pm J^\pm. \quad (\text{A.5})$$

Their matrix representation is

$$J^+ = \begin{pmatrix} 0 & 1 \\ 0 & 0 \end{pmatrix}, \quad J^- = \begin{pmatrix} 0 & 0 \\ 1 & 0 \end{pmatrix}. \quad (\text{A.6})$$

Further, we have

$$\begin{aligned}
J^+ J^- &= (J^x)^2 + (J^y)^2 - i[J^x, J^y] = \mathbf{J}^2 - (J^z)^2 + J^z, \\
J^- J^+ &= \mathbf{J}^2 - (J^z)^2 - J^z.
\end{aligned}
\tag{A.7}$$

These equations imply

$$[J^+, J^-] = 2J^z. \tag{A.8}$$

and

$$J^\pm |j, m\rangle = \sqrt{j(j+1) - m(m \pm 1)} |j, m \pm 1\rangle, \tag{A.9}$$

Here, we have chosen the phases between  $J^- |j, m\rangle$  and  $|j, m \pm 1\rangle$  real.

The spin  $\mathbf{S}$  is one type of angular momentum and thus obeys the  $SU(2)$  Lie algebra. A spin 1/2-systems can be represented by a two-dimensional matrix representation of  $SU(2)$ . The Pauli matrices can be generalized to represent higher spin systems in three spatial dimensions. A three-dimensional representation is needed for spin 1. In this case, the Pauli matrices are

$$S^x = \frac{1}{\sqrt{2}} \begin{pmatrix} 0 & 1 & 0 \\ 1 & 0 & 1 \\ 0 & 1 & 0 \end{pmatrix}, \quad S^y = \frac{1}{\sqrt{2}} \begin{pmatrix} 0 & -i & 0 \\ i & 0 & -i \\ 0 & i & 0 \end{pmatrix}, \quad S^z = \begin{pmatrix} 1 & 0 & 0 \\ 1 & 0 & 0 \\ 0 & 0 & -1 \end{pmatrix}. \tag{A.10}$$

As we also analyze spin systems with spin 3/2 in this thesis, the corresponding Pauli matrices are listed as well,

$$\begin{aligned}
S^x &= \frac{1}{2} \begin{pmatrix} 0 & \sqrt{3} & 0 & 0 \\ \sqrt{3} & 0 & 2 & 0 \\ 0 & 2 & 0 & \sqrt{3} \\ 0 & 0 & \sqrt{3} & 0 \end{pmatrix}, \quad S^y = \frac{1}{2} \begin{pmatrix} 0 & -\sqrt{3}i & 0 & 0 \\ \sqrt{3}i & 0 & -2i & 0 \\ 0 & 2i & 0 & -\sqrt{3}i \\ 0 & 0 & \sqrt{3}i & 0 \end{pmatrix}, \\
S^z &= \frac{1}{2} \begin{pmatrix} 3 & 0 & 0 & 0 \\ 0 & 1 & 0 & 0 \\ 0 & 0 & -1 & 0 \\ 0 & 0 & 0 & -3 \end{pmatrix}.
\end{aligned}
\tag{A.11}$$

## Appendix B

### Tensor decompositions of spin operators

In Chapter 4, the parent Hamiltonians of the chiral spin liquid consist of up to four neighboring interacting spins. In this appendix, we decompose the product of one, two and three spin operators into their irreducible components.

#### B.1 One spin operator

A single spin operator transforms as a vector under rotations. We choose the normalization such that the  $m = 0$ -component is equal to  $S^z$ . The three components are

$$\begin{aligned}
 V^1 &= -\frac{1}{\sqrt{2}}S^+, \\
 V^0 &= \frac{1}{\sqrt{2}}[S^-, V^1] = S^z, \\
 V^{-1} &= \frac{1}{\sqrt{2}}[S^-, V^0] = \frac{1}{\sqrt{2}}S^-.
 \end{aligned}
 \tag{B.1.1}$$

#### B.2 Two spin operators

The direct product of two vectors, representing two spin operators  $\mathbf{S}_1$  and  $\mathbf{S}_2$ , can be decomposed into the direct sum of a scalar, a vector and a second order tensor,

$$\mathbf{1} \otimes \mathbf{1} = \mathbf{0} \oplus \mathbf{1} \oplus \mathbf{2}.$$

The scalar component is the scalar product

$$U_{12} = \mathbf{S}_1 \cdot \mathbf{S}_2 = \frac{1}{2}(S_1^+ S_2^- + S_1^- S_2^+) + S_1^z S_2^z, \tag{B.2.1}$$

and the vector is  $-i(\mathbf{S}_1 \times \mathbf{S}_2)$ ,

$$\begin{aligned}
V_{12}^1 &= \frac{i}{\sqrt{2}}(\mathbf{S}_1 \times \mathbf{S}_2)^+ = \frac{1}{\sqrt{2}}(S_1^+ S_2^z - S_1^z S_2^+), \\
V_{12}^0 &= -i(\mathbf{S}_1 \times \mathbf{S}_2)^z = \frac{1}{2}(S_1^+ S_2^- - S_1^- S_2^+), \\
V_{12}^{-1} &= -\frac{i}{\sqrt{2}}(\mathbf{S}_1 \times \mathbf{S}_2)^- = \frac{1}{\sqrt{2}}(S_1^- S_2^z - S_1^z S_2^-).
\end{aligned} \tag{B.2.2}$$

For the second order tensor, we start with the term  $S_1^+ S_2^+$ , since it is the only operator of two spin operators which raises the  $S^z$ -quantum number by two. Therefore, it is proportional to the  $m = 2$ -component of the second order tensor. Since the normalization is free to choose, we set

$$T_{12}^2 = S_1^+ S_2^+. \tag{B.2.3}$$

The remaining tensor components are derived using the angular momentum ladder operators of (4.3.14), reducing the  $m$ -component consecutively by 1. We obtain

$$\begin{aligned}
T_{12}^1 &= \frac{1}{2}[S_1^- + S_2^-, T_{12}^2] = -S_1^z S_2^+ - S_1^+ S_2^z, \\
T_{12}^0 &= \frac{1}{\sqrt{6}}[S_1^- + S_2^-, T_{12}^1] = \frac{1}{\sqrt{6}}(4S_1^z S_2^z - S_1^+ S_2^- - S_1^- S_2^+), \\
T_{12}^{-1} &= \frac{1}{\sqrt{6}}[S_1^- + S_2^-, T_{12}^0] = S_1^z S_2^- + S_1^- S_2^z, \\
T_{12}^{-2} &= \frac{1}{2}[S_1^- + S_2^-, T_{12}^{-1}] = S_1^- S_2^-.
\end{aligned} \tag{B.2.4}$$

These expressions allow us to reformulate the scalar product  $\mathbf{S}_1 \cdot \mathbf{S}_2$  in terms of its irreducible representations. In particular, Equations (B.2.1), (B.2.3) and (B.2.4) imply

$$\frac{1}{2}(S_1^+ S_2^- + S_1^- S_2^+) = \frac{2}{3}\mathbf{S}_1 \cdot \mathbf{S}_2 - \frac{1}{\sqrt{6}}T_{12}^0, \tag{B.2.5}$$

$$S_1^z S_2^z = \frac{1}{3}\mathbf{S}_1 \cdot \mathbf{S}_2 + \frac{1}{\sqrt{6}}T_{12}^0. \tag{B.2.6}$$

The combination of (B.2.5) and (B.2.2) yields

$$\begin{aligned}
S_1^+ S_2^- &= \frac{2}{3}\mathbf{S}_1 \cdot \mathbf{S}_2 - i(\mathbf{S}_1 \times \mathbf{S}_2)^z - \frac{1}{\sqrt{6}}T_{12}^0, \\
S_1^- S_2^+ &= \frac{2}{3}\mathbf{S}_1 \cdot \mathbf{S}_2 + i(\mathbf{S}_1 \times \mathbf{S}_2)^z - \frac{1}{\sqrt{6}}T_{12}^0.
\end{aligned} \tag{B.2.7}$$

### B.3 Three spin operators

The direct product of three vector operators, for instance three spin operators  $\mathbf{S}_1$ ,  $\mathbf{S}_2$ , and  $\mathbf{S}_3$ , can be decomposed into a scalar, three vectors, two second order tensors and one third-order tensor,

$$\mathbf{1} \otimes \mathbf{1} \otimes \mathbf{1} = \mathbf{0} \oplus \mathbf{3} \cdot \mathbf{1} \oplus \mathbf{2} \cdot \mathbf{2} \oplus \mathbf{3}.$$

The scalar is constructed out of the triple product,



$$\begin{aligned}
U_{123} &= -i\mathbf{S}_1 \cdot (\mathbf{S}_2 \times \mathbf{S}_3) \\
&= \frac{1}{2}S_1^z (S_2^+ S_3^- - S_2^- S_3^+) + 2 \text{ cyclic permutations} \\
&= \frac{1}{2}(S_1^z S_2^+ S_3^- + S_1^+ S_2^- S_3^z + S_1^- S_2^z S_3^+ \\
&\quad - S_1^z S_2^- S_3^+ - S_1^- S_2^+ S_3^z - S_1^+ S_2^z S_3^-).
\end{aligned} \tag{B.3.1}$$

Note that, for  $\mathbf{S}_2 \neq \mathbf{S}_3$ , this operator can be rewritten as the sum of scalar products,

$$-i\mathbf{S}_1 \cdot (\mathbf{S}_2 \times \mathbf{S}_3) = -(\mathbf{S}_1 \cdot \mathbf{S}_2)(\mathbf{S}_1 \cdot \mathbf{S}_3) + (\mathbf{S}_1 \cdot \mathbf{S}_3)(\mathbf{S}_1 \cdot \mathbf{S}_2). \tag{B.3.2}$$

In the case of  $\mathbf{S}_2 = \mathbf{S}_3$ , since  $\mathbf{S}_j \times \mathbf{S}_j = i\mathbf{S}_j$ , the triple product reduces to

$$-i\mathbf{S}_1 \cdot (\mathbf{S}_2 \times \mathbf{S}_2) = \mathbf{S}_1 \cdot \mathbf{S}_2. \tag{B.3.3}$$

The three vectors are

$$\mathbf{S}_1(\mathbf{S}_2\mathbf{S}_3), \quad S_1^\alpha(\mathbf{S}_2)S_3^\alpha, \quad \text{and} \quad (\mathbf{S}_1\mathbf{S}_2)\mathbf{S}_3, \tag{B.3.4}$$

where Einstein's sum convention is used in the second expression,  $\alpha = x, y, z$ . For later purposes, the  $m = 0$ -component is explicitly written out,

$$\begin{aligned}
V_{a,123}^0 &= S_1^z(\mathbf{S}_2\mathbf{S}_3) = \frac{1}{2}(S_1^z S_2^+ S_3^- + S_1^z S_2^- S_3^+) + S_1^z S_2^z S_3^z, \\
V_{b,123}^0 &= \mathbf{S}_1(S_2^z)\mathbf{S}_3 = \frac{1}{2}(S_1^- S_2^z S_3^+ + S_1^+ S_2^z S_3^-) + S_1^z S_2^z S_3^z, \\
V_{c,123}^0 &= (\mathbf{S}_1\mathbf{S}_2)S_3^z = \frac{1}{2}(S_1^+ S_2^- S_3^z + S_1^- S_2^+ S_3^z) + S_1^z S_2^z S_3^z.
\end{aligned} \tag{B.3.5}$$

The  $m = 2$ -component of the tensor of second order is obtained by forming the product of two vector operators which are constructed out of the three spins. Two choices are possible

$$\begin{aligned}
T_{a,123}^2 &= -iS_1^+(\mathbf{S}_2 \times \mathbf{S}_3)^+, \\
T_{b,123}^2 &= -i(\mathbf{S}_1 \times \mathbf{S}_2)^+ S_3^+.
\end{aligned} \tag{B.3.6}$$

There is no third operator of this form, as the sum of the three operators obtained by cyclic permutation of the superscripts equals zero.

As in (B.2.4), the remaining components are derived by applying the ladder operator. As it is needed in the following, the  $m = 0$ -component is written out explicitly,

$$\begin{aligned}
T_{a,123}^0 &= -\frac{i}{\sqrt{6}}[4S_1^z(\mathbf{S}_2 \times \mathbf{S}_3)^z - S_1^+(\mathbf{S}_2 \times \mathbf{S}_3)^- - S_1^-(\mathbf{S}_2 \times \mathbf{S}_3)^+] \\
&= \frac{1}{\sqrt{6}}[2S_1^z (S_2^+ S_3^- - S_2^- S_3^+) - S_1^+ S_2^- S_3^z + S_1^+ S_2^z S_3^- \\
&\quad + S_1^- S_2^+ S_3^z - S_1^- S_2^z S_3^+].
\end{aligned} \tag{B.3.7}$$

The same holds for  $T_{b,123}^0$ , which is obtained from  $T_{a,123}^0$  by a cyclically permutating the superscripts  $z, +, -$ .

The tensor of third order is obtained with the same method as used for (B.2.3), this time for three spin operators,

$$W_{123}^3 = -S_1^+ S_2^+ S_3^+,$$

$$\begin{aligned}
W_{123}^2 &= \frac{1}{\sqrt{6}} [S_1^- + S_2^- + S_3^-, W_{123}^3] \\
&= -\frac{1}{\sqrt{6}} [S_1^-, S_1^+] S_2^+ S_3^+ + 2 \text{ cycl. permutations} \\
&= \sqrt{\frac{2}{3}} S_1^z S_2^+ S_3^+ + 2 \text{ cycl. permutations,} \\
W_{123}^1 &= \frac{1}{\sqrt{10}} [S_1^- + S_2^- + S_3^-, W_{123}^2] \\
&= \frac{1}{\sqrt{15}} ([S_1^-, S_1^+] S_2^+ S_3^+ + S_1^z [S_2^- + S_3^-, S_2^+ S_3^+]) + 2 \text{ cycl. perms.} \\
&= \frac{1}{\sqrt{15}} (S_1^- S_2^+ S_3^+ - 4S_1^z S_2^z S_3^z) + 2 \text{ cycl. permutations,} \\
W_{123}^0 &= \frac{1}{\sqrt{12}} [S_1^- + S_2^- + S_3^-, W_{123}^1] \\
&= \frac{1}{6\sqrt{5}} \left( S_1^- [S_2^- + S_3^-, S_2^+ S_3^+] - 4 [S_1^- + S_2^-, S_1^z S_2^z] S_3^+ \right. \\
&\quad \left. - 4S_1^z S_2^z [S_3^-, S_3^+] \right) + 2 \text{ cycl. permutations} \\
&= -\frac{1}{\sqrt{5}} (S_1^- S_2^+ S_3^z + 5 \text{ permutations}) + \frac{4}{\sqrt{5}} S_1^z S_2^z S_3^z, \tag{B.3.8} \\
W_{123}^{-1} &= \frac{1}{\sqrt{12}} [S_1^- + S_2^- + S_3^-, W_{123}^0] \\
&= -\frac{1}{\sqrt{15}} (S_1^- S_2^- S_3^+ - 4S_1^- S_2^z S_3^z) + 2 \text{ cycl. permutations,} \\
W_{123}^{-2} &= \frac{1}{\sqrt{10}} [S_1^- + S_2^- + S_3^-, W_{123}^{-1}] \\
&= \sqrt{\frac{2}{3}} S_1^- S_2^- S_3^z + 2 \text{ cycl. permutations,} \\
W_{123}^{-3} &= \frac{1}{\sqrt{6}} [S_1^- + S_2^- + S_3^-, W_{123}^{-2}] \\
&= S_1^- S_2^- S_3^-.
\end{aligned}$$

Here, the permutations always refer to the superscripts  $z, +, -$ , otherwise, we would have to assume that none of the spin operators are identical.

We can now express certain spin operator products in terms of their irreducible tensor components. For instance, by combining (B.3.5) and the expression for  $W_{123}^0$  from (B.3.8), we obtain

$$S_1^z S_2^z S_3^z = \frac{1}{5} (V_{a,123}^0 + V_{b,123}^0 + V_{c,123}^0) + \frac{1}{2\sqrt{5}} W_{123}^0. \tag{B.3.9}$$

This results into

$$\frac{1}{2} S_1^z (S_2^+ S_3^- + S_2^- S_3^+) = V_{a,123}^0 - S_1^z S_2^z S_3^z$$

$$= \frac{4}{5} V_{a,123}^0 - \frac{1}{5} V_{b,123}^0 - \frac{1}{5} V_{c,123}^0 - \frac{1}{2\sqrt{5}} W_{123}^0. \quad (\text{B.3.10})$$

Further, Eqs. (B.3.1) and (B.3.7) can be combined to

$$\frac{1}{2} S_1^z (S_2^+ S_3^- - S_2^- S_3^+) = \frac{1}{3} U_{123} + \frac{1}{\sqrt{6}} T_{a,123}^0. \quad (\text{B.3.11})$$

In total, this yields

$$\begin{aligned} S_1^z S_2^+ S_3^- &= +\frac{1}{3} U_{123} + \frac{1}{5} (4V_{a,123}^0 - V_{b,123}^0 - V_{c,123}^0) + \frac{1}{\sqrt{6}} T_{a,123}^0 - \frac{1}{2\sqrt{5}} W_{123}^0 \\ &= +\frac{1}{3} \mathbf{S}_1 (\mathbf{S}_2 \times \mathbf{S}_3) + \frac{1}{5} [4S_1^z (\mathbf{S}_2 \mathbf{S}_3) - \mathbf{S}_1 (S_2^z \mathbf{S}_3) - (\mathbf{S}_1 \mathbf{S}_2) S_3^z] \\ &\quad + \frac{1}{\sqrt{6}} T_{a,123}^0 - \frac{1}{2\sqrt{5}} W_{123}^0, \end{aligned} \quad (\text{B.3.12})$$

$$\begin{aligned} S_1^z S_2^- S_3^+ &= -\frac{1}{3} U_{123} + \frac{1}{5} (4V_{a,123}^0 - V_{b,123}^0 - V_{c,123}^0) - \frac{1}{\sqrt{6}} T_{a,123}^0 - \frac{1}{2\sqrt{5}} W_{123}^0 \\ &= -\frac{1}{3} \mathbf{S}_1 (\mathbf{S}_2 \times \mathbf{S}_3) + \frac{1}{5} [4S_1^z (\mathbf{S}_2 \mathbf{S}_3) - \mathbf{S}_1 (S_2^z \mathbf{S}_3) - (\mathbf{S}_1 \mathbf{S}_2) S_3^z] \\ &\quad - \frac{1}{\sqrt{6}} T_{a,123}^0 - \frac{1}{2\sqrt{5}} W_{123}^0. \end{aligned} \quad (\text{B.3.13})$$

## B.4 Four spin operators

In the case of a direct product of four spin operators  $\mathbf{S}_1$ ,  $\mathbf{S}_2$ ,  $\mathbf{S}_3$  and  $\mathbf{S}_4$ , the decomposition consists of tensors up to order four,

$$\mathbf{1} \otimes \mathbf{1} \otimes \mathbf{1} \otimes \mathbf{1} = 3 \cdot \mathbf{0} \oplus 6 \cdot \mathbf{1} \oplus 6 \cdot \mathbf{2} \oplus 3 \cdot \mathbf{3} \oplus \mathbf{4}.$$

The three scalars are

$$\begin{aligned} U_{a,1234} &= (\mathbf{S}_1 \cdot \mathbf{S}_2)(\mathbf{S}_3 \cdot \mathbf{S}_4), \\ U_{b,1234} &= S_1^i (\mathbf{S}_2 \cdot \mathbf{S}_3) S_4^i, \\ U_{c,1234} &= S_1^i S_2^j S_3^i S_4^j, \end{aligned} \quad (\text{B.4.1})$$

with the indices  $i, j = x, y, z$ .

For the six vectors, we have

$$\begin{aligned} V_{a,1234} &= (\mathbf{S}_1 \cdot \mathbf{S}_2)(\mathbf{S}_3 \times \mathbf{S}_4), \\ V_{b,1234} &= (\mathbf{S}_1 \times \mathbf{S}_2)(\mathbf{S}_3 \cdot \mathbf{S}_4), \\ V_{c,1234} &= \epsilon^{ijk} \hat{e}^k S_1^i S_2^l S_3^j S_4^l, \\ V_{d,1234} &= \epsilon^{ijk} \hat{e}^k S_1^i (\mathbf{S}_2 \cdot \mathbf{S}_3) S_4^j, \\ V_{e,1234} &= \epsilon^{ijk} \hat{e}^k S_1^l S_2^i S_3^l S_4^j, \\ V_{f,1234} &= S_1^l (\mathbf{S}_2 \times \mathbf{S}_3) S_4^l. \end{aligned} \quad (\text{B.4.2})$$

The  $m = 2$ -components of the six tensors of second order are

$$\begin{aligned}
T_{a,1234}^2 &= (\mathbf{S}_1 \times \mathbf{S}_2)^+ (\mathbf{S}_3 \times \mathbf{S}_4)^+, \\
T_{b,1234}^2 &= S_1^\bullet S_2^\circ S_3^\bullet S_4^\circ, \\
T_{c,1234}^2 &= S_1^\bullet (\mathbf{S}_2 \times \mathbf{S}_3) S_4^\bullet, \\
T_{d,1234}^2 &= S_1^+ (\mathbf{S}_2 \times (\mathbf{S}_3 \times \mathbf{S}_4))^+, \\
T_{e,1234}^2 &= S_2^+ ((\mathbf{S}_1 \times \mathbf{S}_4) \times \mathbf{S}_3)^+, \\
T_{f,1234}^2 &= S_3^+ (\mathbf{S}_1 \times (\mathbf{S}_2 \times \mathbf{S}_4))^+.
\end{aligned} \tag{B.4.3}$$

The expressions for  $T_{b,1234}$  and  $T_{c,1234}$  need some explanation: We define

$$S_1^\bullet S_2^\bullet := (\mathbf{S}_1 \times \mathbf{S}_2)^+. \tag{B.4.4}$$

The same holds for the open symbols. This notation allows us to keep the order of the spin operators unaltered.

Similarly to above, the remaining components can be derived by applying the ladder operator.

For the three tensors of third order, the  $m = 3$ -component is

$$\begin{aligned}
W_{a,1234}^3 &= S_1^+ S_2^+ (\mathbf{S}_3 \times \mathbf{S}_4)^+, \\
W_{b,1234}^3 &= S_1^+ (\mathbf{S}_2 \times \mathbf{S}_3)^+ S_4^+, \\
W_{c,1234}^3 &= (\mathbf{S}_1 \times \mathbf{S}_2)^+ S_3^+ S_4^+.
\end{aligned} \tag{B.4.5}$$

Finally, the  $m = 4$ -component of the fourth-order tensor is

$$X_{1234}^4 = S_1^+ S_2^+ S_3^+ S_4^+. \tag{B.4.6}$$

## Appendix C

### The Jacobi theta function

With the help of the Jacobi theta functions, plane boundary wave functions can be rephrased to the torus geometry of periodic boundary conditions.

The theta functions with characteristics  $a, b$  are defined in general by

$$\vartheta_{a,b}(z|\tau) = \sum_{n=-\infty}^{\infty} e^{i\pi(n+a)^2\tau} e^{i2\pi(n+a)(z+b)}. \quad (\text{C.0.1})$$

with  $z \in \mathbb{C}$  and  $\tau \in \mathbb{C}$  with  $\Im(\tau) > 0$ , living in the upper half plane. They satisfy the quasi-periodicity relations on a lattice  $\Lambda = m' + m\tau$  with  $m, m' \in \mathbb{Z}$ ,

$$\begin{aligned} \vartheta_{a,b}(z + 1|\tau) &= e^{i2\pi a} \vartheta_{a,b}(z|\tau), \\ \vartheta_{a,b}(z + \tau|\tau) &= e^{-i\pi\tau} e^{-i2\pi(z+b)} \vartheta_{a,b}(z|\tau). \end{aligned} \quad (\text{C.0.2})$$

The latter formula implies

$$\vartheta_{a,b}(z + n\tau|\tau) = e^{-i\pi n^2\tau} e^{-i2\pi n(z+b)} \vartheta_{a,b}(z|\tau). \quad (\text{C.0.3})$$

The series converge absolutely and uniformly on compact sets [104].

Especially important are the four theta functions with half-integer characteristics, of which three are even,

$$\vartheta_{0,0}(z|\tau), \vartheta_{\frac{1}{2},0}(z|\tau), \vartheta_{0,\frac{1}{2}}(z|\tau), \quad (\text{C.0.4})$$

with  $\vartheta_{a,b}(-z|\tau) = \vartheta_{a,b}(z|\tau)$ , and one odd function,

$$\vartheta_{\frac{1}{2},\frac{1}{2}}(-z|\tau) = -\vartheta_{\frac{1}{2},\frac{1}{2}}(z|\tau). \quad (\text{C.0.5})$$

Theta functions are multivalued on the torus  $T_\tau = C/\Lambda$ , but its zeros are well-defined, being located at

$$\left(-a + \frac{1}{2}\right)\tau + \left(-b + \frac{1}{2}\right) \pmod{\Lambda}, \quad (\text{C.0.6})$$

as illustrated in Figure C.1.

By a rotation of  $\pi/2$  around the origin, the odd  $\vartheta$ -function  $\vartheta_{\frac{1}{2},\frac{1}{2}}$  as well as the even  $\vartheta$ -function  $\vartheta_{0,0}$  remain unchanged, whereas  $\vartheta_{\frac{1}{2},0}$  maps into  $\vartheta_{0,\frac{1}{2}}$  and vice versa. If we rotate by  $\pi/3$  around the origin, only the odd  $\vartheta$ -function is invariant. The even  $\vartheta$ -functions map into each other via  $(0,0) \rightarrow (0,\frac{1}{2}) \rightarrow (\frac{1}{2},0) \rightarrow (0,0)$ .

As one example for a physical application, the four theta functions  $\vartheta_{a,b}(z|\tau)$ ,  $a, b \in \{0, 1/2\}$  provide periodic solutions of the partial differential equation

$$\partial\vartheta(z|\tau)/\partial\tau = \kappa\partial^2\vartheta(z|\tau)/\partial z^2, \quad (\text{C.0.7})$$

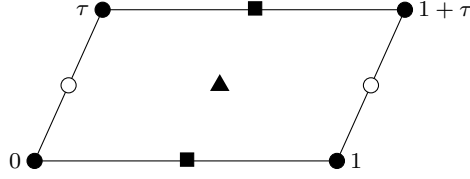


**Fig. C.1** Zeros of the theta-functions in the complex plane: ● zeros of  $\vartheta_{\frac{1}{2},\frac{1}{2}}(z|\tau)$ , ■ zeros of  $\vartheta_{\frac{1}{2},0}(z|\tau)$ , ○ zeros of  $\vartheta_{0,\frac{1}{2}}(z|\tau)$ , ▲ zeros of  $\vartheta_{0,0}(z|\tau)$ .

with  $\kappa = -i\pi/4$ . For  $\tau = it$  and  $t, z \in \mathbb{R}$ , (C.0.7) has the form of a real-time  $t$  diffusion equation, also called heat equation,

$$\partial\vartheta/\partial t = \alpha\partial^2\vartheta/\partial z^2, \quad (\text{C.0.8})$$

with a diffusion constant  $\alpha = \pi/4$ . The non-periodic Gaussian

$$g(z, t) = \sqrt{\frac{\pi}{4\alpha t}} \exp\left(-\frac{z^2}{4\alpha t}\right) \quad (\text{C.0.9})$$

is a solution of (C.0.8) and approaches the Dirac delta distribution for  $t \rightarrow 0$ . Since

$$\sqrt{\frac{\pi}{4\alpha t}} \sum_{n=-\infty}^{\infty} e^{-(n\pi+z)^2/4\alpha t} = \vartheta_{0,0}(z|i4\alpha t/\pi) \quad (\text{C.0.10})$$

and

$$\sqrt{\frac{\pi}{4\alpha t}} \sum_{n=-\infty}^{\infty} (-1)^n e^{-(n\pi+z)^2/4\alpha t} = \vartheta_{0,\frac{1}{2}}(z|i4\alpha t/\pi) \quad (\text{C.0.11})$$

the classical theta functions are "periodized" and "anti-periodized" Gaussians [8].

Appendix D  
Mathematica notebooks for tensor decompositions

## Tensor operations :

Package file with functions to calculate a scalar product ("ScalarProd") of two spins and to calculate a tensor of a specific spin product ("ArbTensor"). (Spin-1/2 system with 1 or 2 or 3 spins communicating with two external spins  $S_m$  and  $S_n$ )

```
BeginPackage["Spin12CreateTensors20140817`"]
LL::usage = "Generate all permutations of x,y,z"
RR::usage = "List of site order for five sites"
RR4::usage = "List of site order for four sites"
RR3::usage = "List of site order for three sites"
ScalarProd::usage = "Calculate scalar product"
Tens::usage = "Create flattened tensor"
ArbTensor::usage = "Calculate arbitrary tensor"

Begin["`Private`"]
(*Define spin operators*)
id := IdentityMatrix[2];
sp := {{0, 1}, {0, 0}};
sm := {{0, 0}, {1, 0}};
sid := 3/4*id; (*sid=sz.sz+1/2*(sp.sm+sm.sp)*)
sz := {{1/2, 0}, {0, -1/2}};
S:={sp,sz,sm};
Sup := {1, 0};
Sdown := {0, 1};
Nil := {0, 0};

(*Function to generate all permutations of {x,y,z} for 3 spins, {x,y}
for 2 spins, {x} for 1 spin *)
LL[x_,y_,z_,NoS_] := Which[NoS==5,Permute[{x,y,z},SymmetricGroup[3]],
  NoS==4,Permute[{x,y},SymmetricGroup[2]],NoS==3,Permute[{x},
  SymmetricGroup[1]]];

(*RR defines the order of the sites*)
RR[x_,y_,z_,m_,n_] := {x,y,z,x,y,z,m,n};

(*Function to create a scalar product of two spin operators S_a.S_b,
returns flattened tensor,a and b being the site index of the two
spins*)
(*SiteList:list with NN elements indicating spin positions,1:spin,
0:vacancy,eg.SiteList={1,1,0,0,0}*)
ScalarProd[SiteList_] :=
Module[{NN,IndexListOdd,IndexListEven,SpinIndex,SiteArgs,Prod,
  FlatProd},
```



```

NN=Length[SiteList];
IndexListOdd=Table[2*i-1,{i,NN}];
IndexListEven=Table[2*i,{i,NN}];
SpinIndex=Flatten[Position[SiteList,1]];(*list of positions
of spins*)
SiteArgs=(SiteList/.{0->id,1->sz});
Prod=(TensorProduct@@@{SiteArgs})[[1]];
If[(NN==5 && SiteList=={0,0,0,0,0})
|| (NN==4 && SiteList=={0,0,0,0})
|| (NN==3 && SiteList=={0,0,0})],
(
(* In this case: flattened identity tensor is created. *)
FlatProd=Flatten[Prod,{IndexListOdd,IndexListEven}];
Return[FlatProd];
),
(
SiteArgs[[SpinIndex[[1]]]]=sp;
SiteArgs[[SpinIndex[[2]]]]=sm;
Prod+=1/2*(TensorProduct@@@{SiteArgs})[[1]];
SiteArgs[[SpinIndex[[1]]]]=sm;
SiteArgs[[SpinIndex[[2]]]]=sp;
Prod+=1/2*(TensorProduct@@@{SiteArgs})[[1]];
FlatProd=Flatten[Prod,{IndexListOdd,IndexListEven}];
Return[FlatProd];
)
]
]

```

(\* Function to create a flattened tensor whose argument is given by one component of the N-dimensional matrix L: L[[a]][[b]]; each element of L has the structure like {sp,id,sm,id,id} \*)

```

Tens[n_, x_, L_, IndexListOdd_, IndexListEven_] :=
  Flatten[(TensorProduct @@@ {L[[n]][[x]])[[1]],
    {IndexListOdd,IndexListEven}];

```

(\* Function to create a tensor given by a spin product [as for instance  $S^a_x S^a_y S^b_m S^b_n$  (with Einstein's sum convention for the upper indices a,b)] and all possible permutations of the sites x,y,z, returning the sum of all tensors (example: if we have 3 sites, there are 3! permutations); RR[x,y,z] defines the order of the sites and P defines pairing of the spin operators; The tensors live in a space with five spin sites a,b,c,m,n.; e.g. RR={x,y,m,n} and P={1,2,3,4,5,6,7,8} gives a spin product  $S^a_x S^a_y S^b_m S^b_n$ ; The argument P always has eight elements 1,...,8. However, if RR has M<8 elements, only the first

M elements of P are relevant. \*)  
 (\* !!!! What cannot be calculated: (A) Self-products of spins as  
 ( $S^a_x S^a_x$ ); (B) In RR, the elements of a) the 1st and 2nd, b) 3rd  
 and 4th, c) 5th and 6th cannot be of the same site. E.g.  $RR=\{x,x,y,z\}$   
 cannot be calculated. However, this is equal to  $RR=\{y,x,x,z\}$ , which can  
 be calculated. \*)

```

ArbTensor[P_,NoS_] :=
Module[{t1, t2, NN, IndexListOdd, IndexListEven, L, DL, Temp1, posm, posn,
pos, case1, ArgList, NoPerm, LEN, LengthEl, T1, T2, T3, Tprod, fac1, fac2,
fac3, fac4, OutP, SUM},
  t1 = SessionTime[];
  NN = NoS; (* NN: Number of sites *)
  IndexListOdd = Table[2*i - 1, {i, NN}];
  IndexListEven = Table[2*i, {i, NN}];

  Temp1 = LL[1, 2, 3, NoS];
  LEN = Length[Temp1];
  Which[NoS==5, For[i = 1, i <= LEN, i++,
    Temp1[[i]] = Append[Temp1[[i]], NoS-2+1];
    Temp1[[i]] = Append[Temp1[[i]], NoS-2+2]],
    NoS==4, For[i = 1, i <= LEN, i++,
    Temp1[[i]] = Append[Temp1[[i]], NoS-2+1];
    Temp1[[i]] = Append[Temp1[[i]], NoS-2+2]],
    NoS==3, For[i = 1, i <= LEN, i++,
    Temp1[[i]] = Append[Temp1[[i]], NoS-2+1];
    Temp1[[i]] = Append[Temp1[[i]], NoS-2+2]]];
  Which[NoS==5,
  (
    ArgList = (RR @@@ Temp1);
    (* Get all possible permutations of the sites x,y,z *)
  ), NoS==4,
  (
    ArgList = (RR4 @@@ Temp1);
    (* Get all possible permutations of the sites x,y *)
  ), NoS==3,
  (
    ArgList = (RR3 @@@ Temp1);
    (* Get all possible permutations of the sites x (just one) *)
  )
  ];
  (*Print[ArgList];*)
  ArgList = DeleteDuplicates[ArgList];
  Print[ArgList];
  NoPerm = Length[ArgList]; (* NoPerm: Number of permutations *)
  LengthEl = Length[ArgList[[1]]];

```

```

L = Table[0, {k, NoPerm}, {i, LengthEl/2}, {m, NN}];
OutP = Table[0, {i, NoPerm}]; (* List to save the tensors of the
different site permutations *)
For[i = 1, i <= NoPerm, i++, For[j = 1, j <= LengthEl, j++,
L[[i]][[IntegerPart[(j + 1)/2]]][[ArgList[[i]][[j]]]]
= P[[j]]];
fac1 = 1;
fac2 = 1;
fac3 = 1;
fac4 = 1;

Which[LengthEl == 2, Goto[SC1], LengthEl == 4,
Goto[SC2], LengthEl == 6, Goto[SC3]];

Label[SC1];
Print["SC1"];
For[h = 1, h <= NoPerm, h++, Tprod = 0;
For[i = 1, i <= 3, i++, a1 = S[[i]]; a2 = S[[4 - i]];
DL = (L /. {0 -> id, 1 -> a1, 2 -> a2});
fac1 = If[a1 == sz, 1, 1/2];
T1 = Tens[h, 1, DL, IndexListOdd, IndexListEven];
Tprod += fac1*T1(*; Print[i]*); OutP[[h]] = Tprod];
SUM = Total[OutP];
(*Print[SUM];*)
t2 = SessionTime[] - t1;
Print["Calculation time = ",t2," s"];
Return[SUM];

Label[SC2];
Print["SC2"];
For[h = 1, h <= NoPerm, h++, Tprod = 0;
For[i = 1, i <= 3, i++, a1 = S[[i]]; a2 = S[[4 - i]];
fac1 = If[a1 == sz, 1, 1/2];
For[j = 1, j <= 3, j++, b1 = S[[j]]; b2 = S[[4 - j]];
DL = (L /. {0 -> id, 1 -> a1, 2 -> a2, 3 -> b1, 4 -> b2});
fac2 = If[b1 == sz, 1, 1/2];
T1 = Tens[h, 1, DL, IndexListOdd, IndexListEven];
T2 = Tens[h, 2, DL, IndexListOdd, IndexListEven];
Tprod += (fac1*fac2)*(T1.T2)(*; Print[i, j]*)];
OutP[[h]] = Tprod];
SUM = Total[OutP];
(* Print[SUM];*)
t2 = SessionTime[] - t1;
Print["Calculation time = ",t2," s"];

```

```

Return[SUM];

Label[SC3];
Print["SC3"];
For[h = 1, h <= NoPerm, h++, Tprod = 0;
  For[i = 1, i <= 3, i++, a1 = S[[i]]; a2 = S[[4 - i]];
    fac1 = If[a1 == sz, 1, 1/2];
    For[j = 1, j <= 3, j++, b1 = S[[j]]; b2 = S[[4 - j]];
      fac2 = If[b1 == sz, 1, 1/2];
      For[k = 1, k <= 3, k++, c1 = S[[k]]; c2 = S[[4 - k]];
        DL = (L /. {0 -> id, 1 -> a1, 2 -> a2, 3 -> b1, 4 -> b2,
          5 -> c1, 6 -> c2});
        fac3 = If[c1 == sz, 1, 1/2];
        T1 = Tens[h, 1, DL, IndexListOdd, IndexListEven];
        T2 = Tens[h, 2, DL, IndexListOdd, IndexListEven];
        T3 = Tens[h, 3, DL, IndexListOdd, IndexListEven];
        Tprod += (fac1*fac2*fac3*fac4)*(T1.T2.T3)]]];
OutP[[h]] = Tprod];
SUM = Total[OutP];
(* Print[SUM]; *)
t2 = SessionTime[] - t1;
Print["Calculation time = ",t2," s"];
Return[SUM];
]

End[]
EndPackage[]

```

# Finding the prefactors of the scalar terms in the tensor decomposition :

Package file with functions to create the tensor projection  $\{T^{m1} T^{m2}\}_j$  whose prefactors are to be calculated (Spin - 1/2 system, arbitrary number of sites)

```
BeginPackage["Spin12FindFactors20140817`"]
CreateTensor::usage = "Create tensor of order M"
TProject::usage = "Project two tensors onto each other"
ResStructure::usage = "Create the tensor product whose prefactors are to be
  found"

Begin["`Private`"]
  (* Define spin operators *)
  id := IdentityMatrix[2]
  sp := {{0, 1}, {0, 0}}
  sm := {{0, 0}, {1, 0}}
  sid := 3/4*
  id (*sid=sz.sz+1/2*(sp.sm+sm.sp)*)
  sz := {{1/2, 0}, {0, -1/2}}

  (* Define commutator *)
  Commutator[A_, B_] := A.B - B.A;

  (* Function to create tensor of order M (M≥1) for a system of NN sites whose
  maximum component is of the form S+a S+b ... S+M *)
  (* TMList: list with NN elements indicating how often which sites appear in
  index of tensor, the number per site can be 0, 1, 2, e.g. TMList={1,1,0,0,1}
  for the tensor Tabn *)
  (* Function returns a list of the components of the tensor in increasing
  order from m=+M to m=-M; e.g. for Tab: {T2ab,T1ab,T0ab,T-1ab,T-2ab} *)
  CreateTensor[TMList_] :=
Module[{NN, M, MM, IndexListOdd, IndexListEven, SpinIndex, TMArgs, TM, FlatTM,
  ListFlatT, Smtemp, SmArgs, Smtot},
  NN = Length[TMList];(* # of sites *)
  M = Count[TMList, 1] ;(* # of spin operators in the tensor *)
  MM = Count[TMList, 1] ;(* # of occupied sites *)
  IndexListOdd = Table[2*i - 1, {i, NN}];
  IndexListEven = Table[2*i, {i, NN}];
  SpinIndex = Flatten[Position[TMList, x_ /; x > 0]];(* list of positions
  of spins *)

  TMArgs = (TMList /. {0 -> id, 1 -> sp}); (* transform list of spin
```

```

positions into list of spin matrices sp and id *)
TM = (TensorProduct @@@ {TMArgs})[[1]]; (* create tensor of order
M, m=M *)
FlatTM = Flatten[(-1)^(M)*TM, {IndexListOdd, IndexListEven}];
ListFlatT = Table[0, {i, 2*M + 1}];
ListFlatT[[1]] = FlatTM;
Smtemp = 0; (* creation of total spin flip down operator *)
SmArgs = Table[id, {i, NN}];

For[j = 1, j < (MM + 1), SmArgs[[SpinIndex[[j]]]] = sm;
  Smtemp += (TensorProduct @@@ {SmArgs})[[1]];
  SmArgs = Table[id, {i, NN}]; j++;
  Smtot := Flatten[Smtemp, {IndexListOdd, IndexListEven}];
For[i = 2, i < (2*M + 2), ListFlatT[[i]] =
  Simplify[1/Sqrt[M*(M + 1) - (M - i + 2)*(M - i + 1)]
  *Commutator[Smtot, ListFlatT[[i - 1]]]]; i++;
  (* create all tensor components *)
  (* Test if correct tensor components are created *)
TMArgs = (TMlist /. {0 -> id, 1 -> sm});
TM = (TensorProduct @@@ {TMArgs})[[1]];
If[ListFlatT[[2*M + 1]] == Flatten[TM, {IndexListOdd, IndexListEven}],
  Return[ListFlatT],
  Return[Print["Error in tensor calculation occured!"]]]
]

(* Function to calculate the projection of two tensors
{T(j1)m1 T(j2)m2}_jres *)
TProject[Tm1List_, Tm2List_, m1_, m2_, jres_] :=
Module[{j1, j2, mmin, mmax, T1, T2, Contraction},
  j1 = Count[Tm1List, 1];
  j2 = Count[Tm2List, 1];
  mmin = Max[-j1, -j2 + m1 + m2];
  mmax = Max[j1, j2 + m1 + m2];
  T1 = CreateTensor[Tm1List];
  T2 = (-1)^j2*CreateTensor[Tm2List];
  fterm[m_] := ClebschGordan[{j1, m}, {j2, m1 + m2 - m}, {jres, m1 + m2}]
  *(T1[[mmax + 1 + m]].T2[[mmax + 1 + m1 + m2 - m]]);
  Contraction = ClebschGordan[{j1, m1}, {j2, m2}, {jres, m1 + m2}]
  *Sum[fterm[m], {m, mmin, mmax}];
  Return[Contraction];
]

(* Function to create the function which defines the structure of the result;
it takes a list of the terms which contribute to the structure and the
parameters for every term: Params={a,b,c,...} *)

```

```

ResStructure[Tm1List_, Tm2List_, m1_, m2_, jres_, ResTerms_] :=
Module[{Num, alphabet, ParamList, ResFunction, NN, TensorProject, FlatStateVec,
Bres, Res},
  Num = Length[ResTerms];
  ParamList = Take[ParamListTotal, {1, Num}];
  ResFunction[X_] := Sum[ResTerms[[i]] X[[i]], {i, Num}];
  NN = Length[Tm1List];
  TensorProject = TProject[Tm1List, Tm2List, m1, m2, jres];
  Bres = ResFunction[ParamList];
  Res = Solve[DeleteCases[Flatten[Table[Bres[[i]][[j]] ==
  TensorProject[[i]][[j]], {i, 1, 2^NN}, {j, 1, 2^NN}]], True],
  Table[ParamList[[kh]], {kh, Num}]];
  Return[Res];
]

End[]
EndPackage[]

```

---

## Main program : Decompose the small Hamiltonian for a spin - 1 system with a 3 - site interaction

```
Needs["Spin12CreateTensors20140817`"]
```

```
Needs["Spin12FindFactors20140817`"]
```

### Part 1 :

External spins are not equal,  $m \neq n$

```
A1 = ScalarProd[{0, 0, 0, 1, 1}];
```

```
RR[x_, y_, z_, m_, n_] := {x, y};
```

```
PA2 = {1, 2, 3, 4, 5, 6};
```

```
A2 = (ArbTensor[PA2, 5].A1);
```

```
RR[x_, y_, z_, m_, n_] := {x, m, x, n};
```

```
PB3 = {1, 2, 3, 4, 5, 6};
```

```
B3p = ArbTensor[PB3, 5];
```

```
RR[x_, y_, z_, m_, n_] := {x, n, x, m};
```

```
B4p = ArbTensor[PB3, 5];
```

```
B3 = B3p - B4p;
```

```
B4 = B3p + B4p;
```

```
RR[x_, y_, z_, m_, n_] := {y, z, x, m, x, n};
```

```
PB5 = {1, 2, 3, 4, 5, 6};
```

```
B5p = ArbTensor[PB5, 5];
```

```
RR[x_, y_, z_, m_, n_] := {y, z, x, n, x, m};
```

```
B6p = ArbTensor[PB5, 5];
```

```
B5 = B5p - B6p;
```

```
B6 = B5p + B6p;
```

```
RR[x_, y_, z_, m_, n_] := {x, m, y, n};
```

```
PC7 = {1, 2, 3, 4, 5, 6};
```

```
C7 = ArbTensor[PC7, 5];
```

```
ResTerms = {A2, A1, B5, B3, C7};
```

(\* Terms B4 and B6 do not occur in the final result \*)

```
ResStructure[{1, 1, 1, 1, 0}, {1, 1, 1, 0, 1}, 4, -4, 0, ResTerms]
```

```
{{aa →  $\frac{1}{15}$ , bb →  $\frac{1}{12}$ , cc →  $-\frac{1}{30}$ , dd →  $-\frac{1}{12}$ , ee →  $-\frac{1}{30}$ }}
```



## References

- [1] *OpenMP Application Program Interface (API)*.
- [2] *Linear Algebra Package (LAPACK, Fortran and C libraries)* (2012).
- [3] *The Numerical Algorithms Group library (NAG, commercial library)* (2012).
- [4] P. W. Anderson, *Infrared Catastrophe in Fermi Gases with Local Scattering Potentials*, Physical Review Letters **18**, 1049 (1967).
- [5] D. Arovas, J. R. Schrieffer, and F. Wilczek, *Fractional Statistics and the Quantum Hall Effect*, Phys. Rev. Lett. **53**, 722 (1984).
- [6] G. Baskaran, *Novel local symmetries and chiral-symmetry-broken phases in  $S=1/2$  triangular-lattice Heisenberg model*, Physical Review Letters **63**, 2524 (1989).
- [7] G. Baym, *Lectures on Quantum Mechanics* (The Benjamin / Cummings Publishing Company, New York, NY, 1969).
- [8] R. Bellman, *A Brief Introduction to Theta Functions*, Athena Series: Selected Topics in Mathematics (Holt, Rinehart and Winston, New York, 1961).
- [9] B. Bernevig and T. Hughes, *Topological Insulators and Topological Superconductors* (Princeton University Press, 2013).
- [10] B. A. Bernevig, D. Giuliano, and R. B. Laughlin, *Coordinate representation of the two-spinon wave function and spinon interaction in the Haldane-Shastry model*, Physical Review B **64**, 024425 (2001).
- [11] —, *Spinon Attraction in Spin-1/2 Antiferromagnetic Chains*, Physical Review Letters **86**, 3392 (2001).
- [12] B. A. Bernevig, T. L. Hughes, and S.-C. Zhang, *Quantum Spin Hall Effect and Topological Phase Transition in HgTe Quantum Wells*, Science **314**, 1757 (2006).
- [13] B. A. Bernevig and S.-C. Zhang, *Quantum Spin Hall Effect*, Physical Review Letters **96**, 106802 (2006).
- [14] M. V. Berry, *Quantal Phase Factors Accompanying Adiabatic Changes*, Proceedings of the Royal Society A: Mathematical, Physical and Engineering Sciences **392**, 45 (1984).
- [15] J. C. Boettger and S. B. Trickey, *First-principles calculation of the spin-orbit splitting in graphene*, Physical Review B **75**, 121402 (2007).
- [16] J. Bonner and M. Fisher, *Linear Magnetic Chains with Anisotropic Coupling*, Phys. Rev. **135**, A640 (1964).
- [17] T. Chakraborty and P. Pietiläinen, *The Fractional Quantum Hall Effect*, volume 85 of *Springer Series in Solid-State Sciences* (Springer Berlin Heidelberg, Berlin, Heidelberg, 1988).
- [18] C.-Z. Chang, J. Zhang, X. Feng, J. Shen, Z. Zhang, M. Guo, K. Li, Y. Ou, P. Wei, L.-L. Wang, Z.-Q. Ji, Y. Feng, S. Ji, X. Chen, J. Jia, X. Dai, Z. Fang, S.-C. Zhang, K. He, Y. Wang, L. Lu, X.-C. Ma, and Q.-K. Xue, *Experimental Observation of the Quantum Anomalous Hall Effect in a Magnetic Topological Insulator*, Science **340**, 167 (2013).
- [19] V. Chari and A. Pressley, *A Guide to Quantum Groups* (Cambridge University Press, 1995).
- [20] Y. L. Chen, J. G. Analytis, J.-H. Chu, Z. K. Liu, S.-K. Mo, X. L. Qi, H. J. Zhang, D. H. Lu, X. Dai, Z. Fang, S. C. Zhang, I. R. Fisher, Z. Hussain, and Z.-X. Shen, *Experimental Realization of a Three-Dimensional Topological Insulator,  $Bi_2Te_3$* , Science **325**, 178 (2009).

- [21] J. Cornelis Talstra, *Integrability and Applications of the Exactly-Solvable Haldane-Shastry One-Dimensional Quantum Spin Chain*, Ph.D. thesis, Princeton University (1995).
- [22] P. A. M. Dirac, *Quantised Singularities in the Electromagnetic Field*, Proceedings of the Royal Society A: Mathematical, Physical and Engineering Sciences **133**, 60 (1931).
- [23] M. Dolev, M. Heiblum, V. Umansky, A. Stern, and D. Mahalu, *Observation of a quarter of an electron charge at the  $\nu = 5/2$  quantum Hall state*, Nature **452**, 829 (2008).
- [24] V. G. Drinfeld, *Hopf algebras and the quantum Yang-Baxter equation*, Sov. Math. Dokl. **32**, 254 (1985).
- [25] G. Fano, F. Ortolani, and E. Colombo, *Configuration-interaction calculations on the fractional quantum Hall effect*, Physical Review B **34**, 2670 (1986).
- [26] L. Fu, *Topological Crystalline Insulators*, Physical Review Letters **106**, 106802 (2011).
- [27] L. Fu and C. L. Kane, *Topological insulators with inversion symmetry*, Physical Review B **76**, 045302 (2007).
- [28] L. Fu, C. L. Kane, and E. J. Mele, *Topological Insulators in Three Dimensions*, Physical Review Letters **98**, 106803 (2007).
- [29] M. Gaudin, *Gaz coulombien discret à une dimension*, Journal de Physique **34**, 511 (1973).
- [30] F. Gebhard and D. Vollhardt, *Correlation functions for Hubbard-type models: The exact results for the Gutzwiller wave function in one dimension*, Phys. Rev. Lett. **59**, 1472 (1987).
- [31] M. Gmitra, S. Konschuh, C. Ertler, C. Ambrosch-Draxl, and J. Fabian, *Band-structure topologies of graphene: Spin-orbit coupling effects from first principles*, Physical Review B **80**, 235431 (2009).
- [32] K. Gottfried and T. Yan, *Quantum Mechanics: Fundamentals* (Springer New York, 2003).
- [33] I. S. Gradshteyn and I. M. Ryzhik, *Table of Integrals, Series, and Products* (Academic, New York, 1980).
- [34] M. Greiter, *Microscopic formulation of the hierarchy of quantized Hall states*, Physics Letters B **336**, 48 (1994).
- [35] —, *S=1 Spin Liquids: Broken Discrete Symmetries Restored*, Journal of Low Temperature Physics **126**, 1029 (2002).
- [36] —, *Landau level quantization on the sphere*, Physical Review B **83**, 115129 (2011).
- [37] —, *Mapping of Parent Hamiltonians*, volume 244 of *Springer Tracts in Modern Physics* (Springer Berlin Heidelberg, Berlin, Heidelberg, 2011).
- [38] M. Greiter and I. A. McDonald, *Hierarchy of quantized Hall states in double-layer electron systems*, Nuclear Physics B **410**, 521 (1993).
- [39] M. Greiter, V. Schnells, and R. Thomale, *The 1D Ising model and the topological Kitaev chain*, Annals of Physics **351**, 1026 (2014).
- [40] —, *Laughlin states and their quasiparticle excitations on the torus*, Physical Review B **93**, 245156 (2016).
- [41] —, *Method to identify parent Hamiltonians for trial states*, Physical Review B **98**, 081113 (2018).
- [42] M. Greiter, D. F. Schroeter, and R. Thomale, *Parent Hamiltonian for the non-Abelian chiral spin liquid*, Physical Review B **89**, 165125 (2014).
- [43] M. Greiter and D. Schuricht, *No attraction between spinons in the Haldane-Shastry model*, Physical Review B **71**, 224424 (2005).
- [44] —, *Many-Spinon States and the Secret Significance of Young Tableaux*, Physical Review Letters **98**, 237202 (2007).
- [45] M. Greiter and R. Thomale, *Non-Abelian Statistics in a Quantum Antiferromagnet*, Physical Review Letters **102**, 207203 (2009).
- [46] —, *Generalizations of Perelomov's identity on the completeness of coherent states*, Physical Review B **85**, 155145 (2012).
- [47] M. Greiter, X.-G. Wen, and F. Wilczek, *Paired Hall state at half filling*, Physical Review Letters **66**, 3205 (1991).
- [48] M. Greiter, X. G. Wen, and F. Wilczek, *Paired Hall states*, Nuclear Physics B **374**, 567 (1992).
- [49] M. Greiter and F. Wilczek, *Exact solutions and the adiabatic heuristic for quantum Hall states*, Nuclear Physics B **370**, 577 (1992).

- [50] C. Gros, R. Joynt, and T. M. Rice, *Antiferromagnetic correlations in almost-localized Fermi liquids*, Physical Review B **36**, 381 (1987).
- [51] M. C. Gutzwiller, *Effect of Correlation on the Ferromagnetism of Transition Metals*, Physical Review Letters **10**, 159 (1963).
- [52] P. S. Häfliger, S. Gerber, R. Pramod, V. Schnells, B. dalla Piazza, R. Chati, V. Pomjakushin, K. Conder, E. Pomjakushina, L. Le Dreau, N. B. Christensen, O. F. Syljurasen, B. Normand, and H. M. Rønnow, *Quantum and thermal ionic motion, oxygen isotope effect, and superexchange distribution in  $\text{La}_2\text{CuO}_4$* , Physical Review B **89**, 085113 (2014).
- [53] F. D. M. Haldane, *Fractional Quantization of the Hall Effect: A Hierarchy of Incompressible Quantum Fluid States*, Physical Review Letters **51**, 605 (1983).
- [54] —, *Exact Jastrow-Gutzwiller resonating-valence-bond ground state of the spin- $(1/2)$  antiferromagnetic Heisenberg chain with  $1/r^2$  exchange*, Physical Review Letters **60**, 635 (1988).
- [55] —, *Model for a Quantum Hall Effect without Landau Levels: Condensed-Matter Realization of the "Parity Anomaly"*, Physical Review Letters **61**, 2015 (1988).
- [56] —, *Fractional statistics" in arbitrary dimensions: A generalization of the Pauli principle*, Physical Review Letters **67**, 937 (1991).
- [57] —, *Spinon gas" description of the  $S = 1/2$  Heisenberg chain with inverse-square exchange: Exact spectrum and thermodynamics*, Physical Review Letters **66**, 1529 (1991).
- [58] F. D. M. Haldane, Z. N. C. Ha, J. C. Talstra, D. Bernard, and V. Pasquier, *Yangian symmetry of integrable quantum chains with long-range interactions and a new description of states in conformal field theory*, Physical Review Letters **69**, 2021 (1992).
- [59] F. D. M. Haldane and E. H. Rezayi, *Periodic Laughlin-Jastrow wave functions for the fractional quantized Hall effect*, Physical Review B **31**, 2529 (1985).
- [60] —, *Periodic Laughlin-Jastrow wave functions for the fractional quantized Hall effect*, Physical Review B **31**, 2529 (1985).
- [61] B. I. Halperin, *Quantized Hall conductance, current-carrying edge states, and the existence of extended states in a two-dimensional disordered potential*, Physical Review B **25**, 2185 (1982).
- [62] —, *Theory of the quantized Hall conductance*, Helv. Phys. Acta **56**, 75 (1983).
- [63] —, *Statistics of Quasiparticles and the Hierarchy of Fractional Quantized Hall States*, Physical Review Letters **52**, 1583 (1984).
- [64] M. Z. Hasan and C. L. Kane, *Colloquium : Topological insulators*, Reviews of Modern Physics **82**, 3045 (2010).
- [65] D. Hsieh, D. Qian, L. Wray, Y. Xia, Y. S. Hor, R. J. Cava, and M. Z. Hasan, *A topological Dirac insulator in a quantum spin Hall phase*, Nature **452**, 970 (2008).
- [66] —, *A topological Dirac insulator in a quantum spin Hall phase*, Nature **452**, 970 (2008).
- [67] D. Hsieh, Y. Xia, L. Wray, D. Qian, A. Pal, J. H. Dil, J. Osterwalder, F. Meier, G. Bihlmayer, C. L. Kane, Y. S. Hor, R. J. Cava, and M. Z. Hasan, *Observation of Unconventional Quantum Spin Textures in Topological Insulators*, Science **323**, 919 (2009).
- [68] T. H. Hsieh, H. Lin, J. Liu, W. Duan, A. Bansil, and L. Fu, *Topological crystalline insulators in the  $\text{SnTe}$  material class*, Nature Communications **3**, 982 (2012).
- [69] D. Huertas-Hernando, F. Guinea, and A. Brataas, *Spin-orbit coupling in curved graphene, fullerenes, nanotubes, and nanotube caps*, Physical Review B **74**, 155426 (2006).
- [70] V. I. Inozemtsev, *On the connection between the one-dimensional  $S=1/2$  Heisenberg chain and Haldane-Shastry model*, Journal of Statistical Physics **59**, 1143 (1990).
- [71] R. Jackiw and C. Rebbi, *Solitons with fermion number*, Physical Review D **13**, 3398 (1976).
- [72] J. Jain, *Composite Fermions* (Cambridge University Press, Cambridge, 2007).
- [73] V. Kalmeyer and R. B. Laughlin, *Equivalence of the resonating-valence-bond and fractional quantum Hall states*, Physical Review Letters **59**, 2095 (1987).
- [74] —, *Theory of the spin liquid state of the Heisenberg antiferromagnet*, Physical Review B **39**, 11879 (1989).
- [75] C. L. Kane and E. J. Mele, *Quantum Spin Hall Effect in Graphene*, Physical Review Letters **95**, 226801 (2005).

- [76] T. A. Kaplan, P. Horsch, and P. Fulde, *Close Relation between Localized-Electron Magnetism and the Paramagnetic Wave Function of Completely Itinerant Electrons*, Physical Review Letters **49**, 889 (1982).
- [77] N. Kawakami, *Asymptotic Bethe-ansatz solution of multicomponent quantum systems with  $1/r^2$  long-range interaction*, Physical Review B **46**, 1005 (1992).
- [78] —,  *$SU(N)$  generalization of the Gutzwiller-Jastrow wave function and its critical properties in one dimension*, Physical Review B **46**, 3191 (1992).
- [79] A. Kitaev, *Fault-tolerant quantum computation by anyons*, Annals of Physics **303**, 2 (2003).
- [80] K. v. Klitzing, G. Dorda, and M. Pepper, *New Method for High-Accuracy Determination of the Fine-Structure Constant Based on Quantized Hall Resistance*, Physical Review Letters **45**, 494 (1980).
- [81] M. König, S. Wiedmann, C. Brune, A. Roth, H. Buhmann, L. W. Molenkamp, X.-L. Qi, and S.-C. Zhang, *Quantum Spin Hall Insulator State in HgTe Quantum Wells*, Science **318**, 766 (2007).
- [82] C. Lacroix, P. Mendels, and F. Mila, eds., *Introduction to Frustrated Magnetism*, volume 164 of *Springer Series in Solid-State Sciences* (Springer Berlin Heidelberg, Berlin, Heidelberg, 2011).
- [83] L. Landau, *Theory of phase transformations I*, Phys. Z. Sowjetunion **11**, 26 (1937).
- [84] —, *Theory of phase transformations II*, Phys. Z. Sowjetunion **11**, 545 (1937).
- [85] R. B. Laughlin, *Quantized Hall conductivity in two dimensions*, Physical Review B **23**, 5632 (1981).
- [86] —, *Anomalous Quantum Hall Effect: An Incompressible Quantum Fluid with Fractionally Charged Excitations*, Physical Review Letters **50**, 1395 (1983).
- [87] —, *Primitive and composite ground states in the fractional quantum hall effect*, Surface Science **142**, 163 (1984).
- [88] R. B. Laughlin, D. Giuliano, R. Caracciolo, and O. L. White, *Quantum Number Fractionalization in Antiferromagnets*, in G. Morandi, P. Sodano, A. Tagliacozzo, and V. Tognetti, eds., *Field Theories for Low-Dimensional Condensed Matter Systems*, 83–115 (Springer, Berlin, 2000).
- [89] R. B. Laughlin and Z. Zou, *Properties of the chiral-spin-liquid state*, Physical Review B **41**, 664 (1990).
- [90] C. H. Lee, Z. Papić, and R. Thomale, *Geometric Construction of Quantum Hall Clustering Hamiltonians*, Physical Review X **5**, 041003 (2015).
- [91] R. Lehoucq, K. Maschhoff, D. Sorensen, and C. Yang, *ARPACK (the ARnoldi PACKage)*.
- [92] J. Leinaas and J. Myrheim, *On the theory of identical particles*, Nuovo Cimento B Serie **37**, 1 (1977).
- [93] M. Levin and A. Stern, *Fractional Topological Insulators*, Physical Review Letters **103**, 196803 (2009).
- [94] C.-X. Liu, S.-C. Zhang, and X.-L. Qi, *The quantum anomalous Hall effect*, (2015).
- [95] Y.-M. Lu and Y. Ran, *Symmetry-protected fractional Chern insulators and fractional topological insulators*, Physical Review B **85**, 165134 (2012).
- [96] M. L. Mehta and G. C. Mehta, *Discrete Coulomb gas in one dimension: Correlation functions*, Journal of Mathematical Physics **16**, 1256 (1975).
- [97] T. Meng and E. Sela, *Time reversal symmetry broken fractional topological phases at zero magnetic field*, Physical Review B **90**, 235425 (2014).
- [98] W. Metzner and D. Vollhardt, *Ground-state properties of correlated fermions: Exact analytic results for the Gutzwiller wave function*, Physical Review Letters **59**, 121 (1987).
- [99] H. Min, J. E. Hill, N. A. Sinitsyn, B. R. Sahu, L. Kleinman, and A. H. MacDonald, *Intrinsic and Rashba spin-orbit interactions in graphene sheets*, Physical Review B **74**, 165310 (2006).
- [100] G. Moore and N. Read, *Nonabelions in the fractional quantum hall effect*, Nuclear Physics B **360**, 362 (1991).
- [101] J. E. Moore and L. Balents, *Topological invariants of time-reversal-invariant band structures*, Physical Review B **75**, 121306 (2007).
- [102] M. Moretti Sala, V. Schnells, S. Boseggia, L. Simonelli, A. Al-Zein, J. G. Vale, L. Paolasini, E. C. Hunter, R. S. Perry, D. Prabhakaran, A. T. Boothroyd, M. Krisch, G. Monaco, H. M. Rønnow, D. F. McMorrow, and F. Mila, *Evidence of quantum dimer excitations in Sr3Ir2O7*, Physical Review B **92**, 024405 (2015).
- [103] R. Morf and B. I. Halperin, *Monte Carlo evaluation of trial wavefunctions for the fractional quantized Hall effect: Spherical geometry*, Zeitschrift für Physik B Condensed Matter **68**, 391 (1987).

- [104] D. Mumford, *Tata Lectures on Theta I, II* (Birkhäuser Boston, Basel, 1983).
- [105] C. Nayak, S. H. Simon, A. Stern, M. Freedman, and S. Das Sarma, *Non-Abelian anyons and topological quantum computation*, *Reviews of Modern Physics* **80**, 1083 (2008).
- [106] T. Neupert, L. Santos, C. Chamon, and C. Mudry, *Fractional Quantum Hall States at Zero Magnetic Field*, *Physical Review Letters* **106**, 236804 (2011).
- [107] R. M. Noack, *Diagonalization- and Numerical Renormalization-Group-Based Methods for Interacting Quantum Systems*, in *AIP Conference Proceedings*, volume 789, 93–163 (AIP, 2005).
- [108] E. G. Novik, A. Pfeuffer-Jeschke, T. Jungwirth, V. Latussek, C. R. Becker, G. Landwehr, H. Buhmann, and L. W. Molenkamp, *Band structure of semimagnetic HgMnTe quantum wells*, *Physical Review B* **72**, 035321 (2005).
- [109] J. Oitmaa and D. D. Betts, *The ground state of two quantum models of magnetism*, *Can. J. Phys.* **56**, 897 (1978).
- [110] A. M. Perelomov, *On the completeness of a system of coherent states*, *Theoretical and Mathematical Physics* **6**, 156 (1971).
- [111] A. Pfeuffer-Jeschke, *No Title*, Ph.D. thesis, Universität Würzburg (2000).
- [112] R. E. Prange and S. M. Girvin, eds., *The Quantum Hall Effect*, *Graduate Texts in Contemporary Physics* (Springer New York, New York, NY, 1990).
- [113] W. H. Press, W. T. Vetterling, S. A. Teukolsky, and B. P. Flannery, *Numerical Recipes in C++: the art of scientific computing* (Cambridge University Press, New York, NY, USA, 2002), 2nd edition.
- [114] X.-L. Qi, *Generic Wave-Function Description of Fractional Quantum Anomalous Hall States and Fractional Topological Insulators*, *Physical Review Letters* **107**, 126803 (2011).
- [115] X.-L. Qi and S.-C. Zhang, *The quantum spin Hall effect and topological insulators*, *Physics Today* **63**, 33 (2010).
- [116] —, *Topological insulators and superconductors*, *Reviews of Modern Physics* **83**, 1057 (2011).
- [117] J. Quinn and A. Wójs, *Composite fermions and the fractional quantum Hall effect: essential role of the pseudopotential*, *Physica E: Low-dimensional Systems and Nanostructures* **6**, 1 (2000).
- [118] I. P. Radu, J. B. Miller, C. M. Marcus, M. A. Kastner, L. N. Pfeiffer, and K. W. West, *Quasi-Particle Properties from Tunneling in the Formula Fractional Quantum Hall State*, *Science* **320**, 899 (2008).
- [119] N. Read and E. Rezayi, *Quasiholes and fermionic zero modes of paired fractional quantum Hall states: The mechanism for non-Abelian statistics*, *Physical Review B* **54**, 16864 (1996).
- [120] —, *Beyond paired quantum Hall states: Parafermions and incompressible states in the first excited Landau level*, *Physical Review B* **59**, 8084 (1999).
- [121] N. Regnault and B. A. Bernevig, *Fractional Chern Insulator*, *Physical Review X* **1**, 021014 (2011).
- [122] R. Roy, *Topological phases and the quantum spin Hall effect in three dimensions*, *Physical Review B* **79**, 195322 (2009).
- [123] V. Schnells, R. Thomale, and M. Greiter, *Fractional insulators*, to be published (2019).
- [124] —, *Local parent Hamiltonian for the chiral spin liquid*, to be published (2019).
- [125] D. F. Schroeter, E. Kapit, R. Thomale, and M. Greiter, *Spin Hamiltonian for which the Chiral Spin Liquid is the Exact Ground State*, *Physical Review Letters* **99**, 097202 (2007).
- [126] B. S. Shastri, *Taking the square root of the discrete  $1/r^2$  model*, *Physical Review Letters* **69**, 164 (1992).
- [127] S. Shastri, *Exact solution of an  $S = 1/2$  Heisenberg antiferromagnetic chain with long-ranged interactions*, *Physical Review Letters* **60**, 639 (1988).
- [128] D. Sheng, Z.-C. Gu, K. Sun, and L. Sheng, *Fractional quantum Hall effect in the absence of Landau levels*, *Nature Communications* **2**, 389 (2011).
- [129] B. Simon, *Holonomy, the Quantum Adiabatic Theorem, and Berry's Phase*, *Physical Review Letters* **51**, 2167 (1983).
- [130] S. H. Simon, F. Harper, and N. Read, *Fractional Chern insulators in bands with zero Berry curvature*, *Physical Review B* **92**, 195104 (2015).
- [131] S. H. Simon, E. Rezayi, and N. R. Cooper, *Pseudopotentials for multiparticle interactions in the quantum Hall regime*, *Physical Review B* **75**, 195306 (2007).
- [132] A. Stern, *Anyons and the quantum Hall effect: A pedagogical review*, *Annals of Physics* **323**, 204 (2008).

- [133] —, *Fractional Topological Insulators: A Pedagogical Review*, Annual Review of Condensed Matter Physics **7**, 349 (2016).
- [134] Y. W. Suen, L. W. Engel, M. B. Santos, M. Shayegan, and D. C. Tsui, *Observation of a  $\nu=1/2$  fractional quantum Hall state in a double-layer electron system*, Physical Review Letters **68**, 1379 (1992).
- [135] J. C. Y. Teo, L. Fu, and C. L. Kane, *Surface states and topological invariants in three-dimensional topological insulators: Application to BiSb*, Physical Review B **78**, 045426 (2008).
- [136] R. Thomale, *Fractional Excitations in low-dimensional spin systems*, Ph.D. thesis, University of Karlsruhe (2008).
- [137] R. Thomale and B. A. Bernevig, *Private Communication*, (2016).
- [138] R. Thomale, E. Kapit, D. F. Schroeter, and M. Greiter, *Parent Hamiltonian for the chiral spin liquid*, Physical Review B **80**, 104406 (2009).
- [139] D. J. Thouless, M. Kohmoto, M. P. Nightingale, and M. den Nijs, *Quantized Hall Conductance in a Two-Dimensional Periodic Potential*, Physical Review Letters **49**, 405 (1982).
- [140] D. C. Tsui, H. L. Stormer, and A. C. Gossard, *Two-Dimensional Magnetotransport in the Extreme Quantum Limit*, Physical Review Letters **48**, 1559 (1982).
- [141] Y.-F. Wang, Z.-C. Gu, C.-D. Gong, and D. N. Sheng, *Fractional Quantum Hall Effect of Hard-Core Bosons in Topological Flat Bands*, Physical Review Letters **107**, 146803 (2011).
- [142] A. Weiße and H. Fehske, *Exact Diagonalization Techniques*, in H. Fehske, R. Schneider, and A. Weiße, eds., *Computational Many-Particle Physics*, volume 739 of *Lecture Notes in Physics*, Berlin Springer Verlag, 529 (2008).
- [143] X. G. Wen, *Non-Abelian statistics in the fractional quantum Hall states*, Physical Review Letters **66**, 802 (1991).
- [144] X.-G. Wen, *Topological orders and edge excitations in fractional quantum Hall states*, Advances in Physics **44**, 405 (1995).
- [145] X. G. Wen, *Quantum Field Theory of Many-Body Systems* (OUP Oxford, 2004).
- [146] X. G. Wen, F. Wilczek, and A. Zee, *Chiral spin states and superconductivity*, Physical Review B **39**, 11413 (1989).
- [147] H. Weng, R. Yu, X. Hu, X. Dai, and Z. Fang, *Quantum anomalous Hall effect and related topological electronic states*, Advances in Physics **64**, 227 (2015).
- [148] E. Wigner, *Gruppentheorie und ihre Anwendung auf die Quantenmechanik der Atomspektren* (Vieweg+Teubner Verlag, Wiesbaden, 1931).
- [149] F. Wilczek, *Quantum Mechanics of Fractional-Spin Particles*, Physical Review Letters **49**, 957 (1982).
- [150] —, *Fractional Statistics and Anyon Superconductivity* (World Scientific, Singapore, 1990).
- [151] R. Willett, J. P. Eisenstein, H. L. Störmer, D. C. Tsui, A. C. Gossard, and J. H. English, *Observation of an even-denominator quantum number in the fractional quantum Hall effect*, Physical Review Letters **59**, 1776 (1987).
- [152] A. Wójs and J. J. Quinn, *Composite fermion approach to the quantum Hall hierarchy: when it works and why*, Solid State Communications **108**, 493 (1998).
- [153] S. Wolfram, *An Elementary Introduction to the Wolfram Language* (Wolfram Media, 2017), 2nd edition.
- [154] C. Wu, B. A. Bernevig, and S.-C. Zhang, *Helical Liquid and the Edge of Quantum Spin Hall Systems*, Physical Review Letters **96**, 106401 (2006).
- [155] Y.-L. Wu, N. Regnault, and B. A. Bernevig, *Gauge-fixed Wannier wave functions for fractional topological insulators*, Physical Review B **86**, 085129 (2012).
- [156] Y. Xia, D. Qian, D. Hsieh, L. Wray, A. Pal, H. Lin, A. Bansil, D. Grauer, Y. S. Hor, R. J. Cava, and M. Z. Hasan, *Observation of a large-gap topological-insulator class with a single Dirac cone on the surface*, Nature Physics **5**, 398 (2009).
- [157] Y. Yao, F. Ye, X.-L. Qi, S.-C. Zhang, and Z. Fang, *Spin-orbit gap of graphene: First-principles calculations*, Physical Review B **75**, 041401 (2007).
- [158] M. W. Young, S.-S. Lee, and C. Kallin, *Fractionalized quantum spin Hall effect*, Physical Review B **78**, 125316 (2008).

- [159] H. Zhang, C.-X. Liu, X.-L. Qi, X. Dai, Z. Fang, and S.-C. Zhang, *Topological insulators in Bi<sub>2</sub>Se<sub>3</sub>, Bi<sub>2</sub>Te<sub>3</sub> and Sb<sub>2</sub>Te<sub>3</sub> with a single Dirac cone on the surface*, Nature Physics **5**, 438 (2009).
- [160] Z. Zou, B. Doucot, and S. Shastry, *Equivalence of fractional quantum Hall and resonating-valence-bond states on a square lattice*, Physical Review B **39**, 11424 (1989).